

# Quantum spin squeezing

Jian Ma<sup>a,b</sup>, Xiaoguang Wang<sup>a,b</sup>, C. P. Sun<sup>a,c</sup>, Franco Nori<sup>a,d</sup>

<sup>a</sup>Advanced Science Institute, RIKEN, Wako-shi, Saitama 351-0198, Japan

<sup>b</sup>Zhejiang Institute of Modern Physics, Department of Physics, Zhejiang University, Hangzhou 310027, China

<sup>c</sup>Institute of Theoretical Physics, Chinese Academy of Sciences, Beijing 100190, China

<sup>d</sup>Physics Department, The University of Michigan, Ann Arbor, Michigan 48109-1040, USA

## Abstract

This paper reviews quantum spin squeezing, which characterizes the sensitivity of a state with respect to SU(2) rotations, and is significant for both entanglement detection and high-precision metrology. We first present various definitions of spin squeezing parameters, explain their origin and properties for typical states, and then discuss spin-squeezed states produced with nonlinear twisting Hamiltonians. Afterwards, we explain pairwise correlations and entanglement in spin-squeezed states, as well as the relations between spin squeezing and quantum Fisher information, where the latter plays a central role in quantum metrology. We also review the applications of spin squeezing for detecting quantum chaos and quantum phase transitions, as well as the influence of decoherence on spin squeezing. Finally, we review several experimental realizations of spin squeezing, as well as their corresponding theoretical backgrounds, including: producing spin-squeezed states via particle collisions in Bose-Einstein condensates, transferring photon squeezing to atomic ensembles, and generating spin squeezing via quantum non-demolition measurements.

## Contents

<b>1</b>	<b>Introduction</b>	<b>3</b>
<b>2</b>	<b>Definitions of spin squeezing</b>	<b>5</b>
2.1	Coherent state and bosonic squeezing	5
2.1.1	Coherent state	6
2.1.2	Generation of bosonic squeezed state	6
2.2	Coherent spin state	7
2.3	Spin-squeezing parameters based on the Heisenberg uncertainty relation	9
2.4	Squeezing parameter $\xi_S^2$ given by Kitagawa and Ueda	10
2.5	Squeezing parameter $\xi_R^2$ given by Wineland <i>et al.</i>	12
2.6	Other spin-squeezing parameters	14
2.7	Rotationally invariant extensions of squeezing parameters	16
2.8	Spin-squeezing parameters for states with parity	18
2.8.1	Spin-squeezing parameters $\xi_S^2$ and $\xi_R^2$	18
2.8.2	Spin-squeezing parameter $\tilde{\xi}_E^2$	20
2.8.3	Dicke States	21
2.9	Relations between spin squeezing and bosonic squeezing	21

Email address: xgwang@zimp.zju.edu.cn (Xiaoguang Wang)

<b>3</b>	<b>Generation of spin squeezing with nonlinear twisting Hamiltonians</b>	<b>22</b>
3.1	One-axis twisting Hamiltonian	23
3.1.1	One-axis twisted states	23
3.1.2	One-axis twisting with a transverse field	25
3.1.3	One-axis twisting in Bose-Einstein condensates	25
3.1.4	One-axis twisting from large-detuned atom-field interaction	27
3.2	Two-axis twisted states	28
<b>4</b>	<b>Spin squeezing, negative pairwise correlations, and entanglement</b>	<b>30</b>
4.1	Spin squeezing and pairwise correlations	30
4.1.1	Spin-squeezing parameter $\xi_S^2$ and correlation $G_{\vec{n}_\perp, \vec{n}_\perp}$	31
4.1.2	Spin-squeezing parameter $\xi_E^2$ and correlation $G_{1\vec{n}, 2\vec{n}}$	31
4.2	Spin squeezing and pairwise entanglement	32
4.3	Spin squeezing and many-body entanglement	36
4.4	Spin-squeezing inequalities for higher spin- $j$ systems	37
4.5	Two-mode spin-squeezed states	38
<b>5</b>	<b>Spin squeezing, Fisher information, and quantum metrology</b>	<b>39</b>
5.1	Quantum Fisher information	39
5.2	Spin squeezing and quantum Fisher information	40
5.3	Spin squeezing, Fisher information and metrology	42
<b>6</b>	<b>Spin squeezing, quantum phase transitions, and quantum chaos</b>	<b>46</b>
6.1	Spin squeezing and quantum phase transitions in the Lipkin-Meshkov-Glick model	46
6.2	Spin squeezing and quantum chaos in the Quantum kicked-top model	48
6.3	Spin squeezing and quantum chaos in the Dicke model	50
<b>7</b>	<b>Spin squeezing under decoherence</b>	<b>52</b>
7.1	Decoherence and spin squeezing generation	52
7.2	Spin-squeezed states under particle loss	53
7.3	Spin squeezing under decoherence channels	54
7.3.1	Decoherence channels	55
7.3.2	Spin squeezing parameters under decoherence	56
7.4	Effects of decoherence on spin squeezing in Ramsey processes	59
<b>8</b>	<b>Theoretical proposals and experimental realizations of squeezing generation</b>	<b>62</b>
8.1	Generating spin squeezing in Bose-Einstein condensations	62
8.1.1	Experimental realizations	62
8.2	Squeezing transferred from light to atoms	69
8.2.1	Theoretical proposals	69
8.2.2	Experimental realizations	73
8.3	Generating spin squeezing via quantum nondemolition measurements	75
8.3.1	Theoretical background	75
8.3.2	Experimental results	79
<b>9</b>	<b>Conclusion</b>	<b>84</b>
<b>Appendix A</b>	<b>Principal squeezing parameter</b>	<b>86</b>
<b>Appendix B</b>	<b>Variances of <math>J_{\vec{n}}</math> for the CSSs</b>	<b>86</b>
<b>Appendix C</b>	<b>The minimum value of the quantity <math>\vec{n}^T \Gamma \vec{n}</math></b>	<b>88</b>

<b>Appendix D</b>	<b>Expectations for the one-axis twisted state</b>	<b>89</b>
<b>Appendix E</b>	<b>Photon polarization and Stokes operators</b>	<b>91</b>

## 1. Introduction

In the past two decades, spin squeezing [1, 2, 3] has attracted considerable attention, both theoretically and experimentally. The notion of spin squeezing has arisen mainly from two considerations: The study of particle correlations and entanglement [4, 5, 6], and the improvement of measurement precision in experiments [2, 3, 7, 8]. However, the definition of spin-squeezing parameter is not unique, and we will here review several definitions that have been used in the past. The most widely studied squeezing parameters were proposed by Kitagawa and Ueda in Ref. [1], denoted by  $\xi_S^2$ , and by Wineland *et al.* in Ref. [2, 3], denoted by  $\xi_R^2$ . The spin squeezing parameter  $\xi_S^2$  [1] was inspired by the well-known photon squeezing; while the parameter  $\xi_R^2$  [2, 3] was introduced naturally in the standard Ramsey spectroscopy experiment, where the squeezing parameter is the ratio of the phase resolution when using a correlated state versus that when using a coherent spin state (CSS).

One application of spin squeezing is to detect quantum entanglement [6, 9, 10], which plays a key role in both the foundations of quantum physics and quantum-information processing [11, 12]. Parameter  $\xi_S^2$ , found to be related to negative pairwise correlations [13] and concurrence [14, 15], is able to characterize pairwise entanglement for a class of many-body spin-1/2 states. Reference [4] proved that a many-body spin-1/2 state is entangled if it is spin squeezed corresponding to  $\xi_R^2 < 1$ . Indeed, spin-squeezing parameters are multipartite entanglement witnesses [6]. Another important reason for choosing spin-squeezing parameters as measures of multipartite correlations is that spin squeezing is relatively easy to be generated and measured experimentally [16, 17, 18, 19, 20, 21, 22, 23, 24, 25]. Spin-squeezing parameters only involve the first and second moments of the collective angular momentum operators, and in many practical cases, e.g., in Bose-Einstein condensations (BECs), particles cannot be addressed individually, and only the collective operators can be measured. To detect entanglement for realistic experiments, a class of spin squeezing inequalities were proposed [26, 27, 28], based the first, second, and even the third moments of collective spin operators. The use of spin-squeezing parameters as entanglement detectors has already been discussed in a recent review [6]. Besides, spin squeezing could also be useful for quantum computation (see, e.g., the reviews in [29, 30, 31]), as well as for quantum simulations (see, e.g., the reviews in [32]).

Another application of spin squeezing, especially in experiments, is to improve the precision of measurements, e.g., in the Ramsey spectroscopy [2, 3, 33, 34, 35, 36, 37, 38, 8, 39], and in making more precise atom clocks [3, 5, 7, 23, 40, 41, 42, 43, 44] and gravitational-wave interferometers [45, 46, 47]. Therefore, many efforts have been devoted to the generation of squeezing in atomic systems. Basically, these works can be sorted by two categories.

(i) Generating spin squeezing in atomic ensembles via atom-photon interactions [48]. Within this category, a very natural idea is to transfer squeezing from light to atoms [3, 16, 21, 49, 50, 51, 52, 53, 54, 55, 56, 57, 58, 59, 60, 61, 62], and many proposals focused on transferring squeezing via electromagnetically induced transparency [63, 64, 65, 66, 67, 68, 69, 70, 71, 72]. When considering light-atom interactions, the detuning between the light and the atoms are very important. In the large detuning regime, an effective Hamiltonian is obtained, consisting of a dispersive interaction term and a nonlinear interaction term, and the magnitude of the two terms can be adjusted. (a) The dispersive interaction between the light and atoms, results in a Faraday rotation of the polarization of the light [73]. Then by performing a quantum nondemolition (QND) measurement of the output light, the atomic ensembles can be squeezed conditioned to the measurement results [74, 75, 76, 77, 78, 79, 80, 73, 81, 82, 38, 83, 84, 85, 86, 40, 87, 88, 89, 90, 42, 91, 92, 93, 94, 95, 23, 24, 96, 97, 25, 98, 99, 100, 101], and this method was realized in experiments [74, 63, 21, 23, 24, 102, 103, 104]. (b) The nonlinear term, which describes interactions between atoms, is a one-axis twisting Hamiltonian [1, 105, 106], and can be used to generate spin squeezing [107, 108, 109, 110, 111, 22]. There are also some other proposals, including placing atoms in a high-Q cavity such that the atoms interact with a single field mode (not squeezed) repeatedly [112], illuminating bichromatic light on the atoms in a bad cavity [113] without requiring strong atom-cavity coupling. The

intrinsic spin squeezing in a large atomic radiating system was studied in Ref. [114], where spin-squeezed states are generated due to photon-exchanging induced strong interatomic correlations. Spin squeezing can also be produced via squeezing exchange between the motional and internal degrees of freedom [115]. In addition, squeezing can also be transferred from the atomic ensembles to photons [116, 117, 118].

(ii) Generating spin squeezing in the BEC via atomic collisions. In the last decade, generating spin-squeezed states in a BEC attracted many interests. The nonlinear atom-atom collisions in a two-component BEC can be described by a one-axis twisting Hamiltonian [4, 17, 119, 120, 121, 122, 123, 124, 125, 126, 127, 128, 129, 130, 131, 132, 133, 18, 134, 135, 136], which can generate spin-squeezed states. Besides, two-axis twisting Hamiltonian can be realized via Raman processes [137, 138], or via two-component condensates in a double-well potential [139]. Bragg scattering induced spin squeezing was studied in Refs. [140, 141]. Spin squeezing can also be created in a spinor-1 BEC [142, 143], via spin-exchange interactions [144, 145], or free dynamical evolution [146, 147]. As studied in Ref. [148], the ground state of a  $F = 1$  dipolar spinor BEC with transverse external magnetic field is spin squeezed. The squeezing of the ground state of spin-1 condensates in an optical lattice has been studied in [149, 150], where spin squeezing occurs in the Mott insulator phase. The particle collisions induced decoherence in the generation of spin squeezing was studied in [151], and spin-squeezed states generated in BEC are robust to dissipation [152], and particle losses [126, 153, 154]. Photodissociation induced spin squeezing was studied in Refs. [155, 156]. The spin-squeezed states in BEC have been used to perform sub-shot-noise measurements [46, 157], detect weak forces [158]. Experimental realizations of spin-squeezed states in BEC were reported in Refs. [17, 159, 160, 161, 18, 19, 20]. Recently, spin squeezing in BEC was re-examined by considering the effects of indistinguishable of particles [162, 163], where spin squeezing is neither necessary to achieve sub-shot noise accuracies in quantum metrology, nor in general an entanglement witness. Below, we only consider distinguishable cases. Besides the above two categories, other proposals such as using Ising Hamiltonian to generate squeezed states was studied in Ref. [41, 164, 165, 166].

This review is organized as follows. First, in Sec. 2, we present a full list of definitions of spin squeezing, which were proposed for different tasks, and give the relations between the spin squeezing and the bosonic squeezing. We make a comparison between bosonic squeezing and spin squeezing. We demonstrate their relations under the large- $N$  limit and small excitations. In this case spin squeezing will reduce to bosonic squeezing.

In Sec. 3, we review the generation of spin-squeezed states via the one-axis twisting and two-axis twisting Hamiltonians, which have both fixed parity and particle-exchange symmetry. The proposal of using nonlinear Hamiltonians to generate spin-squeezed states originates from quantum optics, where the nonlinear Kerr effect is employed to prepare squeezed light. The dynamics controlled by the one-axis twisting Hamiltonian can be solve analytically. This type of Hamiltonian is widely studied in the regime of spin squeezing, and could be implemented in BEC [4, 17, 18, 19, 20], and large detuning atom-field interaction models [167, 107, 22], etc. The two-axis twisting has advantages in generating spin squeezing as compared to the one-axis twisting, however, it is not easy to implemented in experiments, and analytical results cannot be obtained for arbitrary system size.

Since the nonlinear Hamiltonians involve two-body interactions, one can infer that spin-squeezed states may be pairwise correlated or entangled. This is reviewed in Sec. 4. We study the relations between spin squeezing and negative pairwise correlation. Then we review the relations between spin squeezing and entanglement, and this is one of the most important branches in the study of spin squeezing. The spin-squeezing parameter  $\xi_S^2$  is closely related to pairwise entanglement. Moreover, the squeezing parameter proposed in [28, 15] has been found to be qualitatively equivalent to the concurrence for systems with exchange symmetry and parity. The parameter  $\xi_R^2$  can provide a criterion for multipartite entanglement. Thus, spin squeezing parameters can also be used to detect entanglement beyond pairwise entanglement. Spin-squeezing parameters can also be used to detect entanglement in a system of spin- $j$  particles. In the end of this section, we also discuss the concept of two-mode spin squeezing, of which the bipartite entanglement is a valuable quantum information resource.

In Sec. 5, we discuss spin squeezing and quantum Fisher information (QFI) in quantum metrology. The spin squeezing parameter  $\xi_R^2$  arises in the Ramsey interferometer, and the QFI lies at the heart of parameter estimation theory. Both quantities characterize the entanglement enhanced quantum metrology. Their

relations are reviewed and compared in the Ramsey interferometry. In Sec. 6, we discuss the applications of spin squeezing in quantum phase transitions (QPTs) and quantum chaos. In this section, we first employ the Lipkin-Meshkov-Glick model, which has a second-order QPT, to show that spin squeezing can be used to identify the critical point. Then, we review spin squeezing in quantum chaos. Two typical chaotic models are described: the quantum kicked-top model and the Dicke model. Some quantities, like entropy and concurrence, have been studied in these two models, and spin-squeezing parameters can also reflect their chaotic behaviors. The lifetime of a spin-squeezed state is much shorter when the system is chaotic than when the system is regular.

In Sec. 7, we consider the effects of decoherence. Firstly, in Sec. 7.1, we discuss how decoherence affects the generation of spin squeezing. Then in Sec. 7.2 and 7.3, we discuss the robustness and lifetime of spin squeezing in the presence of decoherence. Finally in Sec. 7.4, we discuss how decoherence affects the ability of spin-squeezed states to the improvement of phase resolution in Ramsey processes.

Finally, in Sec. 8, we review the generation of spin squeezing in experiments, including BEC, light-matter interaction, QND measurements. The closely related theoretical backgrounds are provided as well. For each physical system, we give a brief yet comprehensive summary of a series experimental results, as well as detailed discussions of several notable experimental improvements. We first discuss experiments on BEC, which involves Mott insulator transitions and the one-axis twisting. Then we review the transfer of squeezing, from light to atomic ensemble, via absorption of squeezed vacuum. Atomic ensembles can be viewed as quantum memories, and light is a very promising information carrier. Spin-squeezed states have been prepared in an optically thick Cesium atomic ensemble by using a squeezed vacuum. We also discuss a QND-measurement scheme, which generates conditional spin-squeezed states; and by utilizing feedback techniques, one can produce unconditional spin-squeezed states. Finally, we summarize some useful results and derivations in the appendices.

## 2. Definitions of spin squeezing

The definition of spin squeezing is not unique, and it depends on the context where squeezing is considered. The most popular definitions are proposed by Kitagawa and Ueda [1], in analogy to photon squeezing, and by Wineland *et al.* [2, 3], in Ramsey experiments. The latter one is directly associated with quantum metrology. Besides these two widely studied definitions, there are some other definitions of spin squeezing, which were introduced for certain considerations. Before we discuss spin squeezing, we first give a brief review on bosonic squeezing, widely studied in quantum optics. These will give some initial indications on the possible definitions and the generation of spin squeezing.

### 2.1. Coherent state and bosonic squeezing

Let us first review some basic concepts of bosonic squeezing, which is widely studied in quantum optics [168, 169, 170, 171], and has applications in practical precision measurements [172, 173]. Squeezed states have also been studied in other contexts, including squeezed phonons in condensed matter physics [174, 175, 176, 177] and squeezed states of microwave radiation in a superconducting resonant circuit [178].

Consider the bosonic creation and annihilation operators  $a^\dagger$  and  $a$ , with the corresponding commutation relation

$$[a, a^\dagger] = 1, \quad (1)$$

satisfying  $a|n\rangle = \sqrt{n}|n-1\rangle$  and  $a^\dagger|n\rangle = \sqrt{n+1}|n+1\rangle$ , where  $|n\rangle$  is the number state, i.e.,  $a^\dagger a|n\rangle = n|n\rangle$ . Below we consider two dimensionless operators  $X$  and  $P$  given by

$$X \equiv a + a^\dagger, \quad P \equiv \frac{a - a^\dagger}{i}, \quad (2)$$

which are the position and momentum amplitudes, respectively. The commutator

$$[X, P] = 2i \quad (3)$$

results in the Heisenberg uncertainty relation

$$\Delta X \Delta P \geq 1, \quad (4)$$

where  $\Delta A = \sqrt{\langle A^2 \rangle - \langle A \rangle^2}$  is the standard deviation, and  $(\Delta A)^2$  is the variance.

### 2.1.1. Coherent state

The coherent state [179, 180, 181], usually called the minimum uncertainty state, satisfies the following simple condition

$$\Delta X = \Delta P = 1. \quad (5)$$

The coherent state and its applications have been reviewed in [182, 183]. From the above criterion (5), the simplest coherent state is the vacuum state  $|0\rangle$ . A coherent state is defined as

$$a|\alpha\rangle = \alpha|\alpha\rangle, \quad (6)$$

from which the first moments of  $X$  and  $P$  for the coherent state are directly obtained as Eq. (5).

The uncertainty relation (4) cannot be violated. However, we can choose a state to make  $\Delta X$  (or  $\Delta P$ ) smaller than 1, and this type of state is called coherent squeezed state. Generally, squeezing occurs when variance is less than 1 in any direction of the  $X$ - $P$  plane. We introduce an operator in the  $X$ - $P$  plane as

$$\begin{aligned} X_\theta &= e^{i\theta a^\dagger a} X e^{-i\theta a^\dagger a} \\ &= a e^{-i\theta} + a^\dagger e^{i\theta}, \end{aligned} \quad (7)$$

with  $X = X_0$  and  $P = X_{\pi/2}$  being special cases. We see that the generalized operator  $X_\theta$  can be obtained by rotating operator  $X$  in the phase space. The so-called principal quadrature squeezing [184, 185] is characterized by a parameter

$$\zeta_B^2 = \min_{\theta \in (0, 2\pi)} (\Delta X_\theta)^2, \quad (8)$$

which is the minimum value of  $(\Delta X_\theta)^2$  with respect to  $\theta$ , and  $\zeta_B^2 < 1$  indicates bosonic principal squeezing. The minimization in the above definition can be easily performed (See Appendix A)

$$\zeta_B^2 = 1 + 2(|\langle a^\dagger a \rangle - \langle a \rangle|^2 - 2|\langle a^2 \rangle - \langle a \rangle^2|), \quad (9)$$

which only contains expectation values  $\langle a \rangle$ ,  $\langle a^2 \rangle$ , and  $\langle a^\dagger a \rangle$ .

### 2.1.2. Generation of bosonic squeezed state

A bosonic squeezed state can be generated by applying the following nonlinear Hamiltonian

$$H = i(ga^{\dagger 2} - g^*a^2) \quad (10)$$

on a coherent states as

$$|\alpha, \eta\rangle = S(\eta) |\alpha\rangle, \quad (11)$$

with squeezing operator  $S$ :

$$S(\eta) = \exp(-iHt) = \exp\left(\frac{1}{2}\eta^* a^2 - \frac{1}{2}\eta a^{\dagger 2}\right) \quad (12)$$

and complex number  $\eta = r \exp(i\theta)$ , where  $r = -2|g|t$ .

In Sec. 3.2, we will see that the two-axis twisting Hamiltonian that generates spin-squeezed states is inspired from this squeezing operator  $S$ . The nonlinear operator  $S$  mixes the  $X$  and  $P$  components and thus performs not only a rotation, but also squeezing. As shown in Ref. [170], the standard deviations for the rotated operators are derived as

$$\Delta X_{\theta/2} = e^{-r}, \quad \Delta P_{\theta/2} = e^r, \quad (13)$$

The variance in  $X_{\theta/2}$  is reduced with a factor  $e^{-r}$ , and the squeezing is determined by  $r$ , which is usually called the squeezing parameter. Computer animations showing various types of squeezed states, including squeezed wave packets are available online at [186].

Bosonic squeezed states can also be generated from the Kerr interaction Hamiltonian [187]

$$H = \kappa(a^\dagger a)^2. \quad (14)$$

Choosing an initial state be the coherent state, we have the state at time  $t$ ,

$$|\psi(t)\rangle_{\text{Kerr}} = \exp[-i\kappa t(a^\dagger a)^2] |\alpha\rangle. \quad (15)$$

## 2.2. Coherent spin state

Now we turn to spin systems. Hereafter, we will mainly consider the system consisting of  $N$  spin-1/2 particles, since in many practical cases we deal with two-level systems or qubits. A two-level atom interacting with the radiation field can be treated as a spin-1/2 particle in a magnetic field. The angular momentum operators for this ensemble of spin-1/2 particles are given by

$$J_\alpha = \frac{1}{2} \sum_{l=1}^N \sigma_{l\alpha}, \quad \alpha = x, y, z \quad (16)$$

where  $\sigma_{l\alpha}$  is the Pauli matrix for the  $l$ -th particle. Before we discuss spin squeezing, we introduce the CSS.

The CSS is defined as a direct product of single spin states

$$|\theta, \phi\rangle = \bigotimes_{l=1}^N \left[ \cos \frac{\theta}{2} |0\rangle_l + e^{i\phi} \sin \frac{\theta}{2} |1\rangle_l \right], \quad (17)$$

where  $|0\rangle_l$  and  $|1\rangle_l$  are the eigenstates of  $\sigma_{lz}$  with eigenvalues 1 and  $-1$ , respectively. The above definition (17) gives an intuitive geometric description as shown in Fig. 1, i.e., all the spins point in the same direction.

The CSS can also be written as

$$|\eta\rangle \equiv |\theta, \phi\rangle = (1 + |\eta|^2)^{-j} \sum_{m=-j}^j \binom{2j}{j+m}^{1/2} \eta^{j+m} |j, m\rangle, \quad \eta \in \mathbb{C}, \quad (18)$$

in terms of the Dicke states  $|j, m\rangle$ , which are the eigenstates of  $J_z$  with eigenvalue  $m$ , and

$$\eta = -\tan \frac{\theta}{2} \exp(-i\phi). \quad (19)$$

Note that, when  $\theta = \pi$ ,  $\eta$  is divergent, and only the coefficient before  $|j, j\rangle$  is nonzero, thus  $|\theta = \pi, \phi\rangle = |j, j\rangle$ . The above form is expressed as the projection of a coherent state onto Dicke states  $|j, m\rangle$ , and  $|\langle j, m|\eta\rangle|^2$  are related to the projection noise [188], obeying a binomial distribution, shown in Fig. 1.

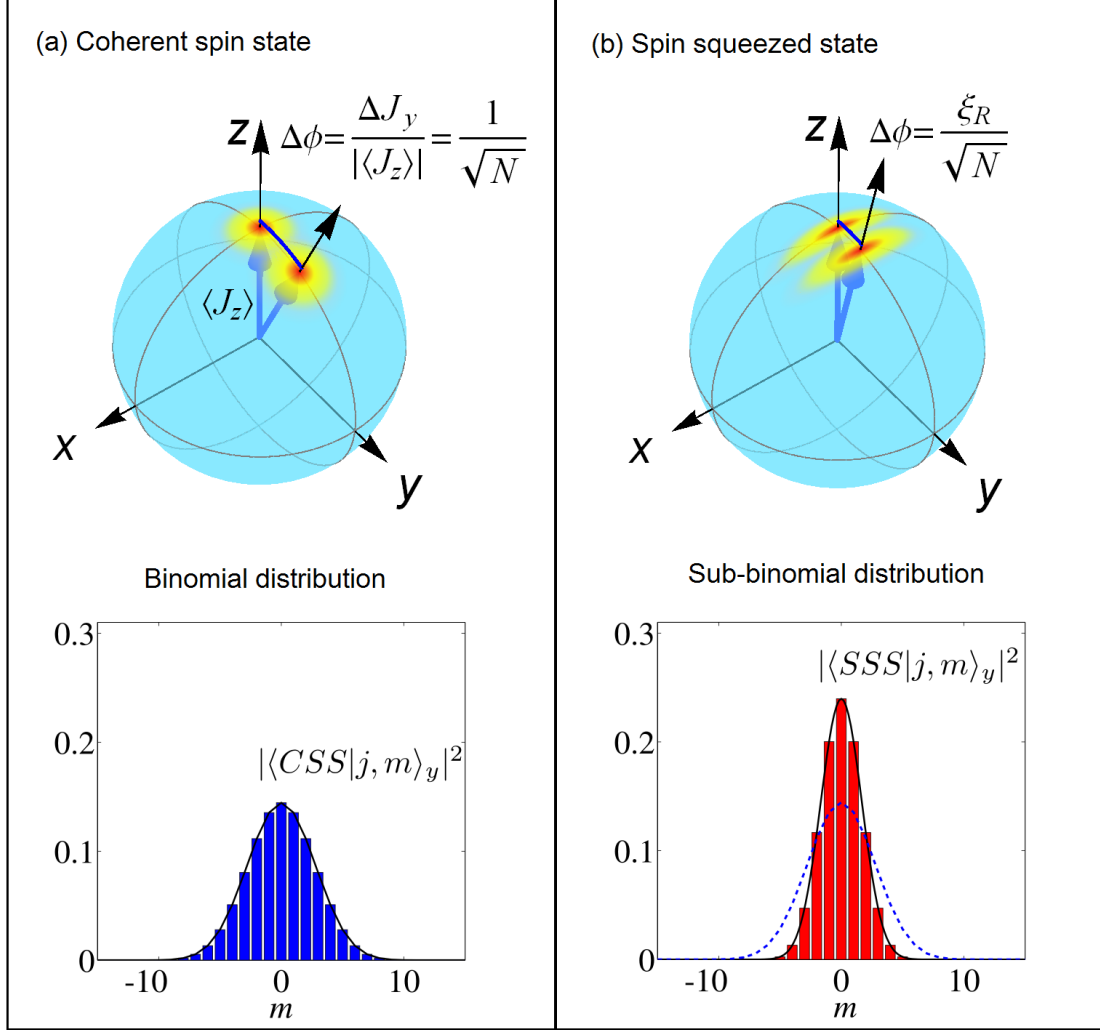


Figure 1: (Color online) Bloch sphere representations for a coherent spin state  $|CSS\rangle$  shown in (a), and a spin-squeezed state  $|SSS\rangle$  in (b). The radius of the Bloch sphere is  $|\langle \vec{J} \rangle|$ . The fluctuations of the spin components are represented by the circular multi-color disks in (a) and the multi-color elliptical disks in (b). The phase variance  $\Delta\phi$ , determined by spin fluctuation disks and spin lengths, is the resolution of the spin state with respect to rotations, which characterizes the frequency precision in Ramsey spectroscopy. For a CSS, the projection noise is characterized by a binomial distribution, as shown in (a), while for a SSS, the projection noise is not binomial, and may be a sub-binomial distribution (b).

Below, we shall derive Eq. (18). By using the identity

$$\exp[i(\xi\sigma_+ + \eta\sigma_-)] = \cos\sqrt{\xi\eta} + i\frac{\sin\sqrt{\xi\eta}}{\sqrt{\xi\eta}}(\xi\sigma_+ + \eta\sigma_-), \quad (20)$$

one can write the CSS in the following form

$$|\theta, \phi\rangle = \bigotimes_{l=1}^N R_l(\theta, \phi) |0\rangle_l = \bigotimes_{l=1}^N \exp(\zeta\sigma_{l+} - \zeta^*\sigma_{l-}) |0\rangle_l, \quad (21)$$

where

$$\zeta = -\frac{\theta}{2} \exp(-i\phi). \quad (22)$$



It can be further written as

$$|\theta, \phi\rangle = R(\theta, \phi)|j, j\rangle = \exp(\zeta J_+ - \zeta^* J_-)|j, j\rangle, \quad (23)$$

where  $|j, j\rangle \equiv \bigotimes_{l=1}^N |0\rangle_l$  is the eigenstate of  $J_z$  with eigenvalue  $j = N/2$ , which represents all the spins polarize to the  $z$ -direction. Here

$$J_{\pm} = J_x \pm iJ_y \quad (24)$$

are the ladder operators and  $R(\theta, \phi)$  is the rotation operator, which can be also given by

$$R(\theta, \phi) = \exp(-i\theta J_{\vec{n}}) = \exp[i\theta (J_x \sin \phi - J_y \cos \phi)], \quad (25)$$

where  $\vec{n} = (-\sin \phi, \cos \phi, 0)$ .

Now we write Eq. (23) in a more explicit form by using the formula [189, 183]

$$\exp(\zeta J_+ - \zeta^* J_-) = \exp(\eta J_+) \exp\left[\ln\left(1 + |\eta|^2\right) J_z\right] \exp(-\eta^* J_-), \quad (26)$$

where  $\eta$  is defined as Eq. (19). The above relations can be verified as below. The rotation operator  $R(\theta, \phi)$  can be expressed in a product form as

$$R(\theta, \phi) = \bigotimes_{l=1}^N R_l(\theta, \phi) = \bigotimes_{l=1}^N \exp(\zeta \sigma_{l+} - \zeta^* \sigma_{l-}), \quad (27)$$

and  $R_l(\theta, \phi)$  can be evaluated readily as

$$R_l(\theta, \phi) = \begin{pmatrix} \cos |\zeta| & -e^{-i\phi} \sin |\zeta| \\ e^{i\phi} \sin |\zeta| & \cos |\zeta| \end{pmatrix}, \quad (28)$$

similarly, we find

$$\exp(\eta \sigma_+) \exp\left[\ln \sqrt{1 + |\eta|^2} \sigma_z\right] \exp(-\eta^* \sigma_-) = \begin{pmatrix} (1 + |\eta|^2)^{-1/2} & \eta (1 + |\eta|^2)^{-1/2} \\ -\eta^* (1 + |\eta|^2)^{-1/2} & (1 + |\eta|^2)^{-1/2} \end{pmatrix}. \quad (29)$$

Then, taking Eqs. (22) and (19) into the above two matrices, the relation (26) is obtained.

### 2.3. Spin-squeezing parameters based on the Heisenberg uncertainty relation

The definition of spin squeezing is not unique. When talking about spin squeezing, we should specify a certain spin-squeezing parameter. The uncertainty relation for angular momentum operators results from the commutation relation

$$[J_\alpha, J_\beta] = i\varepsilon_{\alpha\beta\gamma} J_\gamma, \quad (30)$$

where  $\alpha, \beta, \gamma$  denote the components in any three orthogonal directions, and  $\varepsilon_{\alpha\beta\gamma}$  is the Levi-Civita symbol. The uncertainty relation is

$$(\Delta J_\alpha)^2 (\Delta J_\beta)^2 \geq |\langle J_\gamma \rangle|^2 / 4. \quad (31)$$

In analogy to bosonic squeezing, spin squeezing could be defined when one of the fluctuations in the left-hand side of Eq. (31) satisfies [45, 190]  $(\Delta J_\alpha)^2 \leq |\langle J_\gamma \rangle| / 2$ , and consequently, a squeezing parameter  $\xi_H^2$  is given by

$$\xi_H^2 = \frac{2(\Delta J_\alpha)^2}{|\langle J_\gamma \rangle|}, \quad \alpha \neq \gamma \in (x, y, z), \quad (32)$$

and if  $\xi_H^2 < 1$ , the state is squeezed. The subscript  $H$  refers to the Heisenberg uncertainty relations. More generally, one can define

$$\xi_H^2 = \frac{2(\Delta J_{\vec{n}_1})^2}{|\langle J_{\vec{n}_2} \rangle|}, \quad (33)$$

where  $\vec{n}_1$  and  $\vec{n}_2$  are two orthogonal unit vectors.

Below, we calculate  $\xi_H^2$  for a CSS  $|\theta, \phi\rangle$ . According to the definition (32), the value of  $\xi_H^2$  depends on the choice of the directions  $\vec{n}_1$  and  $\vec{n}_2$ , and also on the parameter  $\theta$  and  $\phi$  of the CSS. From Eq. (B.6), one can find that

$$\xi_H^2 = \frac{1 - (\vec{n}_0 \cdot \vec{n}_1)^2}{|\vec{n}_0 \cdot \vec{n}_2|}. \quad (34)$$

More specifically, let  $\vec{n}_0$  be the  $z$ -direction and  $\vec{n}_1$  the  $x$ -direction. The squeezing parameter then becomes

$$\xi_H^2 = \left| \frac{\sin \theta}{\cos \phi} \right|, \quad (35)$$

where we have used Eq. (B.8). It is found that  $\xi_H^2$  may be less than 1 for a CSS, and this is not expected, since a CSS should not be spin squeezed.

Now we discuss a generalized spin-squeezing parameter, introduced in Refs. [191, 192], for which spin squeezing could occur in two orthogonal directions simultaneously. The subscript  $H'$  indicates that this parameter is also related to the Heisenberg uncertainty relation. We first discuss spin squeezing in the  $x$ -axis, considering two orthogonal angular momentum operators in the  $y$ - $z$  plane

$$\begin{aligned} J_\theta &\equiv J_y \cos \theta + J_z \sin \theta, \\ J_{\theta+\pi/2} &\equiv -J_y \sin \theta + J_z \cos \theta, \end{aligned} \quad (36)$$

and the commutation relations  $[J_x, J_\theta] = iJ_{\theta+\pi/2}$ ,  $[J_x, J_{\theta+\pi/2}] = -iJ_\theta$ . The state is squeezed in the  $x$ -axis if

$$(\Delta J_x)^2 < \frac{1}{2} |\langle J_{\theta+\pi/2} \rangle|, \quad \text{and/or} \quad (\Delta J_x)^2 < \frac{1}{2} |\langle J_\theta \rangle|. \quad (37)$$

Since the maximum value of  $\langle J_\theta \rangle$  is  $\sqrt{\langle J_z \rangle^2 + \langle J_y \rangle^2}$ , we can say that the state is  $J_x$ -squeezed if  $(\Delta J_x)^2 < \frac{1}{2} \sqrt{\langle J_z \rangle^2 + \langle J_y \rangle^2}$ , otherwise, the state is  $J_y$ -squeezed if  $(\Delta J_y)^2 < \frac{1}{2} \sqrt{\langle J_z \rangle^2 + \langle J_x \rangle^2}$ . The above two inequalities could hold simultaneously.

More generally, we could write the above squeezing parameter as follows

$$\xi_{H'}^2 = \frac{2(\Delta J_{\vec{n}_1})^2}{\sqrt{\langle J_{\vec{n}_2} \rangle^2 + \langle J_{\vec{n}_3} \rangle^2}}. \quad (38)$$

For the CSS  $|\theta, \phi\rangle$ , from Eq. (B.6), one can find that  $\xi_{H'}^2 = \sqrt{1 - (\vec{n}_0 \cdot \vec{n}_1)^2}$ . More specifically, let  $\vec{n}_0$  be the  $z$ -direction, we have

$$\xi_{H'}^2 = |\sin \theta|. \quad (39)$$

The above equation indicates that the CSS can be squeezed, implying that  $\xi_{H'}^2$  is not a desirable definition for spin squeezing.

#### 2.4. Squeezing parameter $\xi_S^2$ given by Kitagawa and Ueda

Unlike the bosonic systems where the variance is equal in any direction for a bosonic coherent state, for a CSS the variance of spin operators depends on  $\vec{n}$ , and there exists *a priori* direction: the mean-spin direction (MSD)

$$\vec{n}_0 = \frac{\langle \vec{J} \rangle}{|\langle \vec{J} \rangle|} = \frac{\langle \vec{\sigma}_1 \rangle}{|\langle \vec{\sigma}_1 \rangle|}, \quad (40)$$

where the second inequality results from the exchange symmetry.

Below, we use  $\vec{n}_\perp$  to denote the direction perpendicular to the MSD. For a CSS, we have  $(\Delta J_{\vec{n}_\perp})^2 = j/2$  (See [Appendix B](#)), thus a state is spin squeezed if the variance of  $J_{\vec{n}_\perp}$  is less than  $j/2$ . Compared with the principal squeezing (8), we arrive at the spin-squeezing parameter [1]

$$\xi_S^2 = \frac{\min(\Delta J_{\vec{n}_\perp}^2)}{j/2} = \frac{4 \min(\Delta J_{\vec{n}_\perp}^2)}{N}, \quad (41)$$

where  $j = N/2$ , and  $\vec{n}_\perp$  refers to an axis perpendicular to the MSD and the minimization is over all directions  $\vec{n}_\perp$ . It is desirable that the spin-squeezing parameter  $\xi_S^2$  is equal to 1 for the CSS.

To calculate the parameter  $\xi_S^2$ , the first step is to compute the MSD determined by the expectation values  $\langle J_\alpha \rangle$ , with  $\alpha \in \{x, y, z\}$ . The MSD  $\vec{n}_0$  can be written in spherical coordinates as

$$\vec{n}_0 = (\sin \theta \cos \phi, \sin \theta \sin \phi, \cos \theta), \quad (42)$$

where  $\theta$  and  $\phi$  are polar and azimuthal angles, respectively. The angles  $\theta$  and  $\phi$  are given by [193]

$$\begin{aligned} \theta &= \arccos\left(\frac{\langle J_z \rangle}{|\vec{J}|}\right), \\ \phi &= \begin{cases} \arccos\left(\frac{\langle J_x \rangle}{|\vec{J}| \sin(\theta)}\right) & \text{if } \langle J_y \rangle > 0, \\ 2\pi - \arccos\left(\frac{\langle J_x \rangle}{|\vec{J}| \sin(\theta)}\right) & \text{if } \langle J_y \rangle \leq 0, \end{cases} \end{aligned} \quad (43)$$

where  $|\vec{J}| = \sqrt{\langle J_x \rangle^2 + \langle J_y \rangle^2 + \langle J_z \rangle^2}$  is the magnitude of the mean spin. With respect to  $\vec{n}_0$ , the other two orthogonal bases are given as

$$\vec{n}_1 = (-\sin \phi, \cos \phi, 0), \quad (44)$$

$$\vec{n}_2 = (\cos \theta \cos \phi, \cos \theta \sin \phi, -\sin \theta). \quad (45)$$

The above expressions are valid for  $\theta \neq 0, \pi$ . For  $\theta = 0, \pi$ , the mean spin is along the  $\pm z$  direction, and the possible choices of  $\phi$  can be 0 or  $\pi$ .

The second step now is to find the minimal variance of  $J_{\vec{n}_\perp} = \vec{J} \cdot \vec{n}_\perp$ . The direction  $\vec{n}_\perp$  can be represented as

$$\vec{n}_\perp = \vec{n}_1 O^T = \vec{n}_1 \cos \varphi + \vec{n}_2 \sin \varphi, \quad (46)$$

where  $O$  is a  $2 \times 2$  orthogonal matrix that performs rotations in the normal plane. The variance  $(\Delta J_{\vec{n}_\perp})^2$  can be written as

$$(\Delta J_{\vec{n}_\perp})^2 = \langle J_{\vec{n}_\perp}^2 \rangle = \vec{n}_\perp \Gamma \vec{n}_\perp^T, \quad (47)$$

where the symmetric matrix

$$\Gamma = \begin{pmatrix} \langle J_{\vec{n}_1}^2 \rangle & \text{Cov}(J_{\vec{n}_1}, J_{\vec{n}_2}) \\ \text{Cov}(J_{\vec{n}_1}, J_{\vec{n}_2}) & \langle J_{\vec{n}_2}^2 \rangle \end{pmatrix}, \quad (48)$$

in which

$$\begin{aligned} \text{Cov}(J_{\vec{n}_1}, J_{\vec{n}_2}) &= \frac{1}{2} \langle [J_{\vec{n}_1}, J_{\vec{n}_2}]_+ \rangle - \langle J_{\vec{n}_1} \rangle \langle J_{\vec{n}_2} \rangle \\ &= \frac{1}{2} \langle [J_{\vec{n}_1}, J_{\vec{n}_2}]_+ \rangle, \end{aligned} \quad (49)$$

is the covariance between  $J_{\vec{n}_1}$  and  $J_{\vec{n}_2}$ , and  $[X, Y]_+ = XY + YX$  is the anti-commutator. In the above equation,  $\langle J_{\vec{n}_1} \rangle = \langle J_{\vec{n}_2} \rangle = 0$  since  $\vec{n}_1$  and  $\vec{n}_2$  are perpendicular to the MSD. The variance can be written as

$$(\Delta J_{\vec{n}_\perp})^2 = \vec{n}_1 O^T \Gamma O \vec{n}_1^T, \quad (50)$$

and the matrix  $O$  can be chosen such that

$$O^T \Gamma O = \text{diag}\{\lambda_-, \lambda_+\}, \quad (51)$$

where the eigenvalues

$$\lambda_{\pm} = \frac{1}{2} \left[ \langle J_{\vec{n}_1}^2 + J_{\vec{n}_2}^2 \rangle \pm \sqrt{\left( \langle J_{\vec{n}_1}^2 - J_{\vec{n}_2}^2 \rangle \right)^2 + 4\text{Cov}(J_{\vec{n}_1}, J_{\vec{n}_2})^2} \right], \quad (52)$$

and  $\min(\Delta J_{\vec{n}_\perp})^2 = \lambda_-$  (See [Appendix C](#)), thus the squeezing parameters becomes

$$\xi_S^2 = \frac{4}{N} \lambda_- = \frac{2}{N} \left[ \langle J_{\vec{n}_1}^2 + J_{\vec{n}_2}^2 \rangle \pm \sqrt{\left( \langle J_{\vec{n}_1}^2 - J_{\vec{n}_2}^2 \rangle \right)^2 + 4\text{Cov}(J_{\vec{n}_1}, J_{\vec{n}_2})^2} \right]. \quad (53)$$

The optimal squeezing angle in Eq. (46) is given as

$$\varphi = \begin{cases} \frac{1}{2} \arccos\left(\frac{-A}{\sqrt{A^2+B^2}}\right) & \text{if } B \leq 0, \\ \pi - \frac{1}{2} \arccos\left(\frac{-A}{\sqrt{A^2+B^2}}\right) & \text{if } B > 0, \end{cases} \quad (54)$$

where we define

$$A \equiv \langle J_{\vec{n}_1}^2 - J_{\vec{n}_2}^2 \rangle, \quad B \equiv 2\text{Cov}(J_{\vec{n}_1}, J_{\vec{n}_2}). \quad (55)$$

We know that the parameter  $\xi_S^2 = 1$  for the uncorrelated pure CSS  $|\theta, \phi\rangle$  in Eq. (17). Thus, if there are certain quantum correlations among the elementary spins, we may have  $\xi_S^2 < 1$ , i.e., the fluctuation in one direction is reduced, as shown in Fig. 1. Therefore, the squeezing parameter  $\xi_S^2$  has natural connections with quantum correlations (entanglement). Indeed, it has been found that  $\xi_S^2$  has a very close relation with quantities such as negative correlations [13] and concurrence [15], and we will discuss them in Sec. 4.

### 2.5. Squeezing parameter $\xi_R^2$ given by Wineland *et al.*

Now, we discuss the spin-squeezing parameter proposed by Wineland *et al.* [2, 3] in the study of Ramsey spectroscopy. The squeezing parameter  $\xi_R^2$  is the ratio of the fluctuations between a general state and a CSS in the determination of the resonance frequency in Ramsey spectroscopy. The CSS here acts as a noise reference state. In contrast with  $\xi_S^2$ , which is the analog of bosonic squeezing, the parameter  $\xi_R^2$  is substantially connected to the improvement of the sensitivity of angular-momentum states to rotations, and thus is attractive for experiments.

Here we use a simple graphical way to describe this type of parameter, as shown in Fig. 1, while the mathematical form and essential physics are the same as for Ramsey spectroscopy and the Mach-Zender interferometer employed in Ref. [3]. More details of the Ramsey process will be discussed in Sec. 5.3.

Consider now a spin state  $|\psi\rangle$ . Without loss of generality, we assume the MSD to be along the  $z$  direction, and thus  $\langle J_x \rangle = \langle J_y \rangle = 0$ . This spin state is shown in Fig. 1, the circular or elliptical disks represent the variance  $\Delta J_{\vec{n}_\perp}$ , which is also called the projection noise. This state can be represented by a cone ending in a Bloch sphere.

Let us now rotate the state around the  $x$ -axis. Then, in the Heisenberg picture, we have

$$J_y^{\text{out}} = \exp(i\phi J_x) J_y \exp(-i\phi J_x) = \cos \phi J_y - \sin \phi J_z. \quad (56)$$

From the above equation, we can immediately obtain

$$\langle J_y^{\text{out}} \rangle = -\sin \phi \langle J_z \rangle, \quad (57)$$

$$(\Delta J_y^{\text{out}})^2 = \cos^2 \phi (\Delta J_y)^2 + \sin^2 \phi (\Delta J_z)^2 - \frac{1}{2} \sin(2\phi) \langle [J_y, J_z]_+ \rangle. \quad (58)$$

According to the error propagation formula,  $\Delta x = \Delta f(x) / |\partial \langle f(x) \rangle / \partial x|$ , the phase sensitivity  $\Delta\phi$  can be calculated as

$$\Delta\phi = \frac{\Delta J_y^{\text{out}}}{|\partial \langle J_y^{\text{out}} \rangle / \partial \phi|} = \frac{\Delta J_y^{\text{out}}}{|\cos \phi \langle J_z \rangle|}. \quad (59)$$

For the rotation angle  $\phi \sim 0$ ,  $(\Delta J_y^{\text{out}})^2 \sim (\Delta J_y)^2$  and  $\cos \phi \sim 1$ . Thus, the above equation reduces to

$$\Delta\phi = \frac{\Delta J_y}{|\langle J_z \rangle|}, \quad (60)$$

which allows us to know the phase sensitivity from the expectations and variances of the collective spin operators.

From the above procedure, for the more general case that the MSD is not along the  $z$  direction, we can obtain the phase sensitivity as

$$\Delta\phi = \frac{\Delta J_{\vec{n}_\perp}}{|\langle \vec{J} \rangle|}. \quad (61)$$

For the CSS, we can obtain the phase sensitivity from Eqs. (B.8) and (B.9) as

$$(\Delta\phi)_{\text{CSS}} = \frac{1}{\sqrt{N}}, \quad (62)$$

which is the so-called standard quantum limit (SQL) or shot-noise limit. This is the limit of precision in atomic interferometry experiments when we use uncorrelated atoms.

The squeezing parameter proposed by Wineland *et al.* is defined as [2, 3]

$$\xi_R^2 = \frac{(\Delta\phi)^2}{(\Delta\phi)_{\text{CSS}}^2} = \frac{N (\Delta J_{\vec{n}_\perp})^2}{|\langle \vec{J} \rangle|^2}. \quad (63)$$

This is the ratio of the phase sensitivity of a general state versus the CSS. Here, we choose the direction  $\vec{n}_\perp$  where  $\Delta J_{\vec{n}_\perp}$  is minimized. This definition is related to the  $\xi_S^2$  by Kitagawa and Ueda via

$$\xi_R^2 = \left( \frac{j}{|\langle \vec{J} \rangle|} \right)^2 \xi_S^2. \quad (64)$$

Since  $j = \frac{N}{2} \geq |\langle \vec{J} \rangle|$ , we have  $\xi_S^2 \leq \xi_R^2$ . Even though these two parameters are similar (when  $j = |\langle \vec{J} \rangle|$ ,  $\xi_R^2 = \xi_S^2$ ), their physical meanings are different. When  $\xi_R^2 < 1$ , the state is spin squeezed, and its phase sensitivity to rotation is improved over the shot-noise limit. According to Eq. (61), the phase sensitivity can be written as

$$\Delta\phi = \frac{\xi_R}{\sqrt{N}}. \quad (65)$$

If  $\xi_R^2 < 1$ ,  $\Delta\phi < (\Delta\phi)_{\text{CSS}}$  beats the shot-noise limit.

The lower bound of the phase sensitivity is given by the Heisenberg uncertainty relation  $(\Delta J_{\vec{n}_\perp})^2 (\Delta J_{\vec{n}'_\perp})^2 \geq \frac{1}{4} |\langle J_{\vec{n}} \rangle|^2$ , from which we have  $\xi_R^2 4 (\Delta J_{\vec{n}'_\perp})^2 / N \geq 1$ . Using the relations  $N^2/4 = j^2 \geq \langle J_{\vec{n}}^2 \rangle \geq (\Delta J_{\vec{n}})^2$  and the fact that the largest eigenvalue of  $J_{\vec{n}}^2$  is  $j^2$ , we obtain

$$\xi_R^2 \geq \frac{1}{N}. \quad (66)$$

By using Eq. (65), we further have

$$\Delta\phi \geq (\Delta\phi)_{\text{HL}} = \frac{1}{N}, \quad (67)$$

where  $(\Delta\phi)_{\text{HL}}$  is the Heisenberg limit (HL) [194].

Reference [2] proposed another definition,

$$\xi_{H''}^2 = \frac{j}{|\langle \vec{J} \rangle|} \xi_S^2 = \frac{2(\Delta J_{\vec{n}_\perp})^2}{|\langle \vec{J} \rangle|}. \quad (68)$$

We may choose another set of three orthogonal directions  $\{\vec{n}_\perp, \vec{n}'_\perp, \vec{n}_0\}$ . Then the uncertainty relation can be written as

$$(\Delta J_{\vec{n}_\perp})^2 (\Delta J_{\vec{n}'_\perp})^2 \geq |\langle J_{\vec{n}_0} \rangle|^2 / 4. \quad (69)$$

Thus, the parameter  $\xi_{H''}^2$  is naturally defined in this coordinate system. We will show that  $\xi_{H''}^2 = 1$  for the CSS, indicating that this parameter is appropriate for characterizing spin squeezing. For a CSS, the variance of  $J_{\vec{n}_0}$  is zero, i.e., no fluctuations along the MSD (See Appendix B),  $(\Delta J_{\vec{n}_0})^2 = 0$ . The variances of the angular momenta in the plane perpendicular to  $\vec{n}_0$  behave similar to bosonic operators, for which we obtain (See Appendix B)

$$(\Delta J_\alpha)^2 = (\Delta J_\beta)^2 = j/2, \quad (70)$$

where the subscripts  $\alpha$  and  $\beta$  denote two orthogonal axes perpendicular to the mean-spin direction  $\vec{n}_0$ . So, we have  $\xi_{H''}^2 = 1$ .

The three squeezing definitions  $\xi_S^2$ ,  $\xi_{H''}^2$ , and  $\xi_R^2$  discussed above are not equivalent, however, they satisfy the following relation

$$\xi_S^2 \leq \xi_{H''}^2 \leq \xi_R^2, \quad (71)$$

since  $j \geq |\langle \vec{J} \rangle|$  always holds. Therefore, if a state is spin squeezed according to criterion  $\xi_R^2 < 1$ , it is definitely squeezed according to parameter  $\xi_{H''}^2$  and  $\xi_S^2$ , and thus  $\xi_R^2 < 1$  is the most stringent condition of squeezing among these three parameters in Eq. (71).

We also note that, the projection noise can be schematically visualized in Fig. 1, where we show the projection noise distributions for a CSS and a SSS. For CSS, take  $|j, j\rangle$  for example, and the MSD is along the  $z$  direction. If we measure  $J_y$ , the expectation value  $\langle J_y \rangle = 0$ , while the variance  $(\Delta J_y)^2 = j/2$ . The probability of the outcome states  $|j, m\rangle_y$  obeys the binomial distribution

$$P(m) = \left| \langle j, j | j, m \rangle_y \right|^2 = \left| \langle j, m | \exp\left(-i\frac{\pi}{2} J_x\right) | j, j \rangle \right|^2 = \frac{1}{2^N} \binom{N}{N-m}, \quad (72)$$

where  $|j, m\rangle_y = \exp(i\frac{\pi}{2} J_x) |j, m\rangle$  is the eigenstate of  $J_y$  with eigenvalue  $m$ . The phase sensitivity  $\Delta\phi$  is determined by the width of the binomial distribution, and a spin-squeezed state may thus have a sub-binomial distribution [75].

## 2.6. Other spin-squeezing parameters

In this section, we review some other definitions of spin squeezing, and discuss their applications. Reference [4] proposed a spin-squeezing parameter  $\xi_{R'}^2$ , which is a criterion for multipartite entanglement. The subscript  $R'$  indicates the close relationship between the spin squeezing parameters  $\xi_{R'}^2$  and  $\xi_R^2$ . The parameter  $\xi_{R'}^2$  is defined as

$$\xi_{R'}^2 = \frac{N(\Delta J_{\vec{n}_1})^2}{\langle J_{\vec{n}_2} \rangle^2 + \langle J_{\vec{n}_3} \rangle^2}. \quad (73)$$

For spin-1/2 many-body systems, it has been proved [4] that, if  $\xi_{R'}^2 < 1$  the state is entangled. However, an entangled state may not be necessarily squeezed. Based on this parameter, spin squeezing is directly connected to multipartite entanglement. Inspired by this finding, many works studied the relations between spin squeezing and entanglement (see, e.g., [6]). The choices of the directions  $\vec{n}_i$  are arbitrary, and if  $\vec{n}_2$  is chosen to be the MSD, while  $\vec{n}_1$  is chosen to minimize the variance  $\Delta J_{\vec{n}_1}$ , then  $\xi_{R'}^2$  reduces to  $\xi_R^2$ .

Below, we show that for the CSS,  $\xi_{R'}^2 = 1$ . Substituting Eq. (B.6) into Eq. (73), we obtain

$$\xi_{R'}^2 = \frac{1 - (\vec{n}_0 \cdot \vec{n}_1)^2}{(\vec{n}_0 \cdot \vec{n}_2)^2 + (\vec{n}_0 \cdot \vec{n}_3)^2} = 1. \quad (74)$$

In summary,  $\xi_R^2$  can be viewed as a generalization of  $\xi_D^2$ , and also provides a useful criterion for many-body entanglement.

In the study of Dicke states  $|j, m\rangle$  in BEC, Raghavan *et al.* [121] proposed a new kind of squeezing parameter

$$\xi_D^2 = \frac{N (\Delta J_{\vec{n}})^2}{N^2/4 - \langle J_{\vec{n}} \rangle^2}, \quad (75)$$

where the subscript  $D$  indicates that this parameter can detect entanglement in Dicke states. If  $\xi_D^2 < 1$ , the state is squeezed along  $\vec{n}$ . Actually, in Ref. [121], the authors only consider the variance  $(\Delta J_z)^2$  along the  $z$ -axis. For a CSS  $|\theta, \phi\rangle$ ,  $\xi_D^2 = 1$ , which can be directly proved by substituting Eq. (B.6) into Eq. (75). For all entangled symmetric Dicke states  $|j, m\rangle$ , we will show that this parameter can detect entanglement in Dicke states in Sec. 3.

As discussed previously, an important application of the spin squeezing parameter is to detect entanglement. This kind of entanglement criterion is based on collective-spin inequalities, and it is attractive for experiments, because in practice we cannot always address individual particles, while the expectation values and variances for collective spin operators are easier to measure, such as in population spectroscopies. Therefore, Tth *et al.* [28] generalized the spin squeezing definitions and gave a set of spin inequalities. We find that one of the spin inequalities is suitable to be rewritten as a new type of spin-squeezing parameter, and this inequality reads

$$(N-1) (\Delta J_{\vec{n}_1})^2 \geq \langle J_{\vec{n}_2}^2 \rangle + \langle J_{\vec{n}_3}^2 \rangle - N/2, \quad (76)$$

which holds for any separable states, and the violation of this inequality indicates entanglement. This inequality can be further written in the following form

$$N (\Delta J_{\vec{n}_1})^2 \geq \langle \vec{J}^2 \rangle - \langle J_{\vec{n}_1} \rangle^2 - N/2, \quad (77)$$

and one can define a spin squeezing parameter related to entanglement

$$\xi_E^2 = \frac{N (\Delta J_{\vec{n}_1})^2}{\langle \vec{J}^2 \rangle - N/2 - \langle J_{\vec{n}_1} \rangle^2}, \quad (78)$$

whose form is similar to  $\xi_D^2$ . In fact, for symmetric states with only Dicke states populated,  $\langle \vec{J}^2 \rangle = N/2(N/2 + 1)$ , and then  $\xi_E^2$  reduces to  $\xi_D^2$ . Thus, for the CSS,  $\xi_E^2 = \xi_D^2 = 1$ . In Table 1, we give a summary of the spin squeezing parameters discussed above, and we also show their values for the CSS state  $|\theta, \phi\rangle$  in Eq. (17).

Table 1: This table shows the definitions for different spin-squeezing parameters. Except for  $\xi_H^2$  and  $\xi_{H'}^2$ , the other spin-squeezing parameters all equal to 1 for the CSS.

Squeezing parameters	Definitions	Coherent spin state	References
$\xi_H^2$	$\frac{2(\Delta J_{\vec{n}_1})^2}{ \langle J_{\vec{n}_2} \rangle }$	$\frac{1 - (\vec{n}_0 \cdot \vec{n}_1)^2}{ \langle \vec{n}_0 \cdot \vec{n}_2 \rangle }$	[45]
$\xi_{H'}^2$	$\frac{2(\Delta J_{\vec{n}_1})^2}{\sqrt{\langle J_{\vec{n}_2} \rangle^2 + \langle J_{\vec{n}_3} \rangle^2}}$	$\sqrt{1 - (\vec{n}_0 \cdot \vec{n}_1)^2}$	[191]
$\xi_{H''}^2$	$\frac{2(\Delta J_{\vec{n}_\perp})_{\min}^2}{ \langle \vec{J} \rangle }$	1	[2]
$\xi_S^2$	$\frac{4(\Delta J_{\vec{n}_\perp})_{\min}^2}{N}$	1	[1]
$\xi_R^2$	$\frac{N^2}{4\langle \vec{J} \rangle^2} \xi_S^2$	1	[3]
$\xi_{R'}^2$	$\frac{N(\Delta J_{\vec{n}_1})^2}{\langle J_{\vec{n}_2} \rangle^2 + \langle J_{\vec{n}_3} \rangle^2}$	1	[4]
$\xi_D^2$	$\frac{N(\Delta J_{\vec{n}})^2}{N^2/4 - \langle J_{\vec{n}} \rangle^2}$	1	[121]
$\xi_E^2$	$\frac{N(\Delta J_{\vec{n}_1})^2}{\langle \vec{J}^2 \rangle - N/2 - \langle J_{\vec{n}_1} \rangle^2}$	1	[28]

### 2.7. Rotationally invariant extensions of squeezing parameters

As discussed above, for a given state, the denominators of parameters  $\xi_{R'}^2$ ,  $\xi_D^2$ , and  $\xi_E^2$  depend on the choice of the directions. Unlike parameters  $\xi_S^2$  and  $\xi_R^2$ , for which the denominators are constants. Thus it is difficult to determine the minima of  $\xi_{R'}^2$ ,  $\xi_D^2$ , and  $\xi_E^2$ . Inspired by Töhr's discussions [28, 195, 196], we will give slightly different definitions for  $\xi_{R'}^2$  and  $\xi_D^2$ , and the new definitions provide us a simple way to determine whether a state is spin squeezed.

Spin squeezing with respect to  $\xi_{R'}^2$ ,  $\xi_D^2$ , and  $\xi_E^2$  are equivalent to the following three inequalities

$$\begin{aligned}
N(\Delta J_{\vec{n}_1})^2 &< \langle J_{\vec{n}_2} \rangle^2 + \langle J_{\vec{n}_3} \rangle^2, \\
N(\Delta J_{\vec{n}})^2 &< \frac{N^2}{4} - \langle J_{\vec{n}} \rangle^2, \\
N(\Delta J_{\vec{n}})^2 &< \langle \vec{J} \rangle^2 - \frac{N}{2} - \langle J_{\vec{n}} \rangle^2,
\end{aligned} \tag{79}$$

The right-hand sides of the above three inequalities can be written in a rotation-invariant form by adding  $\langle J_{\vec{n}_1} \rangle^2$  to both sides of the first inequality, and  $\langle J_{\vec{n}} \rangle^2$  to the second and third ones. Then we obtain

$$\begin{aligned}
(N-1)(\Delta J_{\vec{n}})^2 + \langle J_{\vec{n}}^2 \rangle &< \langle \vec{J} \rangle^2, \\
(N-1)(\Delta J_{\vec{n}})^2 + \langle J_{\vec{n}}^2 \rangle &< \frac{N^2}{4}, \\
(N-1)(\Delta J_{\vec{n}})^2 + \langle J_{\vec{n}}^2 \rangle &< \langle \vec{J} \rangle^2 - \frac{N}{2},
\end{aligned} \tag{80}$$



which are equivalent to the original inequalities, and we replace  $\vec{n}_1$  with  $\vec{n}$  in the first inequality. Note that the right-hand side of the inequality is invariant under rotations. Thus, to detect entanglement, we shall find the minimum value of the left-hand side by rotating the direction  $\vec{n}$ . So, the spin squeezing parameters can be defined as

$$\tilde{\xi}_{R'}^2 = \frac{\min_{\vec{n}}[(N-1)(\Delta J_{\vec{n}})^2 + \langle J_{\vec{n}}^2 \rangle]}{\langle \vec{J} \rangle^2}, \quad (81)$$

$$\tilde{\xi}_D^2 = \frac{4}{N^2} \min_{\vec{n}}[(N-1)(\Delta J_{\vec{n}})^2 + \langle J_{\vec{n}}^2 \rangle], \quad (82)$$

$$\tilde{\xi}_E^2 = \frac{\min_{\vec{n}}[(N-1)(\Delta J_{\vec{n}})^2 + \langle J_{\vec{n}}^2 \rangle]}{\langle \vec{J} \rangle^2 - N/2}. \quad (83)$$

These parameters are rotationally invariant.

The minimization procedure works as below. First the term  $(N-1)(\Delta J_{\vec{n}})^2 + \langle J_{\vec{n}}^2 \rangle$  can be written as [28]

$$(N-1)(\Delta J_{\vec{n}})^2 + \langle J_{\vec{n}}^2 \rangle = \vec{n} \Gamma \vec{n}^T, \quad (84)$$

where the superscript  $T$  denotes the transpose, and  $\Gamma$  is a  $3 \times 3$  matrix, which is defined as

$$\Gamma = (N-1)\gamma + \mathbf{C}, \quad (85)$$

where the covariance matrix  $\gamma$  is given as

$$\gamma_{kl} = \mathbf{C}_{kl} - \langle J_k \rangle \langle J_l \rangle \text{ for } k, l \in \{x, y, z\} = \{1, 2, 3\}, \quad (86)$$

with a correlation matrix

$$\mathbf{C}_{kl} = \frac{1}{2} \langle J_l J_k + J_k J_l \rangle. \quad (87)$$

The minimum value of  $\vec{n} \Gamma \vec{n}^T$  is the minimum eigenvalue of  $\Gamma$  (See Appendix B), and thus the spin-squeezing parameter based on these inequality can be defined as [197]

$$\tilde{\xi}_{R'}^2 = \frac{\lambda_{\min}}{\langle \vec{J} \rangle^2}, \quad \tilde{\xi}_D^2 = \frac{4\lambda_{\min}}{N^2}, \quad \tilde{\xi}_E^2 = \frac{\lambda_{\min}}{\langle \vec{J}^2 \rangle - N/2}. \quad (88)$$

If  $\tilde{\xi}_E^2 < 1$ , the state is spin squeezed and entangled. In the case when  $\langle \vec{J}^2 \text{ big} \rangle = j(j+1)$  and when  $\lambda_{\min}$  is obtained in the  $\vec{n}_\perp$ -direction, we find  $\tilde{\xi}_E^2 = \xi_S^2$ , and thus  $\tilde{\xi}_E^2$  can be regarded as a generalization of  $\xi_S^2$ . For a CSS,  $\lambda_{\min} = j^2$  and  $\tilde{\xi}_E^2 = 1$ .

It is interesting to note that the left-hand sides of the above inequalities are equal to  $\vec{n} \Gamma \vec{n}^T$ , and thus the minimum values are just  $\lambda_{\min}$ . Therefore, the new definitions of squeezing parameters become proportional to  $\lambda_{\min}$ . Although these new parameters are not quantitatively equal to their original ones, they are qualitatively equivalent to the original ones in the sense that they all can detect whether a state is spin squeezed or not.

In the above discussion, spin squeezing was defined for many-qubit states belonging to the maximum multiplicity subspace of the collective angular momentum operator  $\vec{J}$ . This means that these states exhibit particle exchange symmetry. The concept of spin squeezing is therefore restricted to symmetric many-body systems that are accessible to collective operations alone. There is no *a priori* reason for this restriction in real experiments, thus Ref. [198] explored the possibility of extending the concept of spin squeezing to multi-qubit systems, where individual qubits are controllable in the sense that they are accessible to local operations. This requires a criterion of spin squeezing that exhibits invariance under local unitary operations on the qubits.

Now we introduce a local unitary invariant spin squeezing criterion for  $N$  qubits. We denote the mean-spin direction for a local qubit  $i$  by

$$\hat{n}_{i0} = \frac{\langle \vec{\sigma}_i \rangle}{|\langle \vec{\sigma}_i \rangle|}. \quad (89)$$

Associating a mutually-orthogonal set  $\{\hat{n}_{i\perp}, \hat{n}_{i\perp'}, \hat{n}_{i0}\}$  of unit vectors with each qubit, we may define the collective operators

$$\mathcal{J}_\perp = \frac{1}{2} \sum_{i=1}^N \vec{\sigma}_i \cdot \hat{n}_{i\perp}, \quad \mathcal{J}_{\perp'} = \frac{1}{2} \sum_{i=1}^N \vec{\sigma}_i \cdot \hat{n}_{i\perp'}, \quad \mathcal{J}_0 = \frac{1}{2} \sum_{i=1}^N \vec{\sigma}_i \cdot \hat{n}_{i0}, \quad (90)$$

which satisfy the usual angular momentum commutation relations as Eq. (30), and this leads to the uncertainty relation

$$(\Delta \mathcal{J}_\perp) (\Delta \mathcal{J}_{\perp'}) \geq \frac{1}{2} \langle \mathcal{J}_0 \rangle. \quad (91)$$

Analogous to the above spin definitions, like  $\xi_S^2$  and  $\xi_R^2$ , we may define the corresponding squeezing parameters [198] as

$$\tilde{\xi}_S^2 = \frac{4(\Delta \mathcal{J}_\perp)_{\min}^2}{N}, \quad \tilde{\xi}_R^2 = \frac{N(\Delta \mathcal{J}_\perp)_{\min}^2}{\langle \mathcal{J}_0 \rangle^2}. \quad (92)$$

One important advantage of these squeezing parameters [198] is that they are locally unitary invariant due to the definition of  $\mathcal{J}$  in Eq. (90). Immediately, one can verify that for all  $N$ -body separable states, the above two parameters in Eq. (92) equal to one, since the single spin-1/2 particle is never spin squeezed. This is in contrast with the original squeezing parameters  $\xi_S^2$  and  $\xi_R^2$ , which are equal to 1 only for CSS.

### 2.8. Spin-squeezing parameters for states with parity

In preceding discussions, we reviewed several different spin-squeezing parameters presented in the literature. In the following, we mainly focus on two typical spin-squeezing parameters,  $\xi_S^2$  and  $\xi_R^2$ , which have wide applications in detecting entanglement, and in quantum metrology, etc. Besides these two parameters, we also consider parameter  $\tilde{\xi}_E^2$  in some parts of the paper, since  $\tilde{\xi}_E^2$  has close relations with  $\xi_S^2$  and can be viewed as a generalization of  $\xi_S^2$ . Furthermore,  $\tilde{\xi}_E^2$  is significant in discussing spin squeezing and entanglement.

We shall see that most typical spin-squeezed states are of a fixed parity. In this subsection we will study spin-squeezing parameters  $\xi_S^2$ ,  $\xi_R^2$  and  $\tilde{\xi}_E^2$  for states with even (odd) parity, and give relations among them. For general states, it is hard to find explicit relations of these three parameters. At first we explain the parity of a spin state and restrict ourselves to states with exchange symmetry and with only Dicke states being populated. For these states, we may define the parity operator

$$P = (-1)^{J_z + j}, \quad (93)$$

with eigenvalues  $p = 1$  and  $-1$  corresponding to even and odd parity, respectively. Thus the state  $|j, -j\rangle$ , which means each spin pointing to the  $-z$  direction, has even parity, and for a Dicke state  $|j, -j + n\rangle$ , if  $n$  is even (odd), the state has even (odd) parity. In general, if a spin state is spanned only by Dicke states of even (odd) parity, this state is of even (odd) parity. States with parity are very common, e.g., the state generated by the one-axis twisting model, which we will discuss in Sec. 3.

#### 2.8.1. Spin-squeezing parameters $\xi_S^2$ and $\xi_R^2$

Here, we consider spin-squeezing parameters  $\xi_S^2$  and  $\xi_R^2$ . For states with parity, we have the following relations,

$$\langle J_\alpha \rangle = \langle J_\alpha J_z \rangle = \langle J_z J_\alpha \rangle = 0, \quad \alpha = x, y, \quad (94)$$

which mean the MSD is along the  $z$  direction. The above equation leads to the following zero covariance

$$\text{Cov}(J_z, J_{\bar{n}_\perp}) = \frac{1}{2} \langle [J_z, J_{\bar{n}_\perp}]_+ \rangle - \langle J_z \rangle \langle J_{\bar{n}_\perp} \rangle = 0, \quad (95)$$

which implies that there are no spin correlations between the longitudinal ( $z$ ) and transverse directions ( $x$ - $y$  plane). The MSD is along the  $z$ -axis, then the general expression for the spin-squeezing parameter  $\xi_S^2$  in Eq. (53) reduces to [15]

$$\xi_S^2 = \frac{2}{N} (\langle J_x^2 + J_y^2 \rangle - |\langle J_z^- \rangle|). \quad (96)$$

Due to the exchange symmetry, we find

$$\langle J_\alpha \rangle = \frac{N}{2} \langle \sigma_{1\alpha} \rangle, \quad (97)$$

$$\langle J_\alpha^2 \rangle = \frac{N}{4} + \frac{N(N-1)}{4} \langle \sigma_{1\alpha} \sigma_{2\alpha} \rangle, \quad \alpha = x, y, z, \quad (98)$$

$$\langle \vec{J}^2 \rangle = \frac{3N}{4} + \frac{N(N-1)}{4} \langle \vec{\sigma}_1 \cdot \vec{\sigma}_2 \rangle, \quad (99)$$

$$\begin{aligned} (\Delta J_\alpha)^2 &= \frac{N}{4} \left[ 1 + (N-1) \langle \sigma_{1\alpha} \sigma_{2\alpha} \rangle - N \langle \sigma_{1\alpha} \rangle^2 \right] \\ &= \frac{N}{4} [1 + N C_{\alpha\alpha} - \langle \sigma_{1\alpha} \sigma_{2\alpha} \rangle], \end{aligned} \quad (100)$$

where

$$C_{\alpha\alpha} = \langle \sigma_{1\alpha} \sigma_{2\alpha} \rangle - \langle \sigma_{1\alpha} \rangle \langle \sigma_{2\alpha} \rangle \quad (101)$$

is the correlation function along the  $\alpha$ -direction. Furthermore, we obtain

$$\langle J_-^2 \rangle = N(N-1) \langle \sigma_{1-} \sigma_{2-} \rangle, \quad (102)$$

$$\begin{aligned} \langle J_x^2 + J_y^2 \rangle &= \frac{N}{2} + \frac{N(N-1)}{4} \langle \sigma_{1x} \sigma_{2x} + \sigma_{1y} \sigma_{2y} \rangle \\ &= \frac{N}{2} + \frac{N(N-1)}{2} \langle \sigma_{1+} \sigma_{2-} + \sigma_{1-} \sigma_{2+} \rangle. \end{aligned} \quad (103)$$

By substituting Eqs. (102) and (103) into Eq. (96), we obtain

$$\xi_S^2 = 1 - 2(N-1) (|\langle \sigma_{1-} \sigma_{2-} \rangle| - \langle \sigma_{1+} \sigma_{2-} \rangle), \quad (104)$$

where we have used  $\langle \sigma_{1+} \sigma_{2-} \rangle = \langle \sigma_{1-} \sigma_{2+} \rangle$ , which results from the exchange symmetry. From Eq. (97) and the relation between the parameters  $\xi_R^2$  and  $\xi_S^2$ , we find

$$\xi_R^2 = \left( \frac{N}{2|J_z|} \right)^2 \xi_S^2 = \frac{\xi_S^2}{\langle \sigma_{1z} \rangle^2}. \quad (105)$$

The above expressions for the two spin-squeezing parameters establish explicit relations between spin squeezing and local two-spin correlations, and we will further discuss these relations in Sec. 4.

Table 2: Comparison between different squeezing parameters for states with parity (extended from Ref. [197]). In the third column, simplified expressions are displayed for squeezing parameters for states with parity. The squeezing parameters are also expressed in terms of local expectations (fourth column).

Parameters	Definitions	States with parity	In terms of local expectations
$\xi_S^2$	$\frac{4(\Delta J_{\vec{n}_\perp})_{\min}^2}{N}$	$\frac{2}{N} (\langle J_x^2 + J_y^2 \rangle -  \langle J_-^2 \rangle )$	$1 - 2(N-1) ( \langle \sigma_{1-} \sigma_{2-} \rangle  - \langle \sigma_{1+} \sigma_{2-} \rangle)$
$\xi_R^2$	$\frac{N^2}{4\langle \vec{J} \rangle^2} \xi_S^2$	$\frac{\xi_S^2}{4\langle J_z \rangle^2 / N^2}$	$\frac{\xi_S^2}{\langle \sigma_{1z} \rangle^2}$
$\tilde{\xi}_{R'}^2$	$\frac{\lambda_{\min}}{\langle \vec{J} \rangle^2}$	$\frac{\min\{\xi_S^2, \varsigma^2\}}{4\langle J_z \rangle^2 / N^2}$	$\frac{\min\{\xi_S^2, 1 + (N-1)C_{zz}\}}{\langle \sigma_{1z} \rangle^2}$
$\tilde{\xi}_D^2$	$\frac{4\lambda_{\min}}{N^2}$	$\min\{\xi_S^2, \varsigma^2\}$	$\min\{\xi_S^2, 1 + (N-1)C_{zz}\}$
$\tilde{\xi}_E^2$	$\frac{\lambda_{\min}}{\langle \vec{J}^2 \rangle - N/2}$	$\frac{\min\{\xi_S^2, \varsigma^2\}}{4\langle \vec{J}^2 \rangle / N^2 - 2/N}$	$\frac{\min\{\xi_S^2, 1 + (N-1)C_{zz}\}}{(1 - N^{-1})\langle \vec{\sigma}_1 \cdot \vec{\sigma}_2 \rangle + N^{-1}}$

### 2.8.2. Spin-squeezing parameter $\tilde{\xi}_E^2$

Here, we derive explicit expression of  $\tilde{\xi}_E^2$  for states with parity. By using Eq. (95), the correlation matrix (87) is simplified to the following form

$$\mathbf{C} = \begin{pmatrix} \langle J_x^2 \rangle & \mathbf{C}_{xy} & 0 \\ \mathbf{C}_{xy} & \langle J_y^2 \rangle & 0 \\ 0 & 0 & \langle J_z^2 \rangle \end{pmatrix}, \quad (106)$$

where  $\mathbf{C}_{xy} = \langle [J_x, J_y]_+ \rangle / 2$ . From the correlation matrix  $\mathbf{C}$  and the definition of covariance matrix  $\Gamma$  given by Eq. (86), one finds

$$\Gamma = \begin{pmatrix} N \langle J_x^2 \rangle & N \mathbf{C}_{xy} & 0 \\ N \mathbf{C}_{xy} & N \langle J_y^2 \rangle & 0 \\ 0 & 0 & N (\Delta J_z)^2 + \langle J_z^2 \rangle \end{pmatrix}. \quad (107)$$

This matrix has a block-diagonal form and the eigenvalues of the  $2 \times 2$  block are obtained as

$$\lambda_{\pm} = \frac{N}{2} \left( \langle J_x^2 + J_y^2 \rangle \pm |\langle J_-^2 \rangle| \right). \quad (108)$$

Therefore, the smallest eigenvalue  $\lambda_{\min}$  of  $\Gamma$  is obtained as

$$\lambda_{\min} = \min \left\{ \lambda_-, N (\Delta J_z)^2 + \langle J_z^2 \rangle \right\}. \quad (109)$$

It is interesting to see that the eigenvalue  $\lambda_-$  is simply related to the spin squeezing parameter  $\xi_S^2$  in Eq. (96) via

$$\xi_S^2 = \frac{4}{N^2} \lambda_-. \quad (110)$$

Thus, from the definition of  $\tilde{\xi}_E^2$  given by Eq. (83), we finally find

$$\tilde{\xi}_E^2 = \frac{\min \{ \xi_S^2, \varsigma^2 \}}{4 \langle \vec{J}^2 \rangle / N^2 - 2/N}, \quad (111)$$

where

$$\varsigma^2 = \frac{4}{N^2} \left( N (\Delta J_z)^2 + \langle J_z^2 \rangle \right). \quad (112)$$

The meaning of  $\varsigma^2$  will be clear by substituting Eqs. (97) and (100) into the above equation. Then, we obtain

$$\varsigma^2 = N (\Delta J_z)^2 + \langle J_z^2 \rangle = 1 + (N-1) \mathcal{C}_{zz}. \quad (113)$$

Parameter  $\varsigma^2$  is just a linear function of the correlation function  $\mathcal{C}_{zz}$  given in Eq. (101). From Eq. (99) and the above expression, we write parameter  $\tilde{\xi}_E^2$  in terms of expectations of local operators as

$$\tilde{\xi}_E^2 = \frac{\min \{ \xi_S^2, \varsigma^2 \}}{(1 - N^{-1}) \langle \vec{\sigma}_1 \cdot \vec{\sigma}_2 \rangle + N^{-1}}. \quad (114)$$

In the special case when only spin  $j = N/2$  is populated, i.e.,  $\langle \vec{J}^2 \rangle = N/2(N/2 + 1)$ , we have  $\langle \vec{\sigma}_1 \cdot \vec{\sigma}_2 \rangle = 1$ , and therefore, the above equation reduces to

$$\tilde{\xi}_E^2 = \min \{ \xi_S^2, \varsigma^2 \}. \quad (115)$$

Thus, the relations among the spin-squeezing parameters  $\xi_S^2$ ,  $\xi_R^2$ , and  $\tilde{\xi}_E^2$  are clear for states with parity, and in this case, the spin-squeezing parameters are determined by pairwise correlations in the  $z$ -axis and the  $x$ - $y$  plane. The above results are summarized in Table 2 extended from Ref. [199].

### 2.8.3. Dicke States

Below, we first consider Dicke states and simple superpositions of two Dicke states. The Dicke states  $|j, m\rangle$  are entangled state except for  $m = \pm j$ . Since we mainly consider an ensemble of spin-1/2 particles, the state  $|j, m\rangle$  can be written as

$$\begin{aligned} |j, m\rangle &= \sqrt{\frac{(j-m)!}{(j+m)!(2j)!}} J_+^{j+m} |j, -j\rangle \\ &= \sqrt{\frac{(j-m)!}{(j+m)!(2j)!}} \left( \sum_{i=1}^N \sigma_{i+} \right)^{j+m} |1\rangle^{\otimes N}. \end{aligned} \quad (116)$$

Since the Dicke states  $|j, m\rangle$  are eigenstates of  $J_z$  with eigenvalue  $m$ , the MSD is along the  $z$ -axis. A single Dicke state has either even or odd parity. Thus, we can use formulas shown in Table 2, and we only need to calculate  $\xi_S^2$  and  $\zeta^2$ .

From Eq. (96), the squeezing parameter  $\xi_S^2$  can be written as

$$\xi_S^2 = 1 + j - \frac{1}{j} \left( \langle J_z^2 \rangle + |\langle J_-^2 \rangle| \right), \quad (117)$$

which is determined by two expectation values:  $\langle J_z^2 \rangle$  and  $\langle J_-^2 \rangle$ . For the Dicke states, we obtain

$$\xi_S^2 = 1 + \frac{j^2 - m^2}{j} \geq 1, \quad (118)$$

since  $j \geq m$ . The equal sign holds for  $m = \pm j$ , when the Dicke state becomes a CSS. The quantity  $\zeta^2$  is obtained as

$$\zeta^2 = \frac{1}{j^2} \left[ N (\Delta J_z)^2 + \langle J_z \rangle^2 \right] = \frac{m^2}{j^2} \leq 1. \quad (119)$$

Thus, from Table 2, one finds

$$\tilde{\xi}_D^2 = \tilde{\xi}_E^2 = \min(\xi_S^2, \zeta^2) = \zeta^2 \leq 1, \quad (120)$$

indicating that the state is squeezed and entangled for  $m \neq \pm j$ . The parameters  $\xi_R^2$  and  $\tilde{\xi}_{R'}^2$  are given by

$$\xi_R^2 = \left( \frac{j}{m} \right)^2 \xi_S^2 \geq 1, \quad (121)$$

$$\tilde{\xi}_{R'}^2 = \frac{\zeta^2}{m^2/j^2} = 1, \quad (122)$$

thus spin squeezing according to the three parameters  $\xi_S^2$ ,  $\xi_R^2$ , and  $\tilde{\xi}_{R'}^2$  cannot reflect the underlying entanglement in the Dicke states.

### 2.9. Relations between spin squeezing and bosonic squeezing

Above, we reviewed some basic concepts about bosonic and spin squeezing, and now we will demonstrate the relationship between these two mathematically distinct, yet intuitively connected squeezing [200, 201]. It has been shown in Ref. [201] that the spin-squeezing parameter  $\xi_S^2$  reduces to the bosonic squeezing in the limit of large number of atoms and small excitations. For this purpose, we consider the principal quadrature squeezing defined as (8). The definition of  $\zeta_B^2$  provides an atomic squeezing counterpart to bosonic squeezing, and is similar to the definition of  $\xi_S^2$ , both of them searching for minimum squeezing.

It is well-known that the Heisenberg-Weyl algebra describing the bosonic mode can be obtained by contraction from the SU(2) algebra describing the ensemble of atoms [202]. To see this, we define  $b \equiv J_-/\sqrt{2j}$  and  $b^\dagger \equiv J_+/\sqrt{2j}$ . From the commutation relation (1), we have

$$[\mathcal{N}, b^\dagger] = b^\dagger, \quad [\mathcal{N}, b] = -b, \quad [b, b^\dagger] = 1 - \frac{\mathcal{N}}{j}, \quad (123)$$

where  $\mathcal{N} = J_z + j$  is the ‘number operator’, and its eigenvalues vary from 0 to  $N$ , counting the number of excited atoms. In the limit of  $j \rightarrow \infty$  and small  $\langle \mathcal{N} \rangle$ , the operators  $\mathcal{N}$ ,  $b$ , and  $b^\dagger$  satisfy the commutation relations of the Heisenberg-Weyl algebra. Note that, when we take this limit, the average number of excited atoms  $\langle \mathcal{N} \rangle$  should be much less than the total number of atoms  $N$ .

We can also use the usual Holstein-Primakoff transformation [203]:

$$J_+ = a^\dagger \sqrt{2j - a^\dagger a}, \quad J_- = \sqrt{2j - a^\dagger a} a, \quad J_z = a^\dagger a - j. \quad (124)$$

In the limit of  $j \rightarrow \infty$ , we have

$$\frac{J_+}{\sqrt{2j}} \rightarrow a^\dagger, \quad \frac{J_-}{\sqrt{2j}} \rightarrow a, \quad -\frac{J_z}{j} \rightarrow 1, \quad (125)$$

by expanding the square root and neglecting terms of  $O(1/j)$ . We see that the bosonic system and the atomic spin system are connected by the large- $j$  limit from an algebraic point of view.

To display this connection, we consider even (odd) states. These states refer to those being a superposition of even (odd) Fock states for bosonic systems, and those being a superposition of Dicke states  $|n\rangle_j \equiv |j, -j + n\rangle$  with the even (odd) excitations for the atomic systems. The Dicke states  $|n\rangle_j$  satisfy  $\mathcal{N}|n\rangle_j = n|n\rangle_j$ . Specifically, even and odd bosonic coherent states have been realized experimentally in various physical systems. The even (odd) states serve as examples for demonstrating connections between bosonic and atomic squeezing. For even (odd) states,  $\langle a \rangle = 0$ ; thus, from Eq. (8), we obtain

$$\zeta_B^2 = 1 + 2|\langle a^\dagger a \rangle - 2|\langle a^2 \rangle|. \quad (126)$$

Obviously, one necessary condition for squeezing is that  $|\langle a^2 \rangle| \neq 0$ .

For even (odd) atomic states, the squeezing parameter  $\xi_S^2$  has already been given in Eq. (96), and we rewrite it as

$$\xi_S^2 = 1 + 2\langle \mathcal{N} \rangle - \frac{\langle \mathcal{N}^2 \rangle}{j} - \frac{|\langle J_-^2 \rangle|}{j}. \quad (127)$$

Using Eq. (125), in the limit of  $j \rightarrow \infty$ , we find that Eq. (127) reduces to Eq. (126) for even (odd) states. Also, we may find that the squeezing parameter  $\xi_R^2$  also reduce to  $\zeta_B^2$  in this limit. This result displays a direct connection between bosonic squeezing and atomic squeezing. From an experimental point of view, the number of atoms is typically large enough, so the observed atomic squeezing is expected to approximate the bosonic quadrature squeezing. As a remark, Eqs. (126) and (127) obtained for even and odd states are also applicable to arbitrary states, which is discussed in Ref. [201].

### 3. Generation of spin squeezing with nonlinear twisting Hamiltonians

In this section, we discuss generating spin-squeezed states with the one-axis twisting and two-axis twisting Hamiltonians. The one-axis twisting Hamiltonian is one of the most important models studied in generating spin squeezing, both theoretically and experimentally. It also describes a nonlinear rotator, and was studied in Ref. [204] before its applications in spin squeezing. The proposal of using these two types of twisting Hamiltonians to generate spin-squeezed states is directly inspired by using the nonlinear Hamiltonian (10) to produce bosonic squeezing.

In Sec. 3.1, we first present the analytical results of the evolution of the one-axis twisting. Then we discuss how to implement this Hamiltonian in a two-component BEC, and by using large-detuned light-atom interactions. The experimental progresses are reviewed in Sec. 8.1. Then in Sec. 3.2, we discuss the two-axis twisted state. As compared with the one-axis twisting, one can obtain higher degree of squeezing by using the two-axis twisting Hamiltonian. However, this type of Hamiltonian is not easy to be implemented in experiments, and analytical results are not available for arbitrary system size.

### 3.1. One-axis twisting Hamiltonian

Here we discuss the generation of spin squeezing by using the one-axis twisting Hamiltonian [1, 204]. The one-axis twisting model is very simple, and is one of the most widely studied models in generating spin-squeezed state [167, 107, 22, 119, 121, 123, 122, 205, 126, 127, 206, 129, 130, 207, 110, 157, 111, 131, 132, 18, 22, 135, 208, 209, 210]. It works in analogy to the squeezing operator, Eq. (15), in photon system and has been implemented in BEC via atomic collisions [4, 17, 18, 19, 20] and in atomic ensembles [167, 107, 111, 22, 210, 209]. Moreover, it allows simple derivations of various analytical results.

#### 3.1.1. One-axis twisted states

Consider now an ensemble of  $N$  spin-1/2 particles with exchange symmetry, and assume that its dynamical properties can be described by collective operators  $J_\alpha$ ,  $\alpha = x, y, z$ . The one-axis twisting Hamiltonian reads

$$H_{\text{OAT}} = \chi J_x^2 = \frac{\chi}{4} \sum_{k,l=1}^N \sigma_{kx} \sigma_{lx}, \quad (128)$$

which is a nonlinear operator with coupling constant  $\chi$  and involves all pairwise interactions, which indicates that the spin-squeezed states generated by this Hamiltonian may exhibit pairwise correlations. The most commonly used twisting Hamiltonian is along the  $z$ -axis, with the initial state being a CSS pointing along the  $x$ -axis. Since the twisting is along the  $x$ -axis, we choose the initial CSS along the  $z$ -axis to make our analysis consistent with the  $z$ -axis twisting version. Here we prefer the  $x$ -axis twisting Hamiltonian satisfying

$$[H_{\text{OAT}}, P] = 0, \quad (129)$$

where  $P$  is the parity operator given by Eq. (93). We choose the initial state as  $|j, -j\rangle = |1\rangle^{\otimes N}$ . Considering its dynamic evolution, the spin-squeezed state at time  $t$  is formally written as

$$|\Psi(t)\rangle = \exp(-i\theta J_x^2/2) |1\rangle^{\otimes N}, \quad (130)$$

where

$$\theta = 2\chi t \quad (131)$$

is the one-axis twisting angle. This state is the one-axis twisted state with even parity, and the MSD is along the  $z$  direction, thus the results derived in Sec. 2 can be directly used here.

Table 3: Expectation values of local observables for the one-axis twisted state.

$\langle \sigma_{1z} \rangle$	$-\cos^{N-1}(\theta/2)$
$\langle \sigma_{1z} \sigma_{2z} \rangle$	$\frac{1}{2}(1 + \cos^{N-2}\theta)$
$\langle \sigma_{1+} \sigma_{2-} \rangle$	$\frac{1}{8}(1 - \cos^{N-2}\theta)$
$\langle \sigma_{1-} \sigma_{2-} \rangle$	$-\frac{1}{8}(1 - \cos^{N-2}\theta) - \frac{i}{2} \sin(\theta/2) \cos^{N-2}(\theta/2)$

The expectation values needed for calculating spin squeezing parameters are derived in Appendix D, and are summarized in Table 3. By substituting expressions  $\langle \sigma_{1+} \sigma_{2-} \rangle$  and  $\langle \sigma_{1-} \sigma_{2-} \rangle$  into Eq. (104), we obtain

$$\xi_S^2 = 1 - C_r = 1 - (N-1)C, \quad (132)$$

where

$$C = \frac{1}{4} \left\{ \left[ \left(1 - \cos^{N-2}\theta\right)^2 + 16 \sin^2\left(\frac{\theta}{2}\right) \cos^{2N-4}\left(\frac{\theta}{2}\right) \right]^{1/2} - \left(1 - \cos^{N-2}\theta\right) \right\}. \quad (133)$$

It will be clear in Sec. 4 that the quantity  $C$  is the concurrence [14], measuring entanglement of two spin  $s = 1/2$  particles.

In the case that  $N \gg 1$  and  $|\theta| \ll 1$ , while  $N|\theta| \gg 1$  and  $N|\theta|^2 \ll 1$ , we can expand Eq. (133) and find that the spin-squeezing parameter scales as [1]

$$\xi_S^2 \sim N^{-2/3}, \quad (134)$$

at  $|\theta| = \theta_0 = 12^{1/6} (N/2)^{-2/3}$ . Since  $\theta$  is very small and  $N$  is large, at  $\theta_0$  we find

$$\langle \sigma_{1z} \rangle \sim -\exp \left[ -\left( \frac{4}{3} N \right)^{-1/3} \right], \quad (135)$$

and then, for large enough  $N$ , we have

$$\xi_R^2 \sim N^{-2/3}. \quad (136)$$

Therefore, the projection noise is reduced by a factor of  $N^{-2/3}$ . The optimal squeezing angle for the one-axis twisting is [1]

$$\delta \sim \frac{1}{2} \arctan \left( N^{-1/3} \right), \quad (137)$$

which varies with the particle number  $N$ ; although if  $N$  is large enough,  $\delta$  is close to 0.

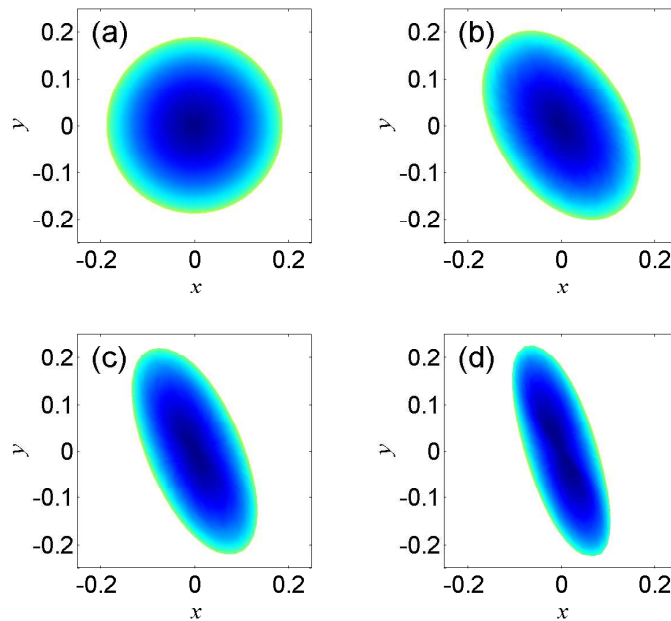


Figure 2: (Color online) Husimi  $Q$  function of spin-squeezed states generated by the one-axis twisting model for various times: (a)  $\chi t = 0$ , (b)  $\chi t = 0.1$ , (c)  $\chi t = 0.2$  and (d)  $\chi t = 0.3$ . The system size is  $N = 60$ , and at the beginning  $\chi t = 0$ , the state is a CSS and thus the  $Q$  function is a circle. The optimal squeezing angle rotates with time.

The squeezing and the dynamic evolution of the state can also be illustrated by calculating the Husimi- $Q$  function

$$Q(\theta_0, \phi_0) = |\langle \theta_0, \phi_0 | \Psi(t) \rangle|^2, \quad (138)$$



Table 4: Spin-squeezing parameters in terms of the rescaled concurrence  $C_r$  given by Eqs. (132) and (133) for the one-axis twisted state.

$\xi_S^2$	$1 - C_r$
$\xi_R^2$	$\frac{1 - C_r}{\langle \sigma_{1z} \rangle^2}$
$\tilde{\xi}_E^2$	$1 - C_r$

which represents the quasiprobability distribution of  $|\Psi(t)\rangle$ , and  $|\theta_0, \phi_0\rangle$  is the CSS given in Eq. (17). The Husimi- $Q$  function is shown in Fig. 2, where the coordinate we used is determined by

$$\begin{aligned} x &= Q \cos \theta_0 \cos \phi_0, \\ y &= Q \cos \theta_0 \sin \phi_0. \end{aligned} \quad (139)$$

As we can see that, the initial CSS is a circle given by the Husimi function, and during the evolution, the Husimi- $Q$  function becomes squeezed and elliptical, while the squeezing angle rotates.

Now we discuss another two parameters  $\xi_R^2$  and  $\tilde{\xi}_E^2$ . Parameter  $\xi_R^2$  is easily obtained, as we know both  $\xi_S^2$  and  $\langle \sigma_{1z} \rangle^2$ . To obtain  $\tilde{\xi}_E^2$ , we also need to derive  $\mathcal{C}_{zz}$  and  $\langle \vec{\sigma}_1 \cdot \vec{\sigma}_2 \rangle$  as seen from Table 2. For this state,  $\langle \vec{\sigma}_1 \cdot \vec{\sigma}_2 \rangle = 1$ , thus the expression of  $\tilde{\xi}_E^2$  reduces to

$$\begin{aligned} \tilde{\xi}_E^2 &= \min \{ \xi_S^2, \varsigma^2 \} \\ &= \min \{ 1 - C_r, 1 + (N - 1)\mathcal{C}_{zz} \}. \end{aligned} \quad (140)$$

By substituting expressions of  $\langle \sigma_{1z}\sigma_{2z} \rangle^2$  and  $\langle \sigma_{1z} \rangle^2$  (Table 3) into definition of the correlation function, we obtain,

$$\mathcal{C}_{zz} = \frac{1}{2} (1 + \cos^{N-2} \theta) - \cos^{2N-2} (\theta/2) \geq 0. \quad (141)$$

The proof of the above inequality is given in Appendix C of Ref. [197].

As the correlation function  $\mathcal{C}_{zz}$  and the rescaled concurrence  $C_r$  are always larger than zero, Eq. (140) reduces to

$$\tilde{\xi}_E^2 = \xi_S^2 = 1 - C_r. \quad (142)$$

So, for the state given by Eq. (130), the spin-squeezing parameters  $\tilde{\xi}_E^2$  and  $\xi_S^2$  are equal, and we summarize these results in Table 4.

### 3.1.2. One-axis twisting with a transverse field

In Ref. [119], it was found that a one-axis twisting Hamiltonian with a transverse control field

$$H = \chi J_x^2 + B J_z, \quad (143)$$

is more effective in generating squeezed states, where  $B$  is the strength of the external field. Reference [211] proved that the optimally spin-squeezed states that maximize the sensitivity of the Ramsey spectroscopy are eigensolutions of this Hamiltonian. This type of Hamiltonian was considered in BEC [123, 122, 129, 130, 132, 135], and atomic ensembles [111]. The initial state is also a CSS  $|j, -j\rangle$ , while the dynamic evolution cannot be solved analytically, except for  $N \leq 3$ , and numerical results show that the external field leads to an improvement of the degrees of squeezing in an extended period of time.

### 3.1.3. One-axis twisting in Bose-Einstein condensates

Below, we discuss how to derive the one-axis twisting Hamiltonian from a two-component BEC, which can be regarded as a BEC with atoms in two internal states, or similarly, a BEC in a double-well potential.

We consider the case of  $N$  atoms in two internal states  $|A\rangle$  and  $|B\rangle$ . The Hamiltonian of the system is given by [4, 125] ( $\hbar \equiv 1$ )

$$H = \int d\vec{r} \sum_{k=A,B} \left[ \hat{\psi}_k^\dagger(\vec{r}) \hat{h}_k \hat{\psi}_k(\vec{r}) + \frac{g_{kk}}{2} \hat{\psi}_k^\dagger(\vec{r}) \hat{\psi}_k^\dagger(\vec{r}) \hat{\psi}_k(\vec{r}) \hat{\psi}_k(\vec{r}) \right] + \int d\vec{r} g_{AB} \hat{\psi}_A^\dagger(\vec{r}) \hat{\psi}_B^\dagger(\vec{r}) \hat{\psi}_A(\vec{r}) \hat{\psi}_B(\vec{r}) \quad (144)$$

where the single-particle Hamiltonian

$$\hat{h}_k = -\frac{\nabla^2}{2m} + V_k(\vec{r}) \quad (145)$$

governs atoms in the internal state  $k$ , with atom mass  $m$  and trapping potential  $V_k(\vec{r})$ . The bosonic field operator  $\hat{\psi}_k(\vec{r})$  annihilates an atom at position  $\vec{r}$  in the internal state  $k$ , which obeys

$$\left[ \hat{\psi}_k(\vec{r}), \hat{\psi}_k^\dagger(\vec{r}') \right] = \delta(\vec{r} - \vec{r}'). \quad (146)$$

The interaction strengths

$$g_{kl} = \frac{4\pi a_{kl}}{m}, \quad (147)$$

with  $a_{kl}$  the  $s$ -wave scattering length and  $g_{AA}$ ,  $g_{BB}$ , and  $g_{AB}$  are for collisions between atoms in states  $A$ ,  $B$ , and interspecies collisions, respectively.

Now we employ the single-mode approximation for each of the components,

$$\hat{\psi}_A(\vec{r}) = \phi_A(\vec{r}) a, \quad \hat{\psi}_B(\vec{r}) = \phi_B(\vec{r}) b, \quad (148)$$

where  $\phi_A(\vec{r})$  and  $\phi_B(\vec{r})$  are assumed to be real,  $a$  and  $b$  are the bosonic annihilation operators that satisfy  $[a, a^\dagger] = [b, b^\dagger] = 1$  and  $[a, b] = 0$ . In the single-mode approximation, the Hamiltonian is rewritten as

$$H = (\omega_A - U_{AA}) a^\dagger a + (\omega_B - U_{BB}) b^\dagger b + U_{AA} (a^\dagger a)^2 + U_{BB} (b^\dagger b)^2 + 2U_{AB} a^\dagger a b^\dagger b, \quad (149)$$

where

$$\omega_k = \int d\vec{r} \phi_k^*(\vec{r}) \hat{h}_k \phi_k(\vec{r}), \quad U_{kl} = \frac{g_{kl}}{2} \int d\vec{r} |\phi_k(\vec{r})|^2 |\phi_l(\vec{r})|^2. \quad (150)$$

Note that,  $\phi_k(\vec{r})$  obeys the coupled Gross-Pitaevskii equation, thus  $\omega_k$  and  $U_{kl}$  depend on the time  $t$ . Now the effective Hamiltonian is rewritten by using angular momentum operators via the following Schwinger representation

$$J_z = \frac{1}{2} (a^\dagger a - b^\dagger b), \quad J_+ = a^\dagger b, \quad J_- = ab^\dagger, \quad (151)$$

where the operator  $2J_z$  measures the population difference between states  $|A\rangle$  and  $|B\rangle$ , and  $J_\pm$  describe the atomic tunneling between the two internal states. The total atom number operator  $\hat{N} = a^\dagger a + b^\dagger b$  is a conserved quantity here. Using the Schwinger representation (151) the Hamiltonian (149) can be written as

$$H = e(t) \hat{N} + E(t) \hat{N}^2 + \delta(t) J_z + \chi(t) J_z^2, \quad (152)$$

where the nonlinear interaction coefficient is

$$\chi(t) = U_{AA} + U_{BB} - 2U_{AB}, \quad (153)$$

and the other coefficients are

$$\begin{aligned} e(t) &= (\omega_A + \omega_B - U_{AA} - U_{BB})/2, \\ E(t) &= (U_{AA} + U_{BB} + 2U_{AB})/4, \\ \delta(t) &= \omega_A - \omega_B + (U_{AA} - U_{BB})(\hat{N} - 1). \end{aligned} \quad (154)$$

As the number operator  $\hat{N}$  is a conserved quantity, if  $\chi(t) \neq 0$  as presented in Sec. 8.1, spin-squeezed states are generated as discussed previously. The validity of using the single-mode assumption to calculate spin squeezing was verified in Refs. [120, 125], based on both Bogoliubov theory and positive- $P$  simulations. Note that, the original Hamiltonian (144) entangles the internal and motional states of the atoms, which is a source of decoherence for the spin squeezing. With direct numerical simulation [4, 154], spin squeezing produced via the original Hamiltonian (144) is roughly in agreement with the one-axis twisting Hamiltonian (152).

We now consider that a driving microwave field is applied [129], and the Hamiltonian becomes

$$H_1 = H + \frac{1}{2} \int d\vec{r} \left[ \hat{\psi}_A^\dagger(\vec{r}) \hat{\psi}_B(\vec{r}) \Omega_R e^{-i\Delta t} + \text{h.c.} \right], \quad (155)$$

where  $\Delta$  is the detuning of the field from resonance and  $\Omega_R$  is the effective Rabi frequency assumed to be positive. Following the same steps, we effectively obtain the Hamiltonian in terms of the angular-momentum operators as

$$H_1 = \delta(t) J_z + \chi(t) J_z^2 + \Omega [J_+ e^{-i\delta t} + J_- e^{i\delta t}], \quad (156)$$

where

$$\Omega = \Omega_R \int d\vec{r} \phi_A^*(\vec{r}) \phi_B(\vec{r}). \quad (157)$$

Usually, we can assume  $\tilde{\delta}(t) = 0$ . As presented in Ref. [119], by using the control field to assist the one-axis twisting, spin squeezing can be maintained for an extended period of time. In Ref. [131],  $\chi(t)$  is assumed to be independent of time  $t$ , and the external field is turned off rapidly at a time  $t_M$ , so that  $\Omega(t) = \Omega_R \Theta(t_M - t)$ , where  $\Theta(t)$  is the usual step function, and the maximal-squeezing time  $t_M$  is obtained analytically

$$\chi t_M \simeq \frac{\pi}{4} \sqrt{\frac{\chi}{\Omega_R N}}, \quad (158)$$

which is valid for large  $N$  ( $\geq 10^3$ ). The time-dependent field  $\Omega(t)$  provides the control for storing the spin squeezing.

### 3.1.4. One-axis twisting from large-detuned atom-field interaction

Next we discuss the derivation of the one-axis twisting Hamiltonian from a collection of two-level atoms interacting with a large detuned field [107, 108, 109, 110, 111, 22]. Consider an ideal model, a collection of  $N$  two-level atoms laid in a cavity, the Hamiltonian for the whole system is

$$H = H_0 + H_I, \quad (159)$$

where

$$\begin{aligned} H_0 &= \omega_0 J_z + \omega_c a^\dagger a, \\ H_I &= g (J_+ a + J_- a^\dagger). \end{aligned} \quad (160)$$

$H_0$  describes the free dynamics of the atoms and field, and  $H_I$  is the interaction term under the rotating wave approximation. The spin operators  $J_{z,\pm}$  describe the atomic system,  $a, a^\dagger$  describe the cavity field, and  $g$  is the atom-field interaction strength. We can see from the Hamiltonian that, atoms interact with the cavity field, while no direct interaction exists between atoms. However, under the large detuning condition,

i.e. the atom-field detuning  $\Delta = \omega_0 - \omega_c$  is very large as compared to  $g$  such that  $|\Delta| \gg g\sqrt{N}$ , and we can perform the Fröich-Nakajima transform to obtain an effective Hamiltonian describing nonlinear atom-atom interaction. The Fröich-Nakajima transform is performed as,

$$H_S = e^{-S} H e^S, \quad (161)$$

where  $S$  is of the same order as the interaction term  $H_I$ . Expand the above transform to the second order of  $S$ , we have

$$\begin{aligned} H_S &= H + [H, S] + \frac{1}{2} [[H, S], S] \\ &= H_0 + (H_I + [H_0, S]) + \frac{1}{2} [(H_I + [H_0, S]), S] + \frac{1}{2} [H_I, S], \end{aligned} \quad (162)$$

and let  $H_I + [H_0, S] = 0$ , which gives

$$H_S = H_0 + \frac{1}{2} [H_I, S], \quad (163)$$

where

$$S = \frac{g}{\Delta} (a^\dagger J_- - a J_+). \quad (164)$$

Inserting Eq. (164) into Eq. (163), we obtain the effective Hamiltonian

$$H_S = H_0 - \eta [J_z^2 - (2a^\dagger a + 1) J_z], \quad (165)$$

and the factor  $\eta = g^2/\Delta$ . Note that, the effective Hamiltonian (165) contains a one-axis twisting term  $J_z^2$ , and a dispersive interaction term proportional to  $a^\dagger a J_z$ , which is employed in the QND measurement and shall be discussed in Sec. 8.

If photon loss is taken into account, the effective Hamiltonian is of the same form as Eq. (165), while the interaction strength is modified to be [107]

$$\eta = \frac{g^2 \Delta}{\Delta^2 + \gamma^2/4}, \quad (166)$$

where  $\gamma$  is the decay rate of the cavity field and satisfies  $\gamma \ll \Delta$ . The derivation of Eq. (166) can refer to Ref. [107], where the atoms are laid in a cavity that is highly detuned from the atomic transition frequency, while the atomic dissipation induced by spontaneous emission was considered to be negligibly small as compared to the time scale of interaction. Spin squeezing of atoms in cavity was also studied in [108, 109, 110]. In experiments, the effective one-axis twisting Hamiltonian was demonstrated for squeezing individual high spin ( $F = 4$  [22], and  $F = 3$  [89, 111]) Cs atoms that interacts with off-resonant light field.

References [207, 210, 209] proposed an interesting method to generate effective one-axis twisting Hamiltonian via cavity feedback. The large detuned atom-field interaction in cavity induces an effective QND-type Hamiltonian,

$$H = \alpha a^\dagger a J_z, \quad (167)$$

while the backaction of the cavity light causes the photon number operator  $a^\dagger a$  to be linearly proportional to  $J_z$ , thus the QND Hamiltonian becomes a one-axis twisting Hamiltonian. In a recent experiment [209], an effective one-axis twisting Hamiltonian was generated by cavity feedback, and achieved 5.6(6) improvement in signal-to-noise ratio for  $|F = 1, m_F = 0\rangle \leftrightarrow |F = 2, m_F = 0\rangle$  hyperfine clock transition in  $^{87}\text{Rb}$  atoms.

### 3.2. Two-axis twisted states

Although spin squeezing can be produced by the one-axis twisting model effectively, the optimal squeezing angle depends on the system size and evolution time. This problem is solved if the twisting is performed simultaneously clockwise and counterclockwise about two orthogonal axes in the plane normal to the MSD. The initial state is also  $|j, -j\rangle$ , and the twisting is about two axes in the  $\theta = \pi/2$ ,  $\phi = \pm\pi/4$  directions. The relevant two spin operators are written as

$$J_{\frac{\pi}{2}, \frac{\pi}{4}} = \cos\left(\frac{\pi}{4}\right) J_x + \sin\left(\frac{\pi}{4}\right) J_y = \frac{1}{\sqrt{2}}(J_x + J_y), \quad (168)$$

$$J_{\frac{\pi}{2}, -\frac{\pi}{4}} = \cos\left(\frac{\pi}{4}\right) J_x - \sin\left(\frac{\pi}{4}\right) J_y = \frac{1}{\sqrt{2}}(J_x - J_y). \quad (169)$$

The two-axis twisting Hamiltonian is written as [1]

$$H_{\text{TAT}} = J_{\frac{\pi}{2}, \frac{\pi}{4}}^2 - J_{\frac{\pi}{2}, -\frac{\pi}{4}}^2 = \chi(J_x J_y + J_y J_x) = \frac{\chi}{2i}(J_+^2 - J_-^2), \quad (170)$$

which is analogous to the Hamiltonian (10) for producing squeezed light that creates and annihilates photons in pairs. By replacing  $a$  and  $a^\dagger$  with  $J_-/\sqrt{N}$  and  $J_+/\sqrt{N}$ , respectively, we will obtain the two-axis twisting Hamiltonian shown in Eq. (170). Various approaches for implementing this Hamiltonian were studied in Refs. [137, 212, 213, 205, 138, 214]. The MSD is also along the  $z$ -axis. Unfortunately, the two-axis twisting model cannot be solved analytically for arbitrary  $N$ , except for  $N \leq 3$ . Below, we list two advantages of the two-axis twisting compared with the one-axis twisting case.

Table 5: Comparison of squeezing parameters when using either one-axis twisting or two-axis twisting Hamiltonian.

	One-axis Twisting	Two-axis Twisting
Minimum $\xi_S^2$ and $\xi_R^2$	$\propto \frac{1}{N^{2/3}}$	$\propto \frac{1}{N}$
Optimal squeezing angle	$\delta \sim \frac{1}{2} \arctan(N^{-1/3})$	Unchanged
Physical implementations	(i) Bose-Einstein condensation [17, 18, 19, 20]; (ii) Large detuning atom-field interaction [107, 111].	Effective atom-atom interaction via photon exchange [215, 212].

(i) The optimal squeezing angle is invariant during the evolution. Since the MSD for the two-axis twisting Hamiltonian is along the  $z$ -axis, according to Eq. (54), the optimal squeezing angle is determined by two quantities,  $\langle J_x^2 - J_y^2 \rangle$ , and  $\langle J_x J_y + J_y J_x \rangle$ . Due to

$$[J_x J_y + J_y J_x, H_{\text{TAT}}] = 0, \quad (171)$$

$\langle J_x J_y + J_y J_x \rangle$  is invariant during the time evolution. Here, the initial state is the CSS  $|j, -j\rangle$ , thus  $\langle J_x J_y + J_y J_x \rangle = 0$ . Then, the optimal squeezing direction is  $\varphi = 0, \pi/2$  during the evolution. The Husimi function is shown in Fig. 3, and it is clear that the optimal squeezing angle is invariant.

(ii) The degree of squeezing is high. By numerical calculations, the spin squeezing parameters scales as [1]

$$\xi_R^2 \propto \frac{1}{N}, \quad \xi_S^2 \propto \frac{1}{N}, \quad (172)$$

in the two-axis twisting model. Thus, according to Eq. (65), the phase noise approaches the Heisenberg limit. Comparisons between the one-axis twisting and two-axis twisting Hamiltonians are displayed in Table 5.

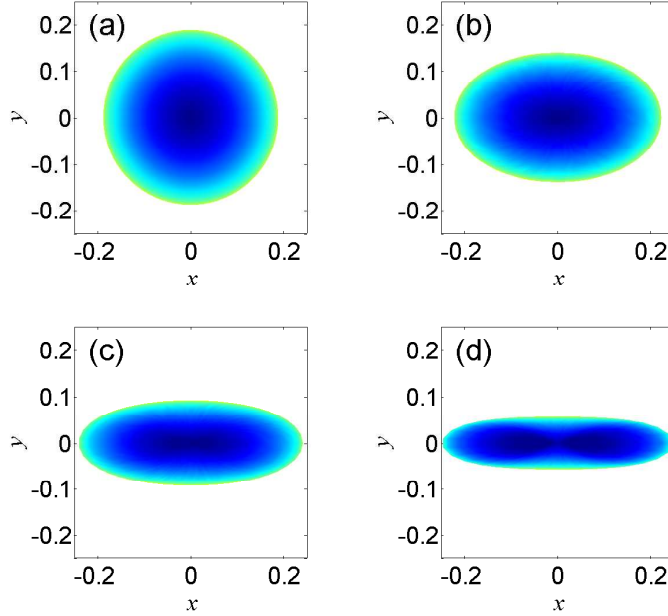


Figure 3: (Color online) Husimi  $Q$  function of spin-squeezed states generated by the two-axis twisting model for various times: (a)  $\chi t = 0$ , (b)  $\chi t = 0.1$ , (c)  $\chi t = 0.2$ , and (d)  $\chi t = 0.3$ . The system size is  $N = 60$ . Compared with the one-axis twisting, the optimal squeezing angle here is invariant during the time evolution.

#### 4. Spin squeezing, negative pairwise correlations, and entanglement

In this and the following sections, we mainly concentrate on spin squeezing, quantum correlations, and entanglement. Here, we first consider spin squeezing and pairwise correlations in a system with exchange symmetry, and consider the squeezing parameters  $\xi_S^2$  and  $\xi_E^2$ . Note that for a CSS, which has no pairwise correlation, the variance of  $J_{\vec{n}_\perp}$  is evenly distributed on individual spin components in the  $\vec{n}_\perp$ -direction, thus if a state has negative pairwise correlations in the  $\vec{n}_\perp$ -direction, the variance  $J_{\vec{n}_\perp}$  could be reduced as compared with CSSs. Below, we show that, as discussed in Ref. [13], spin squeezing with respect to  $\xi_S^2 < 1$  implies negative pairwise correlation in the  $\vec{n}_\perp$  direction. Moreover, the minimum pairwise correlation is associated with parameter  $\tilde{\xi}_E^2$ , and  $\tilde{\xi}_E^2 < 1$  is equivalent to the existence of negative pairwise correlation.

##### 4.1. Spin squeezing and pairwise correlations

As discussed in Refs. [1, 13], the spin-squeezing parameter  $\xi_S^2$  is well defined in the  $j = N/2$  subspace, where the states are of exchange symmetry. Thus, the expectation values and variances of the angular momentum operators  $J_\alpha$  can be expressed in terms of the local pairwise correlations, which helps us to obtain the relations between spin squeezing parameters and the pairwise correlations. The pairwise correlation function is defined as

$$G_{i\vec{n},j\vec{n}} \equiv \langle \sigma_{i\vec{n}} \sigma_{j\vec{n}} \rangle - \langle \sigma_{i\vec{n}} \rangle \langle \sigma_{j\vec{n}} \rangle = \langle \sigma_{1\vec{n}} \sigma_{2\vec{n}} \rangle - \langle \sigma_{1\vec{n}} \rangle^2, \quad (173)$$

with  $i, j$  being particle indices, and the second equality holds due to exchange symmetry. One can further define the minimum pairwise correlation as

$$G_m = \min_{\vec{n}} G_{1\vec{n},2\vec{n}}, \quad (174)$$

where the minimization is over an arbitrary direction  $\vec{n}$ .

#### 4.1.1. Spin-squeezing parameter $\xi_S^2$ and correlation $G_{\vec{n}_\perp, \vec{n}_\perp}$

First, we consider the spin-squeezing parameter  $\xi_S^2$ . From the relation  $J_{\vec{n}} = 1/2 \sum_{i=1}^N \sigma_{i\vec{n}}$ , one finds the variance of  $J_{\vec{n}}$ , which is given by

$$\begin{aligned} (\Delta J_{\vec{n}})^2 &= \frac{1}{4} \sum_{ij} (\langle \sigma_{i\vec{n}} \sigma_{j\vec{n}} \rangle - \langle \sigma_{i\vec{n}} \rangle \langle \sigma_{j\vec{n}} \rangle) \\ &= \frac{1}{4} [N(1 - \langle \sigma_{1\vec{n}} \rangle^2) + N(N-1)G_{1\vec{n}, 2\vec{n}}], \end{aligned} \quad (175)$$

where we used the symmetry property in deriving the last equality. From this equation, the correlation function can be written as

$$G_{1\vec{n}, 2\vec{n}} = \frac{4 [N (\Delta J_{\vec{n}})^2 + \langle J_{\vec{n}} \rangle^2]}{N^2(N-1)} - \frac{1}{N-1}. \quad (176)$$

If the correlation function is along the direction  $\vec{n}_\perp$ , Eq. (176) reduces to

$$G_{1\vec{n}_\perp, 2\vec{n}_\perp} = \frac{4 \langle J_{\vec{n}_\perp}^2 \rangle - N}{(N-1)N}, \quad (177)$$

where we have used the fact  $\langle J_{\vec{n}_\perp} \rangle = 0$ . From the relation between the spin squeezing parameter  $\xi_S^2$  and the expectation value  $\langle J_{\vec{n}_\perp}^2 \rangle$ ,

$$\min_{\vec{n}_\perp} \langle J_{\vec{n}_\perp}^2 \rangle = \frac{N}{4} \xi_S^2, \quad (178)$$

one obtain the minimum pairwise correlation [13]

$$\min_{\vec{n}_\perp} G_{\vec{n}_\perp, \vec{n}_\perp} = \frac{\xi_S^2 - 1}{N-1}, \quad (179)$$

where we have used Eq. (177). This implies that  $\min_{\vec{n}_\perp} G_{\vec{n}_\perp, \vec{n}_\perp} < 0$  is equivalent to  $\xi_S^2 < 1$ . Therefore, a spin-squeezed state ( $\xi_S^2 < 1$ ) has negative pairwise correlation in the  $\vec{n}_\perp$  direction ( $G_{\vec{n}_\perp, \vec{n}_\perp} < 0$ ).

#### 4.1.2. Spin-squeezing parameter $\xi_E^2$ and correlation $G_{1\vec{n}, 2\vec{n}}$

Now, we investigate the relation between the correlation function  $G_{1\vec{n}, 2\vec{n}}$  and the squeezing parameter  $\xi_E^2$ . It is more convenient to rewrite the correlation function as

$$G_{1\vec{n}, 2\vec{n}} = \langle \vec{n}^T \vec{\sigma}_1 \vec{\sigma}_2^T \vec{n} \rangle - \langle \vec{n}^T \vec{\sigma}_1 \rangle \langle \vec{\sigma}_2^T \vec{n} \rangle = \vec{n}^T \mathbf{G} \vec{n}, \quad (180)$$

where the normalized direction  $\vec{n} = (n_x, n_y, n_z)^T$ , and the pairwise correlation matrix  $\mathbf{G}$  is given by

$$\mathbf{G} = \langle \vec{\sigma}_1 \vec{\sigma}_2^T \rangle - \langle \vec{\sigma}_1 \rangle \langle \vec{\sigma}_2^T \rangle. \quad (181)$$

The matrix elements of  $\mathbf{G}$  are

$$\mathbf{G}_{k,l} = \langle \sigma_{1k} \sigma_{2l} \rangle - \langle \sigma_{1k} \rangle \langle \sigma_{2l} \rangle, \quad k, l = x, y, z. \quad (182)$$

From Eq. (176), we know that the correlation function  $G_{1\vec{n}, 2\vec{n}}$  is a linear function of the quantity  $N (\Delta J_{\vec{n}})^2 + \langle J_{\vec{n}} \rangle^2$ , which can be written as

$$N (\Delta J_{\vec{n}})^2 + \langle J_{\vec{n}} \rangle^2 = \vec{n}^T \left[ N \left( \frac{\langle \vec{J} \vec{J}^T \rangle + \langle \vec{J} \vec{J}^T \rangle^T}{2} - \langle \vec{J} \rangle \langle \vec{J} \rangle^T \right) + \langle \vec{J} \rangle \langle \vec{J} \rangle^T \right] \vec{n}. \quad (183)$$

The matrix

$$N \left( \frac{\langle \vec{J} \vec{J}^T \rangle + \langle \vec{J} \vec{J}^T \rangle^T}{2} - \langle \vec{J} \rangle \langle \vec{J} \rangle^T \right) + \langle \vec{J} \rangle \langle \vec{J} \rangle^T \quad (184)$$

is just the matrix  $\Gamma$  given by Eq. (85). Therefore, we have

$$N (\Delta J_{\vec{n}})^2 + \langle J_{\vec{n}} \rangle^2 = \vec{n}^T \Gamma \vec{n}. \quad (185)$$

Substituting Eqs. (180) and (185) into Eq. (176) leads to the following relation

$$\mathbf{G} = \frac{4\Gamma}{N^2(N-1)} - \frac{\mathbb{I}}{(N-1)}, \quad (186)$$

where  $\mathbb{I}$  is a  $3 \times 3$  identity matrix, and thus  $\mathbf{G}$  and  $\Gamma$  can be diagonalized simultaneously. This indicates that,  $G_{\vec{n}, \vec{n}}$  can be expressed in terms of  $\xi_S^2$  or  $\tilde{\xi}_E^2$  by choosing a specific direction  $\vec{n}$ .

Now we look for the relation between the parameter  $\tilde{\xi}_E^2$  and the minimum pairwise correlation. From Eq. (180), the minimum pairwise correlation

$$G_m = \min_{\vec{n}} G_{\vec{n}, \vec{n}} = \min_{\vec{n}} (\vec{n} \mathbf{G} \vec{n}^T) = g_{\min}, \quad (187)$$

where  $g_{\min}$  is the minimum eigenvalue of the pairwise correlation matrix  $\mathbf{G}$ . From Eq. (186), we find

$$g_{\min} = \frac{4\lambda_{\min} - N^2}{N^2(N-1)}. \quad (188)$$

In the symmetric case ( $j = N/2$ ), as we have assumed here,  $\tilde{\xi}_E^2 = 4\lambda_{\min}/N^2$ , and thus

$$G_m = \frac{\tilde{\xi}_E^2 - 1}{N-1}. \quad (189)$$

If the minimal pairwise correlation is in the plane normal to the MSD, the above relation will degenerate to Eq. (179). In another form, we write

$$\tilde{\xi}_E^2 = 1 + (N-1)G_m. \quad (190)$$

This exact result indicates that the spin squeezing defined by the parameter  $\tilde{\xi}_E^2$  is equivalent to the negative pairwise correlation, i.e.,  $G_m < 0$  implies  $\tilde{\xi}_E^2 < 1$  and vice versa.

#### 4.2. Spin squeezing and pairwise entanglement

One of the most useful applications of spin squeezing is to detect entanglement for many-qubit system. To determine whether a state is entangled, we just need to measure the collective operators, which are particle populations in many cases. Moreover, in many experiments, such as BEC, particles are not accessed individually, and the spin-squeezing parameter is easier to obtain than the concurrence and the entanglement entropy. Different kinds of spin-squeezing inequalities may be used to detect various types of entanglement [26, 27, 28, 6]. In Refs. [13, 216, 15, 217, 218], the relationships between negative pairwise correlation, concurrence, and  $\xi_S^2$  for symmetric states and even (odd)-parity states were found. References [219, 220] showed that for a two-qubit Dicke system, parameter  $\xi_S^2$  is better than  $\xi_R^2$  to measure entanglement. A multipartite entanglement criterion for spin-squeezing parameter was given in Ref. [4]. Inspired by this work, some other generalized spin squeezing inequalities were proposed. In Refs. [26, 27], by employing a positive partial transpose method, they found generalized spin squeezing inequalities as criteria for two- and three-qubit entanglement. In Refs. [221, 28], optimal spin squeezing inequalities were proposed.

At the time when squeezing parameters  $\xi_S^2$  and  $\xi_R^2$  were proposed, Refs. [1, 2, 3] noticed the potential relationship between spin squeezing and entanglement. Since  $\xi_S^2 = 1$  for CSS, Ref. [1] expected that for an appropriate correlated state,  $\xi_S^2 < 1$ . As shown above, the one-axis twisting Hamiltonian can produce



squeezed states, and this Hamiltonian involves pairwise interactions. This indicates that spin squeezing is associated with pairwise entanglement.

To detect two-qubit entanglement, it was proven [26, 27, 222] that if the inequality

$$\left[ \langle J_{\bar{n}_1}^2 \rangle + \frac{N(N-2)}{4} \right]^2 \geq \left[ \langle J_{\bar{n}_2}^2 \rangle + \langle J_{\bar{n}_3}^2 \rangle - \frac{N}{2} \right]^2 + (N-1)^2 \langle J_{\bar{n}_1} \rangle^2 \quad (191)$$

is violated then the state is two-qubit entangled. For symmetric states, the above inequality is simplified to

$$1 - \frac{4 \langle J_{\bar{n}} \rangle^2}{N^2} \geq \frac{4 (\Delta J_{\bar{n}})^2}{N}, \quad (192)$$

and a symmetric state is two-qubit entangled if and only if it violates the above inequality.

Entanglement of two-qubit systems is characterized by the concurrence [14]. The concurrence  $C$ , quantifying the entanglement of a pair of qubits, is defined as [14]

$$C = \max(0, \lambda_1 - \lambda_2 - \lambda_3 - \lambda_4), \quad (193)$$

where the quantities  $\lambda_i$ 's are the square roots of the eigenvalues, in descending order, of the matrix

$$\varrho_{12} = \rho_{12}(\sigma_{1y} \otimes \sigma_{2y}) \rho_{12}^*(\sigma_{1y} \otimes \sigma_{2y}), \quad (194)$$

where  $\rho_{12}$  is the two-qubit density matrix, and  $\rho_{12}^*$  is the complex conjugate of  $\rho_{12}$ . From its definition (193), the concurrence  $C \geq 0$ , and the existence of two-qubit entanglement is equivalent to  $C > 0$ .

For example, we calculate the concurrence of a pure state

$$|\psi\rangle = a|00\rangle + b|01\rangle + c|10\rangle + d|11\rangle. \quad (195)$$

Then density matrix of  $|\psi\rangle$  is

$$\rho = |\psi\rangle\langle\psi|, \quad (196)$$

and its conjugate  $\rho^*$  is a pure state. Since  $\sigma_{1y} \otimes \sigma_{2y}$  is a unitary operation,

$$\tilde{\rho} = \sigma_{1y} \otimes \sigma_{2y} \rho_{12}^* \sigma_{1y} \otimes \sigma_{2y}, \quad (197)$$

is still a pure state. Therefore, the rank of  $\rho\tilde{\rho}$  is less than or equal to one, and it has at most one nonzero eigenvalue  $\lambda$ , and the concurrence

$$\begin{aligned} C &= \sqrt{\lambda} = \sqrt{\text{Tr}(\rho\tilde{\rho})} = |\langle\psi|\sigma_{1y} \otimes \sigma_{2y} (|\psi\rangle)^*| \\ &= 2|ad - bc|. \end{aligned} \quad (198)$$

If  $a = d = 1/\sqrt{2}$  and  $b = c = 0$ , then  $|\psi\rangle$  is the Bell state and is entangled since  $C = 1$ .

Following the previous discussion, we proceed to give a quantitative relation between the squeezing parameter and the concurrence for states with even (odd) parity and nonzero mean spin, i.e.,  $\langle J_z \rangle \neq 0$ . The two-spin reduced density matrix for a parity state with exchange symmetry can be written in a block-diagonal form [216]

$$\rho_{12} = \begin{pmatrix} v_+ & u^* \\ u & v_- \end{pmatrix} \oplus \begin{pmatrix} w & y \\ y & w \end{pmatrix}, \quad (199)$$

in the basis  $\{|00\rangle, |11\rangle, |01\rangle, |10\rangle\}$ , where

$$\begin{aligned} v_{\pm} &= \frac{N^2 - 2N + 4\langle J_z^2 \rangle \pm 4\langle J_z \rangle(N-1)}{4N(N-1)}, \\ w &= \frac{N^2 - 4\langle J_z^2 \rangle}{4N(N-1)}, \quad u = \frac{\langle J_+^2 \rangle}{N(N-1)}, \\ y &= \frac{4\langle J_x^2 + J_y^2 \rangle - 2N}{4N(N-1)}, \end{aligned} \quad (200)$$

which can be written in terms of local expectations as

$$v_{\pm} = \frac{1}{4} (1 \pm 2\langle\sigma_{1z}\rangle + \langle\sigma_{1z}\sigma_{2z}\rangle), \quad (201)$$

$$w = \frac{1}{4} (1 - \langle\sigma_{1z}\sigma_{2z}\rangle), \quad (202)$$

$$u = \langle\sigma_{1-}\sigma_{2-}\rangle, \quad (203)$$

$$y = \langle\sigma_{1+}\sigma_{2-}\rangle. \quad (204)$$

The concurrence is then given by [14]

$$C = 2 \max \{0, |u| - w, y - \sqrt{v_+v_-}\}. \quad (205)$$

From the above expressions we know that, the spin-squeezing parameters and concurrence are determined by the expectation value  $\langle\sigma_{1z}\rangle$ , correlations  $\langle\sigma_{1+}\sigma_{2-}\rangle$ ,  $\langle\sigma_{1-}\sigma_{2-}\rangle$ , and  $\langle\sigma_{1z}\sigma_{2z}\rangle$ .

Since  $\langle J^2 \rangle = N/2(N/2 + 1)$ , from Eq. (200), one can straightforwardly verify that

$$w = y. \quad (206)$$

Thus the concurrence given by Eq. (205) becomes

$$C = 2 \max \{0, |u| - y, y - \sqrt{v_+v_-}\}. \quad (207)$$

Since the density matrix should be positive, we find

$$\sqrt{v_+v_-} \geq |u|. \quad (208)$$

From this inequality, one may find that if  $|u| - y > 0$ , then  $y - \sqrt{v_+v_-} < 0$  and if  $y - \sqrt{v_+v_-} > 0$ ,  $|u| - y < 0$ . In other words, two quantities  $|u| - y$  and  $y - \sqrt{v_+v_-}$  cannot be simultaneously larger than zero.

Table 6: Spin squeezing parameters  $\xi_S^2$  and  $\tilde{\xi}_E^2$  as well as the concurrence  $C$  for parity states. Symbols are defined in the text

	Pairwise entangled ( $C > 0$ )		Unentangled
Concurrence	$C = 2( u  - y) > 0$	$C = 2(y - \sqrt{v_+v_-}) > 0$	$C = 0$
$\xi_S^2$	$\xi_S^2 = 1 - (N - 1)C < 1$	$\xi_S^2 > 1$	$\xi_S^2 \geq 1$
$\tilde{\xi}_E^2$	$\tilde{\xi}_E^2 = 1 - (N - 1)C < 1$	$\tilde{\xi}_E^2 = 1 - 2(N - 1)(y + \sqrt{v_+v_-})C < 1$	$\tilde{\xi}_E^2 \geq 1$

From Table 2 and Eqs. (203) and (204), we can write the spin-squeezing parameter  $\xi_S^2$  in terms of the reduced matrix elements  $u$  and  $y$  as

$$\xi_S^2 = 1 - 2(N - 1)(|u| - y). \quad (209)$$

Again from Table 2,  $\tilde{\xi}_E^2$  contains the quantity

$$\zeta^2 = 1 + (N - 1)\mathcal{C}_{zz}. \quad (210)$$

So, to write  $\tilde{\xi}_E^2$  in terms of the matrix elements, we consider the correlation function  $\mathcal{C}_{zz}$ . From Eqs. (201), (202), and (206), we obtain

$$y^2 - v_+v_- = -\frac{1}{4}\mathcal{C}_{zz}. \quad (211)$$

This is a key step. Thus, from Eq. (210), we have

$$\varsigma^2 = 1 - 4(N-1)(y + \sqrt{v_+v_-})(y - \sqrt{v_+v_-}). \quad (212)$$

From the above equation and Table 2, we obtain

$$\tilde{\xi}_E^2 = \min \{ \xi_S^2, 1 - 4(N-1)(y + \sqrt{v_+v_-})(y - \sqrt{v_+v_-}) \}. \quad (213)$$

The relations between spin squeezing and concurrence are displayed in Table 6. From it we can see that, for a symmetric state,  $\tilde{\xi}_E^2 < 1$  is qualitatively equivalent to  $C > 0$ , implying that spin squeezing according to  $\tilde{\xi}_E^2$  is equivalent to pairwise entanglement [223]. Although  $\xi_S^2 < 1$  indicates  $C > 0$ , when  $C = 2(y - \sqrt{v_+v_-}) > 0$ , we find  $\xi_S^2 > 1$ . Therefore, a spin-squeezed state ( $\xi_S^2 < 1$ ) is pairwise entangled, while a pairwise entangled state may not be spin-squeezed according to the squeezing parameter  $\xi_S^2$  [15].

Below, we give a simple example to illustrate the above results. Consider a simple superposition of Dicke states

$$|\psi_D\rangle = \cos\theta|j, m\rangle + e^{i\varphi}\sin\theta|j, m+2\rangle, \quad n = -j, \dots, j-2 \quad (214)$$

with the angle  $\theta \in [0, \pi)$  and the relative phase  $\varphi \in [0, 2\pi)$ , and  $j = N/2$ . This state is of even parity, and the MSD is along the  $z$  direction. The relevant spin-expectation values can be obtained as

$$\begin{aligned} \langle J_z \rangle &= m + 2\sin^2\theta, \\ \langle J_z^2 \rangle &= m^2 + 4(m+1)\sin^2\theta, \\ \langle J_-^2 \rangle &= \frac{1}{2}e^{i\varphi}\sin 2\theta\sqrt{\mu_m}, \end{aligned} \quad (215)$$

where  $\mu_m = (j+m+1)(j+m+2)(j-m)(j-m-1)$ . With the above results we find

$$\begin{aligned} u &= \frac{e^{i\varphi}\sin 2\theta}{2N(N-1)}\sqrt{\mu_m}, \\ y &= \frac{1}{N-1} \left\{ \frac{N}{4} - \frac{1}{N} [m^2 + 4(m+1)\sin^2\theta] \right\}, \\ \sqrt{v_+v_-} &= \frac{\sqrt{(N^2 - 2N + 4\langle J_z^2 \rangle)^2 - 16(N-1)^2\langle J_z \rangle^2}}{4N(N-1)}, \end{aligned} \quad (216)$$

and thus the spin-squeezing parameters are obtained as

$$\xi_S^2 = 1 - \frac{1}{N} \left\{ |\sin 2\theta| \sqrt{\mu_m} - 2 [m^2 + 4(m+1)\sin^2\theta] - \frac{N^2}{2} \right\}, \quad (217)$$

$$\varsigma^2 = \frac{4}{N} [m^2 + 4(m+1)\sin^2\theta] - \frac{4(N-1)}{N^2} [m + 2\sin^2\theta]^2. \quad (218)$$

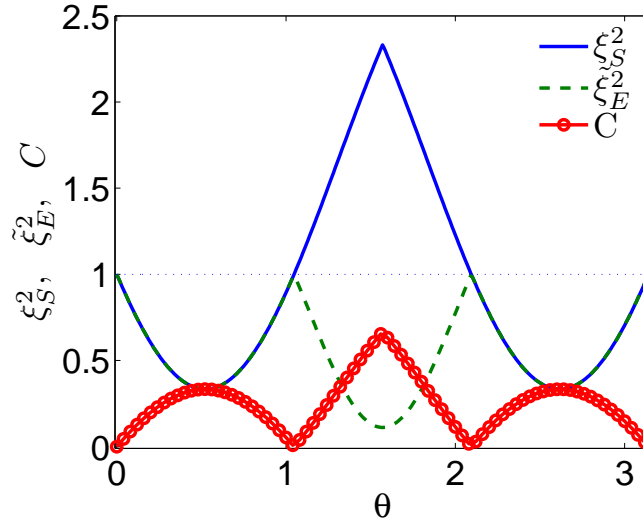


Figure 4: (Color online) Spin-squeezing parameters  $\xi_S^2$ ,  $\xi_E^2$  and concurrence  $C$  as a function of  $\theta$ , with  $N = 3$  and  $m = -N/2$ . The one-to-one correspondence between  $\xi_E^2$  and the concurrence  $C$  is very clear.

In Fig. 4, we plot these two spin-squeezing parameters and concurrence versus  $\theta$  within one period. The system size  $N = 3$  and  $m = -3/2$ . We observe that for  $\theta \in (0, \pi/3) \cup (2\pi/3, \pi)$ ,  $\xi_E^2 = \xi_S^2 < 1$ , therefore the state is spin-squeezed in the  $x$ - $y$  plane. Moreover, as  $C > 0$ , the state is pairwise entangled. For  $\theta \in (\pi/3, 2\pi/3)$ , it is obvious that the state is also pairwise entangled, since  $C > 0$ , while spin squeezing occurs in the  $z$ -axis since  $\xi_E^2 < 1$  and  $\xi_S^2 > 1$ . These results clearly show that  $\xi_E^2 < 1$  is equivalent to  $C > 0$ .

#### 4.3. Spin squeezing and many-body entanglement

To characterize and detect multipartite entanglement is one of the most challenging open problems in quantum information theory [9]. The simplest multipartite state is the three-qubit pure state, for which there exists a good measure of tripartite entanglement based on the concurrence [224]. One can also use the *state preparation fidelity*  $F$  for a  $N$ -qubit state  $\rho$  in order to investigate multipartite entanglement. The state  $\rho$  can be either pure or mixed. The fidelity  $F$  is defined as [225]

$$F(\rho) = \langle \Psi_{\text{GHZ}} | \rho | \Psi_{\text{GHZ}} \rangle, \quad (219)$$

where  $|\Psi_{\text{GHZ}}\rangle = 1/\sqrt{2}(|00\dots 0\rangle + |11\dots 1\rangle)$  is the  $N$ -particle Greenberger-Horne-Zeilinger (GHZ) state. The sufficient condition for  $N$ -particle entanglement is given by [225]

$$F(\rho) > 1/2. \quad (220)$$

We have the freedom to choose other GHZ states such as  $|\Psi_{\text{GHZ}}\rangle = 1/\sqrt{2}(|00\dots 01\rangle \pm |11\dots 10\rangle)$ , etc. By local unitary operations we can transfer these states to the original GHZ state and these operations do not change the entanglement. Detailed discussions on this sufficient condition can be found in Refs. [225, 226]. They also discussed how to use many-body Bell inequalities to detect multipartite entanglement.

Spin squeezing inequalities can act as entanglement criteria (see also Ref. [6]). To detect three-qubit entanglement, it has been proven that it is necessary to measure the third-order moments of the collective angular momenta [26, 27]. It was found that, for a state  $\rho$  and three orthogonal directions  $\vec{n}_1$ ,  $\vec{n}_2$ , and  $\vec{n}_3$ , if the following inequality [27]

$$-\frac{1}{3}\langle J_{\vec{n}_1}^3 \rangle + \langle J_{\vec{n}_2} J_{\vec{n}_1} J_{\vec{n}_2} \rangle - \frac{N-2}{2}\langle J_{\vec{n}_3}^2 \rangle + \frac{1}{3}\langle J_{\vec{n}_1} \rangle + \frac{N(N-1)(5N-2)}{24} < 0, \quad (221)$$

is satisfied, the state  $\rho$  possesses a genuine GHZ-type entanglement. If one of the following inequalities

$$\begin{aligned} & \langle J_{\bar{n}_3}^3 \rangle - 2\langle J_{\bar{n}_2} J_{\bar{n}_3} J_{\bar{n}_2} \rangle - 2\langle J_{\bar{n}_1} J_{\bar{n}_3} J_{\bar{n}_1} \rangle \\ & - \frac{N-2}{2} \left( 2\langle J_{\bar{n}_1}^2 \rangle + 2\langle J_{\bar{n}_2}^2 \rangle - \langle J_{\bar{n}_3}^2 \rangle \right) - \frac{N^2 - 4N + 8}{4} \langle J_{\bar{n}_3} \rangle + \frac{N(N-2)(13N-4)}{24} < 0, \end{aligned} \quad (222)$$

$$- \frac{1}{3} \langle J_{\bar{n}_1}^3 \rangle + \langle J_{\bar{n}_2} J_{\bar{n}_1} J_{\bar{n}_2} \rangle - \frac{N-2}{2} \langle J_{\bar{n}_3}^2 \rangle + \frac{1}{3} \langle J_{\bar{n}_1} \rangle + \frac{N^2(N-2)}{8} < 0, \quad (223)$$

are fulfilled, then the state  $\rho$  possesses a genuine 3-qubit entanglement.

#### 4.4. Spin-squeezing inequalities for higher spin- $j$ systems

The entanglement criteria presented above are all suitable for spin-1/2 systems. However, in most realistic experiments, atoms can have larger spins. In general, we cannot straightforwardly generalize the above criteria to spin- $j$  cases. To introduce the spin-squeezing inequality for higher-spin systems, we first consider the squeezing parameter  $\xi_R^2$  [227]. Unlike  $\xi_S^2$ , it is difficult to determine the minimum value of  $\xi_R^2$ , since its denominator is not a constant. To find the minimum value of  $\xi_R^2$ , which corresponds to the extreme spin squeezing, one can use the Lagrange multiplier method, to find the state that minimizes [227]

$$f = \mu \langle J_z \rangle + (\Delta J_x)^2. \quad (224)$$

Here the  $z$ -direction is assumed to be the MSD and  $\Delta J_x$  is the minimum variance in the  $x$ - $y$  plane. As discussed in Ref. [227], for integer spins the state that minimizes  $\Delta J_x$  for a given  $\langle J_z \rangle$  has vanishing  $\langle J_x \rangle$  and  $\langle J_y \rangle$ , thus  $f = \mu \langle J_z \rangle + \langle J_x^2 \rangle$ . To minimize  $f$ , one could find the ground state of  $H = \mu J_z + J_x^2$ , which is just a transverse-field one-axis twisting Hamiltonian. For half-integer spins, the problem becomes more difficult, since the state that minimizes  $\langle J_x^2 \rangle$  does not minimize  $\Delta J_x$  for a given  $\langle J_z \rangle$ , and then one cannot formulate the problem as the diagonalization of an operator containing a Lagrange multiplier term. A Monte Carlo variational calculation that minimizes  $f$  is presented in Ref. [227].

Now, consider states of  $N$  spin- $j$  particles. The collective spin operator is  $\vec{\mathcal{J}} \equiv \sum_i \vec{J}_i$ , with  $\vec{J}_i$  the spin operator for the  $i$ -th particle. A separable state of  $N$  spin- $j$  particles could also be represented as

$$\rho_{\text{sep}} = \sum_k p_k \rho_k^{(1)} \otimes \rho_k^{(2)} \otimes \dots \otimes \rho_k^{(N)}, \quad (225)$$

where  $\rho_k^{(i)}$  is the density matrix of the  $i$ -th spin- $j$  particle. For separable states, the variance of  $\mathcal{J}_x$  obeys the inequality [227]

$$(\Delta \mathcal{J}_x)^2 \geq \sum_k p_k \sum_{i=1}^N [(\Delta J_x)^2]_i^{(k)} \geq \sum_k p_k \sum_{i=1}^N j F_j \left( \frac{\langle J_z \rangle_i^{(k)}}{j} \right), \quad (226)$$

where the first inequality comes from the concavity of the variance, the function  $F_j(x)$  is the minimum variance of  $J_x$  divided by  $j$  for a given  $x$ ,  $x = \langle J_z \rangle_i^{(k)} / j$ , and  $F_j(x)$  is a convex function. Therefore, by considering Jensen's inequality, we have

$$\begin{aligned} (\Delta \mathcal{J}_x)^2 & \geq \sum_k p_k N j F_j \left( \frac{\sum_{i=1}^N \langle J_z \rangle_i^{(k)}}{N j} \right) \geq N j F_j \left( \sum_k p_k \frac{\sum_{i=1}^N \langle J_z \rangle_i^{(k)}}{N j} \right) \\ & = N j F_j \left( \frac{\langle \mathcal{J}_z \rangle}{N j} \right), \end{aligned} \quad (227)$$

and if the above inequality is violated, the spin- $j$  system is entangled.

Another entanglement criterion is based on the following inequality [228],

$$(\Delta J_x)^2 + (\Delta J_y)^2 + (\Delta J_z)^2 \geq N j, \quad (228)$$

which holds for separable states of a multipartite  $N$  spin- $j$  system. Based on this inequality, Ref. [228] gave a spin-squeezing parameter

$$\xi_{\text{singlet}}^2 = \frac{(\Delta J_x)^2 + (\Delta J_y)^2 + (\Delta J_z)^2}{J}, \quad (229)$$

where  $J = Nj$ . The subscript ‘singlet’ means that this parameter can detect entanglement in singlet states. It has been proven in Ref. [228] that, states satisfying

$$\xi_{\text{singlet}}^2 < 1 \quad (230)$$

are entangled. This inequality can be used to detect entanglement in the vicinity of many-qubit singlet states. These are pure states that are invariant under a simultaneous unitary rotation on all qubits. For example, for two qubits, the only state is the two-qubit singlet state, which is invariant under rotation.

#### 4.5. Two-mode spin-squeezed states

Spin squeezing discussed above is also called one-mode spin squeezing, which describes the fluctuations of collective spin operators  $\hat{J}_\alpha$  ( $\alpha = x, y, z$ ) of a total system. The two-mode spin squeezing [21, 229, 230] is analogous to the definition of the two-mode squeezing of continuous observables [144], and is proved to be a criterion of inseparability between spin variables of two separated atomic samples.

A bipartite system is separable if and only if its state can be written as

$$\rho = \sum_i p_i \rho_i^{(1)} \otimes \rho_i^{(2)}, \quad (231)$$

where  $p_i$  denotes the probability. In continuous case, it has been proven that [231, 232] the following inequality

$$\Delta \left( q^{(1)} + q^{(2)} \right)^2 + \Delta \left( p^{(1)} - p^{(2)} \right)^2 < 2 \quad (232)$$

is a sufficient condition for entanglement between subsystems 1 and 2. The continuous operators  $q^{(i)}$  and  $p^{(i)}$  belong to subsystems  $i$ , satisfying  $[q^{(k)}, p^{(l)}] = i\delta_{k,l}$  ( $k, l = 1, 2$ ).

For spin systems, the observables of interest are spin operators

$$\hat{J}_\alpha^{(\pm)} = \hat{J}_\alpha^{(1)} \pm \hat{J}_\alpha^{(2)}. \quad (233)$$

The usual criterion for two-mode spin squeezing is [233]

$$\left( \Delta J_z^{(+)} \right)^2 + \left( \Delta J_y^{(-)} \right)^2 < \left\langle J_x^{(+)} \right\rangle. \quad (234)$$

It has been shown that [21, 230, 234], two-mode spin squeezing implies entanglement between spin components of the two subsystems. Furthermore, for pure states of two spin systems of equal dimension, two-mode spin squeezing after application of local unitaries is a necessary condition for entanglement, except for a set of bipartite pure states of measure zero [233]. Account for the Heisenberg-Weyl algebra discussed in Sec. 2.9, Eq. (234) can reduce to Eq. (232). In Refs. [21, 230, 234], two spatially separated atomic ensembles, each containing about  $10^{12}$  Cs atoms, were entangled for 0.5 ms via interacting with a polarized field. The entangled state generated in this experiment is similar to a two-mode squeezing but not the maximally entangled state. Besides, the two-mode spin-squeezed states can also be generated via QND measurement with feedback [235]. Due to the considerable long lifetime of entanglement, two-mode spin squeezing was proposed to be a valuable resource of quantum information, and could be used to perform atomic quantum state teleportation and swapping [229, 230].

## 5. Spin squeezing, Fisher information, and quantum metrology

As discussed previously, the squeezing parameter  $\xi_R^2$  characterizes the sensitivity of a state with respect to SU(2) rotations, and has been studied in quantum metrology. In this section, we first introduce the QFI [236, 172, 237, 238], which determines the precision of the parameter estimation. Then, we discuss the relation between QFI and spin squeezing [239, 240, 241, 242]. Finally, we discuss the applications of spin squeezing and QFI in entanglement enhanced quantum metrology, where the Ramsey and Mach-Zehnder interferometers are discussed.

### 5.1. Quantum Fisher information

The Fisher information measures the amount of information of a parameter that we can extract from a probability distribution. It determines how precise we can attain when estimate a parameter, and with a larger Fisher information we can estimate the parameter with higher precision. Firstly, we begin with a brief discussion about the Fisher information in probability theory, and for more information please refer to Chapter 13 in Ref. [238]. In the regime of the parameter estimation theory, the central problem is to estimate the parameter  $\lambda$  in a probability distribution  $p(x|\lambda)$ , where  $x$  is the random variable, and below we only consider the single parameter case.

The minimum variance of our estimation is determined by the Fisher information. Consider a general distribution  $p(x|\lambda)$ , to estimate the parameter  $\lambda$ , we construct an estimator  $E(x)$  which is a map from the experimental data  $x$  to the parameter  $\lambda$ . The expectation value of the estimator is

$$\langle E(x) \rangle = \int dx p(x|\lambda) E(x). \quad (235)$$

We consider the case  $\langle E(x) \rangle = \lambda$ , i.e., so-called unbiased estimation, thus we have

$$\int dx p(x|\lambda) [E(x) - \lambda] = 0. \quad (236)$$

Differentiating both sides with respect to  $\lambda$  gives

$$\int dx p(x|\lambda) L(x, \lambda) [E(x) - \lambda] = 1, \quad (237)$$

where

$$L(x, \lambda) = \frac{\partial \ln p(x|\lambda)}{\partial \lambda}. \quad (238)$$

Now, square both sides of Eq. (237) and use the Cauchy-Schwarz inequality:

$$|\langle f, g \rangle|^2 \leq \langle f, f \rangle \langle g, g \rangle, \quad (239)$$

we obtain the Cramér-Rao inequality:

$$(\Delta E(x))^2 \geq \frac{1}{N \mathcal{I}_\lambda}, \quad (240)$$

where

$$(\Delta E(x))^2 = \int dx p(x|\lambda) [E(x) - \lambda]^2 \quad (241)$$

is the variance of  $E(x)$ , and

$$\mathcal{I}_\lambda = \int dx p(x|\lambda) L(x, \lambda)^2 \quad (242)$$

is the Fisher information with respect to  $\lambda$ .  $N$  is the number of independent experiments (here  $N = 1$ ), i.e., by repeating the experiment  $N$  times, the precision of  $E(x)$  is improved by  $1/N$ . In practice, we need to maximize the precision of  $\lambda$ , while this is fundamentally limited by the Fisher information  $\mathcal{I}_\lambda$ , which can

be regarded as the amount of information of  $\lambda$  that we can get from  $p(x|\lambda)$ , i.e., with more information, we can make more precise estimation.

Now we turn to discuss the QFI [236, 237, 238], which is the extension of the classical Fisher information in the quantum regime. Consider an  $n \times n$  density matrix  $\rho(\lambda)$ , by performing the positive operator valued measure (POVM)  $\{P_i\}$ , the parameter  $\lambda$  resides in the outcomes probability as

$$p_i(\lambda) = \text{Tr}(\rho(\lambda) P_i). \quad (243)$$

According to Eq. (242), we have

$$\mathcal{I}_\lambda = \sum_i \frac{(\text{Re}\{\text{Tr}[L_\lambda \rho(\lambda) P_i]\})^2}{p_i(\lambda)}, \quad (244)$$

where  $L_\lambda$  is the so-called symmetric logarithmic derivative determined by the following equation

$$\frac{\partial \rho(\lambda)}{\partial \lambda} = \frac{1}{2} [\rho(\lambda) L_\lambda + L_\lambda \rho(\lambda)]. \quad (245)$$

The operator  $L_\lambda$  is a quantum analogy of  $L(x, \lambda)$  in Eq. (238). Thus, a set of POVM yields a corresponding probability distribution, which gives the Fisher information  $\mathcal{I}_\lambda$  of the parameter  $\lambda$ . It was proven that [243]

$$\mathcal{I}_\lambda \leq F_\lambda = \text{Tr}[\rho(\lambda) L_\lambda^2], \quad (246)$$

where  $F_\lambda$  is the QFI, which is measurement-independent. The explicit expression of the QFI is given by

$$F_\lambda = \sum_{i=1}^k \frac{(\partial_\lambda p_i)^2}{p_i} + \sum_{i \neq j}^k \frac{2(p_i - p_j)^2}{p_i + p_j} |\langle \varphi_i | \partial_\lambda \varphi_j \rangle|^2, \quad (k \leq n), \quad (247)$$

where  $p_i$  and  $|\varphi_i\rangle$  are the  $i$ th nonzero eigenvalue and eigenvector of  $\rho(\lambda)$ . Therefore, they are all functions of the parameter  $\lambda$ . The probability distribution that gives the maximum Fisher information, i.e. the QFI, is produced by the optimal POVM built of the eigenprojectors of  $L_\lambda$ . However, in some cases  $L_\lambda$  is not a proper physical observable, and the corresponding POVM cannot be realized in experiments, thus the QFI is not always attainable.

The role of the QFI in parameter estimation is given by the quantum Cramér-Rao bound [236, 237],

$$(\Delta \hat{\lambda})^2 \geq (\Delta \lambda)_{\text{QCB}}^2 \equiv \frac{1}{N_m F_\lambda}, \quad (248)$$

where  $N_m$  is the number of independent experiments,  $\hat{\lambda}$  is the so-called unbiased estimator of the parameter  $\lambda$ , i.e.  $\langle \hat{\lambda} \rangle = \lambda$ . Indeed,  $\hat{\lambda}$  is a map from the experimental data to the parameter space. The Cramér-Rao bound gives the ultimate limit for the precision of  $\lambda$  that can be achieved. In a sense, parameter estimation is equivalent to distinguishing neighboring states along the path in parameter space. The QFI has a more intuitive geometric explanation, and it is the geometric metric of the state  $\rho(\lambda)$  in parameter space, since

$$F_\lambda (d\lambda)^2 = 4(ds_B)^2, \quad (249)$$

where  $(ds_B)^2$  is the Bures distance [244]. Thus, the Fisher information is equivalent to the so-called fidelity susceptibility [245], that has been extensively studied for characterizing QPT.

## 5.2. Spin squeezing and quantum Fisher information

Recently, it has been found that QFI gives a more stringent criterion for entanglement than the spin-squeezing parameter  $\xi_R^2$  [239, 241]. However, for identical particles, it was shown that [162, 163], neither spin squeezing nor quantum Fisher information is an entanglement witness. Below, we deal with distinguishable particles. Consider an ensemble of  $N$  spin-1/2 particles represented by a density matrix  $\rho$ . The QFI with respect to  $\theta$  is given by

$$F[\rho(\theta), J_{\vec{n}}] = \text{Tr}[\rho(\theta) L_\theta^2], \quad (250)$$



where

$$\rho(\theta) = \exp(-i\theta J_{\vec{n}}) \rho \exp(i\theta J_{\vec{n}}), \quad (251)$$

and  $J_{\vec{n}}$  is the generator of the rotation along the direction  $\vec{n}$ . For pure states, the QFI becomes [239]

$$F[\rho(\theta), J_{\vec{n}}] = 4(\Delta J_{\vec{n}})^2. \quad (252)$$

For mixed states

$$F[\rho(\theta), J_{\vec{n}}] \equiv \sum_{i \neq j} \frac{2(p_i - p_j)^2}{p_i + p_j} |\langle \varphi_i | J_{\vec{n}} | \varphi_j \rangle|^2. \quad (253)$$

Comparing Eq. (247) with Eq. (253), there are no derivatives of  $p_i$ , since the transformation in Eq. (251) does not change the eigenvalues of  $\rho$ . Actually, as explained in the previous section,  $F[\rho(\theta), J_{\vec{n}}]$  characterizes the geometric properties of  $\rho$  with respect to rotation, and is the rotational sensitivity of the state, thus we need not to perform a true rotation.

According to Eq. (248), the lower bound of the uncertainty of  $\theta$  is given by

$$(\Delta\theta)_{\text{QCB}}^2 = \frac{1}{F[\rho(\theta), J_{\vec{n}}]}, \quad (254)$$

where we set  $N_m = 1$ . If we measure the angular momentum operator  $J$ , the lower bound of  $\Delta\theta$  becomes

$$(\Delta\theta)_{\text{SS}}^2 = \frac{\xi_R^2}{N}, \quad (255)$$

where  $\xi_R^2$  is the spin-squeezing parameter. Since the Cramér-Rao bound [236, 237] gives the ultimate limit of the precision of  $\theta$ , we must have

$$(\Delta\theta)_{\text{QCB}}^2 \leq (\Delta\theta)_{\text{SS}}^2, \quad (256)$$

and thus

$$\chi^2 \equiv \frac{N}{F[\rho(\theta), J_{\vec{n}}]} \leq \xi_R^2, \quad (257)$$

which was proved in Ref. [239]. They also proved that if

$$\chi^2 < 1, \quad (258)$$

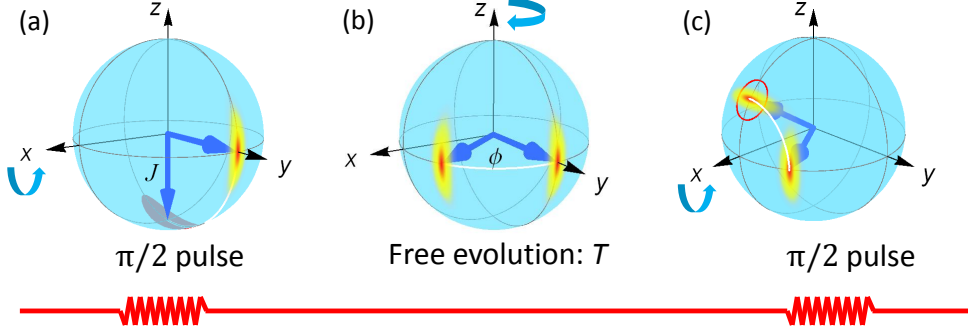
the state is entangled. It is known that  $\xi_R^2 < 1$  also indicates entanglement. Thus,  $\chi^2 < 1$  is more stringent than  $\xi_R^2 < 1$  in detecting multipartite entanglement, regarding the cases when  $\chi^2 < 1$  and  $\xi_R^2 \geq 1$ .

The inequality (257) can be readily proven when  $\rho(\theta)$  is a pure state, since in this case the QFI is just as Eq. (252). By using the Heisenberg uncertainty relation, we have

$$F[\rho(\theta), J_{\vec{n}'_{\perp}}] (\Delta J_{\vec{n}_{\perp}})^2 \geq |\langle J_{\vec{n}} \rangle|^2, \quad (259)$$

where the directions  $\vec{n}_{\perp}$ ,  $\vec{n}'_{\perp}$ , and  $\vec{n}$  are orthogonal to each other. Then, according to the definitions of  $\xi_R^2$  and  $\chi^2$ , we can obtain the inequality (257). Both the spin-squeezing parameters and the QFI could be used as criteria for entanglement, which is a resource for high-precision measurements. Note that, generally, it is difficult for experiments to achieve the precision given theoretically by the QFI due to practical difficulties of the measurements.

### Ramsey interferometer



### Mach-Zehnder interferometer

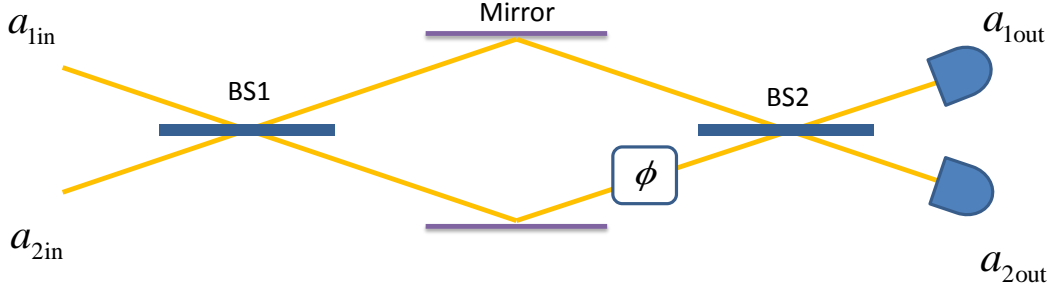


Figure 5: (Color online) Schematic diagrams of the Ramsey (above) and Mach-Zehnder (below) interferometers. For the Ramsey interferometer, the blue arrows represent the states of the spin. The uncertainty of the spin components are represented by the elliptical multi-color disks. The red circle in (c) represent the uncertainty of a CSS. For the Mach-Zehnder interferometer, two beams injected from both sides of the first beam splitter, BS1. The parameter  $\phi$  is the phase difference gained between the two beam splitters BS1 and BS2. After the second beam splitter, BS2, photon numbers are detected, and the number difference between the two detectors is related to the phase difference  $\phi$ . The two beam splitters correspond to the two  $\pi/2$  pulses in the Ramsey process (a) and (c).

### 5.3. Spin squeezing, Fisher information and metrology

Here, we discuss spin squeezing and QFI in quantum metrology [172, 246, 247, 248, 249]. In general, we cannot access parameters of a state or a Hamiltonian directly, since they are not physical observables. But in many cases, the parameter is related to an observable, like in the Ramsey spectroscopy, where the phase  $\phi$  gained in the free evolution is related to the population differences, and the parameters can also be obtained via Landau-Zener-Stckelberg interferometry [31]. This parameter estimation scheme is illustrated below,

$$\begin{aligned}
 &\text{Prepare a state } \rho, \\
 &\quad \downarrow \\
 &\text{Quantum evolution } \rho_\phi = U(\phi) \rho U^\dagger(\phi), \\
 &\quad \downarrow \\
 &\text{Measurement } \langle \hat{O} \rangle_\phi = \text{Tr} [\hat{O} \rho_\phi], \tag{260}
 \end{aligned}$$

where the information of the parameter  $\phi$  is contained in the measurement result  $\langle \hat{O} \rangle_\phi$ , and in some cases the observable  $\hat{O}$  cannot be accessed directly, and this was studied in Ref. [250]. The fluctuation of the

observable  $\hat{O}$  is unavoidable, and the variance of  $\phi$  is

$$\Delta\phi = \frac{(\Delta\hat{O})_\phi}{\left|\partial\langle\hat{O}\rangle_\phi/\partial\phi\right|}. \quad (261)$$

Since  $\phi$  is periodic, its mean and variance are not calculated as non-periodic variables, and this should be declared. To calculate the mean of  $\phi$ , we first obtain the mean of  $\hat{O}$ , that is  $\langle\hat{O}\rangle_\phi$ . Then the mean of  $\phi$  is the inverse function of  $\langle\hat{O}\rangle_\phi$ . For more details, please refer to Ref. [251]. Since in many cases the evolution processes are fixed (or hard to change), we can reduce the variance of  $\phi$  by choosing an appropriate initial state  $\rho$  and operator  $\hat{O}$ . When we measure  $J_z$ , the precision is given by squeezing parameter  $\xi_R^2$  as shown in Eq. (65).

We first give a brief summary of Ramsey processes, shown in Fig. 5. Consider an ensemble of  $N$  two-level particles interacting with an applied magnetic field  $\vec{B}$ . The Hamiltonian of the two-level particles

$$H = -\vec{\mu} \cdot \vec{B}, \quad (262)$$

where  $\vec{\mu} = \mu_0\vec{J}$  is the magnetic moment and  $\vec{B} = B_0\vec{n}_z + \vec{B}_1$ , with a static magnetic field

$$B_0 = -\hbar\omega_0/\mu_0, \quad \mu_0 < 0, \quad (263)$$

and a time-dependent field

$$\vec{B}_1 = B_1 [\vec{n}_x \cos(\omega t) + \vec{n}_y \sin(\omega t)]. \quad (264)$$

The Hamiltonian now becomes

$$H = \hbar\omega_0 J_z + \frac{\hbar\Omega_R}{2} (J_+ e^{-i\omega t} + \text{h.c.}), \quad (265)$$

where  $\Omega_R = |\mu_0 B_1|/\hbar$  is the Rabi frequency. It is convenient to use a frame of reference rotating around  $B_0$  with frequency  $\omega$ ,

$$H_R = \hbar(\omega_0 - \omega) J_z + \hbar\Omega_R J_x, \quad (266)$$

where the second term in Eq. (266) acts as a pulse. When this pulse is applied, the above Hamiltonian is approximated as

$$H_R \simeq \hbar\Omega_R J_x, \quad (267)$$

since  $\Omega_R \gg |\omega_0 - \omega|$ .

As shown in Fig. (5), the Ramsey interferometry consists of two  $\pi/2$ -pulses of length  $t_{\pi/2} = \pi/(2\Omega_R)$  and a free evolution of length  $t$ . The first pulse plays as a  $\pi/2$  rotation around the  $x$ -axis. Thereafter, during the free-evolution period, when  $B_1 = 0$ , the state vector precesses about the  $z$ -axis and acquires a phase  $\phi = (\omega - \omega_0)t$ . Assuming  $t \gg t_{\pi/2}$ , the time of the entire process is

$$t_f = 2t_{\pi/2} + t \simeq t. \quad (268)$$

After the free period, followed by a second Ramsey pulse, the spin direction is rotated around the  $x$ -axis by  $\pi/2$ . The the initial state evolves to

$$|\psi(t)\rangle = U|\psi(0)\rangle,$$

where the unitary operator is

$$\begin{aligned} U &= \exp\left(-i\frac{\pi}{2}J_x\right) \exp(i\phi J_z) \exp\left(-i\frac{\pi}{2}J_x\right) \\ &= \exp(-i\phi J_y) \exp(-i\pi J_x). \end{aligned} \quad (269)$$

Then we could measure the number of atoms in the excited energy level  $|0\rangle$  to estimate  $\phi$ . This is equivalent to measuring  $J_z$ :

$$\langle J_z \rangle_t = \langle J_x \rangle_{t=0} \sin \phi - \langle J_z \rangle_{t=0} \cos \phi, \quad (270)$$

where the subscript  $t$  denotes the time, and in the right-hand side, the average  $\langle \cdot \rangle_{t=0}$  is carried out using the initial state. From the evolution operator  $U$ , we can further find the variance

$$(\Delta J_z)_t^2 = \cos^2 \phi (\Delta J_z)_{t=0}^2 + \sin^2 \phi (\Delta J_x)_{t=0}^2 - \sin(2\phi) \text{Cov}(J_x, J_z)_{t=0}. \quad (271)$$

Then  $\omega_0$  is related to the measurement data of  $\langle J_z \rangle$  via

$$\omega_0 = \omega + \frac{1}{t} \arccos \left( -\frac{\langle J_z \rangle_t}{\langle J_z \rangle_{t=0}} \right). \quad (272)$$

In practice, we repeat the above procedure  $N_m$  times, with a total experimental time  $T = N_m t$ . Then, we can estimate  $\phi$  with the uncertainty

$$(\Delta \phi)^2 = \frac{(\Delta J_z)_t^2}{N_m |\partial \langle J_z \rangle_t / \partial \phi|^2}, \quad (273)$$

which is obtained by using the propagation of the fluctuation (261). Below, we set  $N_m = 1$ .

From Eqs. (270) (271) and (273), the phase uncertainty is related to the initial states and the phase. Below, we discuss the uncertainty of  $\phi$  for different initial states. If the initial state is prepared as a CSS

$$|\psi(0)\rangle_{\text{CSS}} = |j, -j\rangle = |1\rangle^{\otimes N}, \quad (274)$$

i.e., all the atoms are prepared in their ground states and the spin vector points in the  $-z$  direction, as shown in Fig. 13. For this initial state shown in Eq. (274), we can find

$$(\Delta \phi)_{\text{CSS}}^2 = \frac{1}{N}, \quad (275)$$

which is the shot-noise limit, and we have already known in Sec. 2.5 since  $\xi_R^2 = 1$  for a CSS. We can also obtain  $F_\phi = 1$  by using Eq. (247).

Next, we consider a spin-squeezed state

$$|\psi(0)\rangle_{\text{SSS}} = \frac{1}{\sqrt{2}} \left[ |j, 0\rangle_x - \frac{1}{\sqrt{2}} (|j, +1\rangle_x + |j, -1\rangle_x) \right], \quad (276)$$

where the subscript  $x$  denotes the state is the eigenstate of  $J_x$ , i.e.,  $J_x |j, m\rangle_x = m |j, m\rangle_x$ . This state was studied in Ref. [212], the expectation values are

$$\begin{aligned} \langle J_x \rangle_{t=0} &= \langle J_y \rangle_{t=0} = \text{Cov}(J_x, J_z) = 0, \\ \langle J_z \rangle_{t=0} &= \sqrt{\frac{j(j+1)}{2}}, \end{aligned} \quad (277)$$

and

$$\begin{aligned} (\Delta J_x)_{t=0}^2 &= \frac{1}{2}, \\ (\Delta J_y)_{t=0}^2 &= \frac{3}{8} j(j+1) - \frac{1}{4}, \\ (\Delta J_z)_{t=0}^2 &= \frac{1}{8} j(j+1) - \frac{1}{4}. \end{aligned} \quad (278)$$

This state is spin squeezed, since

$$\xi_R^2 = \frac{2}{N/2 + 1}, \quad (279)$$

and the phase uncertainty is optimized at  $\phi \simeq \pi/2$ ,

$$(\Delta\phi)_{\text{SSS}}^2 = \frac{1}{j(j+1)} \propto \frac{1}{N^2}, \quad (280)$$

which attains the Heisenberg limit.

Now, we take the initial state to be a maximally entangled state

$$|\psi(0)\rangle_{\text{GHZ}} = \frac{1}{\sqrt{2}} (|j, j\rangle_y + |j, -j\rangle_y), \quad (281)$$

which is the  $N$ -body GHZ state, or the NOON state in quantum optics. We emphasize that, for this state the phase cannot be estimated by measuring the population difference  $J_z$ , since

$$\langle J_z \rangle_{t=0} = \langle J_x \rangle_{t=0} = 0, \quad (282)$$

that means we cannot get any information about  $\phi$ , and the spin squeezing parameter  $\xi_R^2$  is divergent. On the other hand, after the Ramsey process

$$|\psi(\phi)\rangle_{\text{GHZ}} = U|\psi(0)\rangle_{\text{GHZ}} = \frac{1}{\sqrt{2}} (|j, j\rangle_y + e^{-iN\phi}|j, -j\rangle_y). \quad (283)$$

By using Eq. (247) we find its QFI  $F_\phi = N^2$ , which implies that the precision of  $\phi$  could attain the Heisenberg limit. To achieve this precision, we should measure the parity operator [33, 37, 252]

$$P \equiv \prod_{i=1}^N \sigma_{iz}. \quad (284)$$

The expectation values and variances of  $P$  under the state  $|\psi(\phi)\rangle_{\text{GHZ}}$  are

$$\langle P \rangle_t = \cos N\phi, \quad \langle P^2 \rangle_t = 1, \quad (285)$$

thus the optimal phase uncertainty

$$(\Delta\phi)_{\text{GHZ}}^2 = \frac{1}{N^2} \quad (286)$$

is attained when  $N\phi \simeq \pi/2$ , which is the Heisenberg-limit uncertainty. Although the Heisenberg-limit precision is attained, we should note that, the parity operator  $P$  shown in Eq. (284) is not easy to measure in experiment as compared with the angular momentum operators, especially when  $N$  is large. Additionally, it is also difficult to prepare an  $N$ -body GHZ state with nowadays techniques. In summary, both spin squeezing and QFI are related to the precision in phase estimation. Metrology based on spin squeezing is comparatively easy to implement in experiments, while the ultimate precision is determined by the QFI.

In the end we give a brief review about the Mach-Zehnder interferometer, which can be regarded as an optical version Ramsey interferometer. It consists of two beam splitters (BS) and two mirrors, and the schematic diagram is shown in Fig. 5. Light beams passing through the Mach-Zehnder interferometer undergo transformations as

$$\begin{pmatrix} a_{1\text{out}} \\ a_{2\text{out}} \end{pmatrix} = V_{\text{BS}} V_\phi V_{\text{BS}} \begin{pmatrix} a_{1\text{in}} \\ a_{2\text{in}} \end{pmatrix}, \quad (287)$$

where  $a_i$  ( $i = 1, 2$ ) are the annihilation operators of the  $i$ th path, and

$$V_{\text{BS}} = \exp\left(i\frac{\alpha}{2}\sigma_x\right) = \begin{pmatrix} \cos\frac{\alpha}{2} & i\sin\frac{\alpha}{2} \\ i\sin\frac{\alpha}{2} & \cos\frac{\alpha}{2} \end{pmatrix}, \quad (288)$$

denotes the transform of the BS,  $R = \sin(\alpha/2)^2$  and  $T = \cos(\alpha/2)^2$  are the transmission and reflection rates, respectively. The image number  $i$  arises from the half-wave loss. Below, we consider the 50-50 BS,

that is  $\alpha = \pi/2$ , which acts as the two  $\pi/2$  pulses in the Ramsey process. The difference between the two path lengths gives rise to a phase difference  $\phi$ , and can be represented by acting the transform

$$V_\phi = \exp\left(-i\frac{\phi}{2}\sigma_z\right) = \begin{pmatrix} e^{-i\phi/2} & 0 \\ 0 & e^{i\phi/2} \end{pmatrix} \quad (289)$$

on modes  $a_1$  and  $a_2$ . It is convenient to manipulate these transformations in the Schwinger representation (151) as

$$J_{\alpha,\text{out}} = \left(a_{1\text{out}}^\dagger, a_{2\text{out}}^\dagger\right) \frac{\sigma_\alpha}{2} \begin{pmatrix} a_{1\text{out}} \\ a_{2\text{out}} \end{pmatrix} = U J_{\alpha,\text{in}} U^\dagger, \quad (\alpha = x, y, z), \quad (290)$$

where the unitary transform  $U$  is just as Eq. (269). At the output-port, the information of the phase  $\phi$  is obtained via detecting the photon number difference. Since the Mach-Zehnder interferometry is an optical instrument, it is not easy to prepare well-defined number of photons, unlike the Ramsey interferometer, where the atom number is conserved.

## 6. Spin squeezing, quantum phase transitions, and quantum chaos

In this section, we discuss the applications of spin squeezing in identifying QPTs [253] and quantum chaos [254]. For this task, spin squeezing mainly has three advantages: (i) It is comparatively easy to be measured. (ii) It is an entanglement witness. (iii) It characterizes the sensitivity of a state with respect to SU(2) rotations, thus is promising to detect quantum chaos.

The QPTs occur at absolute zero temperature, and is driven purely by quantum fluctuations. Conventionally, QPTs were first studied by Landau's order parameter theory in the framework of statistics and condensed matter physics. When a QPT occurs, the ground state can change drastically, and the correlation length diverges. Therefore, considering these intrinsic properties of QPT, researchers investigated it by using concepts borrowed from quantum information [11, 12], such as quantum entanglement [9, 6] and fidelity [255]. As discussed previously, spin squeezing is closely related to entanglement, and it is easier to measure experimentally. Therefore, it is desirable to study spin squeezing in QPTs.

Then we discuss using spin squeezing as a signature of quantum chaos. In classical regime, one of the most distinct feature of chaos is the extreme sensitivity of the trajectories with respects to perturbation, however, in the quantum world due to the unitarity of quantum evolutions, the overlap (or fidelity) between two initially separated states is invariant during the evolution, and thus there is no well-accepted definition of quantum chaos. To solve this problem, various signatures of quantum chaos have been identified [254, 256, 257]. Entanglement and spin squeezing [1, 3], which are pure quantum effects, have also been identified as signatures of quantum chaos. Recently, entanglement, measured by the linear entropy, as a signature of quantum chaos has been demonstrated experimentally in an atomic ensemble [258]. The experimental results and the theoretical predictions coincide very well [258].

### 6.1. Spin squeezing and quantum phase transitions in the Lipkin-Meshkov-Glick model

Below, we discuss the spin squeezing for the ground state of the Lipkin-Meshkov-Glick model [259], which occurs a typical second-order QPT [222, 260]. It has been widely studied statistical mechanics of quantum spin system [261], Bose-Einstein condensations [262], and superconducting circuits [263]. It is an exactly solvable [264, 265] many-body interacting quantum system, as well as one of the simplest to show a quantum transition in the strong coupling regime. It is convenient to discuss spin squeezing in this model, since it consists of collective spin operators.

The Hamiltonian of the Lipkin-Meshkov-Glick model reads

$$H = -\frac{\lambda}{N} (J_x^2 + \gamma J_y^2) - h J_z, \quad (291)$$

where  $J_\alpha = \sum_{i=1}^N \sigma_\alpha^i/2$  ( $\alpha = x, y, z$ ) are the collective spin operators;  $\sigma_\alpha^i$  are the Pauli matrices;  $N$  is the total spin number;  $\gamma \in [0, 1]$  is the anisotropic parameter;  $\lambda$  and  $h$  are the spin-spin interaction strengths

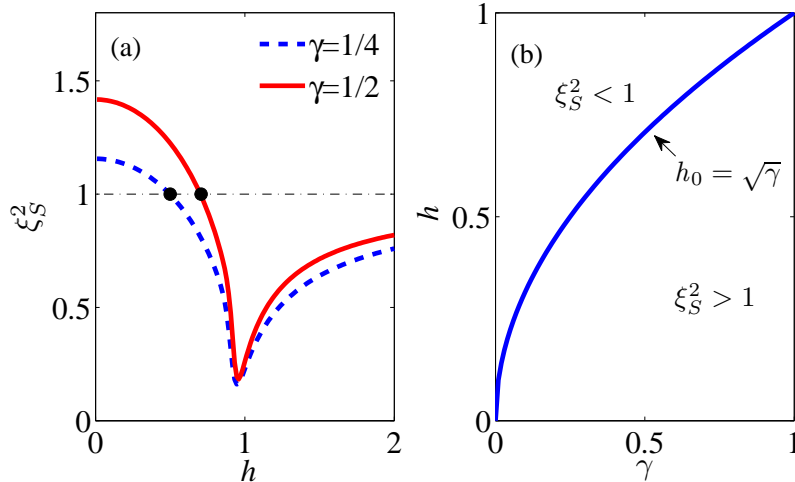


Figure 6: (Color online) Squeezing parameter  $\xi_S^2$  versus the applied magnetic field  $h$  (a), and the ‘phase diagram’ of spin squeezing in the  $h-\gamma$  plane (b), for the ground state of the Lipkin-Meshkov-Glick model. The system size used here is  $N = 2^7$ . The maximal squeezing occurs at the critical point. The two black dots denote  $\xi_S^2 = 1$ , at these points the ground states are coherent spin states. In (b), we show the squeezed and non-squeezed regions that are separated by  $h_0 = \sqrt{\gamma}$ ,  $\xi_S^2 = 1$  in the thermodynamic limit.

and the effective external field, respectively. Here we set  $\lambda = 1$ , where the Lipkin-Meshkov-Glick model describes ferromagnetism. The QPT of this model originates from the competition between the spin-spin interaction and the external field. With mean-field approach [266]; we can see that, when  $h > 1$ , all spins tends to be polarized in the field direction ( $\langle \sigma_z^i \rangle = 1$ ). However, when  $h < 1$ , it is two-fold degenerate with  $\langle \sigma_z^i \rangle = h$ . Therefore, a spontaneous symmetry breaking occurs at  $h = 1$ , which is a second-order QPT point between the so-called symmetric ( $h \geq 1$ ) phase and symmetry broken ( $h < 1$ ) phase. However, by considering the quantum effects, the exact ground state is not degenerate in the symmetry broken phase ( $\gamma \neq 1$ ). Since the Hamiltonian is of spin-flip symmetry, i.e.,  $[H, \prod_{i=1}^N \sigma_z^i] = 0$ , we have  $\langle J_x \rangle = \langle J_y \rangle = 0$ ,  $\langle J_x J_z \rangle = \langle J_y J_z \rangle = 0$ , and the MSD is along the  $z$  direction. In addition,  $[H, \mathbf{J}^2] = 0$ , and the ground state lies in the  $j = N/2$  symmetric sector.

In the isotropic case,  $\gamma = 1$ , the ground state is simply the Dicke state, as discussed in Sec. 2, and  $\xi_{S,R}^2 \geq 1$  for all Dicke state, indicating that there is no spin squeezing with respect to  $\xi_S^2$  and  $\xi_R^2$ . For the Dicke state  $|j, m\rangle$ , we have

$$\tilde{\xi}_E^2 = \frac{m^2}{j^2} \leq 1, \quad (292)$$

thus the squeezing occurs along the  $z$ -axis direction with respect to  $\tilde{\xi}_E^2$ .

In the anisotropic case,  $\gamma \neq 1$ , there is a second-order QPT. Since the system is of exchange symmetry, and the ground state has a fixed parity,  $\xi_S^2$  and  $\tilde{\xi}_E^2$  are closely related to the concurrence, as demonstrated in Refs. [222, 260, 223]. In the thermodynamic limit, we could calculate the squeezing parameter by using the Holstein-Primakoff transformation. The results are [240]

$$\xi_S^2 = \begin{cases} \sqrt{(h-1)/(h-\gamma)}, & \text{for } h \geq 1, \\ \sqrt{(1-h^2)/(1-\gamma)}, & \text{for } h < 1. \end{cases} \quad (293)$$

As shown in Fig. 6, there is no spin squeezing when  $h$  is smaller than  $h_0 = \frac{N-1}{N} \sqrt{\gamma}$ . At the point  $h = h_0$ , the ground state is a CSS, for which the squeezing parameters are equal to one.

To demonstrate the QPT, we calculate the values of  $\xi_S^2$  and  $\partial_h \xi_S^2$  in the vicinity of the critical point.

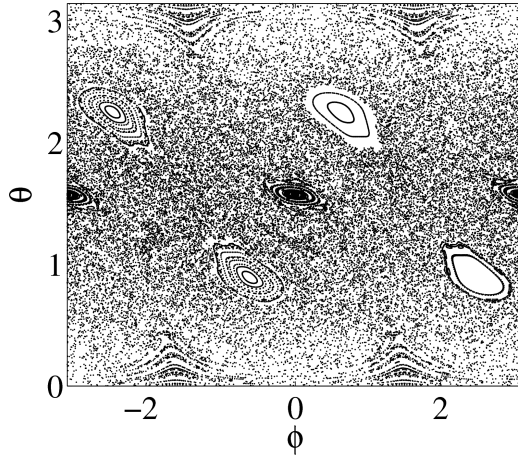


Figure 7: Stroboscopic phase-space dynamics of the classical kicked top for  $\kappa = 3$ . Two hundred stroboscopic trajectories are plotted, each for a duration of 233 kicks. This figure is from Ref. [193].

Reference [260] found that at the critical point

$$\begin{aligned}\xi_S^2 &\sim 1/N^{-0.33\pm 0.01}, \\ \partial_\lambda \xi_S^2 &\sim -1/N^{-0.33\pm 0.03}.\end{aligned}\tag{294}$$

The above results are immediate consequences of the concurrence  $C$ , as shown in Ref. [260]. If  $\xi_S^2 \leq 1$ , we find  $\xi_S^2 = 1 - (N - 1)C$  due to the exchange symmetry. Generalized spin squeezing inequalities can be used to detect the ground state entanglement for lattice models [6]. However, as these inequalities are not given in terms of parameters like  $\xi_S^2$ , there are no such scaling laws, and we do not focus on them here.

Besides spin squeezing and concurrence, other measures such as negativity [267], geometric entanglement [268], and entropy [269] have also been studied. Due to its symmetry, the spin-squeezing parameter  $\xi_S^2$  is closely related to the concurrence in this model. At the critical point, the derivative of the parameter  $\xi_S^2$  with respect to the external driving field strength tends to diverge.

### 6.2. Spin squeezing and quantum chaos in the Quantum kicked-top model

In this section and the following, we discuss the behaviors of spin squeezing in two typical quantum chaotic systems: the quantum kicked-top model and the Dicke model. To facilitate the correspondence between the classical and quantum regimes, the initial states are chosen as CSSs. To connect the quantum dynamics to classical chaos, we choose the initial states located in both chaotic and regular regions. The dynamics of the squeezing parameters distinguish well between regular and chaotic regions, and we conclude that spin squeezing could be a good signature for quantum chaos.

The quantum kicked-top model can be realized in cold atomic ensembles [38, 111], and it is familiar to us since it has the form of a one-axis twisting Hamiltonian with a periodic pulse,

$$H = \frac{\kappa}{2j\tau} J_z^2 + pJ_y \sum_{n=-\infty}^{\infty} \delta(t - n\tau),\tag{295}$$

where the second term is the periodic driven pulse (with discrete kicks). The dynamics of this model is described by the Floquet operator

$$F = \exp\left(-i\frac{\kappa}{2j} J_z^2\right) \exp(-ipJ_y),\tag{296}$$



where we choose  $p = \pi/2$  and  $\tau = 1$  for convenience. The evolution of an initial state  $|\psi(0)\rangle$  is given by  $|\psi(n)\rangle = F^n|\psi(0)\rangle$ . The spin-squeezing dynamics can be obtained from this state. The chaotic behavior of this model has been recently demonstrated experimentally via linear entropy [258], by using the tensor part of an effective Hamiltonian for the dispersive atom-field interaction, and just in the same system, spin-squeezed states have been created [38, 111]. Therefore, the theoretical proposal of using spin squeezing as a signature of quantum chaos could be realized using current techniques. Below, we present numerical results for the dynamics of the spin-squeezing parameters.

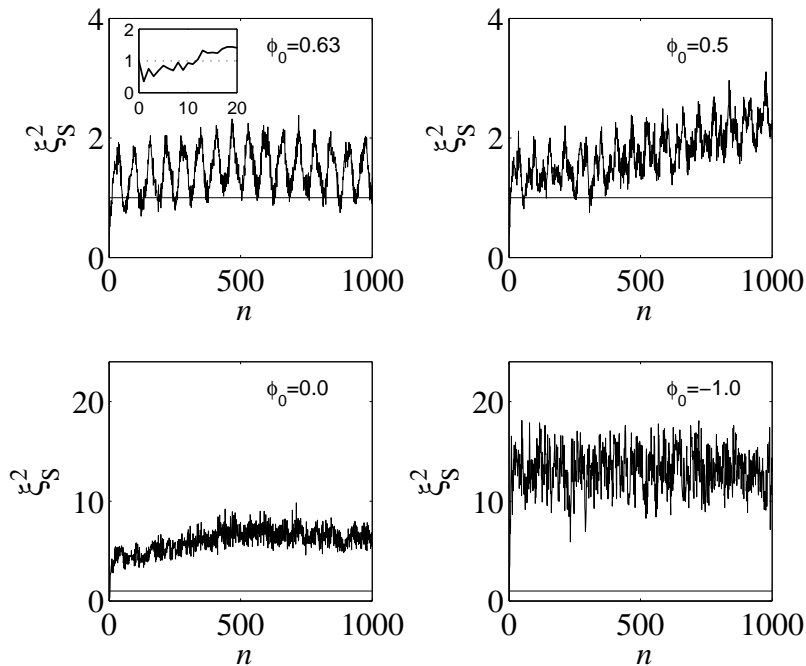


Figure 8: Dynamical evolution of the spin squeezing parameter  $\xi_S^2$  for the initial CSS with  $\theta_0 = 2.25$  for different values of  $\phi_0$ . The other parameters are fixed here at  $\kappa = 3$  and  $j = 25$ . The inset displays the initial dynamics when  $\phi_0 = 0.63$ . This figure is from Ref. [193].

To demonstrate the chaotic properties for this model, one could represent the model Hamiltonian under the CSS in large- $j$  limit. The classical limit of the quantum kicked top is obtained by expressing  $(X, Y, Z) = (\langle J_x \rangle, \langle J_y \rangle, \langle J_z \rangle) / j$ , and factorizing all the second moments to products of first moments, such as  $\langle J_x J_y \rangle / j^2 = XY$ . Then the classical equations of motion can be obtained from the Heisenberg operator equations of motion with the factorization rule. The classical normalized angular momentum variables  $(X, Y, Z)$  can be parameterized in spherical coordinates as  $(X, Y, Z) = (\sin \theta \cos \phi, \sin \theta \sin \phi, \cos \theta)$ , where  $\theta$  and  $\phi$  are the polar and azimuthal angles, respectively. Thus, the map is essentially two dimensional.

The stroboscopic plot with parameter  $\kappa = 3$  is displayed in Fig. 7. The parameter  $\kappa$  is chosen such as to yield a mixture of regular and chaotic areas. Elliptic fixed points surrounded by the chaotic sea are evident. Two such elliptic fixed points have coordinates  $(\theta, \phi) = (2.25, -2.5)$  and  $(\theta, \phi) = (2.25, 0.63)$ . As we will see, this phase-space structure of the classical kicked top determines spin squeezing in the quantum kicked top. If the initial state  $|\theta_0, \phi_0\rangle$  is chosen at one of these two points, the classical dynamics is regular.

Now, we return to the quantum Hamiltonian. The initial state is also a CSS, while the evolution is via the Floquet operator. The numerical results for the squeezing parameter  $\xi_S^2$  are shown in Fig. 8. The polar angle  $\theta = 2.25$  is chosen for all the initial states. The four plots show very clear variations of the dynamics of  $\xi_S^2$  for the fixed point ( $\phi_0 = 0.63$ ), regular region ( $\phi_0 = 0.5$ ), and the chaotic region ( $\phi_0 = 0.0$

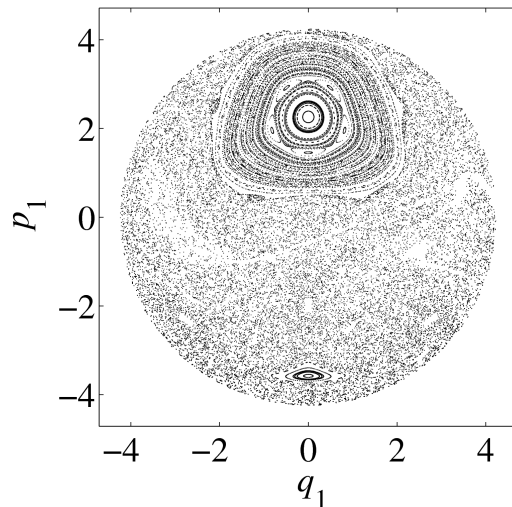


Figure 9: Poincaré section for the spin degrees of freedom (section with  $q_2 = 0.0$  and  $p_2 > 0.0$ ) in the resonant case ( $\omega = \omega_0 = 1$ ), energy  $E = 8.5$ . This figure is from Ref. [272].

and  $\phi_0 = -1.0$ ).

Spin squeezing is drastically suppressed in the chaotic region. As shown in Fig. 8, spin squeezing occurs frequently for the initial state located at the elliptic fixed point  $\phi_0 = 0.63$ , whereas spin squeezing vanishes after a very short time ( $n = 2$ ) for the initial state is in the ‘deep’ chaotic region ( $\phi_0 = -1.0$ ). When the initial state is in the regular region ( $\phi_0 = 0.5$ ), spin squeezing exists over a relatively long time, and only when steps  $n > 318$ , the spin squeezing vanishes. When the initial state is centered in the ‘shallow’ chaotic sea  $\phi_0 = 0$ , spin squeezing disappears after  $n = 4$  and never revives. The strong spin-squeezing oscillations mainly originate from the periodic kicks. Without kicks, the spin squeezing exhibits only periodic regular oscillations. Thus, we see that spin squeezing is very sensitive to classical chaos, and classical chaos strongly suppresses spin squeezing.

### 6.3. Spin squeezing and quantum chaos in the Dicke model

In this section, we consider the Dicke model, which characterizes the interaction between optical field and atoms. The Dicke model describes an ensemble of two-level particles interacting with a single-mode cavity bosonic field, and the corresponding Hamiltonian reads ( $\hbar = 1$ )

$$H = \omega_0 J_z + \omega a^\dagger a + \frac{R}{\sqrt{2j}} (J_+ a + J_- a^\dagger) + \frac{R'}{\sqrt{2j}} (J_+ a^\dagger + J_- a), \quad (297)$$

where the collective pseudo-spin operators are  $J_\alpha = \sum_{i=1}^N \sigma_{i\alpha}/2$ , ( $\alpha = x, y, z$ ) with  $\sigma_{i\alpha}$  being the Pauli operator for the  $i$ -th particle, and  $R, R'$  are the coupling strengths. The denominator  $\sqrt{2j}$  arises from that the dipole coupling strength is proportional to  $1/\sqrt{V}$ , where  $V$  is the volume of the cavity. When we consider the ground state, the system undergoes a second-order QPT between a normal phase and a super-radiant phase [270, 271]. This Hamiltonian is integrable under the rotating-wave approximation, i.e.  $R' = 0$ , which is used to demonstrate the transfer of squeezing between the field and atoms, while in this case no chaos exists. In the non-rotating-wave-approximation regime,  $R' \neq 0$ , its classical dynamics exhibits chaos. Therefore, this system is a desirable model for studying the interface between quantum and classical chaos.

As discussed previously, to study the quantum chaos, we write the Hamiltonian in the classical limit (in the coherent-state representation). As this system consists of the atomic and optical parts, the initial

quantum states are chosen as follows:

$$|\psi(0)\rangle = |\eta\rangle \otimes |\alpha\rangle, \quad (298)$$

where  $|\eta\rangle$  and  $|\alpha\rangle$  are the coherent spin and bosonic states, respectively. Here the variables  $\eta$  and  $\alpha$  can be written as functions of the classical variables in the corresponding phase spaces,  $(q_1, p_1)$  for the atomic degree of freedom, and  $(q_2, p_2)$  for the bosonic field  $\eta = (p_1 + iq_1)/\sqrt{4j - (p_1^2 + q_1^2)}$ ,  $\alpha = \frac{1}{\sqrt{2}}(p_2 + iq_2)$ , where  $q_1, p_1, q_2, p_2$  describe the phase space of the system under consideration, and the indices 1 and 2 denote the atomic and field subsystem, respectively. The classical Hamiltonian corresponding to Eq. (297) can be obtained under the CSS representation.

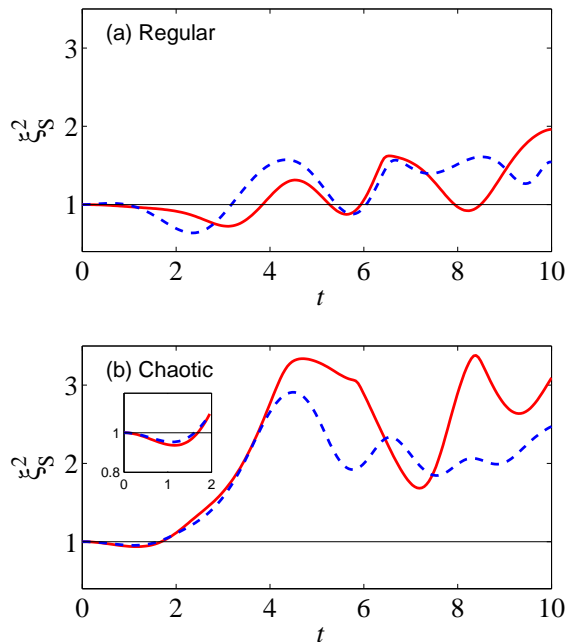


Figure 10: (Color online) Dynamical evolution of the spin-squeezing parameter  $\xi_S^2$  for the initial states with  $q_1 = 0$  and different  $p_1$ . (a) The regular region corresponding to Fig. 9:  $p_1 = 2.0$  (solid line) and  $p_1 = -3.5$  (dashed line); (b) Chaotic region corresponding to Fig. 9:  $p_1 = 0$  (solid line) and  $p_1 = -1.0$  (dashed line). This figure is from Ref. [273].

The classical dynamics associated with the Dicke Hamiltonian was explored in Ref. [274]. It was shown that the integrable cases are recovered when either  $R$  or  $R'$  is zero, and the most chaotic dynamics is associated to the condition  $R = R'$ . In Fig. 9, we show the Poincaré section for the classical counterpart of the spin degrees of freedom, defined by the section  $q_2 = 0$  in the four-dimensional phase space so that every time a trajectory pierces this section with  $p_2 > 0$ , the corresponding point  $(q_1, p_1)$  is plotted. Here, the total energy is fixed at  $E = 8.5$ ,  $j = 4.5$ ,  $\omega = \omega_0 = 1$ . The limit of atomic phase space is indicated by a border of radius equal to  $\sqrt{4j}$ . In Fig. 9, we choose the coupling parameters  $R = 0.5$  and  $R' = 0.2$ , which yield a mixture of regular and chaotic areas of significant sizes. Many fixed points and near-periodic orbits surrounded by the chaotic sea are evident.

The dynamic behavior of the spin-squeezing parameter  $\xi_S^2$  is computed by choosing the initial states in the chaotic and regular regions with respect to the Poincaré section. The results are shown in Fig. 10. We choose two fixed points at  $q_1 = 0, p_1 = 2.0$  and  $q_1 = 0, p_1 = -3.5$ , which are in the regular regions, and two additional points  $q_1 = 0, p_1 = 0$  and  $q_1 = 0, p_1 = -1.0$ , well inside the chaotic sea.

For the regular regions [see Fig. 10 (a)], spin squeezing vanishes after a relatively longer time ( $t \approx 9.0$ ), whereas for the chaotic region [see Fig. 10 (b)], the spin squeezing vanishes after a short time ( $t \approx 1.8$ ).

In summary, spin squeezing is sensitive to and suppressed by chaos. In contrast to this, chaos enhances the bipartite entanglement quantified by the linear entropy in the Dicke model [272]. So, the underlying chaos affects differently the two typical pure quantum mechanical phenomena, spin squeezing and bipartite entanglement. These results are very similar to the case of quantum kicked top model. Numerical results for the quantum kicked top and Dicke models suggest that spin squeezing is a good signature of chaos. Furthermore, by considering the advantage of the spin-squeezing parameter in measurement, it may have good applications in experiments.

## 7. Spin squeezing under decoherence

In this section, we take into account decoherence [275, 276, 277, 278], which is induced by unavoidable technical noise, and interactions with the environment. We shall discuss the effects of decoherence in three aspects.

(i) Decoherence in the generation of spin squeezing. In Sec. 7.1 we shall show that, if the decoherence effect is sufficiently weak, although the ability of squeezing generation is weakened, considerable large amount of squeezing can still be obtained.

(ii) The robustness and lifetime of spin squeezing in the presence of decoherence. In Sec. 7.2, we show that spin-squeezed states are more robust to particle-loss [279] as compared to the GHZ state. In Sec. 7.3, the lifetime of spin squeezing is studied in three types of decoherence channels, which are quite general to describe decoherence processes, and spin squeezing sudden death is observed.

(iii) Decoherence in the quantum metrology process. In Sec. 7.4, we discuss how decoherence affects the ability of spin-squeezed states to the improvement of phase resolution in Ramsey processes. Although the degree of spin squeezing is weakened by decoherence, sub-shot noise phase resolution can still be achieved [13], in contrast with the maximal entangled state, with which we could only attain the shot-noise level precision in the presence of decoherence [280].

### 7.1. Decoherence and spin squeezing generation

In Sec. 3, we have discussed generating spin-squeezed states via ideal one-axis twisting Hamiltonian, where decoherence effects are not taken into account, and the best squeezing scales as  $\xi_R^2 \propto 1/N^{2/3}$  for the one-axis twisting and  $\xi_R^2 \propto 1/N^2$  for the two-axis twisting. It is natural to expect that, decoherence is detrimental to spin squeezing generation, while if the decoherence effect is sufficiently weak, considerable large amount of squeezing can still be obtained. Below, we mainly consider the particle loss induced decoherence, which is an unavoidable source of decoherence in cold atom systems, such as BEC, due to collisions of condensed atoms with the background gas.

We first consider the one-axis twisting Hamiltonian. In Ref. [4], to estimate the effect of particle losses in a two-mode BEC, they have performed a Monte Carlo simulation of the evolution of squeezing from the one-axis twisting Hamiltonian  $H = \chi J_z^2$ . The particle loss is phenomenologically taken into account by introducing a loss rate  $\Gamma$ . Their simulations indicated that even under the conditions that approximately 10% atoms are lost, squeezing of  $\xi_R^2 \sim 0.01$  may be obtained. In Refs. [153, 154], the authors presented a more detailed analysis of spin squeezing generation in the presence of particle loss in a two-mode BEC. The time evolution of the squeezing parameter is derived as

$$\xi_R^2(t) = \xi_{R0}^2(t) \left[ 1 + \frac{1}{3} \frac{\Gamma_{\text{sq}} t}{\xi_{R0}^2(t)} \right], \quad (299)$$

where  $\xi_R^2(t)$  is the squeezing without particle loss, and

$$\Gamma_{\text{sq}} = \sum_m \Gamma_{\text{sq}}^{(m)}, \quad \text{and} \quad \Gamma_{\text{sq}}^{(m)} = m\Gamma^{(m)}, \quad (300)$$

where  $\Gamma^{(m)}$  is the  $m$ -body loss rate. They then found that, for one-body losses, the best obtainable spin squeezing scales as

$$\xi_R^2 \propto N^{-4/15} \text{ for } N \rightarrow \infty, \quad (301)$$

for two-body loss, in the limit  $N \rightarrow \infty$  the best squeezing is independent of  $N$ , and for three-body losses, the best squeezing

$$\xi_R^2 \propto N^{4/15} \text{ for } N \rightarrow \infty. \quad (302)$$

Thus for one-body losses, we can obtain arbitrary small squeezing parameter by increasing the particle number, while for three-body losses case, there is a finite optimum number of particles for squeezing. For two-axis twisting model, the decoherence effects induced by particle loss was studied in Ref. [212], where they established a Raman-scattering based approach to implement the two-axis twisting Hamiltonian as Eq. (170). They found that, to achieve the Heisenberg limit squeezing, it is required that  $\chi \geq \Gamma$ , where  $\chi$  is the twisting strength in Eq. (170), and  $\Gamma$  is the one-body loss rate. To achieve any squeezing, it requires  $N\chi \geq \Gamma$ , where  $N$  is the particle number. Quantum-limited metrology in the presence of collisional dephasing was studied in [281, 242], although these works are associated with nonlinear estimation scheme, their analysis can also be extended to the discussion of spin squeezing. Otherwise, a detailed analysis of decoherence in quantum light-atom interfaces, such as QND-type interactions, was studied in [282].

### 7.2. Spin-squeezed states under particle loss

In the above subsection, we discussed how decoherence affects the production of spin squeezing. Below, we consider the effects of particle loss on the generated spin-squeezed states, which was studied in Refs. [279, 126, 153]. For convenience, the system is now assumed to be symmetric under particle exchange. Based on this assumption, the spin squeezing after particle loss is equivalent to the spin squeezing of the subsystem composed of the remaining particles. The state after particle loss is obtained by tracing over the degrees of freedom of the lost particles, and this procedure is what we used when deriving the reduced density matrix of the state for the subsystem. Therefore, we immediately arrive at the conclusion that concurrence is not affected by particle loss.

Consider an  $N$ -body system with exchange symmetry, represented by a density matrix  $\rho_N$ . The reduced states also have exchange symmetry. After particle loss, the reduced state for the remaining  $N_r$  particles becomes

$$\rho_{N_r} = \text{Tr}_{(N-N_r)}\{\rho_N\}, \quad (303)$$

where we trace over the  $(N - N_r)$  lost particles. As the state is of exchange symmetry, we have

$$\begin{aligned} \langle \sigma_{1\alpha} \rangle &\equiv \langle \sigma_{i\alpha} \rangle_N = \langle \sigma_{i\alpha} \rangle_{N_r}, \\ \langle \sigma_{1\alpha} \sigma_{2\alpha} \rangle &\equiv \langle \sigma_{i\alpha} \sigma_{j\alpha} \rangle_N = \langle \sigma_{i\alpha} \sigma_{j\alpha} \rangle_{N_r}, \end{aligned} \quad (304)$$

where the subscripts  $N$  and  $N_r$  denote the state before and after particle loss, respectively. The indices  $i, j$  denote any two remaining particles. Note that, according to Eq. (304), the MSD is invariant under particle loss.

From the expression  $J_{\vec{n}} = \frac{1}{2} \sum_{i=1}^N \sigma_{i\vec{n}}$ , one can verify that

$$\langle J_{\vec{n}}^2 \rangle_N = \frac{N}{4} + \frac{N^2 - N}{4} \langle \sigma_{1\vec{n}} \sigma_{2\vec{n}} \rangle, \quad (305)$$

where we have used the symmetry of the state. Conversely, one finds

$$\langle \sigma_{1\vec{n}} \sigma_{2\vec{n}} \rangle = \frac{1}{N-1} \left( \frac{4\langle J_{\vec{n}}^2 \rangle_N}{N} - 1 \right). \quad (306)$$

For the state after loss, similarly, we obtain

$$\langle \sigma_{1\vec{n}} \sigma_{2\vec{n}} \rangle = \frac{1}{N_r-1} \left( \frac{4\langle J_{\vec{n}}^2 \rangle_{N_r}}{N_r} - 1 \right). \quad (307)$$

Thus, from Eqs. (306) and (307), we obtain the following relation

$$\frac{4\langle J_{\vec{n}}^2 \rangle_{N_r}}{N_r} = \frac{N_r-1}{N-1} \frac{4\langle J_{\vec{n}}^2 \rangle_N}{N} + \frac{N-N_r}{N-1}, \quad (308)$$

which is applicable to an arbitrary direction  $\vec{n}$ . Then, we have a similar expression for the direction  $\vec{n}_\perp$  (perpendicular to the invariant mean-spin direction),

$$\frac{4\langle J_{\vec{n}_\perp}^2 \rangle_{N_r}}{N_r} = \frac{N_r - 1}{N - 1} \frac{4\langle J_{\vec{n}_\perp}^2 \rangle_N}{N} + \frac{N - N_r}{N - 1}. \quad (309)$$

The two quantities  $4\langle J_{\vec{n}_\perp}^2 \rangle_{N_r}/N_r$  and  $4\langle J_{\vec{n}_\perp}^2 \rangle_N/N$  are just linearly related to each other, and  $N_r - 1 > 0$ . So, if we choose  $\vec{n}_\perp$  be the direction where the minimal variance is obtained for the state before loss, the direction  $\vec{n}_\perp$  also corresponds to the minimal variance after loss. Finally, from the definition of the squeezing parameter  $\xi_S^2$  (Table 1), we obtain [279]

$$\xi_{S,N_r}^2 = \frac{N_r - 1}{N - 1} \xi_{S,N}^2 + \frac{N - N_r}{N - 1}, \quad (310)$$

which gives the relation of the spin-squeezing parameters before and after loss.

Now, we discuss the spin-squeezing parameter  $\xi_R^2$ , which is simply related to the parameter  $\xi_S^2$  via

$$\xi_{R,N}^2 = \frac{N^2}{4\langle \vec{J} \rangle_N^2} \xi_{S,N}^2 = \frac{1}{\langle \vec{\sigma}_1 \rangle^2} \xi_{S,N}^2. \quad (311)$$

A similar expression holds for the squeezing parameters after loss, and it is given by

$$\xi_{R,N_r}^2 = \frac{1}{\langle \vec{\sigma}_1 \rangle^2} \xi_{S,N_r}^2. \quad (312)$$

Multiplying Eq. (310) by  $\langle \vec{\sigma}_1 \rangle^{-2}$ , one immediately obtains [279]

$$\xi_{R,N_r}^2 = \frac{N_r - 1}{N - 1} \xi_{R,N}^2 + \frac{N - N_r}{N - 1} \frac{1}{\langle \vec{\sigma}_1 \rangle^2}. \quad (313)$$

The squeezing parameter  $\xi_{S,N_r}^2$  only requires the knowledge of  $\xi_{S,N}^2$ , while the parameter  $\xi_{R,N_r}^2$  is related to both  $\xi_{R,N}^2$  and  $\langle \vec{\sigma}_1 \rangle^2$ .

Note that the GHZ state, which is maximally entangled, is extremely fragile under particle loss. Indeed, the entanglement is totally destroyed when only one particle is lost. However, the spin-squeezed states, which are only partially correlated (e.g., pairwise correlated) are more robust. We emphasize that the robustness is different in the depolarizing channel. It has been found that in the limit  $N \rightarrow \infty$ , GHZ states can stand more than 55% local depolarization, while for spin-squeezed states it can stand more than 29% local depolarization [283].

### 7.3. Spin squeezing under decoherence channels

In the previous subsection, the decoherence is induced by particle loss. Here, the decoherence effects are described by three types of decoherence channels: the amplitude damping channel (ADC), the phase damping channel (PDC), and the depolarizing channel (DPC). In general, decoherence processes can be described by these three typical channels. They are prototype models of decoherence relevant to various experimental systems. They provide “a revealing caricature of decoherence in realistic physical situations, with all inessential mathematical details stripped away” [284]. But yet this “caricature of decoherence” leads to theoretical predictions being often in good agreement with experimental data. Examples include multiphoton systems, ion traps, atomic ensembles, or a solid-state spin systems such as quantum dots or nitrogen-vacancy centers, where qubits are encoded in electron or nuclear spins. Let us first introduce the three decoherence channels.

### 7.3.1. Decoherence channels

*Amplitude-damping channel.*— The ADC is defined by

$$\mathcal{E}_{\text{ADC}}(\rho) = E_0\rho E_0^\dagger + E_1\rho E_1^\dagger, \quad (314)$$

where  $E_0 = \sqrt{s}|0\rangle\langle 0| + |1\rangle\langle 1|$  and  $E_1 = \sqrt{p}|1\rangle\langle 0|$  are the Kraus operators,  $p = 1 - s$ ,  $s = \exp(-\gamma t/2)$ , and  $\gamma$  is the damping rate. In the Bloch representation, the ADC squeezes the Bloch sphere into an ellipsoid and shifts it toward the north pole. The radius in the  $x$ - $y$  plane is reduced by a factor  $\sqrt{s}$ , while in the  $z$ -direction it is rescaled by a factor  $s$ . The ADC is a prototype model of a dissipative interaction between a qubit and its environment. For example, the ADC model can be applied to describe the spontaneous emission of a photon by a two-level system into an environment of photon or phonon modes at zero (or very low) temperature in (usually) the weak Born-Markov approximation.

*Phase-damping channel.*—The PDC is a prototype model of dephasing or pure decoherence, i.e., loss of coherence of a two-level state without any loss of the system's energy. The PDC is described by the map

$$\mathcal{E}_{\text{PDC}}(\rho) = s\rho + p(\rho_{00}|0\rangle\langle 0| + \rho_{11}|1\rangle\langle 1|), \quad (315)$$

and obviously the three Kraus operators are given by  $E_0 = \sqrt{s}\mathbb{I}$ ,  $E_1 = \sqrt{p}|0\rangle\langle 0|$  and  $E_2 = \sqrt{p}|1\rangle\langle 1|$ , where  $\mathbb{I}$  is the identity operator. For the PDC, there is no energy change and a loss of decoherence occurs with probability  $p$ . As a result of the action of the PDC, the Bloch sphere is compressed by a factor  $(1 - 2p)$  in the  $x$ - $y$  plane. It is evident that the action of the PDC is nondissipative. This means that, in the standard computational basis  $|0\rangle$  and  $|1\rangle$ , the diagonal elements of the density matrix  $\rho$  remain unchanged, while the off-diagonal elements are suppressed. Moreover, the qubit states  $|0\rangle$  and  $|1\rangle$  are also unchanged under the action of the PDC, although any superposition of them (i.e., any point in the Bloch sphere, except the poles) becomes entangled with the environment. The PDC can be interpreted as elastic scattering between a (two-level) system and a reservoir. The PDC is also a suitable model to describe  $T_2$  relaxation in spin resonance.

*Depolarizing channel.*—The definition of the DPC is given by the map

$$\mathcal{E}_{\text{DPC}}(\rho) = s\rho + p\frac{\mathbb{I}}{2}. \quad (316)$$

We see that for the DPC, the spin is unchanged with probability  $s = 1 - p$ , or is depolarized to the maximally-mixed state  $\mathbb{I}/2$  with probability  $p$ . It is seen that due to the action of the DPC, the radius of the Bloch sphere is reduced by a factor  $s$ , but its shape remains unchanged.

Table 7: Analytical results for the time-evolutions of all relevant expectations, correlations, spin-squeezing parameters, and concurrence, as well as the critical values  $p_c$  of the decoherence strength  $p$  [197]. This is done for the three decoherence channels considered here. For the concurrence  $C$ , we give the expression for  $C'_r$ , which is related to the rescaled concurrence  $C_r$  via  $C_r = \max(0, C'_r)$ . The parameters  $x_0 = 1 + 2\langle\sigma_z\rangle_0 + \langle\sigma_{1z}\sigma_{2z}\rangle_0$ ,  $a_0 = (N-1)(1 - \langle\sigma_{1z}\sigma_{2z}\rangle_0)$ . The critical values  $p_c^{(1)}$ ,  $p_c^{(2)}$ , and  $p_c^{(3)}$  correspond to the concurrence, squeezing parameter  $\xi_R^2$ , and  $\xi_E^2$ , respectively. See Ref. [197]

	Amplitude-damping channel (ADC)	Phase-damping channel (PDC)	Depolarizing channel (DPC)
$\langle\sigma_{1z}\rangle$	$s\langle\sigma_{1z}\rangle_0 - p$	$\langle\sigma_{1z}\rangle_0$	$s\langle\sigma_{1z}\rangle_0$
$\langle\sigma_{1z}\sigma_{2z}\rangle$	$s^2\langle\sigma_{1z}\sigma_{2z}\rangle_0 - 2sp\langle\sigma_{1z}\rangle_0 + p^2$	$\langle\sigma_{1z}\sigma_{2z}\rangle_0$	$s^2\langle\sigma_{1z}\sigma_{2z}\rangle_0$
$\langle\sigma_{1+}\sigma_{2-}\rangle$	$s\langle\sigma_{1+}\sigma_{2-}\rangle_0$	$s^2\langle\sigma_{1+}\sigma_{2-}\rangle_0$	$s^2\langle\sigma_{1+}\sigma_{2-}\rangle_0$
$\langle\sigma_{1-}\sigma_{2-}\rangle$	$s\langle\sigma_{1-}\sigma_{2-}\rangle_0$	$s^2\langle\sigma_{1-}\sigma_{2-}\rangle_0$	$s^2\langle\sigma_{1-}\sigma_{2-}\rangle_0$
$\langle\vec{\sigma}_1 \cdot \vec{\sigma}_2\rangle$	$1 - spx_0$	$s^2(1 - \langle\sigma_{1z}\sigma_{2z}\rangle_0) + \langle\sigma_{1z}\sigma_{2z}\rangle_0$	$s^2$
$C_{zz}$	$s^2C_{zz}(0)$	$C_{zz}(0)$	$s^2C_{zz}(0)$
$\xi_S^2$	$1 - sC_r(0)$	$1 - s^2C_r(0)$	$1 - s^2C_r(0)$
$\xi_R^2$	$\frac{1 - sC_r(0)}{(s\langle\sigma_{1z}\rangle_0 - p)^2}$	$\frac{1 - s^2C_r(0)}{\langle\sigma_{1z}\rangle_0^2}$	$\frac{1 - s^2C_r(0)}{s^2\langle\sigma_{1z}\rangle_0^2}$
$\xi_E^2$	$\frac{1 - sC_r(0)}{1 + (1 + N^{-1})spx_0}$	$\frac{1 - s^2C_r(0)}{(1 - \frac{1}{N})[s^2 + (1 - s^2)\langle\sigma_{1z}\sigma_{2z}\rangle_0] + \frac{1}{N}}$	$\frac{1 - s^2C_r(0)}{(1 - N^{-1})s^2 + N^{-1}}$
$C'_r$	$sC_r(0) - (N-1)spx_0/2$	$s^2C_r(0) + a_0(s^2 - 1)/2$	$s^2C_r(0) + \frac{N-1}{2}(s^2 - 1)$
$p_c^{(1)}$	$\frac{2C_r(0)}{(N-1)x_0}$	$1 - \left(\frac{a_0}{2C_r(0) + a_0}\right)^{\frac{1}{2}}$	$1 - \left(\frac{N-1}{2C_r(0) + N-1}\right)^{\frac{1}{2}}$
$p_c^{(2)}$	$\frac{\langle\sigma_{1z}\rangle_0^2 + C_r(0) - 1}{1 + 2\langle\sigma_{1z}\rangle_0 + \langle\sigma_z\rangle_0^2}$	$1 - \left(\frac{1 - \langle\sigma_{1z}\rangle_0^2}{C_r(0)}\right)^{\frac{1}{2}}$	$1 - \left(\frac{1}{C_r(0) + \langle\sigma_{1z}\rangle_0^2}\right)^{\frac{1}{2}}$
$p_c^{(3)}$	$\frac{NC_r(0)}{(N-1)x_0}$	$1 - \left(\frac{a_0}{NC_r(0) + a_0}\right)^{\frac{1}{2}}$	$1 - \left(\frac{N-1}{NC_r(0) + N-1}\right)^{\frac{1}{2}}$

### 7.3.2. Spin squeezing parameters under decoherence

Now we begin to study spin squeezing under the above three different decoherence channels. The spin-squeezed states are prepared by a one-axis twisting Hamiltonian, and the spin-squeezing parameters  $\xi_S^2$ ,  $\xi_R^2$  and  $\xi_E^2$  can be evaluated by using Eqs. (104) and (111), since the system has exchange symmetry, and the decoherence channels act independently on each particle. Therefore, all the spin-squeezing parameters and the concurrence are determined by some correlation functions and expectations, and they can be calculated via the Heisenberg approach shown below.

The spin-squeezing parameters and concurrence for the initial state are shown in Table 7. The state under decoherence is given by

$$\mathcal{E}(\rho) = \sum_{\mu_1, \dots, \mu_N} (\otimes_{i=1}^N K_{\mu_i}) \rho (\otimes_{i=1}^N K_{\mu_i}^\dagger), \quad (317)$$



where  $K_{\mu_i}$  denotes the Kraus operator for the  $i$ -th particle. The spin-squeezing parameters and concurrence consist of some correlation functions and expectations, and we need just to calculate the evolution of these quantities by employing Heisenberg picture without writing the state explicitly. The evolution of operator  $A$  can be put forward by employing the Heisenberg picture with

$$\langle A \rangle = \text{Tr} [A\mathcal{E}(\rho)] = \text{Tr} [\mathcal{E}^\dagger(A)\rho], \quad (318)$$

where

$$\mathcal{E}^\dagger(A) = \sum_{\mu_1, \dots, \mu_N} \left( \otimes_{i=1}^N K_{\mu_i}^\dagger \right) A \left( \otimes_{i=1}^N K_{\mu_i} \right) \quad (319)$$

is relatively easy to calculate for our cases.

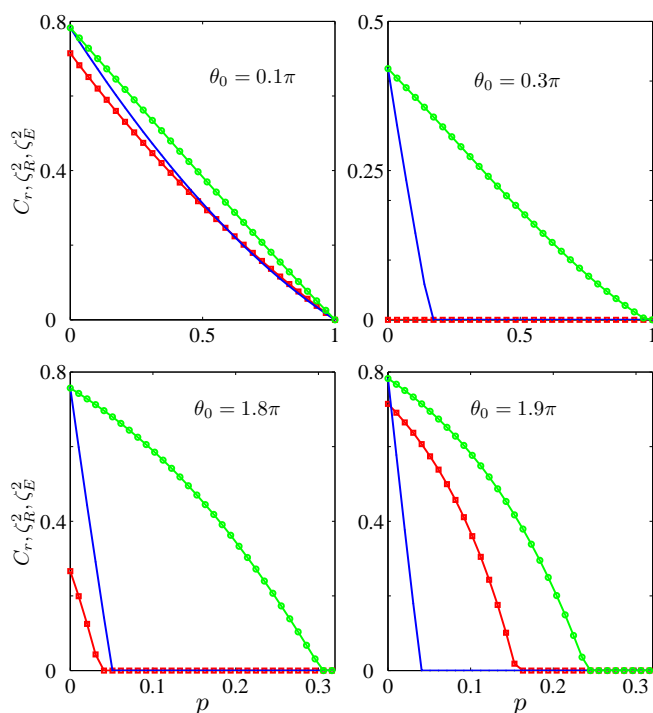


Figure 11: (Color online) Spin-squeezing parameters  $\zeta_R^2$  (red curve with squares),  $\zeta_E^2$  (top green curve with circles), and the concurrence  $C_r$  (solid curve) versus the decoherence strength  $p = 1 - \exp(-\gamma t)$  for the amplitude damping channel, where  $\gamma$  is the damping rate. Here,  $\theta_0$  is the initial twist angle given by Eq. (323). In all figures, we consider an ensemble of  $N = 12$  spins. Note that for small initial twist angle  $\theta_0$  (e.g.,  $\theta_0 = 0.1\pi$ ), the two squeezing parameters and the concurrence all concur. For larger values of  $\theta_0$ , then  $\zeta_R^2$ ,  $\zeta_E^2$ , and  $C$  become quite different, and all vanish for sufficiently large values of the decoherence strength. This figure is from Ref. [197].

In order to characterize spin squeezing more conveniently, we now define the following squeezing parameters:

$$\zeta_k^2 = \max(0, 1 - \xi_k^2), \quad k \in \{S, R, E\}. \quad (320)$$

Spin squeezing appears when  $\zeta_k^2 > 0$ , and there is no squeezing when  $\zeta_k^2$  vanishes. Thus, the definition of the first parameter  $\zeta_S^2$  has a clear meaning: namely, it is the *strength* of the negative correlations as seen from Eq. (179). More explicitly, for the initial state, we have  $\xi_S^2 = 1 - (N - 1)C_0$  as shown in Eq. (132), so  $\zeta_S^2$  is just the *rescaled concurrence*

$$C_r(0) = (N - 1)C_0. \quad (321)$$

To study the decoherence of spin squeezing, we choose a state which is initially squeezed. One typical class of such spin-squeezed states is the one-axis twisting collective spin state [1],

$$|\Psi(\theta_0)\rangle = e^{-i\theta_0 J_x^2/2} |1\rangle^{\otimes N}, \quad (322)$$

which could be prepared by the one-axis twisting Hamiltonian  $H = \chi J_x^2$ , where

$$\theta_0 = 2\chi t \quad (323)$$

is the *one-axis twist angle* and  $\chi$  is the coupling constant.

The numerical results for the squeezing parameters and concurrence are illustrated in Fig. 11 for different initial values of  $\theta$ . For the smaller value of  $\theta_0$ , e.g.,  $\theta_0 = \pi/10$ , we see that there is no entanglement sudden death (ESD) and spin squeezing sudden death (SSSD). The spin squeezing and the pairwise entanglement are completely robust against decoherence. Intuitively, the larger is the squeezing, the larger is the vanishing time for the squeezing. However, here, in contrast to this, no matter how small the squeezing parameters and concurrence are, they vanish only in the asymptotic limit. This results from the complex correlations in the initial state and the special characteristics of the ADC. For larger values of  $\theta_0$ , as the decoherence strength  $p$  increases, the spin squeezing decreases until it suddenly vanishes, so the phenomenon of SSSD occurs. There exists a critical value  $p_c$ , after which there is no spin squeezing. The vanishing time of  $\tilde{\xi}_E^2$  is always larger than those of  $\xi_R^2$  and the concurrence. We note that depending on the initial state, the concurrence can vanish before or after  $\xi_R^2$ . This means that in our model, the parameter  $\tilde{\xi}_E^2 < 1$  implies the existence of pairwise entanglement, while  $\xi_R^2$  does not.

We can calculate all the relevant correlation functions, squeezing parameters, concurrence and the critical values of the decoherence strength  $p$ , which are given in Table 7. Initially, the state is spin-squeezed, i.e.,  $\xi_S^2(0) < 1$  or  $C_r(0) > 0$ . As seen from the Table, one can find that  $\xi_S^2 < 1$ , except in the asymptotic limit of  $p = 1$ . Thus, we conclude that according to  $\xi_S^2$ , the initially spin-squeezed state is always squeezed for  $p \neq 1$ , irrespective of both the decoherence strength and decoherence models. In other words, there exists no SSSD if we quantify spin squeezing by the first parameter  $\xi_S^2$ .

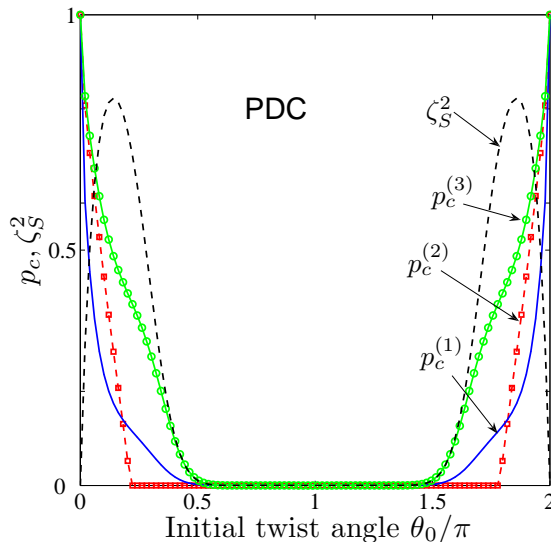


Figure 12: (Color online) Critical values of the decoherence strength  $p_c^{(1)}$  (blue solid curve),  $p_c^{(2)}$  (red curve with squares),  $p_c^{(3)}$  (top green curve with circles), and the squeezing parameter  $\xi_S^2$  (black dashed curve) versus the initial twist angle  $\theta_0$  given by Eq. (323) for the amplitude-damping channel, PDC. Here,  $p_c$  is related to the vanishing time  $t_v$  via  $p_c = 1 - \exp(-\gamma t_v)$ . At vanishing times, SSSD occurs. This figure is from Ref. [197].

The SSSD for the three decoherence channels with respect to different initial twisting angles was also studied [197], here, we only take the PDC for example. In Fig. 12, we plot the decoherence strength  $p_c$  versus the twist angle  $\theta_0$  of the initial state for the PDC. For this decoherence channel, the critical values  $p_c$ 's first decrease, until they reach zero. Also, it is symmetric with respect to  $\theta_0 = \pi$ , which is in contrast to the ADC. There are also intersections between the concurrence and parameter  $\xi_R^2$ , and the critical value  $p_c^{(3)}$  is always larger than  $p_c^{(1)}$  and  $p_c^{(2)}$ .

As summarized in Ref. [197], the common features of the three decoherence channels are: (i) The critical value  $p_c^{(3)}$  is always larger than or equal to the other two, namely, the spin-squeezing correlations according to  $\xi_E^2$  are more robust; (ii) There always exist two intersections between the concurrence and the parameter  $\xi_R^2$ , for  $\theta_0$  from 0 to  $2\pi$ , irrespective of the decoherence channels; (iii) When there is no squeezing (central area of Fig. 12), all vanishing times are zero. Table 7 conveniently lists all the analytical results obtained in this section.

#### 7.4. Effects of decoherence on spin squeezing in Ramsey processes

In this section, we present the effects of decoherence on spin-squeezed states in Ramsey interferometry, which was discussed in Sec. 5.3. Now we take into account decoherence, and each spin-1/2 particle is assumed to evolve independently via the master equation

$$\frac{\partial \rho}{\partial t} = -\frac{i}{2} [(\omega_0 - \omega) \sigma_z, \rho] + \frac{\gamma}{2} (\sigma_z \rho \sigma_z - \rho), \quad (324)$$

where  $\gamma$  is the decoherence rate. Under the above master equation, which describes a dephasing process, nondiagonal elements of  $\rho$  decay as  $\exp(-\gamma t)$ , while the diagonal terms are invariant. Spin squeezing weakened by dissipation effects was studied in Refs. [62, 285]. By using the results obtain in Table 7, we now derive

$$\begin{aligned} \langle J_z \rangle_t &= -\cos \phi \langle J_z \rangle_{t=0} \exp(-\gamma t), \\ (\Delta J_z^2)_t &= \left[ \sin^2 \phi \langle J_x^2 \rangle_{t=0} + \cos^2 \phi (\Delta J_z)_{t=0}^2 - \sin(2\phi) \text{Cov}(J_x, J_z)_{t=0} \right] \exp(-2\gamma t) \\ &\quad + \frac{N}{4} [1 - \exp(-2\gamma t)], \end{aligned} \quad (325)$$

where the exponential terms come from the free evolution, when the system is rotating around the  $z$ -axis. Thus, from the above equations, the decoherence effects on the spin-squeezing parameter  $\xi_R^2$  are clear: the length of the spin becomes shorter, while the fluctuation, which maybe squeezed at the beginning, becomes larger. Therefore, the degree of squeezing becomes smaller.

Since  $\phi$  is time dependent, it is more convenient to estimate  $\omega_0$ . By using Eqs. (273) and (325), we obtain

$$\Delta\omega_0 = \left[ \frac{\sin^2 \phi \langle J_x^2 \rangle + \cos^2 \phi (\Delta J_z)^2 + \frac{N}{4} [\exp(2\gamma t) - 1]}{tT \sin^2 \phi \langle J_z \rangle^2} \right]^{1/2}, \quad (326)$$

where we omit the subscript  $t = 0$ , and assume  $\text{Cov}(J_x, J_z)_{t=0} = 0$ , which is usually satisfied when the initial states have parity, e.g. the spin-squeezed states generated via the twisting Hamiltonian.

Now, we search for the point  $(\phi_{\text{opt}}, t_{\text{opt}})$  where the minimum of  $\Delta\omega_0$  is attained. The minimization of  $\Delta\omega_0$  is equivalent to the minimization of  $(\Delta\omega_0)^2$ , which is given by

$$(\Delta\omega_0)^2 = \frac{\langle J_x^2 \rangle - (\Delta J_z)^2}{tT \langle J_z \rangle^2} + \frac{(\Delta J_z)^2 + \frac{N}{4} [\exp(2\gamma t) - 1]}{tT \sin^2 \phi \langle J_z \rangle^2}. \quad (327)$$

It is evident that  $(\Delta\omega_0)^2$  decreases monotonically with the increase of  $\sin \phi$ , thus

$$\phi_{\text{opt}} = \frac{k\pi}{2} \quad (k \text{ odd}). \quad (328)$$

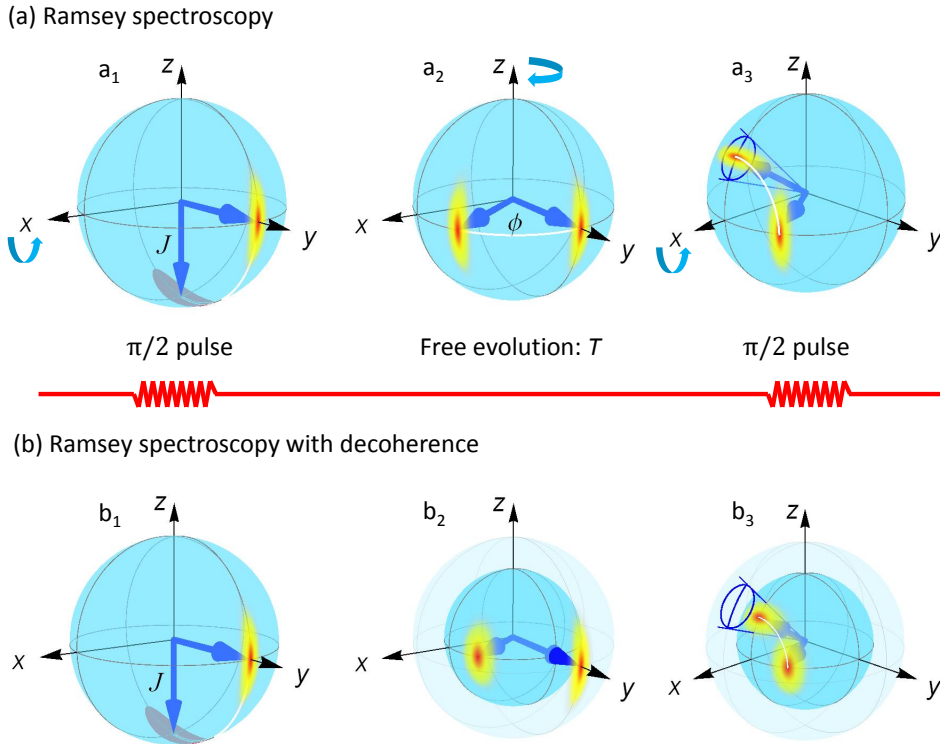


Figure 13: (Color online) Schematic diagram of the state evolution for Ramsey spectroscopy. Here the initial state is spin-squeezed in the  $x$ -direction, with spin length  $J$ . At each “snapshot”, the initial and final states are joined by a white “path” or trajectory on the Bloch sphere. The phase  $\phi$  gained in the free-evolution period is determined by measuring the population differences, between particles in states  $|0\rangle$  and  $|1\rangle$ , which is equivalent to measuring  $J_z$ . The precision of  $\phi$  is thus determined by the spin length and the fluctuation in  $J_z$ . In the absence of decoherence (a), a squeezed state (fuzzy elliptic rainbow) performs better (i.e., has smaller fluctuations in  $J_z$ ) than a coherent spin state (blue circle), shown in  $a_3$ . When decoherence is considered, during the free-evolution period, the spin length is shorter and the fluctuations become larger. Thus, in the final population measurement,  $b_3$ , the precision of  $\phi$  becomes lower.

And at this point,  $(\Delta\omega_0)^2$  becomes

$$(\Delta\omega_0)^2(\phi = \phi_{\text{opt}}) = \frac{\langle J_x^2 \rangle + \frac{N}{4} [\exp(2\gamma t) - 1]}{tT \langle J_z \rangle^2}. \quad (329)$$

It is interesting to see that this minimal value is independent of the variance  $(\Delta J_z)^2$ , irrespective of decoherence. Now, we minimize  $(\Delta\omega_0)^2$  with respect to  $t$ . The value of  $t_{\text{opt}}$  is determined by the conditions

$$\begin{aligned} \frac{\partial}{\partial t} [(\Delta\omega_0)^2(\phi = \phi_{\text{opt}})] &= 0, \\ \frac{\partial^2}{\partial t^2} [(\Delta\omega_0)^2(\phi = \phi_{\text{opt}})] &> 0, \end{aligned} \quad (330)$$

and thus  $t_{\text{opt}}$  is the solution of

$$(2\gamma t - 1) \exp(2\gamma t) + 1 = \xi_x^2, \quad (331)$$

where

$$\xi_x^2 = \frac{4 \langle J_x^2 \rangle}{N}, \quad (332)$$

which is equal to  $\xi_S^2$  if  $\langle J_x^2 \rangle$  is the minimal spin variance in the  $\vec{n}_\perp$  direction. When  $t = t_{\text{opt}}$ , one finds

$$\frac{\partial^2}{\partial t^2} [(\Delta\omega_0)^2(\phi = \phi_{\text{opt}})] = \frac{N\gamma^2 \exp(2\gamma t)}{Tt \langle J_z \rangle^2}, \quad (333)$$

which is obviously larger than zero. Thus, at the optimal point, we obtain the minimal value.

From Eqs. (329) and (331), we obtain the minimal  $\Delta\omega_0$  as

$$\min(\Delta\omega_0) = \sqrt{\frac{2\gamma \exp(2\gamma t_{\text{opt}})}{TN\eta_z}}, \quad (334)$$

where  $\eta_z = 4 \langle J_z \rangle^2 / N^2$ , which is always less than or equal to one. For the CSS  $|j, -j\rangle$ , we have  $\eta_z = 1$ ,  $\xi_x^2 = 1$  and  $t_{\text{opt}} = 1/(2\gamma)$ . Thus according to Eq. (334), we have

$$\min(\Delta\omega_0)_{\text{CSS}} = \sqrt{\frac{2\gamma \exp(1)}{TN}}. \quad (335)$$

A relative improvement in the precision over the above minimal uncertainty may be given by

$$P(t_{\text{opt}}, \eta_z) = 1 - \frac{\min(\Delta\omega_0)}{\min(\Delta\omega_0)_{\text{CSS}}} = 1 - \sqrt{\frac{\exp(2\gamma t_{\text{opt}})}{\exp(1)\eta_z}}. \quad (336)$$

Then in the idealized case,  $t_{\text{opt}} \rightarrow 0$  and  $\eta_z \rightarrow 1$ , the theoretical absolute decoherence limit in the precision improvement is

$$P_{\text{abs}} = 1 - \exp\left(-\frac{1}{2}\right) \simeq 0.39. \quad (337)$$

which is independent of  $N$ . Here, we emphasize that, the limit  $t \rightarrow 0$  implies  $\xi_x^2 \rightarrow 0$  according to Eq. (331).

In Ref. [280], a similar issue was studied with the maximally entangled state, the GHZ state, which is not spin-squeezed but can be used to achieve the Heisenberg limit [33, 37, 252]. Compared with spin-squeezed states, for Markovian dephasing processes as discussed in this section, the best precision given by the GHZ state is the shot-noise limit, the same as a CSS. Recently, the lifetime of spin-squeezed states under the influence of dephasing noise was measured in Ref. [44], where the spin-squeezed state was generated in a collection of atoms in a cavity via feedback mechanism. For experimental conditions in [44], the lifetime is  $\tau \simeq 600 \mu\text{s}$  for an initial spin-squeezed state with  $(\xi_R^2)^{-1} \simeq 4 \text{ dB}$ . Since the CSS is also affected by the same dephasing noise, at the time,  $\tau = 600 \mu\text{s}$ , even though the initially squeezed states becomes unsqueezed,  $\xi_R^2 = 1$ , it still improves the signal-to-noise ratio by  $\sim 3 \text{ dB}$  over that of an initially CSS.

## 8. Theoretical proposals and experimental realizations of squeezing generation

Above we have discussed many theoretical works about spin squeezing and its applications. Below, we review the generation of squeezing in several physical systems, with both theoretical proposals and experimental realizations. In Sec. 8.1, we review experimental progresses of generating spin squeezing in the BEC, for which the theoretical proposals have been discussed in Sec. 3.1.3. Then in Sec. 8.2, we discuss the transfer of squeezing from squeezed lights to atoms. Afterwards, spin squeezing produced by QND measurement is reviewed in Sec. 8.3.

### 8.1. Generating spin squeezing in Bose-Einstein condensations

In this section, we discuss how to generate spin-squeezed states in BEC. There are two main advantages for producing spin-squeezed states in this system: the considerable long coherence times, and the strong atom-atom interactions, which induce nonlinearity and squeezing. The simplest and most widely studied scheme to generate spin-squeezed states in a two-component BEC is to utilize particle collisions. Under the single-mode approximation, the BEC Hamiltonian can be mapped to the one-axis twisting Hamiltonian in the Schwinger representation [4, 17, 119, 120, 121, 122, 123, 124, 125, 126, 127, 129, 130, 131, 132, 133, 18, 134, 135, 136], which was realized in experiments [17, 18, 19, 20]. The validity of the two-mode approximation has been confirmed by using perturbation-based Bogoliubov theory [125], and also by employing the positive- $P$  method [120], both gave a more detailed analysis than using a single-mode approximation. References [137, 138] presented an effective two-axis twisting Hamiltonian resulting from Raman scattering. Spin squeezing in a spinor-1 BEC was studied in Refs. [145, 144, 146, 147, 142, 148, 143]. There, spin-squeezed states could be generated via spin-exchange interactions [145, 144]. For a spinor-1 BEC, which should be described by the SU(3) algebra, spin-squeezed states can be created in an SU(2) subspace [146, 147, 143], and even simultaneously in all the three SU(2) subspaces [147]. Decoherence in the generation of spin squeezing was studied in the cases of particle collisions [151, 141], and particle losses [126, 153, 154]. Below, we present some recent experiments about producing spin-squeezed states.

#### 8.1.1. Experimental realizations

In the BEC system, we use the concept of spin squeezing since physical observables associated with the  $N$  two-level atoms can be described by a fictitious spin  $J = N/2$  in the Schwinger representation, shown in Eq. (151). Below, we show some very recent experimental results [19, 20]. To illustrate these results, we explain the so-called number-squeezing parameter, which is defined as

$$\xi_N^2 = \frac{4(\Delta J_z)^2}{N}. \quad (338)$$

It is called number-squeezing parameter because  $J_z$  measures the number difference between the two components, it is related to the metrological squeezing parameter as

$$\xi_R^2 = \frac{\xi_N^2}{C^2}, \quad (339)$$

where

$$C = \frac{2|\langle \vec{J} \rangle|}{N}, \quad (340)$$

is the contrast of the Ramsey interferometer.

The intrinsic physics of the generation of squeezed states in BEC is the particle collisions, as illustrated in Sec. 3, where we employed a simple two-component BEC, for which an effective one-axis twisting Hamiltonian is derived. In experiments, the BEC can be loaded in a optical lattice, and is described by a Bose-Hubbard model, of which the atom number statistics undergoes a drastic change from a superfluid phase to a Mott insulator phase [149], where the atom number fluctuation is strongly suppressed. The atomic number squeezing has been implemented in Ref. [17]. In this experiment, the condensates were loaded in an optical lattice, and the system can be described by a Bose-Hubbard Hamiltonian, of which the atom number

statistics undergoes a drastic change from a superfluid phase to a Mott insulator phase [149]. For  $N$  atoms loaded in an  $M$ -site lattice, The Bose-Hubbard Hamiltonian reads

$$H = \gamma \sum_{\langle i,j \rangle} \hat{a}_i^\dagger \hat{a}_j + \sum_i \epsilon_i \hat{n}_i + \frac{g\beta}{2} \sum_i \hat{n}_i (\hat{n}_i - 1), \quad (341)$$

where  $\hat{a}_i$  and  $\hat{a}_i^\dagger$  are bosonic operators of atoms on the  $i$ th site,  $\hat{n}_i = \hat{a}_i^\dagger \hat{a}_i$  is the corresponding number operator, and  $\epsilon_i$  denotes the external potential term. The interaction strength  $g$  is associated with the  $s$ -wave scattering length, and is shown in Eq. (147), and

$$\beta \equiv \int d^3r |\phi(r)|^4. \quad (342)$$

The tunneling amplitude  $\gamma$  between the  $i$  and  $j$  sites is

$$\gamma = \int d^3r \phi(r - r_i) \left[ -\frac{\hbar^2}{2m} \nabla^2 + U(r) \right] \phi(r - r_j). \quad (343)$$

In the strong tunneling regime  $g\beta/\gamma \ll 1$ , i.e., the superfluid phase, the interaction term is negligible and the single atomic state will spread the lattice. The many-body ground state is given as [286]

$$|\psi_{\text{SF}}\rangle_{g\beta=0} \propto \left( \sum_{i=1}^M \hat{a}_i^\dagger \right)^N |0\rangle, \quad (344)$$

of which the on-site number fluctuation obeys Poissonian distribution, i.e.,

$$\Delta \hat{n}_i = \langle \hat{n}_i \rangle. \quad (345)$$

Conversely, if the ratio  $g\beta/\gamma$  overcomes a critical point, the ultracold gas enters the Mott insulator phase, where the atomic states are localized and the many-body ground state wavefunction becomes

$$|\psi_{\text{MI}}\rangle_{\gamma=0} \propto \prod_{i=1}^M \left( \hat{a}_i^\dagger \right)^{n_i} |0\rangle, \quad (346)$$

which is a product of local Fock states for each lattice site, with  $n_i$  the on-site atom number, and the corresponding number fluctuations vanish.

In Ref. [17], atom number squeezing was observed in the Mott insulator phase. They loaded about  $10^8$   $^{87}\text{Rb}$  atoms into a time-orbiting potential (TOP) trap and produced about  $10^4$  condensates of  $F = 2$ ,  $m_f = 2$  atoms. After an adiabatic relaxation, the condensate is then loaded in a one-dimensional vertically oriented optical lattice, which consists of  $\sim 12$  weakly linked mesoscopic wells. The squeezing of the particle number was indirectly observed through detecting the phase-sensitivity interference of atoms released from the lattice. The phase variance  $\sigma_\phi$  is related to the number variance  $\sigma_n$  at each lattice as

$$\sigma_n \propto \frac{1}{\sigma_\phi}, \quad (347)$$

due to the phase number uncertainty relation. The increase of the phase variance indicates the reduction of the number variance. As discussed in Sec. 3.2.3, the spin squeezing can be produced in BEC due to nonlinear particle collisions, while in this experiment, besides particle collisions in the same well, there exists a tunneling between neighboring wells. The physics of the formation of number squeezing can be illustrated by considering a simple two-well version of the Bose-Hubbard Hamiltonian (341), written as

$$H = \gamma \left( a_L^\dagger a_R + a_R^\dagger a_L \right) + \frac{g\beta}{2} \left[ \left( a_L^\dagger a_L \right)^2 + \left( a_R^\dagger a_R \right)^2 \right], \quad (348)$$

where the subscripts L and R represent the left and right well, respectively. In the Schwinger representation (151) the above Hamiltonian becomes

$$H = \gamma J_x + \chi J_z^2 + \frac{\chi N^2}{2}, \quad (349)$$

where  $N$  is the total particle number, and the squeezing strength  $\chi = g\beta$ . To create number-squeezed states, they increase the ratio  $N\chi/\gamma$  by varying the intensity of the lattice laser and the initial condensate density. The atomic interference is realized by releasing the atoms to fall under the gravity. The contrast of the resulting interference pattern is used as a phase probe to distinguish between the limits of coherent and Fock states. With the adiabatic increase of the lattice potential depth, they found the increase of the phase variance, characterized by the squeezing factor  $S$ , defined by

$$\sigma_\phi^2 = S\sigma_{\phi 0}^2, \quad (350)$$

where  $\sigma_{\phi 0}^2$  corresponds to non-squeezed case. In the case

$$Ng\beta/\gamma = 10^5, \quad (351)$$

where  $N$  refers to the particle number in the central well, they found that the squeezing factor

$$S_{\text{dB}} = 10 \log_{10} \frac{\sigma_\phi^2}{\sigma_{\phi 0}^2} \simeq 25 \text{ dB}, \quad (352)$$

corresponding to a number variance  $\sigma_n \simeq 1$  in the central well.

In Ref. [149], by using a probe that is sensitive only to the presence of atom pairs at a given lattice, they observed a continuous suppression of number fluctuations when the ultracold sample evolves from the superfluid regime to the Mott insulator regime. In this experiment, the specific two-particle probe are spin-changing collisions, which convert spin  $f = 1$  atoms in the  $m = 0$  Zeeman sublevel to pairs with one atom in  $m = +1$  and the other in the  $m = -1$ . The advantage of the spin-collisional based probes is that they are nondestructive, and they can be resonantly controlled using the differential shift between Zeeman sublevels induced by an off-resonant microwave field. The experiments confirmed that the atom number exhibits near-Poissonian fluctuations for shallow lattices, and strongly suppressed fluctuations for deep lattice. Besides, their results indicate that number squeezing is robust with respect to experimental manipulations.

Experiments of Ref. [160] presented extended coherence times by a factor of 2 over those expected with coherent state BEC interferometry. The coherent time, which is limited due to the mean-field interaction induced decoherence, is probed by using the decay of Bloch oscillations. The theoretical treatment for a BEC in an optical lattice begins with the Bose-Hubbard Hamiltonian (341). The tunneling is weakened by applying a large energy gradient across the array, which benefits from the advantage that the on-site mean-field energy is unaffected. They have demonstrated that, for number squeezed states prepared at potential depth  $U = 22.5E_R$ , where  $E_R = \hbar^2 k^2 / 2m$  and  $k = 2\pi/\lambda$ , with  $\lambda = 852 \text{ nm}$ , the coherence time  $\tau_c = 19.3 \pm 3.5 \text{ ms}$ , which represents an increase of a factor of 2.1 over the expected decay time of an array of coherent states in the same lattice potential. It is interesting to note that here squeezing extends the coherence time: typically, the enhanced fragility of squeezed states to loss mechanisms results in reduced coherence times. Then in Ref. [159], phase coherence of two BEC confined in a double-well potential on an atomic chip was observed. It holds for times up to  $\sim 200 \text{ ms}$  after splitting, a factor of 10 longer than the phase diffusion time expected for a coherent state for the experimental conditions.

In the previous experiments [17, 286, 149, 159, 160], the suppression of atom number fluctuations in a BEC was observed indirectly. The direct determination of squeezing parameter requires access to the on-site atom occupations. This was demonstrated in Ref. [18] by imaging the condensate with a resolution of  $1 \mu\text{m}$  (full-width at half-maximum), which is well below the lattice spacing of  $5.7 \mu\text{m}$ , and fulfils the criterion of local measurement. The condensate was loaded in an optical lattice of two to six wells, and the occupation number per site ranges from 100 to 1,100 atoms. The wells of the lattice are fully resolved, and thus the



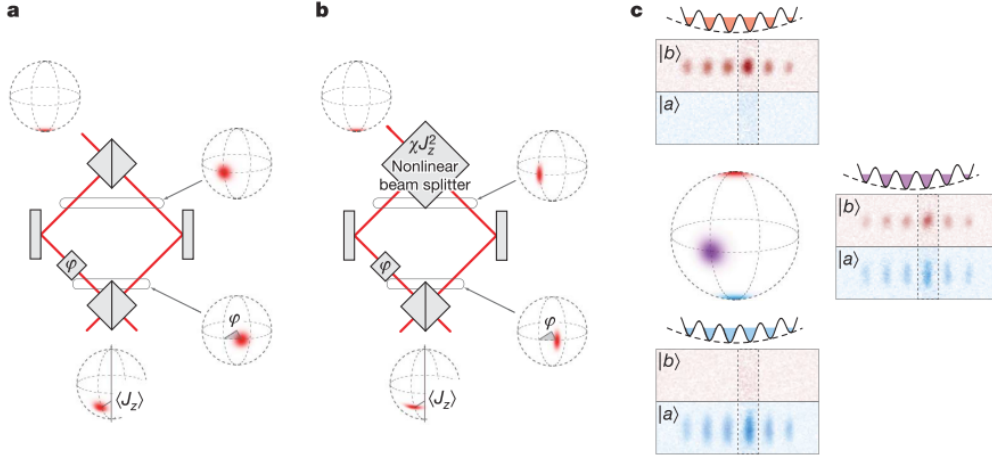


Figure 14: (Color online) Comparison of linear and nonlinear interferometry [19]. **a**, Classical Mach-Zehnder interferometer. The two-mode field is mapped to a Bloch-sphere under the Schwinger representation (151). Here the input state is equivalent to a CSS. **b**, By using a nonlinear beam splitter, which acts as one-axis twisting Hamiltonian and generates spin-squeezed state, the precision of interferometry was improved. **c**, Six independent BECs of  $^{87}\text{Rb}$  were prepared in a one-dimensional optical lattice [19]. State-selective time-delayed imaging causes the atomic clouds to have different shapes. For this trap geometry, the dynamics is described by a one-axis twisting Hamiltonian. This figure is from Ref. [19].

atom number in each lattice site can be determined by direct integration of the atomic density obtained by absorption imaging. The observed spin-squeezed states allow a precision gain of 2.3 dB (two wells) and 3.8 dB (six wells) over the standard quantum limit for interferometric measurements.

Recently, some notable improvements have been reported [19, 20]. Although squeezed states have been generated previously, Ref. [19] first performed a direct experimental demonstration of interferometric phase precision beyond the standard quantum limit in a novel nonlinear Ramsey interferometer. The experimental scheme, shown in Fig. 14, involved six independent BECs of  $^{87}\text{Rb}$  (total number 2,300) prepared in a one-dimensional lattice, enables parallel experiments performed on six wells independently, which results in increased statistics for a given measurement time. The hyperfine states  $|a\rangle = |F = 1, m_F = 1\rangle$  and  $|b\rangle = |F = 2, m_F = -1\rangle$  form a two-level system. The single traps are almost spherical and have dipole frequencies of  $\omega_{\text{trap}} = 2\pi \times 425$  Hz. For this trap geometry, the single mode approximation is well justified, and the dynamics is governed by a one-axis twisting Hamiltonian

$$H/\hbar = \Delta\omega_0 J_z + \chi J_z^2 + \Omega J_\phi, \quad (353)$$

where the third term describes spin rotations around an axis

$$J_\phi = J_x \cos \phi + J_y \sin \phi, \quad (354)$$

due to the coupling of  $|a\rangle$  and  $|b\rangle$  by using two-photon combined microwave and radio-frequency pulses with a Rabi frequency of  $\Omega$  and phase  $\phi$ . In the experiment, the Rabi frequency  $\Omega$  can be switched rapidly between 0 and  $2\pi \times 600$  Hz, allowing for fast diabatic coupling of the states.

Then we consider the nonlinear interaction strength  $\chi$ . When the two states  $|a\rangle$  and  $|b\rangle$  are complete overlap spatially, according to the discussion in Sec. 3.2.3 we have

$$\chi \propto a_{aa} + a_{bb} - 2a_{ab}, \quad (355)$$

where the  $s$ -wave scattering lengths in this experiment [19] satisfy

$$a_{aa} : a_{bb} : a_{ab} = 100 : 97.7 : 95, \quad (356)$$

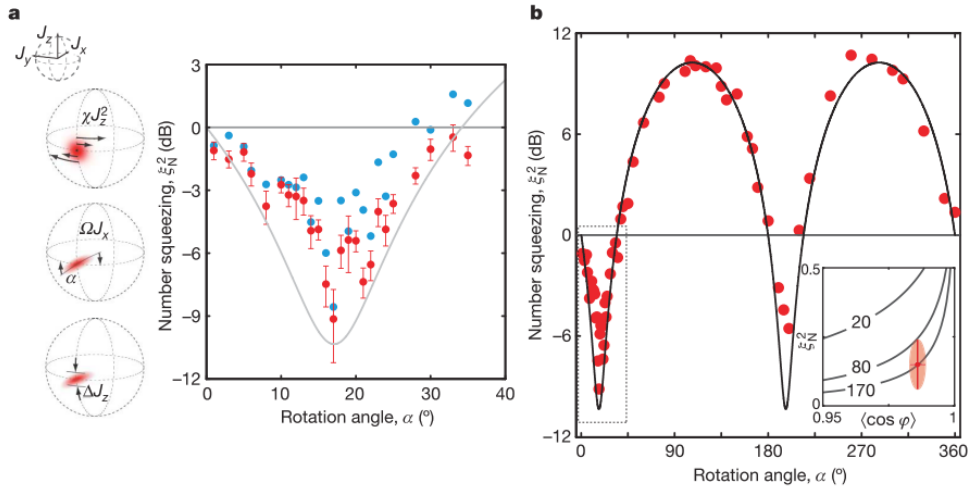


Figure 15: (Color online) Characterization of the quantum state within a nonlinear interferometer [19]. **a**, In the left, the twisting effects of the one-axis twisting Hamiltonian. In the right, the blue data have been corrected for photon shot noise and the red data additionally take the technical noise into account [19]. The best number-squeezing factor was  $\xi_N^2 = -8.2^{+0.9}_{-1.2}$  dB. **b**, Noise tomography of the output state of the nonlinear beam splitter. The dotted box indicates the region detailed in **a**. The largest fluctuations measured have a number-squeezing factor of  $\xi_{N,\max}^2 = +10.3^{+0.3}_{-0.4}$  dB. This figure is from Ref. [19].

which results in very small nonlinear interaction strength,  $\chi \simeq 0$ . To overcome this problem, they used the Feshbach resonance to control scattering lengths. By choosing the magnetic field  $B = 9.10$  G,  $a_{ab}$  can be decreased by a narrow Feshbach resonance and they achieved  $\chi = 2\pi \times 0.063$  Hz. The magnetic field is preserved constant throughout the whole interferometric sequence, while during the coupling pulses the interaction strength  $\chi$  is negligible since the system is in the Rabi regime, that is,  $\chi N/\Omega \ll 1$ .

The experiment begins with a CSS that polarized to the  $-z$  direction according to the chosen coordinate system. After a  $\pi/2$  pulse the state turns to be polarized in the  $x$  direction, thus  $\langle J_z \rangle = \langle J_y \rangle = 0$ . Next, by means of Feshbach resonance, the state evolves under the one-axis twisting Hamiltonian, which causes a shearing effect, shown in Fig. 2, and finally the state has a squeezing angle  $\alpha_0$  with respect to the  $z$  direction. As shown in Fig. 14, to make the state useful for squeezing metrology, it is first rotated around the center of the uncertainty ellipse by  $\alpha = \alpha_0 + \pi/2$ , and then evolves freely for  $\tau = 2 \mu\text{s}$ , during which a phase difference  $\varphi$  is gained between the two states  $|a\rangle$  and  $|b\rangle$ . Followed by a  $\pi/2$  pulse, this phase difference is estimated by a population measurement. This standard Ramsey process is illustrated in Fig. 14. The experimental results for number squeezing are shown in Fig. 15. The minimal fluctuations are found for rotation angle  $\alpha = 16^\circ$ , where the corresponding number squeezing factor is

$$\xi_N^2 = \frac{4(\Delta J_z)^2}{N} = -6.9^{+0.8}_{-0.9} \text{ dB}, \quad (357)$$

for which the photon shot noise due to the imaging process is removed. By additionally taking into account the technical noise due to coupling-pulse imperfections, the squeezing factor can be improved to

$$\xi_N^2 = -8.2^{+0.8}_{-1.2} \text{ dB}, \quad (358)$$

which is close to the atom-loss-limited theoretical optimum for this system [154]. Furthermore, they pointed out that the best spin squeezing factor  $\xi_R^2 = \xi_N^2 / \cos \varphi = -8.2$  dB is obtainable, which implies the entanglement of 170 atoms [227].

In another recent work [20], spin squeezing was generated in an atom chip by controlling the elastic collision interactions through the wavefunction overlap of the two states with a state-dependent microwave

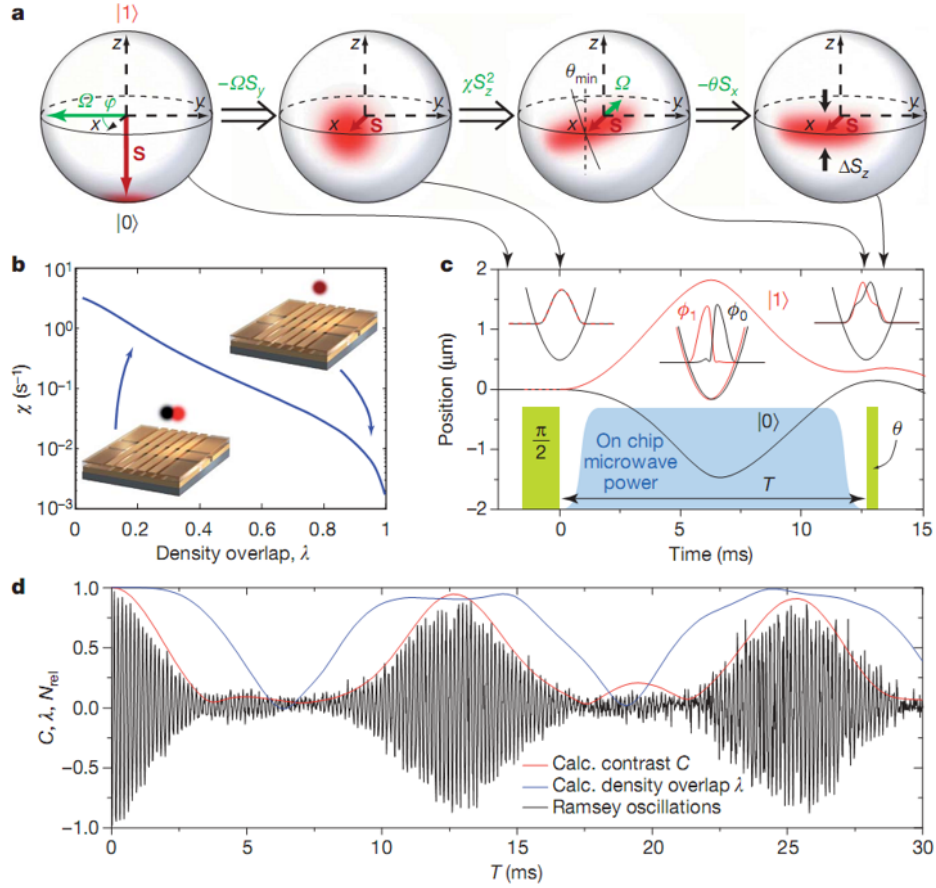


Figure 16: (Color online) Spin squeezing and entanglement through controlled interactions on an atom chip [20]. **a**, Bloch sphere representations of the dynamic evolution of the BEC internal states. The red disks represent spin noise. The one-axis twisting Hamiltonian  $\chi S_z^2$  reduces the spin noise at an angle  $\theta_{\min}$ , and the subsequent pulse rotates the state around  $-x$  by an angle  $\theta$  [20]. **b**, Control of the nonlinearity  $\chi$  on the atomic chip.  $\chi$  depends on the difference of intra- and inter-state atomic interactions. **c**, Experimental sequence and motion of the two BEC components [20]. **d**, Measured Ramsey fringes in the normalized population difference. This figure is from Ref. [20].

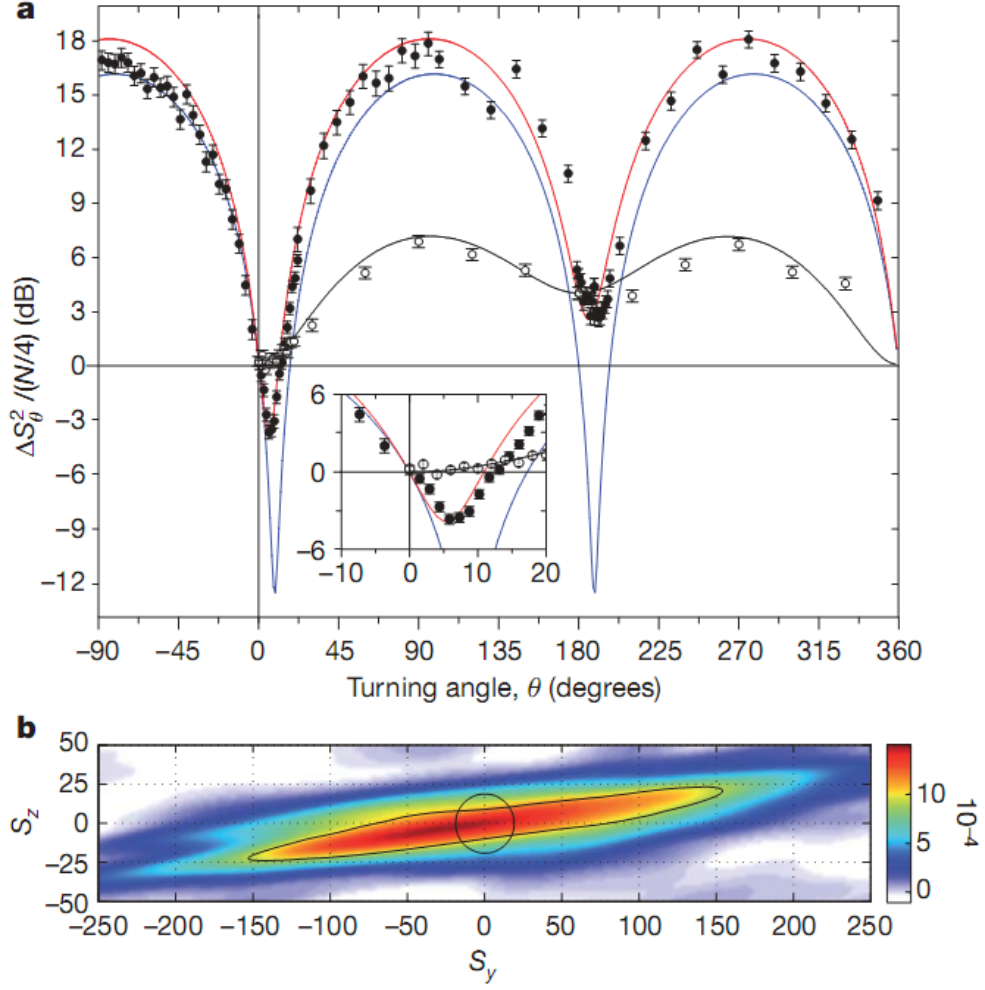


Figure 17: (Color online) Spin noise tomography and reconstructed Wigner function of the spin-squeezed BEC [20]. **a**, Observed spin noise for the spin-squeezed state (filled circles) and for a CSS (open circles). In the squeezed state, a spin noise reduction of  $-3.7 \pm 0.4$  dB is observed for  $\theta_{\min} = 6^\circ$ , corresponding to  $\xi_R^2 = -2.5 \pm 0.6$  dB of metrologically useful squeezing for Ramsey spectroscopy [20]. The blue line describes the simulation results which take account of particle loss but not technical noise, give rise to a minimum variance of -12.8 dB. The technical noise is included in the red line, which is in good agreement with the experimental data. **b**, Reconstructed Wigner function. The black contour line indicates where the Wigner function has fallen to  $1/\sqrt{e}$  of its maximum. For comparison, the circular  $1/\sqrt{e}$  contour of an ideal coherent spin state is shown. This figure is from Ref. [20].

potential. The hyperfine states  $|0\rangle \equiv |F=1, m_F=-1\rangle$  and  $|1\rangle \equiv |F=2, m_F=1\rangle$  of  $^{87}\text{Rb}$  forms a two-level system. The system Hamiltonian is the same as in Eq. (353), while here the notation of the spin operator  $J$  is replaced with  $S$ . A key problem in this experiment is also to produce nonvanishing nonlinear interaction strength, since the  $s$ -wave scattering lengths here satisfy

$$a_{00} : a_{01} : a_{11} = 100.4 : 97.7 : 95.0. \quad (359)$$

They realized  $\chi = 0.49$  Hz though spatially separating the two components of the BEC with a state-dependent potential, during which the  $U_{AB}$  term in Eq. (153) is zero. The Ramsey process here is similar to that in Ref. [19], and is displayed in Fig. 16. At first, a CSS is prepared by a  $\pi/2$  pulse of duration  $120 \mu\text{s}$ . After that, the two components are separated, and the nonlinear interaction is active for a best squeezing time to avoid ‘oversqueezing’. The two states overlap again after 12.7 ms, and the nonlinear interaction stops. As shown in Fig. 16, the transverse spin component

$$S_\theta = S_z \cos \theta - S_y \sin \theta, \quad (360)$$

is measured by rotating the state in the  $y$ - $z$  plane by  $\theta$  before detecting  $S_z$ . The experiment results are shown in Fig. 17, where comparisons between squeezed and coherent states are presented. The normalized variance  $\Delta_n S_\theta^2 = 4\Delta S_\theta^2 / \langle N \rangle$  is plotted so that  $\Delta_n S_\theta^2 = 0$  dB corresponds to the shot noise limit. For squeezed state, a minimum of

$$\Delta_n S_\theta^2 = -3.7 \pm 0.4 \text{ dB} \quad (361)$$

is found at  $\theta_{\min} = 6^\circ$ , with interference contrast  $C = 2|\langle S_x \rangle|/N = (88 \pm 3)\%$ , indicating a squeezing parameter of

$$\xi_R^2 = -2.5 \pm 0.6 \text{ dB}, \quad (362)$$

and reduction of spin noise by  $-3.7 \pm 0.4$  dB was the observed. This could be used to improve interferometric measurements by  $-2.5 \pm 0.6$  dB over the standard quantum limit. The experimental scheme and results [20] are summarized in Figs. 16 and 17. It is pointed out that, the technique for tuning of interactions in a BEC through wavefunction overlap also works in magnetic traps and for atomic state pairs where no convenient Feshbach resonance exists.

## 8.2. Squeezing transferred from light to atoms

Squeezing of photons is not easy to preserve, hence researchers considered how to transfer squeezing from photons to atomic ensembles [50, 112, 51, 16, 54], which are more convenient for storing quantum information. Many efforts have been devoted to use atomic ensembles to realize quantum memories [48, 287, 288], and using photons as information carriers. A practical analysis of generating spin squeezing in an ensemble of atoms, by absorption of squeezed light, was studied theoretically in [51], and soon after it was realized in experiments [16]. Spin-squeezed states can also be generated via electromagnetically induced transparency [64, 66, 67, 68, 69]. In this section, we present the experimental [16] results for generating spin-squeezed states when the atomic ensemble absorbs the squeezed vacuum field of the photons.

### 8.2.1. Theoretical proposals

Here discuss the theoretical proposal [51] of creating spin-squeezed states in atomic ensembles via the absorption of squeezed vacuum, which is illustrated in Fig. 18. The experiment is realized in Ref. [16]. We consider a cloud of Cs atoms [51]. The energy level structure is shown in Fig. 18, where we only consider levels  $|6S_{1/2}, F=4\rangle$ ,  $|6P_{3/2}, F=5\rangle$  and  $|6D_{5/2}, F=6\rangle$ . There are two transition configurations: A  $V$ -type configuration consisting of levels  $|0\rangle$  ( $|6S_{1/2}, m=0\rangle$ ),  $|1\rangle$  ( $|6P_{3/2}, m=-1\rangle$ ) and  $|2\rangle$  ( $|6P_{3/2}, m=1\rangle$ ), which is used to generate spin-squeezed states; a  $\Lambda$ -type configuration consisting of levels  $|1\rangle$ ,  $|2\rangle$  and  $|6D_{5/2}, m=0\rangle$ , which is used for polarization measurement.

Below we mainly consider the  $V$ -type structure and only investigate the subspace spanned by levels  $|1\rangle$  and  $|2\rangle$ . The transition between these two levels is forbidden due to symmetry. However, effective transition processes between these two levels are realized via the level  $|0\rangle$ , and the processes are described by the

operators  $F_{12}$  and  $F_{21}$ . Therefore, we should first derive the dynamical evolution between levels  $|1\rangle$  (or  $|2\rangle$ ) and  $|0\rangle$ , which involves some assumptions and the Heisenberg-Langevin theory [51].

The pseudospin operators are given by

$$\begin{aligned} F_x &= \frac{1}{2} (F_{12} + F_{21}), \\ F_y &= \frac{1}{2i} (F_{12} - F_{21}), \\ F_z &= \frac{1}{2} (F_{11} - F_{22}), \end{aligned} \quad (363)$$

where the collective operators  $F_{ij} = \sum_{\mu} \sigma_{ij}^{(\mu)}$ , ( $i, j = 1, 2$ ), and  $\mu$  is the particle index and  $\sigma_{ij} = |i\rangle\langle j|$ . Note that, since we use the hyperfine states, the angular momentum operators are denoted by  $F$  instead of  $J$ .

As shown in Fig. 18, a left-circularly-polarized coherent field and a right-circularly-polarized squeezed vacuum field propagate along the  $z$ -direction through a cloud of Cs atoms. Due to the selection rule, the coherent field is coupled to levels  $|0\rangle$  and  $|1\rangle$ , and the squeezed vacuum is coupled to  $|0\rangle$  and  $|2\rangle$ . The atomic decay rate  $\gamma$  is assumed to be equal for the two upper states  $|1\rangle$  and  $|2\rangle$ . To describe the interaction between field and atoms, Ref. [51] employs the continuous field operators  $a(\vec{r}, t)$  and atomic operators  $\sigma_{ij}(\vec{r}, t)$ . The continuous atomic operators are given by [51, 289]

$$\sigma_{ij}(\vec{r}, t) = \frac{1}{\rho \Delta V} \sum_{\mu} \exp \left[ i \frac{\omega_{ij}}{c} (z - z^{(\mu)}) \right] \sigma_{ij}^{(\mu)}, \quad (364)$$

where  $\rho$  is the atomic density, and the sum is performed over atoms enclosed in the volume  $\Delta V$  around the position  $\vec{r}$ . The volume  $\Delta V$  is only a small fraction of the entire atom cloud interacting with the field. The frequency between levels  $|i\rangle$  and  $|j\rangle$  is  $\omega_{ij} = (E_i - E_j)/\hbar$ .

Now we consider an important assumption  $\lambda \ll L \sim (\Delta V)^{1/3} \ll \lambda' \lesssim l$ , where  $\lambda$  is the wavelength of the field,  $\lambda'$  is the length-scale of the field changes due to absorption and dispersion, and  $l$  is the length of the atomic cloud along the field propagation direction. This assumption ensures a slow-varying field equation [51, 289]

$$\left( \frac{1}{c} \frac{\partial}{\partial t} + \frac{\partial}{\partial z} \right) a(z, t) = g \rho \int dx \int dy u(x, y) \sigma_{01}(\vec{r}, t), \quad (365)$$

which separates the transverse component of the field  $a(\vec{r}, t)$ . Here,  $u(x, y)$  is the transverse mode function satisfying the normalization condition  $\int dx \int dy u^2(x, y) = 1$ . The interaction strength  $g$  is determined by the atomic dipole moment.

The Heisenberg equation of motion for the continuous atomic dipole operator is given by [289]

$$\begin{aligned} \frac{\partial}{\partial t} \sigma_{01}(\vec{r}, t) &= - \left( \frac{1}{2} \gamma + i \omega_{01} \right) \sigma_{01}(\vec{r}, t) + g u(x, y) a(z, t) [\sigma_{11}(\vec{r}, t) - \sigma_{00}(\vec{r}, t)] \\ &\quad + \sqrt{\gamma} [\sigma_{11}(\vec{r}, t) - \sigma_{00}(\vec{r}, t)] b^{\text{in}}(\vec{r}, t), \end{aligned} \quad (366)$$

where  $\gamma$  is the atom decay rate,  $b^{\text{in}}(\vec{r}, t)$  is the continuous operator of the atomic noise. For different atoms, the noise operators are independent, and thus obey the commutation relations

$$\rho [b^{\text{in}}(\vec{r}, t), b^{\text{in}\dagger}(\vec{r}_1, t_1)] = \delta(\vec{r} - \vec{r}_1) \delta(t - t_1). \quad (367)$$

Now we assume the field to be so weak that the number of excited atoms is negligibly small, and replace  $\sigma_{00}(\vec{r}, t) - \sigma_{11}(\vec{r}, t) = 1$  in Eq. (366). Then we obtain

$$\frac{\partial}{\partial t} \sigma_{01}(\vec{r}, t) = - \left( \frac{1}{2} \gamma + i \omega_{01} \right) \sigma_{01}(\vec{r}, t) - g u(x, y) a(z, t) - \sqrt{\gamma} b^{\text{in}}(\vec{r}, t), \quad (368)$$

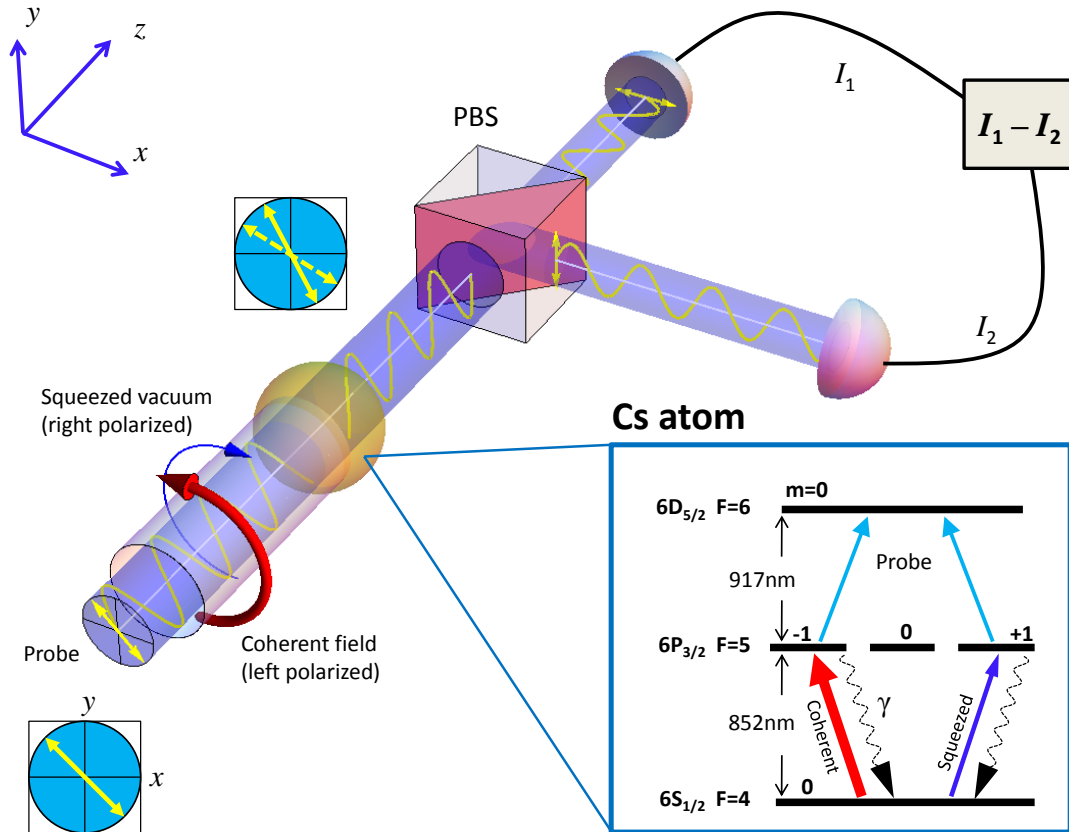


Figure 18: (Color online) Schematic diagram for a polarization measurement [51]. Three input beams propagate through a Cs atom cloud along the  $z$ -direction, a  $\pi/4$ -polarized probe beam which is nearly resonant with  $6P_{3/2}$  to  $6D_{5/2}$  transition, a left-polarized coherent beam that induces transition [51] between levels  $|0\rangle$  ( $6S_{1/2}$ ,  $m=0$ ) and  $|1\rangle$  ( $6P_{3/2}$ ,  $m=-1$ ), and a right-polarized squeezed vacuum which coupled with levels  $|0\rangle$  and  $|2\rangle$  ( $6P_{3/2}$ ,  $m=1$ ). The coherent field is much stronger than the squeezed vacuum. The atom cloud is optically thick for the squeezed vacuum and coherent field, and we assume that these two fields are completely absorbed, while the probe beam is only partially absorbed. Due to the population differences between levels  $|1\rangle$  and  $|2\rangle$ , the refraction index for left- and right-polarization components of the probe beam are different, thus the polarization plane of the probe beam is rotated along the  $z$ -direction. After a polarization beam splitter (PBS), the probe beam is split into  $x$ - and  $y$ -polarized beams and is detected by two photon detectors. As the probe beam is  $\pi/4$  polarized, for the case of no atom clouds, the photocurrent difference is zero. Therefore, when an atom could exist, the photocurrent different is measured to gain information about the population fluctuations of levels  $|1\rangle$  and  $|2\rangle$ . As the absorption is complete, a 50% degree of spin squeezing can be obtained.

The solutions of Eqs. (368) and (365) can be obtained [51] by using the Fourier transform of  $\sigma_{01}$ ,  $b^{\text{in}}$  and  $a$ ,

$$\sigma_{01}(\vec{r}, \omega) = -\frac{g u(x, y) a(z, \omega) + \sqrt{\gamma} b^{\text{in}}(\vec{r}, \omega)}{\gamma/2 - i(\omega - \omega_{01})}, \quad (369)$$

$$a(z, \omega) = a(0, \omega) e^{ik(\omega)z} - \int_0^z dz_1 \frac{\sqrt{\gamma} g \rho e^{ik(\omega)(z-z_1)}}{\gamma/2 - i(\omega - \omega_{01})} b^{\text{in}}(z_1, \omega), \quad (370)$$

with the new dispersion relation

$$k(\omega) = \frac{\omega}{c} + \frac{ig^2\rho}{\gamma/2 - i(\omega - \omega_{01})}. \quad (371)$$

The redefined continuous noise operators become

$$b^{\text{in}}(z, \omega) = \int dx \int dy u(x, y) b^{\text{in}}(\vec{r}, \omega), \quad (372)$$

with commutation relation  $\rho [b^{\text{in}}(z, \omega), b^{\text{in}\dagger}(z_1, \omega_1)] = \delta(z - z_1) \delta(\omega - \omega_1)$ . For a specific field, the expectation values of Eq. (370) can be calculated, and inserted into Eq. (369) to obtain the dynamics of the local dipole operators. Finally, by using Eq. (364) the collective atomic dipole of the sample can be obtained [51].

The above results can be used to compute the collective operators

$$F_{ij} = \sum_{\mu} \sigma_{ij}^{(\mu)} = \rho \int d\vec{r} \sigma_{ij}(\vec{r}), \quad (i, j = 1, 2). \quad (373)$$

Assume now that the coherent field  $a_1$  and squeezed vacuum  $a_2$  have an identical transverse mode function  $u(x, y)$ , and also that the coherent amplitude is much stronger than the squeezed vacuum fluctuations. Thus the operator products can be linearized as

$$\begin{aligned} \sigma_{12}(\vec{r}, t) &= \langle \sigma_{10}(\vec{r}, t) \rangle \sigma_{02}(\vec{r}, t), \\ \sigma_{12}(\vec{r}, \Delta = \omega - \omega_1) &= \langle \sigma_{10}(\vec{r}, t = 0) \rangle \sigma_{02}(\vec{r}, \omega), \end{aligned} \quad (374)$$

where  $\langle \sigma_{10}(\vec{r}, t) \rangle = \langle \sigma_{10}(\vec{r}, t = 0) \rangle \exp(-i\omega_1 t)$ . Now we assume  $\omega_1 = \omega_{01} = \omega_{02}$ , and consider the practical condition

$$g^2\rho \gg \frac{\gamma\Delta}{c}, \quad (375)$$

which implies complete absorption, and that the light traveling time is shorter than the atomic decay time. Finally, the collective operator  $F_{12}$  can be obtained [51]

$$\begin{aligned} F_{12}(\Delta) &\simeq \frac{\alpha^*}{\gamma - i\Delta} [a_2^{\text{in}}(\omega_1 + \Delta) + d_2^{\text{in}}(\omega_1 + \Delta)] \\ &= \kappa e^{-i\phi} [a_2^{\text{in}}(\omega_1 + \Delta) + d_2^{\text{in}}(\omega_1 + \Delta)], \end{aligned} \quad (376)$$

where  $a_2^{\text{in}}(t) \equiv a_2^{\text{in}}(\vec{r} = 0, t)$ , and  $\kappa, \phi$  are the argument and phase of  $\alpha^*/(\gamma - i\Delta)$ , respectively. The spin squeezing is obtained from

$$\langle F_{x,y}^2 \rangle = \frac{1}{4} \langle F_z \rangle (4X_{+,-}^2 + 1), \quad (377)$$

where  $\langle F_z \rangle = \kappa^2 = \frac{|\alpha|^2}{\gamma^2 + \Delta^2}$ , and  $X_{+,-}$  are the quadrature phase amplitudes defined as

$$\begin{aligned} X_+ &= \frac{1}{2} [e^{-i\phi} a_2^{\text{in}} + e^{i\phi} a_2^{\text{in}\dagger}], \\ X_- &= \frac{1}{2i} [e^{-i\phi} a_2^{\text{in}} - e^{i\phi} a_2^{\text{in}\dagger}]. \end{aligned} \quad (378)$$



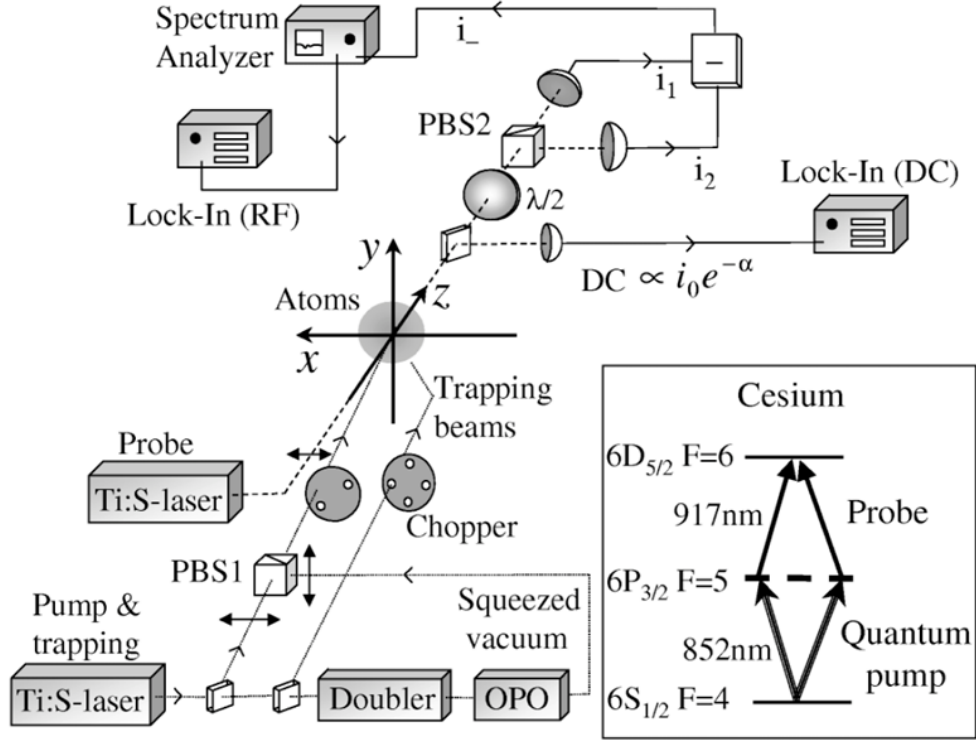


Figure 19: (Color online) Schematic diagram of the experiment in Ref. [16]. The squeezed vacuum is  $y$ -polarized, while the pumping beam is  $x$ -polarized. The probe is also  $x$ -polarized, and after the  $\lambda/2$  wave plate, it turns to  $\pi/4$  polarized. This is from Ref. [16].

For the vacuum input field  $a_2$ , the variance is  $X_{+,-}^2 = 1/4$ , and thus  $\langle F_{x,y}^2 \rangle = \frac{1}{2} \langle F_z \rangle = \frac{1}{2} \langle F \rangle$  for coherent spin state [51]. For squeezed vacuum, as discussed in Sec. 2,

$$4X_+^2 = \exp(-2|\eta|), \quad 4X_-^2 = \exp(2|\eta|), \quad (379)$$

where  $\eta = |\eta| \exp(i2\phi)$  is the bosonic squeezing parameter. Therefore, if the input field is a broadband vacuum, in the limit  $X_+^2 = 0$ , then  $\langle F_x^2 \rangle = \langle F_z \rangle / 4$  and the spin-squeezing parameter becomes (see Table 1)

$$\xi_{H''}^2 = \frac{1}{2}. \quad (380)$$

Thus for an optically thick atomic ensemble, it is possible to achieve 50% spin squeezing when the squeezed vacuum is completely absorbed.

### 8.2.2. Experimental realizations

Soon after the above theoretical proposal [51], an experiment was carried out in Ref. [16], with the experimental setup shown in Fig. 19. They observed a spin-squeezed ensemble of  $10^7$  cold Cs atoms, which is produced via transferring a state of free propagating squeezed light to the atomic ensemble. This experiment also demonstrated storage of quantum information of light in atoms. In this experiment, they

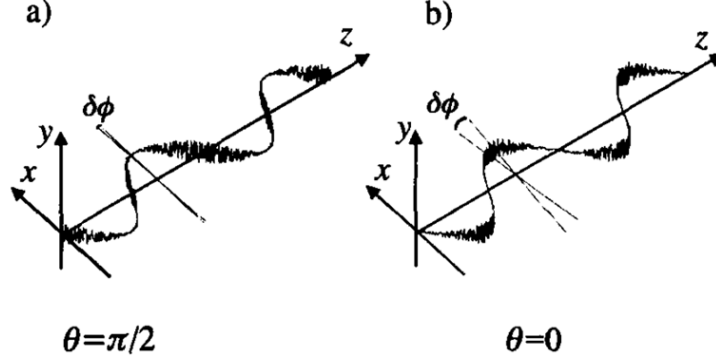


Figure 20: (Color online) Schematic diagram of the electric field for the mixed output beam after PBS1 in Fig. 19 [54]. The fluctuations in the composite field of the coherent pumping beam and the squeezed vacuum depend on their phase difference. If the phase difference  $\theta = 0$ , the so-called out-of-phase case, the field will have reduced fluctuations in the polarization axis direction, while if  $\theta = \pi$ , the so-called in-phase case, the field will have reduced fluctuations. This figure is from Ref. [54].

prepared about  $10^9$  Cs atoms in a magneto-optical trap, and then excited the  $6P$  collective spin with the coherent pump polarized along the  $x$ -direction to establish the quantum limit of the spin noise. The coherent pump is of 50 mW with a beam diameter of 4.0 mm, resonant with the 852 nm transition between  $|6S_{1/2}, F = 4\rangle$  and  $|6D_{5/2}, F = 6\rangle$ , provides weak excitation for the  $6P$  collective spin of about  $10^7$  atoms. Then the atom states are detected by a probe beam, which is linearly polarized parallel to the coherent component of the pump and near resonant with the  $|6P_{3/2}, F = 5\rangle \rightarrow |6D_{5/2}, F = 6\rangle$  (917 nm) transition. The properties of atoms are related to the change in the probe differential photocurrent  $\delta i$ . In the absence of atoms, the differential photocurrent is zero on average, and fluctuates due to shot noise. In the experiment, the fluctuation of the change of the differential photocurrent [52]

$$(\delta i)^2(\Delta) = -[1 - \exp(-\alpha_\Delta)] + s \alpha_0 \exp(-2\alpha_\Delta) (\delta \tilde{J})^2 \quad (381)$$

is measured, where  $(\delta \tilde{J})^2$  is the atomic noise contribution per atom depending on the geometry of the experiment,  $s$  is the probe saturation parameter, and

$$\alpha_\Delta = \alpha_0 \frac{(\gamma/2)^2}{\Delta^2 + (\gamma/2)^2} = \frac{\sigma}{A} N \frac{(\gamma/2)^2}{\Delta^2 + (\gamma/2)^2} \quad (382)$$

is the probe optical depth at the detuning  $\Delta$  [16, 76], with  $N$  the number of atoms interacting with the probe,  $\sigma$  the atomic cross section for unpolarized light,  $A$  the cross section of the probe beam, and  $\gamma$  the atomic decay rate.

The probe beam diameter is 3.7 mm and the power is about 250 mW for the off-resonant spin squeezing measurements  $s = 0.4$ . The squeezing transfer is performed via injecting squeezed vacuum which is linearly polarized along the  $y$ -direction. After the first polarized beam splitter (PBS1), the coherent pumping beam and the squeezed vacuum are mixed, and thus the output field will have fluctuations in either the polarization axis direction or in the ellipticity (depending on the phase as shown in Fig. 20) reduced below the standard quantum limit [16].

In the case of squeezed light, the fluctuations in the intensity difference between the right- and left-polarized components of the pump field is

$$\Delta S_z^2 = \frac{n}{4} (R_- \cos^2 \theta + R_+ \sin^2 \theta), \quad (383)$$

where  $S_z$  is the Stokes operator (E.3),  $\theta$  is the phase difference between the squeezed vacuum and the coherent pumping field, and  $R_\pm$  are determined by the efficiency of the squeezing source, for coherent states

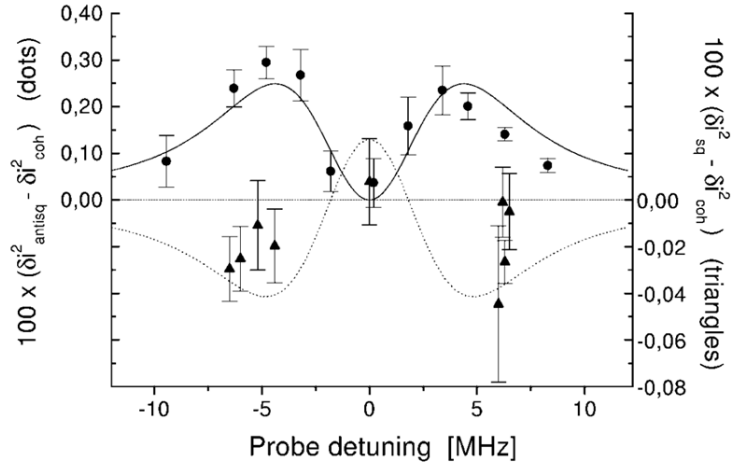


Figure 21: Squeezed spin noise of atoms [16]. Dashed line at zero: spin noise for uncorrelated atoms. Dots (left axis): antisqueezed spin noise. Triangles (right axis): squeezed spin noise. Solid line: square Doppler broadened dispersion function. Dotted line: expected spin squeezing spectrum. The detuning uncertainty is 0.5 MHz. Note that the scales for spin squeezing and spin antisqueezing are different. This figure is from Ref. [16].

$R_{\pm} = 1$ . Therefore, if  $R_- < 1 < R_+$  and in the case of  $\theta = 0$ , the output field has ellipticity fluctuations, and the fluctuations of the intensity difference between the right- and left-polarized components of the output field are reduced below the shot-noise limit [16]. Intuitively, this reduces the fluctuations in the population difference between the  $+m$  and  $-m$  Zeeman levels.

With the squeezed vacuum in phase, the average squeezing of the pump light available at the trap site is  $(-1.8 \pm 0.2)$  dB. The squeezing parameter is defined as [16]

$$\xi = \frac{(\delta i)_{\text{sq}}^2 - (\delta i)_{\text{coh}}^2}{(\delta i)_{\text{coh}}^2}, \quad (384)$$

where  $\delta i^2$  is the change in the probe differential photocurrent noise caused by the atoms. The subscripts “sq” and “coh” denote the spin-squeezed state and CSS, respectively. The best squeezing shown in Fig. 21 is  $-3.0\%$  at  $\pm 6$  MHz. The average value for all of the 183 individual measurements [16] at  $\pm 6$  MHz is  $\xi = -(1.4 \pm 0.4)\%$ . The actual degree of squeezing should be greater, since the relative contribution of the readout efficiency is not known from the overall efficiency  $\eta$ .

### 8.3. Generating spin squeezing via quantum nondemolition measurements

Quantum nondemolition measurements have been studied to generate non-classical photon states [170], and also spin-squeezed states [74, 76, 53, 75, 77, 290, 78, 80, 82, 40, 42, 92, 23, 96, 25, 94, 98]. At first, we briefly introduce the criteria for QND measurements. Then we present a typical QND-type Hamiltonian, implemented via dispersive interactions between light field and atoms. Utilizing this Hamiltonian, spin squeezing was generated in experiments [76, 23, 25]. In this QND-type Hamiltonian, the light field plays the role of a probe, by readout of the light field, the atomic spin state could be squeezed, but is conditioned to the specific readout of the light field, and thus is called conditional spin-squeezed state. By using feedback techniques [53, 290, 235, 78, 73, 99], unconditional spin-squeezed states can be generated.

#### 8.3.1. Theoretical background

We first briefly discuss the basic requirements for a QND measurement (see, e.g. Ref. [170]). Consider two systems  $A$  and  $P$ , where  $A$  is the signal, and  $P$  acts as a probe coupled to the signal. By detecting the probe (e.g., measuring a physical quantity  $P_{\alpha} \in \{P_i\}$  that belongs to  $P$ ), we could gain information about a

signal operator  $A_\alpha \in \{A_i\}$  without perturbing its subsequent evolution. The two sets  $\{A_i\}$  and  $\{P_i\}$  contain conjugate operators of the probe and signal systems, respectively. For example, for a free particle, the two conjugate operators could be the position operator  $x$  and momentum operator  $p$ . The total Hamiltonian for the signal-probe system reads

$$H = H_A + H_P + H_I. \quad (385)$$

The conditions for a QND-type measurement of a signal operator  $A_\alpha$  via detecting a probe operator  $P_\beta$  are listed below:

- (i) For a QND-type measurement of  $A_\alpha$ , the interaction term  $H_I$  must contain the operator  $A_\alpha$ .
- (ii) Backaction-evasion in the measurement of the operator  $A_\alpha$  requires

$$[H_I, A_\alpha] = 0. \quad (386)$$

(iii) The dynamics of  $P_\beta$  should be associated with  $A_\alpha$ , so that the readout of  $P_\beta$  contains information about  $A_\alpha$ ; therefore

$$[H_I, P_\beta] \neq 0. \quad (387)$$

- (iv) Since the successive measurements of  $A_\alpha$  should be predictable, then

$$[H_A, A_\alpha] = 0. \quad (388)$$

From the criteria given above, one of the simplest QND-type Hamiltonians is

$$H_I = A_\alpha P_\alpha, \quad (389)$$

and the probe operator to be detected is  $P_\beta$  with  $\beta \neq \alpha$ . This QND-type Hamiltonian can be implemented through far-off resonant dispersive interactions between light and atomic ensembles, as shown in Fig. 22(b). Two probe light beams,  $a_1$  and  $a_2$ , are coupled to different hyperfine levels, with detuning  $\Delta_1$  and  $\Delta_2$ , respectively. In the large detuning case, the effective Hamiltonian is [23]

$$H = \hbar \sum_{i=1}^2 \frac{g_i^2 \Delta_i}{\gamma_i^2/4 + \Delta_i^2} a_i^\dagger a_i J_{ii} = \hbar \Omega \left( S_z J_z + \frac{1}{4} n N \right), \quad (390)$$

where the  $\gamma_i$ 's are the spontaneous decay rates for the excited levels, and

$$J_{ii} = \sum_{\mu} |i\rangle^{\mu} \langle i| \quad (391)$$

measures the population of atoms in the level  $|i\rangle^{\mu}$ , and  $n$ ,  $N$  are the photon and atom numbers, respectively. The Stokes operator  $S_z$  (E.3) measures the population difference between the left- and right-polarized states. In experiment [23], the detuning  $\Delta_1$  and  $\Delta_2$  are chosen in such a way that

$$\frac{g_1^2 \Delta_1}{\gamma_1^2/4 + \Delta_1^2} = \frac{g_2^2 \Delta_2}{\gamma_2^2/4 + \Delta_2^2} = \frac{\Omega}{2}. \quad (392)$$

This Hamiltonian acts as a Faraday rotation to the photon polarization, and as a fictitious magnetic field to atoms. The Heisenberg equations for the operators  $\vec{S}$  and  $\vec{J}$  are

$$\begin{aligned} \begin{pmatrix} S_x \\ S_y \\ S_z \end{pmatrix}_t &= \begin{pmatrix} \cos(\chi J_z) & -\sin(\chi J_z) & 0 \\ \sin(\chi J_z) & \cos(\chi J_z) & 0 \\ 0 & 0 & 1 \end{pmatrix} \begin{pmatrix} S_x \\ S_y \\ S_z \end{pmatrix}_{\text{in}}, \\ \begin{pmatrix} J_x \\ J_y \\ J_z \end{pmatrix}_t &= \begin{pmatrix} \cos(\chi S_z) & -\sin(\chi S_z) & 0 \\ \sin(\chi S_z) & \cos(\chi S_z) & 0 \\ 0 & 0 & 1 \end{pmatrix} \begin{pmatrix} J_x \\ J_y \\ J_z \end{pmatrix}_{\text{in}}, \end{aligned} \quad (393)$$

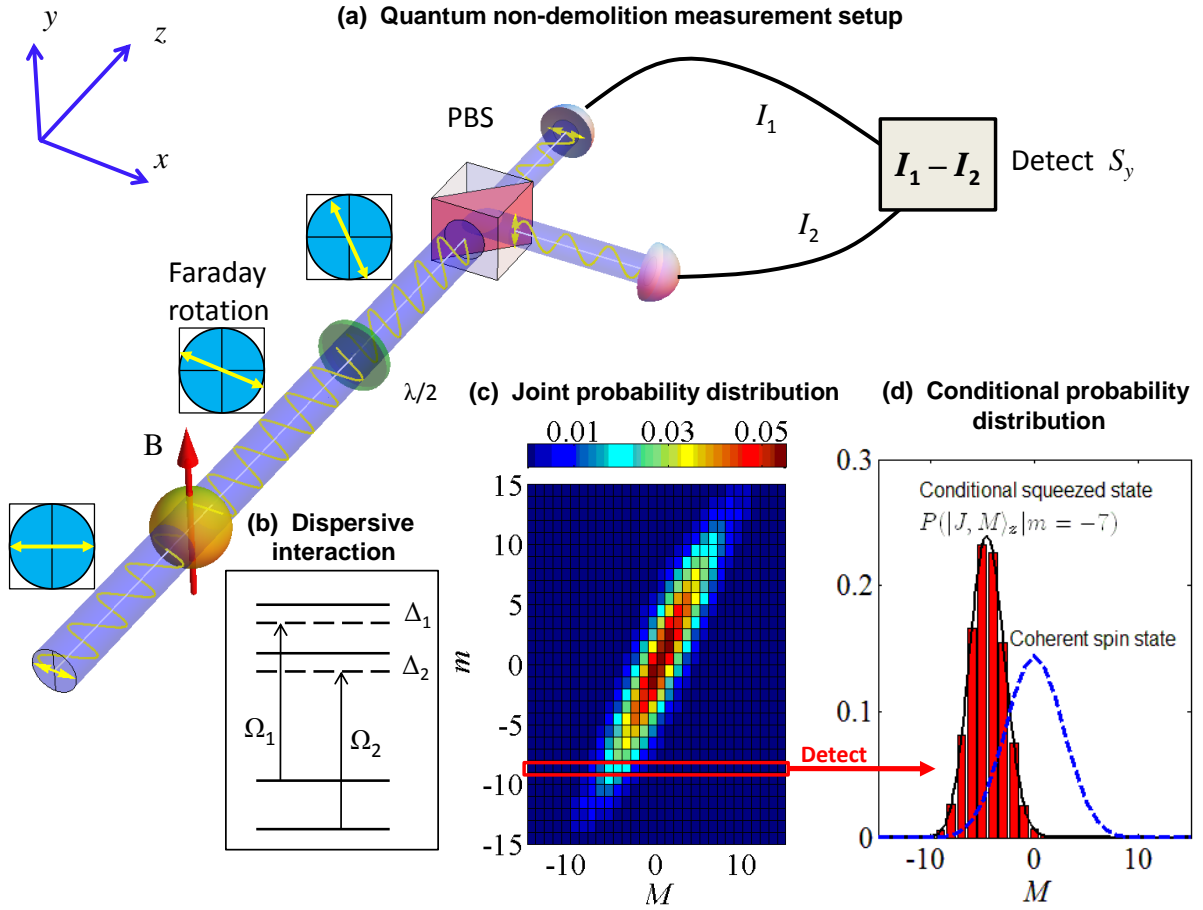


Figure 22: (Color online) (a) Schematic diagram for the QND measurement. The input probe beam is  $x$ -polarized, and the atoms are initially polarized along the  $x$ -axis. The two circular polarized components of the probe beam interact dispersively with atoms, with detuning  $\Delta_1$  and  $\Delta_2$ , as shown in (b),  $\Omega_1$  and  $\Omega_2$  are atom-field couplings. The dispersive interactions induce a rotation of the polarization plane, the Faraday rotation. The  $\lambda/2$  wave plate together with the following PBS and two detectors play the role of QND measurement of  $J_z$  by detecting  $S_y$ , which is readout by the photocurrent difference. (c) Joint probability distributions for a system with  $N = n = 30$  and  $\chi = 0.1$ . (d) When the readout of  $S_y$  gives  $m = -7$ , the conditional squeezed state is plotted and compared with the coherent spin state.

where  $\chi = \Omega t$ . Therefore, a QND measurement on  $J_z$  is performed through the readout of  $S_x(t)$  [or  $S_y(t)$ ].

Now, we consider a specific case, where the initial states for the light field and atoms are both CSSs along the  $x$ -direction,

$$|\varphi(0)\rangle = |S, S\rangle_x |J, J\rangle_x, \quad (394)$$

where  $S = n/2$ ,  $J = N/2$ , and the subscript  $x$  means that the states are represented in the  $S_x$  and  $J_x$  basis. A QND measurement on  $J_z$  is performed by detecting  $S_y$  (or  $S_x$ ), the readout of  $S_y(t)$  becomes

$$\langle S_y(t) \rangle = \frac{n}{2} \langle \sin(\chi J_z) \rangle \simeq \langle S_y \rangle + \frac{n\chi}{2} \langle J_z \rangle, \quad (395)$$

where the average  $\langle \cdot \rangle$  is carried out under the initial states since we are using in the Heisenberg picture. Thus we see that  $\langle J_z \rangle$  and  $\langle S_y \rangle$  are related, the mean value of  $\langle S_y(t) \rangle$  is approximately zero. From (395), the fluctuation of  $S_y(t)$  is also related to  $J_z$  [74].

Below, we demonstrate the QND-measurement-induced spin squeezing from the point of view of state evolution, shown in Fig. 22(c)-(d). As presented in Fig. 1, for a coherent spin state  $|J, J\rangle_x$ , if we measure  $J_z$ , the probability of the readout of states  $|J, M\rangle_z$  obeys a binomial distribution

$$P_J(M) \equiv P(|J, M\rangle_z | |J, J\rangle_x) = \left| {}_z \langle J, M | J, J \rangle_x \right|^2 = \frac{1}{2^N} \binom{N}{N/2 + M}, \quad (396)$$

where  $P(|J, M\rangle_z | |J, J\rangle_x)$  is a conditional distribution. Similarly, in the basis of  $|S, m\rangle_y$ , the measurement basis, we have

$$P_S(m) \equiv P(|S, m\rangle_y | |S, S\rangle_x) = \left| {}_y \langle S, m | S, S \rangle_x \right|^2 = \frac{1}{2^n} \binom{n}{n/2 + m}. \quad (397)$$

The evolution of the state becomes

$$\begin{aligned} |\varphi(t)\rangle &= \exp(-i\chi S_z J_z) |S, S\rangle_x |J, J\rangle_x \\ &= \sum_{M=-J}^J \exp(-i\chi M S_z) \sqrt{P_J(M)} |S, S\rangle_x |J, M\rangle_z. \end{aligned} \quad (398)$$

At time  $t$ , we measure  $S_y$ . For a single trial measurement, the readout will fall in an eigenvalue  $m$  of  $S_y$ , and the photon state collapses into the corresponding eigenstate  $|S, m\rangle$ . After this readout, the atomic state is also changed according to the measurement result of  $S_y$ . Therefore, the focus is on the conditional distribution  $P(|J, M\rangle_z | |S, m\rangle_y)$ , which gives information of the atomic state after a single trial measurement of  $S_y$ . To analyze this problem, we consider the system size to be very large, in which case the binomial distribution becomes a Gaussian normal distribution,

$$\begin{aligned} P_J(M) &= \frac{1}{\sqrt{\pi N/2}} \exp\left(-\frac{2M^2}{N}\right), \\ P_S(m) &= \frac{1}{\sqrt{\pi n/2}} \exp\left(-\frac{2m^2}{n}\right). \end{aligned} \quad (399)$$

With the Bayes theorem

$$P(|J, M\rangle_z | m) P_S(m) = P(|S, m\rangle_y | M) P_J(M), \quad (400)$$

the conditional probability distribution for  $P(|S, m\rangle_y | M)$  is easy to obtain. If the atomic system is in the state  $|J, M\rangle_z$ , according to Eq. (398) the photon state is rotated around the  $z$ -axis with an angle  $\phi = \chi M$ . If the rotation angle is very small, then the photon state after the rotation is still a Gaussian distribution with mean value at  $\sin(\phi) n/2 \simeq \phi n/2$ , and

$$P(|S, m\rangle_y | M) = \frac{1}{\sqrt{\pi n/2}} \exp\left[-\frac{(m - \phi n/2)^2}{n/2}\right]. \quad (401)$$

Therefore, the conditional probability distribution of the atomic state becomes

$$P(|J, M\rangle_z | m) = \frac{1}{\sqrt{\pi \xi_R^2 N/2}} \exp \left[ -\frac{(M - \chi m \xi_R^2 N/2)^2}{\xi_R^2 N/2} \right], \quad (402)$$

where

$$\xi_R^2 = \frac{1}{1 + \kappa^2}, \quad (403)$$

with

$$\kappa^2 = nN\chi^2/4, \quad (404)$$

and the state of the atomic system after detecting  $S_y$  is squeezed, while the expectation value of  $J_z$  is shifted to  $\chi m \xi_R^2 N/2$ .

Note that the spin length is generally shortened due to photon scattering and other noises during the QND measurement, so the above Eq. (403) holds under the condition that the spin length is not affected too much after the QND measurement. An illustrative description of the above procedure is displayed in Fig. 22. The spin state derived above is the so-called conditional squeezed state, which is conditioned to the first measurement output of  $S_y$ . In a “single trial” measurement of  $S_y$ , the output value is random with respect to a specific probability distribution. The conditional squeezed state is generated randomly, so it is not repeatable. To obtain an unconditional squeezed state, we could employ a feedback or filter scheme to shift  $\langle J_z \rangle$  back to zero, which is demonstrated in Refs. [53, 290, 235, 78, 73, 99].

### 8.3.2. Experimental results

Below, we first give a brief introduction about some experimental works, then we present a detailed discussion about a recent notable improvement. In Ref. [76], QND measurement was performed on a collective spin of  $\sim 10^6$  Cs atoms, and sub-shot-noise fluctuations of the collective spin were observed. In this experiment, the probe beam was short pulses of laser light that linearly polarized at  $\pm 45^\circ$ . Then, in Ref. [77], the authors performed continuous QND measurement on a collection of  $\sim 10^7$  Cs atomic spins with an off-resonant laser beam. The continuous QND measurement is an important feature of this work, and the probe laser also serves for measurement of the spin rotation signal. They observed squeezed atomic spin states with spin noise reduction to 70% below the shot-noise limit, and measured a small spin rotation with an accuracy exceeding the shot-noise limit of the phase measurement. Reference [40] proposed a sequence of QND measurements and spin rotations, which require interferometric QND measurement of the atomic population with a sensitivity at the projection-noise level. To achieve this they demonstrated experimentally that a shot-noise-limited fiber optical interferometer at the white-light setting can reach a sensitivity sufficient to detect the projection noise under conditions not far from those of the QND measurement. Increasing the optical density can significantly improve the QND figure of merit  $\kappa^2$ , and thus will enhance the degree of squeezing. In Ref. [92], the authors demonstrated QND measurement of atomic ensembles in a high-finesse optical cavity, which can enhance the optical depth of the atomic sample. In this experiment, a cloud of  $^{87}\text{Rb}$  atoms was cooled in a MOT, located at the center of a hemispherical cavity. The maximum atom-cavity coupling,  $g/(2\pi) = 53$  kHz, is realized for the  $|F = 2, m_F = 2\rangle \rightarrow |F' = 3, m_F = 3\rangle$  cycling transition. The atoms are released from the MOT, further cooled by optical molasses, prepared in an equal superposition of the  $|F = 1, m_F = 0\rangle$  and  $|F = 2, m_F = 0\rangle$  clock states, and probed by a standing wave of intracavity light. They observed 3.8 dB in the variance of  $J_z$  below the projection noise with spontaneous emission of  $\leq 30\%$ .

Reference [103] demonstrated sub-projection-noise sensitivity of QND spin measurements of  $1 \times 10^6$  cold  $^{87}\text{Rb}$  atoms in a broadband atomic magnetometer. The high-bandwidth system avoids decoherence effects through rapid probing. The spin readout noise is 2.8 dB below the thermal spin noise and 1.6 dB below the CSS projection noise. Since the Hamiltonian (390) only appropriate for spin-1/2 or other two-level systems as pointed out by studies of Ref. [104], where they considered larger spins and proposed a decoupling mechanism based on a two-polarization probing technique to recover the ideal QND behavior. The decoupled QND measurement achieves a sensitivity 5.7(6) dB better than the spin projection noise.

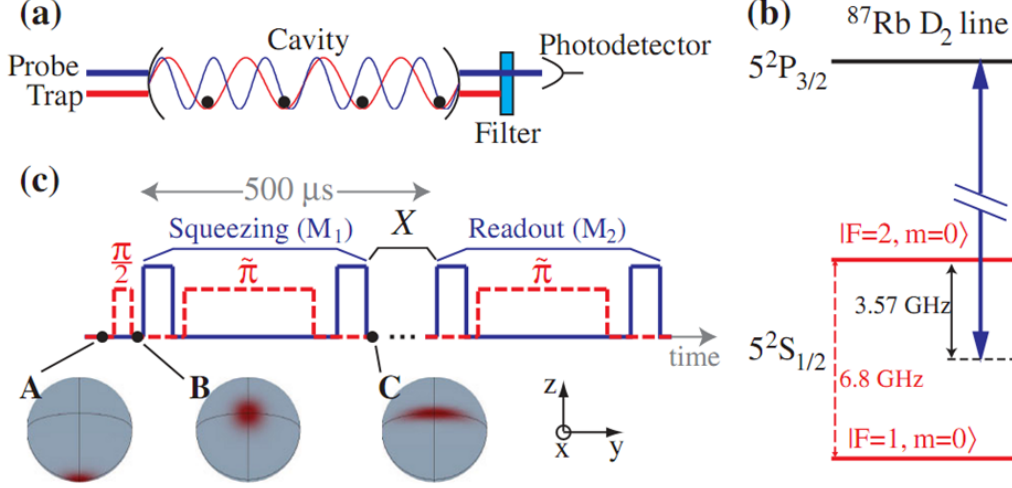


Figure 23: (Color online). Experimental schematic diagram of Ref. [102]. (a) Experimental setup. (b) Level structure of rubidium atom. (c) Experimental sequences. Dashed lines denote the microwave pulses while solid lines denote the probe pulses. The  $\tilde{\pi}$  pulse represents a composite  $\pi$  pulses. Various operations are performed between two readouts ( $M_1$  and  $M_2$ ), denoted by  $X$ , such as the measurement of the variance of the CSS, the operation of a clock. **A-C**: Semiclassical probability distribution functions of the state. This figure is from Ref. [102].

Recently, Ref. [102] demonstrated the generation of spin-squeezed state of  $5 \times 10^4$  trapped  $^{87}\text{Rb}$  atoms on an atom-clock transition by resonator-aided QND measurement. For photon number  $p = 3 \times 10^5$ , they observed noise reduction of 3.0(8) dB below the shot-noise limit. The hyperfine clock states used are  $|1\rangle = |5^2S_{1/2}, F = 1, m_F = 0\rangle$  and  $|2\rangle = |5^2S_{1/2}, F = 2, m_F = 0\rangle$ . They used the metrological spin-squeezing parameter defined as

$$\zeta_m = \frac{2S_{\text{in}} (\Delta S_z)^2}{|\langle \vec{S} \rangle|^2}, \quad (405)$$

where  $S_{\text{in}}$  is the initial spin of the uncorrelated ensemble. Actually, this parameter is equal to  $\xi_R^2$  when  $S_{\text{in}} = N/2$ . The experimental setup is shown in Fig. 23. A strong ensemble-light coupling was achieved by using a near-confocal optical resonator, and the experiments are performed on an ensemble containing up to  $N_a = 5 \times 10^4$  laser-cooled  $^{87}\text{Rb}$  atoms optically trapped inside the resonator in a standing wave of 851-nm light. The wavelength of the probe light is  $2\pi/k = 780$  nm, and the cavity has a finesse  $\mathcal{F} = 5.6(2) \times 10^3$ , a linewidth  $\kappa = 2\pi \times 1.01(3)$  MHz, and a mode waist  $w = 56.9(4)$   $\mu\text{m}$  at the atoms' position, corresponding to a maximal single-atom cooperativity  $\eta_0 = 24\mathcal{F}/(\pi k^2 w^2) = 0.203(7)$ . One resonator mode is tuned 3.57(1) GHz to the blue of the  $|5^2S_{1/2}, F = 2\rangle \rightarrow |5^2P_{3/2}, F' = 3\rangle$  transition in  $^{87}\text{Rb}$  to result in a mode frequency shift  $\omega$  proportional to the population difference  $N = N_2 - N_1$  between the hyperfine clock states

$$\begin{aligned} |1\rangle &= |5^2S_{1/2}, F = 1, m_F = 0\rangle, \\ |2\rangle &= |5^2S_{1/2}, F = 2, m_F = 0\rangle. \end{aligned} \quad (406)$$



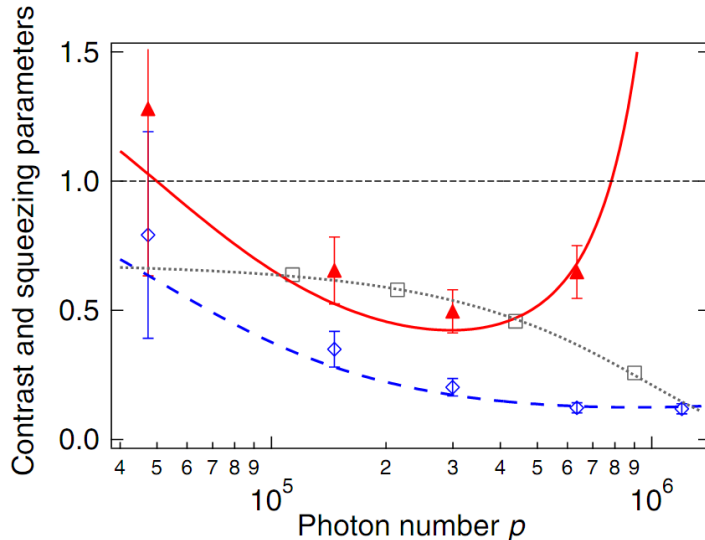


Figure 24: (Color online). Normalized spin noise  $\sigma^2 = (\Delta S_z^2)_{M_1} / (\Delta S_z^2)_{\text{CSS}}$  (open diamonds), contrast  $C$  (open square), and metrological squeezing parameter  $\zeta_m$  (solid triangles). Solid line denotes the fits. This figure is from Ref. [102].

The experimental processes are shown in Fig. 23(c). At first, the atomic ensemble is prepared in state  $|1\rangle$ , after a  $\pi/2$  pulse, the atomic state polarizes in the  $x$ -axis, then after measurements  $M_1$ , the atomic ensemble is conditional spin squeezed as Fig. 23C. To quantify the spin squeezing, they measured  $\Delta S_z^2$  and  $|\langle \vec{S} \rangle|$ , the latter is obtained from the observed contrast  $C$  of Rabi oscillations since  $|\langle \vec{S} \rangle| = CS_0$ , as shown in Fig. 24, from which the metrological squeezing parameter achieves

$$\zeta_m^{-1} = 3.0(8) \text{ dB}$$

for photon number  $p = 3 \times 10^5$ .

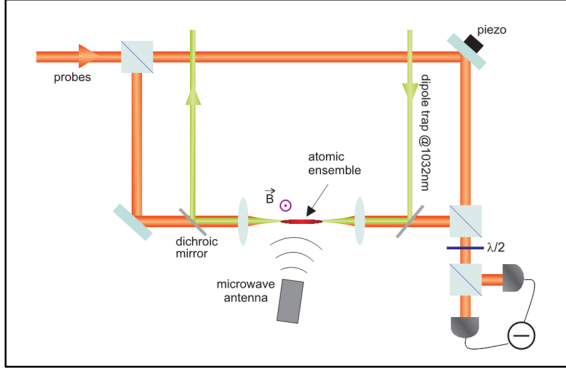
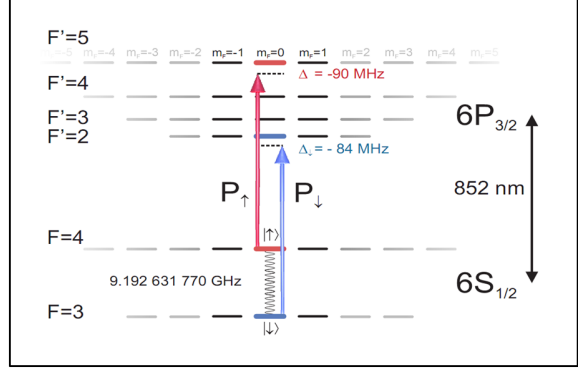
The QND measurements discussed above were all performed on alkali atoms, which have complicated multilevel structures. In Ref. [25], the authors demonstrated a QND measurement with a collective spin of cold ytterbium atoms,  $^{171}\text{Yb}$ , which have the simplest ground state with a nuclear spin of one-half and have no electron spin, and thus the system is robust against stray magnetic fields since the magnetic moment of nuclear spin is a thousandth of that of electron spin. By using short light pulses with a width of 100 ns, more than a hundred time operations are expected to be performed within the coherence time, and experimental results showed  $1.8_{-1.5}^{+2.4}$  dB spin squeezing.

With the above experimental efforts, recently, two successive notable improvements in QND experiment were reported [23, 24], where a complete sub-shot-noise Ramsey process was demonstrated by means of QND measurement. The experimental schemes for these two works [23, 24] are similar, thus here, we mainly discuss the very recent one [24]. The experimental setup is shown in Fig. 25(a). An ensemble of  $\sim 10^5$  cold Cs atoms are located in one of the arms of the Mach-Zehnder interferometer. The atoms are first loaded into a standard MOT, and are then transferred into a far-off resonant optical dipole trap (FORT), generated by a Versadisk laser with a wavelength of 1032 nm and a power of 2.3 W. After loading the FORT, the MOT is turned off and a 1.22 Gauss magnetic field is applied, which defines a quantization axis orthogonal to the trapping beam. The ground levels

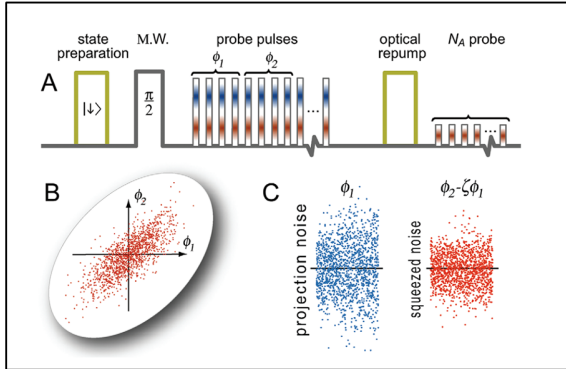
$$\begin{aligned} |\downarrow\rangle &\equiv |6S_{1/2}, F = 3, m_F = 0\rangle, \\ |\uparrow\rangle &\equiv |6S_{1/2}, F = 4, m_F = 0\rangle, \end{aligned} \quad (407)$$

are referred to the clock levels, and by optical pumping, the atoms are prepared in the clock level  $|\downarrow\rangle$ . As described in Ref. [23], atoms remaining in states other than  $|\downarrow\rangle$  due to imperfect optical pumping are

(a) Experimental setup

(b) Cesium  $D_2$ -line level diagram

(c) Pulse sequence and noise data



(d) Projection noise and spin squeezing

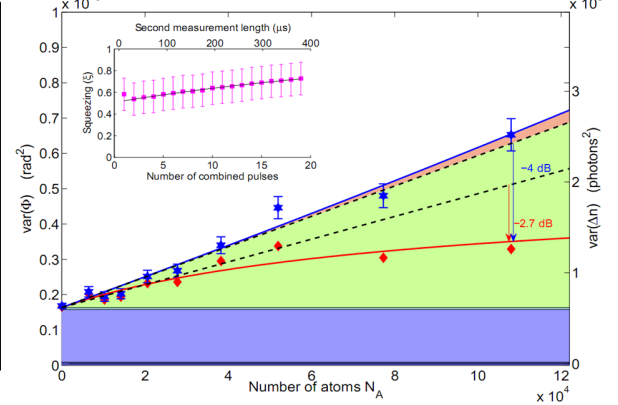


Figure 25: (Color online) (a) Schematic diagram of the QND measurement experimental setup, a Mach-Zehnder interferometer [24, 23]. The elongated Cesium atomic cloud is placed in the probe arm. The probe beam consists of two identical linearly polarized light beams  $P_\uparrow$  and  $P_\downarrow$ , which acquire phase shifts proportional to the number of atoms in the clock states  $N_\uparrow$  and  $N_\downarrow$ , respectively, as also shown in (b). In (c) A, we show an experimental sequence for generating the state  $|J, J\rangle_x$  and QND measurement of  $S_y$ , and in B and C, noise data of  $\phi_2$  and  $\phi_1$  show correlations between  $\phi_2$  and  $\phi_1$ , and reduced noise of  $(\phi_2 - \zeta\phi_1)$ . In (d), we display the experimental results of the projection noise and spin squeezing. Blue stars: variance of the second measurement  $\Delta^2\phi_2$ . Solid blue line: quadratic fit to  $\Delta^2\phi_2$ . Green area: atomic projection noise of the CSS. Red diamonds: conditional variance  $\Delta^2(\phi_2 - \zeta\phi_1)$ . Red line: reduced noise as predicted by the fits to the noise data. This data was obtained by acquiring 4800 experimental runs. Inset: spin squeezing  $\xi_R^2$  as a function of the number of pulses combined to form the second measurement. The data is fitted with an exponential decay (solid line). Figures (a), (b), and (d) are from Ref. [24], and figure (c) is from Ref. [23].

subsequently pushed out of the trap. To prepare the CSS  $\otimes_{i=1}^{N_A} \left[ \frac{1}{\sqrt{2}} (|\downarrow\rangle + |\uparrow\rangle) \right]_i$ , a resonant  $\pi/2$  microwave pulse at the clock frequency is applied. Then, successive QND measurements of the population difference,  $N_\uparrow - N_\downarrow$ , will be performed by measuring the phase shift of the probe light in a balanced homodyne configuration. After the QND measurement, all atoms are pumped into the  $F = 4$  level to determine the total atom number  $N_A$ . The sequence, shown in Fig. 25(c), is repeated several thousand times with a cycle time of  $\simeq 5$  s.

As shown in Fig. 25(a), two identical linear polarized beams  $P_\uparrow$  and  $P_\downarrow$ , which are generated by two extended-cavity diode lasers, enters the interferometer from the same port [Fig. 25(a)], off-resonantly probe transitions  $|F = 3\rangle \rightarrow |F' = 4\rangle$  and  $|F = 4\rangle \rightarrow |F' = 5\rangle$ , respectively. Each beam gains a phase shift

$$\phi_{\uparrow(\downarrow)} = k_{\uparrow(\downarrow)} N_{\uparrow(\downarrow)}, \quad (408)$$

which is proportional to the number of atoms  $N_\uparrow$  and  $N_\downarrow$  corresponding to the clock states  $|\uparrow\rangle$  and  $|\downarrow\rangle$ , respectively. The detuning  $\Delta_\uparrow$  and  $\Delta_\downarrow$  are tuned to ensure  $k_\uparrow = k_\downarrow$ , such that the Hamiltonian for this system is Eq. (390), and thus

$$J_z = (N_\uparrow - N_\downarrow) / 2, \quad (409)$$

where  $N_{\uparrow(\downarrow)}$  are the photon number operators,  $N_A = N_\uparrow + N_\downarrow$  is the total atom number. The photocurrent difference is equivalent to measuring  $S_{y,\text{out}}$ , which is derived from Eq. (395) as

$$S_{y,\text{out}} = S_{y,\text{in}} + \frac{n}{2} \chi J_{z,\text{in}}. \quad (410)$$

The phase difference between the two arms of the Mach-Zehnder interferometer is defined as

$$\phi \equiv \frac{S_{y,\text{out}}}{n}, \quad (411)$$

where  $n = n_\uparrow + n_\downarrow$  is the total photon number. In experiments [23, 24], the photon numbers of the two probe beams  $n_\uparrow$  and  $n_\downarrow$  are set to be almost equal. If the probe beam is in a coherent state, the variance of the phase difference is

$$\Delta^2 \phi = \frac{1}{n} + \chi^2 (\Delta J_{z,\text{in}})^2, \quad (412)$$

which is related to both photon shot-noise  $1/n$ , and atomic spin noise  $(\Delta J_{z,\text{in}})^2$ . As the atomic ensemble is prepared in a CSS,  $\Delta J_{z,\text{in}} = \sqrt{N_A}/2$ . From Fig. 25(c), two successive measurements of  $\phi_1$  and  $\phi_2$  are performed, using probe photons  $n_1$  and  $n_2$ . Thus,

$$\Delta^2 \phi_{1(2)} = \frac{1}{n_{1,(2)}} + \chi^2 \frac{N_A}{4}, \quad \text{Cov}(\phi_1, \phi_2) = \chi^2 \frac{N_A}{4}. \quad (413)$$

The covariance (413) is calculated for the atomic ensemble, which is the same for the two measurements, while the two probe beams have no correlations. As  $\phi_2$  is conditioned to  $\phi_1$  and can be predicted with a better precision, after the measurement of  $\phi_1$ , an appropriate estimate of  $\phi_2$  is chosen as  $\zeta \phi_1$ , and the variance of their difference becomes

$$\begin{aligned} \Delta^2 (\phi_2 - \zeta \phi_1) &= (\Delta^2 \phi_1) \zeta^2 - 2 \text{Cov}(\phi_1, \phi_2) \zeta + \Delta^2 \phi_2 \\ &= \frac{1}{n_2} + \frac{1}{1 + \kappa^2} \chi^2 \frac{N_A}{4}, \end{aligned} \quad (414)$$

where the second line is the minimum of  $\Delta^2 (\phi_2 - \zeta \phi_1)$  at

$$\zeta = \frac{\text{Cov}(\phi_1, \phi_2)}{\Delta^2 \phi_1} = \frac{\kappa^2}{1 + \kappa^2}. \quad (415)$$

Here,

$$\kappa^2 = n_1 N \chi^2 / 4, \quad (416)$$

which is the same result derived in Eq. (403). Now, according to Eq. (414), the spin-squeezing parameter

$$\xi_R^2 = \frac{1}{1 + \kappa^2}. \quad (417)$$

A measurement of  $\kappa^2 = 1.6$  for  $N_A = 1.2 \times 10^5$  atoms gives rise to a reduction of the projection noise by  $-4$  dB compared to the CSS projection noise, displayed in Fig. 25(d).

Now consider the decoherence during a QND measurement. In experiments [23, 24], the employ of two-color QND can suppress the dephasing effects induced by an inhomogeneous AC stark shift due to the transverse intensity profile of the probe beam [96]. Otherwise, since the probe interacts dispersively with the atoms, decoherence is inevitable induced by spontaneous photon scattering [23, 24], which shortens the mean-spin length as

$$\langle \vec{J} \rangle \rightarrow (1 - \eta) \langle \vec{J} \rangle, \quad (418)$$

where  $\eta = 1 - \exp(-n\alpha)$ , with  $n$  the total number of photons in the probe pulse and the parameter  $\alpha = -2.39 \times 10^{-8}$  [24]. The coherence between the clock levels decreases while the phase shifts are almost unaffected, so in the absence of the classical noise, we have

$$\xi_R^2 = \frac{1}{(1 - \eta)^2 (1 + \kappa^2)}. \quad (419)$$

When using  $n_1/2 = 3 \times 10^6$  photons per probe, the reduction is  $\eta = 14\%$ , and experimental data gives  $1/\xi_R^2 = 2.7$  dB as shown in Fig. 25(d). This is very close to the theoretical prediction from Eq. (419),  $1/\xi_R^2 = 2.8$  dB. The above results indicate that experiments must carefully choose photon numbers for optimal spin squeezing.

## 9. Conclusion

We have reviewed both basic notions and recent progresses on spin squeezing. After a short introduction on bosonic squeezing, in Sec. 2, we reviewed various definitions of spin-squeezing parameters and their physical significance. In order to understand these parameters better, we derived explicit analytical expressions of them for states with parity. At the end of Sec. 2, we showed that, in the limit of a large number of atoms and small number of excitations, spin squeezing reduces to bosonic squeezing.

In Sec. 3, we reviewed theoretical approaches toward producing spin-squeezed states via one-axis twisting and two-axis twisting Hamiltonians. The one-axis twisting Hamiltonian has attracted considerable attentions, and has been implemented in BEC, as reviewed in Sec. 8. For this model, we presented analytical results for the spin-squeezing parameters  $\xi_S^2$  and  $\xi_R^2$ , which scale with the particle number as  $1/N^{2/3}$ .

The two-axis twisting Hamiltonian can produce more squeezing than the one-axis case. Moreover, its optimal squeezing angle does not vary with time. However, analytical results are only available for particle number  $N \leq 3$ , and numerical results showed that  $\xi_S^2$  and  $\xi_R^2$  scale as  $1/N$ . This two-axis twisting Hamiltonian can be realized in spinor BEC.

Section 4 showed that spin squeezing has very close relations to both entanglement and negative pairwise correlations. A system consisting of spin-1/2 particles is entangled if  $\xi_R^2 < 1$ . For states with parity and exchange symmetry, close relations between the spin-squeezing parameters  $\xi_S^2$ ,  $\xi_E^2$ , and the concurrence  $C$  have been established. In this case, spin squeezing according to  $\xi_E^2$  is qualitatively equivalent to the existence of pairwise entanglement. Moreover, recent results generalized the proposal of using spin squeezing to detect entanglement, and also developed a set of spin inequalities. In the end, the two-mode spin squeezing is reviewed. It can detect the entanglement between spin variables of two separated atomic samples, and was proposed to be a valuable resource of quantum information processing. As explained in this section, spin-squeezing-based entanglement witnesses should be useful in measurements and are then expected to be of wide applications in experiments.

In Sec. 5, we discussed the relation between spin squeezing and QFI, as well as their applications in quantum metrology. Applications of spin squeezing also deserve more considerations, and in Sec. 6, we explained how spin squeezing can be used to detect quantum chaos and QPTs.

In Sec. 7, we first consider how decoherence affects the generation of spin squeezing. If the decoherence effect is sufficiently weak, considerable large amount of squeezing can still be obtained. Then we showed that spin-squeezed states are more robust than the GHZ state in the presence of particle loss. The lifetime of squeezing is discussed for three typical decoherence channels, and the spin-squeezing sudden death was derived and analyzed. These channels are prototype models, however, are quite general to describe decoherence processes. The results derived by using these channels still make sense when using concrete physical models. In addition, the one parameter in the dephasing, dissipation, or the depolarizing channels may be a very complex function depending on the realistic physical models of decoherence. Afterwards, we show that in the Ramsey spectroscopy, decoherence reduces the ability of spin-squeezed states to help in precision-improvement, however, compared with the GHZ states, spin-squeezed states are more robust to decoherence.

In Sec. 8 we reviewed several recent experiments, as well as their theoretical backgrounds. Spin-squeezed states were realized in BEC and atomic ensembles. In the past two decades, spin squeezing has been studied extensively. It was first proposed in order to overcome the classical shot-noise limit and make high-precision atomic interferometers. This encouraged many theoretical and experimental efforts in the control and manipulation of atomic systems. Afterwards, it was realized that the notion of spin squeezing can provide an insight on entanglement, and this has attracted considerable recent interests. Experiments can now produce spin-squeezed states, and even use them to perform sub-shot noise interference. However, in practice, using spin-squeezed states in an atomic clock or a gravity interferometer still faces many challenges, including how to suppress the decoherence and enlarge the particle number of the spin-squeezed states.

Finally, we summarize and list several main results, some of which are of broad interest:

(a) There are several definitions of squeezing parameters (see Table 1), which one is preferable depends on various situations. For example, when studying the accuracy of Ramsey spectroscopy, the parameter  $\xi_R^2$  is more suitable. In this review, we mainly focused on two parameters,  $\xi_S^2$  and  $\xi_R^2$ , which are widely studied in the literatures.

(b) In general, spin-squeezed states are entangled; however this depends on specific squeezing parameters. From Sec. 4, we know that, for the parameter  $\xi_R^2$ , states are entangled if  $\xi_R^2 < 1$ ; while for the parameter  $\tilde{\xi}_E^2$ , states with parity have pairwise entanglement if  $\tilde{\xi}_E^2 < 1$ . Generalized spin inequalities have also been developed to detect entanglement.

(c) Since spin-squeezing parameters only involve expectations and variances of collective spin operators, they can be measured relatively easy in many physical systems, e.g., BEC and atomic ensembles, while addressing individual atoms is an arduous task.

(d) Among proposals for generating spin-squeezed states, the twisting Hamiltonian, which describes nonlinear two-body interactions, plays an important role. This type of Hamiltonian has been studied and implemented in physical systems like BEC.

(e) In parameter-estimation processes, compared with the GHZ state, spin-squeezed states can also attain the Heisenberg limit, but are more robust to decoherence.

In summary, spin squeezing has provided very useful insight into quantum processes, and will continue to considerably impact quantum optics and quantum information science in the future.

**Acknowledgements** We would like to thank Heng-Na Xiong, Xiaoqian Wang, Xiao-Ming Lu, and Xiaolei Yin for useful discussions. FN acknowledges partial support from the Laboratory of Physical Sciences (LPS), National Security Agency (NSA), Army Research Office (ARO), Defense Advanced Research Projects Agency (DARPA), Air Force Office of Scientific Research (AFOSR), National Science Foundation (NSF) grant No. 0726909, JSPSRFBR contract No. 09-02-92114, Grant-in-Aid for Scientific Research (S), MEXT Kakenhi on Quantum Cybernetics, and the Funding Program for Innovative R&D on Science and Technology (FIRST). Xiaoguang Wang acknowledges support from the NSFC with grant No. 11025527, 10874151, and 10935010. Jian Ma acknowledges support from the Scholarship Award for Excellent Doctoral Student granted by Ministry of Education.

## Appendix A. Principal squeezing parameter

From Eqs. (7) and (8), we have

$$\begin{aligned}\zeta_B^2 &= \min_{\theta \in [0, 2\pi)} \left[ \cos^2 \theta (\Delta X)^2 + \sin^2 \theta (\Delta P)^2 + \sin(2\theta) \text{Cov}(X, P) \right] \\ &= \min_{\theta \in [0, 2\pi)} \left\{ \frac{(\Delta X)^2 + (\Delta P)^2}{2} + \frac{1}{2} \{ \cos(2\theta) [(\Delta X)^2 - (\Delta P)^2] + 2 \sin(2\theta) \text{Cov}(X, P) \} \right\} \\ &= \frac{1}{2} \left\{ \text{Var}(X) + \text{Var}(P) - \sqrt{[\text{Var}(X) - \text{Var}(P)]^2 + 4 \text{Cov}^2(X, P)} \right\},\end{aligned}\tag{A.1}$$

where the variance

$$\text{Var}(X) = \langle X^2 \rangle - \langle X \rangle^2\tag{A.2}$$

and the covariance

$$\text{Cov}(X, P) = \frac{1}{2} \langle XP + PX \rangle - \langle X \rangle \langle P \rangle.\tag{A.3}$$

From the expressions for  $X$  and  $P$  in Eq. (2), one finds

$$\frac{XP + PX}{2} = \frac{a^2 - a^{\dagger 2}}{i},\tag{A.4}$$

which leads to the covariance

$$\text{Cov}(X, P) = \frac{1}{i} [\text{Var}(a) - \text{Var}(a^\dagger)].\tag{A.5}$$

From the identity

$$\text{Var} \left( \sum_{i=1}^N X_i \right) = \sum_{i=1}^N \text{Var}(X_i) + 2 \sum_{i < j} \text{Cov}(X_i, X_j),\tag{A.6}$$

we have

$$\text{Var}(X) = \text{Var}(a) + \text{Var}(a^\dagger) + 2 \text{Cov}(a, a^\dagger),\tag{A.7}$$

$$\text{Var}(P) = -\text{Var}(a) - \text{Var}(a^\dagger) + 2 \text{Cov}(a, a^\dagger),\tag{A.8}$$

which leads to

$$\text{Var}(X) + \text{Var}(P) = 4 \text{Cov}(a, a^\dagger),\tag{A.9}$$

$$\text{Var}(X) - \text{Var}(P) = 2 (\text{Var}(a) + \text{Var}(a^\dagger)).\tag{A.10}$$

Substituting Eqs. (A.5), (A.9), and (A.10) into Eq. (A.1), we finally obtain

$$\zeta_B^2 = 2 \left\{ \text{Cov}(a, a^\dagger) - \sqrt{\text{Var}(a) \text{Var}(a^\dagger)} \right\},\tag{A.11}$$

which is just Eq. (9).

## Appendix B. Variances of $J_{\vec{n}}$ for the CSSs

We obtain the variance  $(\Delta J_{\vec{n}})^2 = \langle J_{\vec{n}}^2 \rangle - \langle J_{\vec{n}} \rangle^2$  for the CSS. The expectation values  $\langle J_{\alpha}^2 \rangle$  are given by

$$\begin{aligned}\langle J_{\alpha}^2 \rangle &= \frac{1}{4} \sum_{i,j=1}^N \langle \sigma_{i\alpha} \sigma_{j\alpha} \rangle \\ &= \frac{N}{4} + \frac{1}{4} \sum_{i \neq j=1}^N \langle \sigma_{i\alpha} \sigma_{j\alpha} \rangle \\ &= \frac{N}{4} + \frac{N^2 - N}{4} \langle \sigma_{1\alpha} \rangle^2.\end{aligned}\tag{B.1}$$

The last equality is valid since we are considering a product state with exchange symmetry. Note that

$$\langle J_\alpha \rangle = \frac{N}{2} \langle \sigma_{1\alpha} \rangle, \quad (\text{B.2})$$

the variance is found to be

$$(\Delta J_\alpha)^2 = \frac{N}{4} (1 - \langle \sigma_{1\alpha} \rangle^2). \quad (\text{B.3})$$

Now, we consider a more general operator  $J_{\vec{n}}$  as

$$J_{\vec{n}} = \vec{J} \cdot \vec{n} = \frac{1}{2} \sum_{i=1}^N \vec{\sigma}_i \cdot \vec{n} = \frac{1}{2} \sum_{i=1}^N \sigma_{i\vec{n}}, \quad (\text{B.4})$$

from which, its variance is given by

$$\begin{aligned} \text{Var}(J_{\vec{n}}) &= (\Delta J_{\vec{n}})^2 \\ &= \frac{1}{4} \sum_{i=1}^N \text{Var}(\sigma_{i\vec{n}}) \\ &= \frac{1}{4} \sum_{i=1}^N (1 - \langle \sigma_{i\vec{n}} \rangle^2) \\ &= \frac{N}{4} (1 - \langle \sigma_{1\vec{n}} \rangle^2). \end{aligned} \quad (\text{B.5})$$

Here, the second equality follows from Eq. (A.6) and the fact that the CSS is a product state and contains no correlations (the covariance  $\text{Cov}(X_i, X_j) = \langle [X_i, X_j]_+ / 2 \rangle - \langle X_i \rangle \langle X_j \rangle = 0$ ). The third equality is from the result  $\sigma_{i\vec{n}}^2 = \mathbb{I}$ .

From Eqs. (B.4) and (100), we obtain

$$\begin{aligned} \langle J_{\vec{n}} \rangle &= \frac{N}{2} \langle \sigma_{1\vec{n}} \rangle = \frac{N}{2} |\langle \vec{\sigma}_1 \rangle| \vec{n}_0 \cdot \vec{n}, \\ (\Delta J_{\vec{n}})^2 &= \frac{N}{4} (1 - \langle \sigma_{1\vec{n}} \rangle^2) = \frac{N}{4} [1 - |\langle \vec{\sigma}_1 \rangle|^2 (\vec{n}_0 \cdot \vec{n})^2], \end{aligned} \quad (\text{B.6})$$

which is valid for any product state with exchange symmetry. The second equality is obtained from the fact

$$\langle \vec{\sigma}_1 \rangle = |\langle \vec{\sigma}_1 \rangle| \vec{n}_0 = |\langle \vec{\sigma}_1 \rangle| (\sin \theta \cos \phi, \sin \theta \sin \phi, \cos \theta). \quad (\text{B.7})$$

From the definition of the CSS, the expectation values  $\langle J_\alpha \rangle$  ( $\alpha = x, y, z$ ) are obtained as

$$\begin{aligned} \langle J_x \rangle &= \frac{N}{2} \sin \theta \cos \phi, \\ \langle J_y \rangle &= \frac{N}{2} \sin \theta \sin \phi, \\ \langle J_z \rangle &= \frac{N}{2} \cos \theta. \end{aligned} \quad (\text{B.8})$$

with  $N = 2j$ , and  $\theta, \phi$  are the polar and azimuth angles, respectively. Substituting Eq. (B.8) into Eq. (B.5) leads to the explicit form of the variances

$$\begin{aligned} (\Delta J_x)^2 &= \frac{N}{4} (1 - \sin^2 \theta \cos^2 \phi), \\ (\Delta J_y)^2 &= \frac{N}{4} (1 - \sin^2 \theta \sin^2 \phi), \\ (\Delta J_z)^2 &= \frac{N}{4} \sin^2 \theta. \end{aligned} \quad (\text{B.9})$$

Using Eq. (1), one finds the variance along the MSD,

$$\text{Var}(J_{\vec{n}_0}) = \frac{N}{4} (1 - |\langle \vec{\sigma}_1 \rangle|^2). \quad (\text{B.10})$$

For the CSS, only Dicke states are populated, and thus,

$$\langle J_x^2 + J_y^2 + J_z^2 \rangle = \frac{N}{2} \left( \frac{N}{2} + 1 \right). \quad (\text{B.11})$$

From the above equation and from the relations between the collective operator  $J_\alpha$  and the local operators (B.4), one finds

$$\frac{1}{N^2 - N} \sum_{i \neq j} \langle \vec{\sigma}_i \cdot \vec{\sigma}_j \rangle = 1. \quad (\text{B.12})$$

As the CSS is a product symmetric state, the above equation reduces to

$$\langle \vec{\sigma}_1 \rangle \cdot \langle \vec{\sigma}_1 \rangle = 1. \quad (\text{B.13})$$

Applying this result to Eq. (B.10), one immediately has

$$\text{Var}(J_{\vec{n}_0}) = 0. \quad (\text{B.14})$$

For the variances along the direction  $\vec{n}_\perp$  perpendicular to the MSD, from Eq. (100), we have

$$\begin{aligned} \text{Var}(J_{\vec{n}_\perp}) &= \frac{N}{4} (1 - \langle \sigma_{1\vec{n}_\perp} \rangle^2) \\ &= \frac{N}{4} [1 - (\langle \vec{\sigma}_1 \rangle \cdot \vec{n}_\perp)^2] \\ &= \frac{N}{4} [1 - |\langle \vec{\sigma}_1 \rangle|^2 (\vec{n}_0 \cdot \vec{n}_\perp)^2] \\ &= \frac{N}{4} = j/2, \end{aligned} \quad (\text{B.15})$$

where the third equality follows from Eq. (40).

### Appendix C. The minimum value of the quantity $\vec{n}^T \Gamma \vec{n}$

Here, we prove that the minimum value of  $\vec{n}^T \Gamma \vec{n}$  is a minimum eigenvalue of  $\Gamma$ . The minimum value of  $\vec{n}^T \Gamma \vec{n}$  is obtained by searching the vector  $\vec{n} = (n_1, n_2, n_3)^T$ . Since the matrix  $\Gamma$  is real and symmetric, we obtain

$$\min_{\vec{n}} (\vec{n}^T \Gamma \vec{n}) = \min_{\vec{n}} [\vec{n}^T O^T (O \Gamma O^T) O \vec{n}] = \min_{\vec{n}'} (\vec{n}'^T \Gamma^d \vec{n}'), \quad (\text{C.1})$$

where  $O$  is an orthogonal  $3 \times 3$  matrix which diagonalizes  $\Gamma$ , and

$$\Gamma^d = \text{diag}(\lambda_1, \lambda_2, \lambda_3), \quad (\text{C.2})$$

where we set  $\lambda_1 \geq \lambda_2 \geq \lambda_3$ . The rotated direction is  $\vec{n}' = O \vec{n} = (n'_1, n'_2, n'_3)^T$ . Now, the minimum value of  $\vec{n}^T \Gamma \vec{n}$  is obtained as

$$\min_{\vec{n}} (\vec{n}^T \Gamma \vec{n}) = \min_{\vec{n}'} (\vec{n}'^T \Gamma^d \vec{n}') = \min_{\vec{n}'} (\lambda_1 n_1'^2 + \lambda_2 n_2'^2 + \lambda_3 n_3'^2) = \lambda_3, \quad (\text{C.3})$$

since  $n_1'^2 + n_2'^2 + n_3'^2 = 1$ . Thus, the minimum value of  $\vec{n}^T \Gamma \vec{n}$  is obtained by choosing  $n_3' = 1$ , and  $n_1' = n_2' = 0$ , therefore,  $\vec{n} = O^T \vec{n}'$  is the direction where the minimum is achieved.



## Appendix D. Expectations for the one-axis twisted state

Here, we will use the Heisenberg picture to derive the relevant expectation values for the one-axis twisted state. To determine the spin-squeezing parameters  $\xi_S^2$  and  $\xi_R^2$ , as seen from Table 2, one needs to know the expectation  $\langle \sigma_{1z} \rangle$ , and correlations  $\langle \sigma_{1+} \sigma_{2-} \rangle$  and  $\langle \sigma_{1-} \sigma_{2-} \rangle$ . We first consider the expectation  $\langle \sigma_{1z} \rangle$ .

The evolution operator can be written as,

$$U = \exp(-i\chi t J_x^2) = \exp\left(-i\theta \sum_{k>l} j_{kx} j_{lx}\right) \quad (\text{D.1})$$

up to a trivial phase, where  $\theta = 2\chi t$ . From this form, the evolution of  $j_{1z}$  can be obtained as

$$U^\dagger j_{1z} U = j_{1z} \cos[\theta j_x^{(2)}] + j_{1y} \sin[\theta j_x^{(2)}],$$

where

$$j_x^{(k)} = \sum_{l=k}^N j_{lx}. \quad (\text{D.2})$$

Therefore, the expectations are

$$\langle j_{1z} \rangle = -\frac{1}{2} \langle \mathbf{1}' | \cos[\theta j_x^{(2)}] | \mathbf{1}' \rangle \quad (\text{D.3})$$

since  $\langle 1 | j_{1y} | 1 \rangle = 0$ . Here,  $|\mathbf{1}'\rangle = |1\rangle_2 \otimes \dots \otimes |1\rangle_N$ . So, one can find the following form for the expectation values

$$\begin{aligned} \langle \mathbf{1} | \cos[\theta J_x] | \mathbf{1} \rangle &= (\langle \mathbf{1} | e^{i\theta J_x} | \mathbf{1} \rangle + \text{c.c.}) / 2 \\ &= (\prod_{k=1}^N \langle 1 | e^{i\theta j_{kx}} | 1 \rangle + \text{c.c.}) / 2 \\ &= \cos^N(\theta'), \end{aligned} \quad (\text{D.4})$$

where  $\theta' = \theta/2$  and  $|\mathbf{1}\rangle = |1\rangle^{\otimes N}$ . By using Eqs. (D.3) and (D.4), one gets

$$\langle \sigma_z \rangle = -\cos^{N-1}(\theta'). \quad (\text{D.5})$$

Since the operator  $\sigma_{1x} \sigma_{2x}$  commutes with the unitary operator  $U$ , we easily obtain

$$\langle \sigma_{1x} \sigma_{2x} \rangle = 0. \quad (\text{D.6})$$

We now compute the correlations  $\langle \sigma_{1z} \sigma_{2z} \rangle$ . From the unitary operator,

$$\begin{aligned} U^\dagger j_{1z} j_{2z} U &= \left[ j_{1z} \cos(\theta j_x^{(2)}) + j_{1y} \sin(\theta j_x^{(2)}) \right] \left[ j_{2z} \cos[\theta(j_{1x} + j_x^{(3)})] + j_{2y} \sin[\theta(j_{1x} + j_x^{(3)})] \right] \\ &= \left[ j_{1z} \cos(\theta j_{2x}) \cos(\theta j_x^{(3)}) - j_{1z} \sin(\theta j_{2x}) \sin(\theta j_x^{(3)}) \right. \\ &\quad \left. + j_{1y} \sin(\theta j_{2x}) \cos(\theta j_x^{(3)}) + j_{1y} \cos(\theta j_{2x}) \sin(\theta j_x^{(3)}) \right] \\ &\quad \times \left[ j_{2z} \cos(\theta j_{1x}) \cos(\theta j_x^{(3)}) - j_{2z} \sin(\theta j_{1x}) \sin(\theta j_x^{(3)}) \right. \\ &\quad \left. + j_{2y} \sin(\theta j_{1x}) \cos(\theta j_x^{(3)}) + j_{2y} \cos(\theta j_{1x}) \sin(\theta j_x^{(3)}) \right]. \end{aligned}$$

Although there are 16 terms after expanding the above equation, only four terms survive when calculating  $\langle j_{1z}j_{2z} \rangle$ . We then have

$$\begin{aligned}
\langle j_{1z}j_{2z} \rangle &= \langle \mathbf{1} | j_{1z}j_{2z} \cos^2(\theta/2) \cos^2(\theta j_x^{(3)}) - j_{1z}j_{2x}j_{2y} \sin(\theta) \sin^2(\theta j_x^{(3)}) \\
&\quad + 4j_{1y}j_{1x}j_{2x}j_{2y} \sin^2(\theta/2) \cos^2(\theta j_x^{(3)}) - j_{1y}j_{1x}j_{2z} \sin(\theta) \sin^2(\theta j_x^{(3)}) | \mathbf{1} \rangle \\
&= \frac{1}{4} \langle \mathbf{1}' | \cos^2(\theta j_x^{(3)}) | \mathbf{1}' \rangle \\
&= \frac{1}{8} \langle \mathbf{1}' | [1 + \cos(2\theta j_x^{(3)})] | \mathbf{1}' \rangle \\
&= \frac{1}{8} [1 + \cos^{N-2}(\theta)], \tag{D.7}
\end{aligned}$$

where  $|\mathbf{1}'\rangle = |1\rangle_3 \otimes \dots \otimes |1\rangle_N$ . The second equality in Eq. (D.7) is due to the property  $j_x j_y = -j_y j_x = i j_z/2$ , and the last equality is from Eq. (D.4). Finally, from the above equation, one finds

$$\langle \sigma_{1z} \sigma_{2z} \rangle = \frac{1}{2} (1 + \cos^{N-2} \theta). \tag{D.8}$$

Due to the relation  $\langle \sigma_{1x} \sigma_{2x} + \sigma_{1y} \sigma_{2y} + \sigma_{1z} \sigma_{2z} \rangle = 1$  for the initial state, the correlation  $\langle \sigma_{1y} \sigma_{2y} \rangle$  is obtained from Eqs. (D.6) and (D.8) as

$$\langle \sigma_{1y} \sigma_{2y} \rangle = \frac{1}{2} (1 - \cos^{N-2} \theta). \tag{D.9}$$

Substituting Eqs. (D.6) and (D.9) into the following relations

$$\sigma_{1x} \sigma_{2x} + \sigma_{1y} \sigma_{2y} = 2(\sigma_{1+} \sigma_{2-} + \sigma_{1-} \sigma_{2+}) \tag{D.10}$$

leads to

$$\langle \sigma_{1+} \sigma_{2-} \rangle = \frac{1}{8} (1 - \cos^{N-2} \theta), \tag{D.11}$$

where the relation  $\langle \sigma_{1+} \sigma_{2-} \rangle = \langle \sigma_{1-} \sigma_{2+} \rangle$  is used due to the exchange symmetry.

To calculate the correlation  $\langle \sigma_{1-} \sigma_{2-} \rangle$ , due to the following relations

$$\sigma_{1x} \sigma_{2x} - \sigma_{1y} \sigma_{2y} = 2(\sigma_{1+} \sigma_{2+} + \sigma_{1-} \sigma_{2-}), \tag{D.12}$$

$$i(\sigma_{1x} \sigma_{2y} + \sigma_{1y} \sigma_{2x}) = 2(\sigma_{1+} \sigma_{2+} - \sigma_{1-} \sigma_{2-}), \tag{D.13}$$

we need to know the expectations  $\langle j_{1x} j_{2y} \rangle$ . The evolution of  $j_{1x} j_{2y}$  is given by

$$U^\dagger s_{1x} s_{2y} U = j_{1x} \left\{ j_{2y} \cos \left[ \theta(j_{1x} + j_x^{(3)}) \right] - j_{2z} \sin \left[ \theta(j_{1x} + j_x^{(3)}) \right] \right\}, \tag{D.14}$$

and the expectation is obtained as

$$\begin{aligned}
\langle j_{1x} j_{2y} \rangle &= \frac{1}{2} \langle \mathbf{1}' | j_{1x} \sin \left[ \theta(j_{1x} + j_x^{(3)}) \right] | \mathbf{1}' \rangle \\
&= \frac{1}{4i} \langle \mathbf{1}' | j_{1x} e^{i\theta j_{1x}} \prod_{k=3}^N e^{i\theta j_{kx}} - j_{1x} e^{-i\theta j_{1x}} \prod_{k=3}^N e^{-i\theta j_{kx}} | \mathbf{1}' \rangle \\
&= \frac{1}{4i} \cos^{N-2}(\theta') \langle 1 | j_{1x} e^{i\theta j_{1x}} - j_{1x} e^{-i\theta j_{1x}} | 1 \rangle \\
&= \frac{1}{2} \cos^{N-2}(\theta') \langle 1 | j_{1x} \sin(\theta j_{1x}) | 1 \rangle \\
&= \frac{1}{4} \sin(\theta') \cos^{N-2}(\theta'). \tag{D.15}
\end{aligned}$$

Here,  $|\mathbf{1}'\rangle = |1\rangle_1 \otimes |1\rangle_3 \otimes \dots \otimes |1\rangle_N$ , where  $|1\rangle_2$  is absent. Moreover,  $\langle j_{1y} j_{2x} \rangle = \langle j_{1x} j_{2y} \rangle$  due to the exchange symmetry, and thus,

$$\langle j_{1x} j_{2y} + j_{1y} j_{2x} \rangle = \frac{1}{2} \sin(\theta') \cos^{N-2}(\theta'). \tag{D.16}$$

For the state (322), we obtain the following expectations

$$\langle \sigma_{1x}\sigma_{2y} + \sigma_{1y}\sigma_{2x} \rangle = 2 \sin(\theta') \cos^{N-2}(\theta'). \quad (\text{D.17})$$

The combination of Eqs. (D.6), (D.9), (D.12), (D.13), and (D.17) leads to the correlation

$$\langle \sigma_{1-}\sigma_{2-} \rangle = -\frac{1}{8} (1 - \cos^{N-2}\theta) - \frac{i}{2} \sin(\theta') \cos^{N-2}(\theta'). \quad (\text{D.18})$$

Substituting Eqs. (D.11) and (D.18) to the expression  $\xi_S^2$  in terms of local expectation values (Table 2) leads to the desirable expression of the squeezing parameter for the one-axis twisted state.

### Appendix E. Photon polarization and Stokes operators

Here, we briefly introduce the Stokes operators for photons. The light field has two orthogonal polarization directions. If the light field propagates along the  $z$ -axis, we use the bases given by  $\hat{e}_x$  and  $\hat{e}_y$ , which denote the vertical and horizontal polarizations, respectively. The other two sets of bases can be expressed with  $\hat{e}'_x$  and  $\hat{e}'_y$ . If the phase difference between the  $\hat{e}_x$ - and  $\hat{e}_y$ -polarized components is  $\pm\pi/2$ , then the light is  $45^\circ$  polarized, with new bases expressed as

$$\hat{e}'_x = \frac{1}{\sqrt{2}} (\hat{e}_x + \hat{e}_y), \quad \hat{e}'_y = \frac{1}{\sqrt{2}} (-\hat{e}_x + \hat{e}_y). \quad (\text{E.1})$$

If the phase difference between the  $\hat{e}_x$  and  $\hat{e}_y$  components is  $\pm\pi/4$ , then the light is circularly polarized, with right- and left-circular bases

$$\hat{e}_+ = -\frac{1}{\sqrt{2}} (\hat{e}_x + i\hat{e}_y), \quad \hat{e}_- = \frac{1}{\sqrt{2}} (\hat{e}_x - i\hat{e}_y). \quad (\text{E.2})$$

The two polarized components can build up an angular momentum operator analogous to the Schwinger representation (151). Denote the  $x$ - and  $y$ -polarized field operators as  $a_x$  and  $a_y$ , respectively. Then, the Stokes operators are defined as

$$\begin{aligned} S_x &= \frac{1}{2} (a_x^\dagger a_x - a_y^\dagger a_y), \\ S_y &= \frac{1}{2} (a_x^\dagger a'_x - a_y^\dagger a'_y), \\ S_z &= \frac{1}{2} (a_+^\dagger a_+ - a_-^\dagger a_-). \end{aligned} \quad (\text{E.3})$$

The three Stokes operators ( $S_x$ ,  $S_y$  and  $S_z$ ) shown in (E.3) measure the photon number differences of the  $x$ - to  $y$ -polarization,  $\pi/4$ - to  $-\pi/4$ -polarization, and right- to left-polarization, respectively. The polarization squeezing of light field was studied in Refs. [291, 292, 293, 294, 295, 296].

## References

- [1] M. Kitagawa and M. Ueda, Squeezed spin states, *Phys. Rev. A* **47**, 5138 (1993).
- [2] D. J. Wineland, J. J. Bollinger, W. M. Itano, F. L. Moore, and D. J. Heinzen, Spin squeezing and reduced quantum noise in spectroscopy, *Phys. Rev. A* **46**, R6797 (1992).
- [3] D. J. Wineland, J. J. Bollinger, W. M. Itano, and D. J. Heinzen, Squeezed atomic states and projection noise in spectroscopy, *Phys. Rev. A* **50**, 67 (1994).
- [4] A. Sørensen, L. Duan, J. Cirac, and P. Zoller, Many-particle entanglement with Bose-Einstein condensates, *Nature* **409**, 63 (2001).
- [5] N. Bigelow, Quantum engineering - Squeezing entanglement, *Nature* **409**, 27 (2001).
- [6] O. Guehne and G. Tóth, Entanglement detection, *Phys. Rep.* **474**, 1 (2009).
- [7] E. S. Polzik, Quantum physics - The squeeze goes on, *Nature* **453**, 45 (2008).
- [8] A. D. Cronin, J. Schmiedmayer, and D. E. Pritchard, Optics and interferometry with atoms and molecules, *Rev. Mod. Phys.* **81**, 1051 (2009).
- [9] L. Amico, R. Fazio, A. Osterloh, and V. Vedral, Entanglement in many-body systems, *Rev. Mod. Phys.* **80**, 517 (2008).
- [10] R. Horodecki, P. Horodecki, M. Horodecki, and K. Horodecki, Quantum entanglement, *Rev. Mod. Phys.* **81**, 865 (2009).
- [11] M. A. Nielsen and I. L. Chuang, *Quantum Computation and Quantum Information*, (Cambridge University Press, Cambridge, England, 2000).
- [12] J. Stolze and D. Suter, *Quantum Computing: A Short Course from Theory to Experiment, Second Edition*, (Wiley-Vch Verlag, Weinheim, 2008).
- [13] D. Ulam-Orgikh and M. Kitagawa, Spin squeezing and decoherence limit in Ramsey spectroscopy, *Phys. Rev. A* **64**, 052106 (2001).
- [14] W. K. Wootters, Entanglement of formation of an arbitrary state of two qubits, *Phys. Rev. Lett.* **80**, 2245 (1998).
- [15] X. Wang and B. C. Sanders, Spin squeezing and pairwise entanglement for symmetric multiqubit states, *Phys. Rev. A* **68**, 012101 (2003).
- [16] J. Hald, J. Sørensen, C. Schori, and E. Polzik, Spin squeezed atoms: A macroscopic entangled ensemble created by light, *Phys. Rev. Lett.* **83**, 1319 (1999).
- [17] C. Orzel, A. Tuchman, M. Fenselau, M. Yasuda, and M. Kasevich, Squeezed states in a Bose-Einstein condensate, *Science* **291**, 2386 (2001).
- [18] J. Estève, C. Gross, A. Weller, S. Giovanazzi, and M. K. Oberthaler, Squeezing and entanglement in a Bose-Einstein condensate, *Nature* **455**, 1216 (2008).
- [19] C. Gross, T. Zibold, E. Nicklas, J. Estève, and M. K. Oberthaler, Nonlinear atom interferometer surpasses classical precision limit, *Nature* **464**, 1165 (2010).
- [20] M. F. Riedel, P. Boehi, Y. Li, T. W. Haensch, A. Sinatra, and P. Treutlein, Atom-chip-based generation of entanglement for quantum metrology, *Nature* **464**, 1170 (2010).
- [21] B. Julsgaard, A. Kozhekin, and E. Polzik, Experimental long-lived entanglement of two macroscopic objects, *Nature* **413**, 400 (2001).
- [22] T. Fernholz, H. Krauter, K. Jensen, J. F. Sherson, A. S. Sørensen, and E. S. Polzik, Spin squeezing of atomic ensembles via nuclear-electronic spin entanglement, *Phys. Rev. Lett.* **101**, 073601 (2008).
- [23] J. Appel, P. J. Windpassinger, D. Oblak, U. B. Hoff, N. Kjaergaard, and E. S. Polzik, Mesoscopic atomic entanglement for precision measurements beyond the standard quantum limit, *PNAS* **106**, 10960 (2009).
- [24] A. Louchet-Chauvet, J. Appel, J. J. Renema, D. Oblak, N. Kjaergaard, and E. S. Polzik, Entanglement-assisted atomic clock beyond the projection noise limit, *New J. Phys.* **12**, 065032 (2010).
- [25] T. Takano, M. Fuyama, R. Namiki, and Y. Takahashi, Spin Squeezing of a Cold Atomic Ensemble with the Nuclear Spin of One-Half, *Phys. Rev. Lett.* **102**, 033601 (2009).
- [26] J. Korbicz, J. Cirac, and M. Lewenstein, Spin squeezing inequalities and entanglement of N qubit states, *Phys. Rev. Lett.* **95**, 120502 (2005).
- [27] J. K. Korbicz, O. Guehne, M. Lewenstein, H. Haefner, C. F. Roos, and R. Blatt, Generalized spin-squeezing inequalities in N-qubit systems: Theory and experiment, *Phys. Rev. A* **74**, 052319 (2006).
- [28] G. Tóth, C. Knapp, O. Guehne, and H. J. Briegel, Spin squeezing and entanglement, *Phys. Rev. A* **79**, 042334 (2009).
- [29] I. Buluta, S. Ashhab, and F. Nori, Natural and artificial atoms for quantum computation, arXiv:1002.1871v2 .
- [30] J. Q. You and F. Nori, Superconducting circuits and quantum information, *Phys. Today* **58**, 42 (2005).
- [31] S. N. Shevchenko, S. Ashhab, and F. Nori, Landau-Zener-Stueckelberg interferometry, *Phys. Rep.* **492**, 1 (2010).
- [32] I. Buluta and F. Nori, Quantum Simulators, *Science* **326**, 108 (2009).
- [33] J. Bollinger, W. Itano, D. Wineland, and D. Heinzen, Optimal frequency measurements with maximally correlated states, *Phys. Rev. A* **54**, R4649 (1996).
- [34] G. Agarwal and M. Scully, Ramsey spectroscopy with nonclassical light sources, *Phys. Rev. A* **53**, 467 (1996).
- [35] P. R. Berman, editor, *Atom Interferometry*, (Academic Press, 1997).
- [36] G. Xu and D. Heinzen, State-selective Rabi and Ramsey magnetic resonance line shapes, *Phys. Rev. A* **59**, R922 (1999).
- [37] V. Meyer, M. Rowe, D. Kielpinski, C. Sackett, W. Itano, C. Monroe, and D. Wineland, Experimental demonstration of entanglement-enhanced rotation angle estimation using trapped ions, *Phys. Rev. Lett.* **86**, 5870 (2001).
- [38] G. Smith, S. Chaudhury, A. Silberfarb, I. Deutsch, and P. Jessen, Continuous weak measurement and nonlinear dynamics in a cold spin ensemble, *Phys. Rev. Lett.* **93**, 163602 (2004).
- [39] D. Döring, G. McDonald, J. E. Debs, C. Figl, P. A. Altin, H. A. Bachor, N. P. Robins, and J. D. Close, Quantum-projection-noise-limited interferometry with coherent atoms in a Ramsey-type setup, *Phys. Rev. A* **81**, 043633 (2010).

- [40] D. Oblak, P. Petrov, C. Garrido Alzar, W. Tittel, A. Vershovski, J. Mikkelsen, J. Sørensen, and E. Polzik, Quantum-noise-limited interferometric measurement of atomic noise: Towards spin squeezing on the Cs clock transition, *Phys. Rev. A* **71**, 043807 (2005).
- [41] A. Sørensen and K. Mølmer, Spin-spin interaction and spin squeezing in an optical lattice, *Phys. Rev. Lett.* **83**, 2274 (1999).
- [42] D. Meiser, J. Ye, and M. J. Holland, Spin squeezing in optical lattice clocks via lattice-based QND measurements, *New J. Phys.* **10**, 073014 (2008).
- [43] A. Andre, A. Sørensen, and M. Lukin, Stability of atomic clocks based on entangled atoms, *Phys. Rev. Lett.* **92**, 230801 (2004).
- [44] I. D. Leroux, M. H. Schleier-Smith, and V. Vuletic, Orientation-Dependent Entanglement Lifetime in a Squeezed Atomic Clock, *Phys. Rev. Lett.* **104**, 250801 (2010).
- [45] D. F. Walls and P. Zoller, Enhanced sensitivity of a gravitational-wave detector, *Phys. Lett. A* **85**, 118 (1981).
- [46] J. Dunningham and K. Burnett, Sub-shot-noise-limited measurements with Bose-Einstein condensates, *Phys. Rev. A* **70**, 033601 (2004).
- [47] K. Goda, O. Miyakawa, E. E. Mikhailov, S. Saraf, R. Adhikari, K. McKenzie, R. Ward, S. Vass, A. J. Weinstein, and N. Mavalvala, A quantum-enhanced prototype gravitational-wave detector, *Nature Phys.* **4**, 472 (2008).
- [48] K. Hammerer, A. S. Sørensen, and E. S. Polzik, Quantum interface between light and atomic ensembles, *Rev. Mod. Phys.* **82**, 1041 (2010).
- [49] G. M. Palma and P. L. Knight, Phase-sensitive population decay: The two-atom Dicke model in a broadband squeezed vacuum, *Phys. Rev. A* **39**, 1962 (1989).
- [50] A. Banerjee, Generation of atomic-squeezed states in an optical cavity with an injected squeezed vacuum, *Phys. Rev. A* **54**, 5327 (1996).
- [51] A. Kuzmich, K. Mølmer, and E. Polzik, Spin squeezing in an ensemble of atoms illuminated with squeezed light, *Phys. Rev. Lett.* **79**, 4782 (1997).
- [52] J. Sørensen, J. Hald, and E. Polzik, Quantum noise of an atomic spin polarization measurement, *Phys. Rev. Lett.* **80**, 3487 (1998).
- [53] K. Mølmer, Twin-correlations in atoms, *Eur. Phys. J. D* **5**, 301 (1999).
- [54] J. Hald, J. Sørensen, C. Schori, and E. Polzik, Entanglement transfer from light to atoms, *J. Mod. Opt.* **47**, 2599 (2000).
- [55] L. Vernac, M. Pinard, and E. Giacobino, Spin squeezing in two-level systems, *Phys. Rev. A* **62**, 063812 (2000).
- [56] L. Vernac, M. Pinard, and E. Giacobino, Quantum state transfer from light beams to atomic ensembles, *Eur. Phys. J. D* **17**, 125 (2001).
- [57] J. Hald and E. Polzik, Mapping a quantum state of light onto atoms, *J. Opt. B-Quantum Semiclassical Opt.* **3**, S83 (2001).
- [58] L. Vernac, M. Pinard, V. Josse, and E. Giacobino, Collective atomic spin squeezing and control, *Eur. Phys. J. D* **18**, 129 (2002).
- [59] A. Dantan, M. Pinard, V. Josse, N. Nayak, and P. Berman, Atomic spin squeezing in a Lambda system, *Phys. Rev. A* **67**, 045801 (2003).
- [60] A. Dantan, G. Reinaudi, A. Sinatra, F. Laloe, E. Giacobino, and M. Pinard, Long-lived quantum memory with nuclear atomic spins, *Phys. Rev. Lett.* **95**, 123002 (2005).
- [61] A. Dantan, V. Josse, J. Cviklinski, A. Bramati, M. Pinard, and E. Giacobino, Generation and storage of quantum states using cold atoms, *J. Mod. Opt.* **53**, 2235 (2006).
- [62] O. Civitarese, M. Reboiro, L. Rebon, and D. Tielas, Spin squeezing in the presence of dissipation, *Phys. Lett. A* **373**, 754 (2009).
- [63] L.-M. Duan, J. I. Cirac, P. Zoller, and E. S. Polzik, Quantum communication between atomic ensembles using coherent light, *Phys. Rev. Lett.* **85**, 5643 (2000).
- [64] M. Fleischhauer and M. Lukin, Dark-state polaritons in electromagnetically induced transparency, *Phys. Rev. Lett.* **84**, 5094 (2000).
- [65] M. Lukin, S. Yelin, and M. Fleischhauer, Entanglement of atomic ensembles by trapping correlated photon states, *Phys. Rev. Lett.* **84**, 4232 (2000).
- [66] A. Dantan, M. Pinard, and P. Berman, EIT-assisted atomic squeezing, *Eur. Phys. J. D* **27**, 193 (2003).
- [67] D. Akamatsu, K. Akiba, and M. Kozuma, Electromagnetically induced transparency with squeezed vacuum, *Phys. Rev. Lett.* **92**, 203602 (2004).
- [68] A. Dantan and M. Pinard, Quantum-state transfer between fields and atoms in electromagnetically induced transparency, *Phys. Rev. A* **69**, 043810 (2004).
- [69] A. Dantan, A. Bramati, and M. Pinard, Atomic quantum memory: Cavity versus single-pass schemes, *Phys. Rev. A* **71**, 043801 (2005).
- [70] A. Dantan, J. Cviklinski, E. Giacobino, and M. Pinard, Spin squeezing and light entanglement in coherent population trapping, *Phys. Rev. Lett.* **97**, 023605 (2006).
- [71] K. Honda, D. Akamatsu, M. Arikawa, Y. Yokoi, K. Akiba, S. Nagatsuka, T. Tanimura, A. Furusawa, and M. Kozuma, Storage and retrieval of a squeezed vacuum, *Phys. Rev. Lett.* **100**, 093601 (2008).
- [72] Z. R. Gong, X. Wang, and C. P. Sun, Adiabatic creation of atomic squeezing in dark states versus decoherences, *Phys. Rev. A* **82**, 012112 (2010).
- [73] G. Smith, S. Chaudhury, and P. Jessen, Faraday spectroscopy in an optical lattice: a continuous probe of atom dynamics, *J. Opt. B-Quantum Semiclassical Opt.* **5**, 323 (2003).
- [74] A. Kuzmich, N. Bigelow, and L. Mandel, Atomic quantum non-demolition measurements and squeezing, *Europhys. Lett.*

- 42, 481 (1998).
- [75] Y. Takahashi, K. Honda, N. Tanaka, K. Toyoda, K. Ishikawa, and T. Yabuzaki, Quantum nondemolition measurement of spin via the paramagnetic Faraday rotation, *Phys. Rev. A* **60**, 4974 (1999).
  - [76] A. Kuzmich, L. Mandel, J. Janis, Y. Young, R. Eijnisman, and N. Bigelow, Quantum nondemolition measurements of collective atomic spin, *Phys. Rev. A* **60**, 2346 (1999).
  - [77] A. Kuzmich, L. Mandel, and N. Bigelow, Generation of spin squeezing via continuous quantum nondemolition measurement, *Phys. Rev. Lett.* **85**, 1594 (2000).
  - [78] L. Thomsen, S. Mancini, and H. Wiseman, Continuous quantum nondemolition feedback and unconditional atomic spin squeezing, *J. Phys. B-At. Mol. Opt. Phys.* **35**, 4937 (2002).
  - [79] I. Bouchoule and K. Mølmer, Preparation of spin-squeezed atomic states by optical-phase-shift measurement, *Phys. Rev. A* **66**, 043811 (2002).
  - [80] J. Zhang, K. Peng, and S. Braunstein, Backaction-induced spin-squeezed states in a detuned quantum-nondemolition measurement, *Phys. Rev. A* **68**, 035802 (2003).
  - [81] H. Saito and M. Ueda, Measurement-induced spin squeezing in a cavity, *Phys. Rev. A* **68**, 043820 (2003).
  - [82] M. Auzinsh, D. Budker, D. F. Kimball, S. M. Rochester, J. E. Stalnaker, A. O. Sushkov, and V. V. Yashchuk, Can a quantum nondemolition measurement improve the sensitivity of an atomic magnetometer?, *Phys. Rev. Lett.* **93**, 173002 (2004).
  - [83] L. B. Madsen and K. Mølmer, Spin squeezing and precision probing with light and samples of atoms in the Gaussian description, *Phys. Rev. A* **70**, 052324 (2004).
  - [84] A. Kuzmich and T. Kennedy, Nonsymmetric entanglement of atomic ensembles, *Phys. Rev. Lett.* **92**, 030407 (2004).
  - [85] S. de Echaniz, M. Mitchell, M. Kubasik, M. Koschorreck, H. Crepaz, J. Eschner, and E. Polzik, Conditions for spin squeezing in a cold Rb-87 ensemble, *J. Opt. B: Quantum Semiclass. Opt.* **7**, S548 (2005).
  - [86] J. Geremia, J. K. Stockton, and H. Mabuchi, Suppression of spin projection noise in broadband atomic magnetometry, *Phys. Rev. Lett.* **94**, 203002 (2005).
  - [87] V. Petersen, L. B. Madsen, and K. Mølmer, Magnetometry with entangled atomic samples, *Phys. Rev. A* **71**, 012312 (2005).
  - [88] C. Genes and P. Berman, Generating conditional atomic entanglement by measuring photon number in a single output channel, *Phys. Rev. A* **73**, 013801 (2006).
  - [89] G. A. Smith, A. Silberfarb, I. H. Deutsch, and P. S. Jessen, Efficient quantum-state estimation by continuous weak measurement and dynamical control, *Phys. Rev. Lett.* **97**, 180403 (2006).
  - [90] J. Cviklinski, A. Dantan, J. Ortalo, and M. Pinard, Conditional squeezing of an atomic alignment, *Phys. Rev. A* **76**, 033830 (2007).
  - [91] A. E. B. Nielsen and K. Mølmer, Atomic spin squeezing in an optical cavity, *Phys. Rev. A* **77**, 063811 (2008).
  - [92] I. Teper, G. Vrijsen, J. Lee, and M. A. Kasevich, Backaction noise produced via cavity-aided nondemolition measurement of an atomic clock state, *Phys. Rev. A* **78**, 051803 (2008).
  - [93] P. J. Windpassinger, D. Oblak, U. B. Hoff, J. Appel, N. Kjaergaard, and E. S. Polzik, Inhomogeneous light shift effects on atomic quantum state evolution in non-destructive measurements, *New J. Phys.* **10**, 053032 (2008).
  - [94] P. J. Windpassinger, D. Oblak, U. B. Hoff, A. Louchet, J. Appel, N. Kjaergaard, and E. S. Polzik, Squeezing of atomic quantum projection noise, *J. Mod. Opt.* **56**, 1993–1998 (2009).
  - [95] B. A. Chase, B. Q. Baragiola, H. L. Partner, B. D. Black, and J. M. Geremia, Magnetometry via a double-pass continuous quantum measurement of atomic spin, *Phys. Rev. A* **79**, 062107 (2009).
  - [96] M. Saffman, D. Oblak, J. Appel, and E. S. Polzik, Spin squeezing of atomic ensembles by multicolor quantum nondemolition measurements, *Phys. Rev. A* **79**, 023831 (2009).
  - [97] M. Kubasik, M. Koschorreck, M. Napolitano, S. R. de Echaniz, H. Crepaz, J. Eschner, E. S. Polzik, and M. W. Mitchell, Polarization-based light-atom quantum interface with an all-optical trap, *Phys. Rev. A* **79**, 043815 (2009).
  - [98] V. Shah, G. Vasilakis, and M. V. Romalis, High bandwidth atomic magnetometry with continuous quantum nondemolition measurements, *Phys. Rev. Lett.* **104**, 013601 (2010).
  - [99] Z. Kurucz and K. Mølmer, Multilevel Holstein-Primakoff approximation and its application to atomic spin squeezing and ensemble quantum memories, *Phys. Rev. A* **81**, 032314 (2010).
  - [100] P. Marek and R. Filip, Noise-resilient quantum interface based on quantum nondemolition interactions, *Phys. Rev. A* **81**, 042325 (2010).
  - [101] W. Wasilewski, K. Jensen, H. Krauter, J. J. Renema, M. V. Balabas, and E. S. Polzik, Quantum Noise Limited and Entanglement-Assisted Magnetometry, *Phys. Rev. Lett.* **104**, 133601 (2010).
  - [102] M. H. Schleier-Smith, I. D. Leroux, and V. Vuletić, States of an Ensemble of Two-Level Atoms with Reduced Quantum Uncertainty, *Phys. Rev. Lett.* **104**, 073604 (2010).
  - [103] M. Koschorreck, M. Napolitano, B. Dubost, and M. W. Mitchell, Sub-Projection-Noise Sensitivity in Broadband Atomic Magnetometry, *Phys. Rev. Lett.* **104**, 093602 (2010).
  - [104] M. Koschorreck, M. Napolitano, B. Dubost, and M. W. Mitchell, Quantum Nondemolition Measurement of Large-Spin Ensembles by Dynamical Decoupling, *Phys. Rev. Lett.* **105**, 093602 (2010).
  - [105] A. Klimov and P. Espinoza, Classical evolution of quantum fluctuations in spin-like systems: squeezing and entanglement, *J. Opt. B-Quantum Semiclassical Opt.* **7**, 183 (2005).
  - [106] P. K. Pathak, R. N. Deb, N. Nayak, and K. Dutta-Roy, B., The quadratic spin squeezing operators, *J. Phys. A-Math. Theor.* **41**, 145302 (2008).
  - [107] G. Agarwal, R. Puri, and R. Singh, Atomic Schrodinger cat states, *Phys. Rev. A* **56**, 2249 (1997).
  - [108] A. Klimov and C. Saavedra, The Dicke model dynamics in a high detuning limit, *Phys. Lett. A* **247**, 14 (1998).

- [109] D. Shindo, A. Chavez, S. Chumakov, and A. Klimov, Dynamical squeezing enhancement in the off-resonant Dicke model, *J. Opt. B-Quantum Semiclassical Opt.* **6**, 34 (2004).
- [110] R. Deb, M. Abdalla, S. Hassan, and N. Nayak, Spin squeezing and entanglement in a dispersive cavity, *Phys. Rev. A* **73**, 053817 (2006).
- [111] S. Chaudhury, S. Merkel, T. Herr, A. Silberfarb, I. H. Deutsch, and P. S. Jessen, Quantum control of the hyperfine spin of a Cs atom ensemble, *Phys. Rev. Lett.* **99**, 163002 (2007).
- [112] M. Ueda, T. Wakabayashi, and M. KuwataGonokami, Synchronous collapses and revivals of atomic dipole fluctuations and photon fano factor beyond the standard quantum limit, *Phys. Rev. Lett.* **76**, 2045 (1996).
- [113] A. Sørensen and K. Mølmer, Entangling atoms in bad cavities, *Phys. Rev. A* **66**, 022314 (2002).
- [114] V. Yukalov and E. Yukalova, Atomic squeezing under collective emission, *Phys. Rev. A* **70**, 053828 (2004).
- [115] G. Ramon, C. Brif, and A. Mann, Governing dynamics by squeezing in a system of cold trapped ions, *Phys. Rev. A* **59**, 736 (1999).
- [116] K. Saito and M. Ueda, Quantum-controlled few-photon state generated by squeezed atoms, *Phys. Rev. Lett.* **79**, 3869 (1997).
- [117] H. Saito and M. Ueda, Squeezed few-photon states of the field generated from squeezed atoms, *Phys. Rev. A* **59**, 3959 (1999).
- [118] U. Poulsen and K. Mølmer, Squeezed light from spin-squeezed atoms, *Phys. Rev. Lett.* **87**, 123601 (2001).
- [119] C. Law, H. Ng, and P. Leung, Coherent control of spin squeezing, *Phys. Rev. A* **63**, 055601 (2001).
- [120] U. Poulsen and K. Mølmer, Positive- $P$  simulations of spin squeezing in a two-component Bose condensate, *Phys. Rev. A* **64**, 013616 (2001).
- [121] S. Raghavan, H. Pu, P. Meystre, and N. Bigelow, Generation of arbitrary Dicke states in spinor Bose-Einstein condensates, *Opt. Commun.* **188**, 149 (2001).
- [122] S. Jenkins and T. Kennedy, Spin squeezing in a driven Bose-Einstein condensate, *Phys. Rev. A* **66**, 043621 (2002).
- [123] D. Jaksch, J. Cirac, and P. Zoller, Dynamically turning off interactions in a two-component condensate, *Phys. Rev. A* **65**, 033625 (2002).
- [124] H. Jing, Mutual coherence and spin squeezing in double-well atomic condensates, *Phys. Lett. A* **306**, 91 (2002).
- [125] A. Sørensen, Bogoliubov theory of entanglement in a Bose-Einstein condensate, *Phys. Rev. A* **65**, 043610 (2002).
- [126] A. Micheli, D. Jaksch, J. Cirac, and P. Zoller, Many-particle entanglement in two-component Bose-Einstein condensates, *Phys. Rev. A* **67**, 013607 (2003).
- [127] K. Mølmer, Quantum atom optics with Bose-Einstein condensates, *New J. Phys.* **5**, 55 (2003).
- [128] M. Jaaskelainen, W. Zhang, and P. Meystre, Limits to phase resolution in matter-wave interferometry, *Phys. Rev. A* **70**, 063612 (2004).
- [129] S. Choi and N. Bigelow, Quantum squeezing and entanglement in a two-mode Bose-Einstein condensate with time-dependent Josephson-like coupling, *Phys. Rev. A* **72**, 033612 (2005).
- [130] M. Jaaskelainen and P. Meystre, Dynamics of Bose-Einstein condensates in double-well potentials, *Phys. Rev. A* **71**, 043603 (2005).
- [131] G.-R. Jin and S. W. Kim, Storage of spin squeezing in a two-component Bose-Einstein condensate, *Phys. Rev. Lett.* **99**, 170405 (2007).
- [132] G.-R. Jin and S. W. Kim, Spin squeezing and maximal-squeezing time, *Phys. Rev. A* **76**, 043621 (2007).
- [133] S. Thanvanthri and Z. Dutton, Spatial dynamics and spin squeezing in Bose-Einstein condensates, *Phys. Rev. A* **75**, 023618 (2007).
- [134] G. R. Jin and C. K. Law, Relationship between spin squeezing and single-particle coherence in two-component Bose-Einstein condensates with Josephson coupling, *Phys. Rev. A* **78**, 063620 (2008).
- [135] J. Grond, J. Schmiedmayer, and U. Hohenester, Optimizing number squeezing when splitting a mesoscopic condensate, *Phys. Rev. A* **79**, 021603 (2009).
- [136] J. Grond, G. von Winckel, J. Schmiedmayer, and U. Hohenester, Optimal control of number squeezing in trapped Bose-Einstein condensates, *Phys. Rev. A* **80**, 053625 (2009).
- [137] K. Helmerson and L. You, Creating massive entanglement of Bose-Einstein condensed atoms, *Phys. Rev. Lett.* **87**, 170402 (2001).
- [138] M. Zhang, K. Helmerson, and L. You, Entanglement and spin squeezing of Bose-Einstein-condensed atoms, *Phys. Rev. A* **68**, 043622 (2003).
- [139] H. T. Ng, C. Law, and P. Leung, Quantum-correlated double-well tunneling of two-component Bose-Einstein condensates, *Phys. Rev. A* **68**, 013604 (2003).
- [140] B. Deb and G. Agarwal, Entangling two Bose-Einstein condensates by stimulated Bragg scattering, *Phys. Rev. A* **67**, 023603 (2003).
- [141] T. Gasenzer, D. Roberts, and K. Burnett, Limitations of entanglement between photons and atoms coupled out from a Bose-Einstein condensate, *Phys. Rev. A* **65**, 021605 (2002).
- [142] S. Yi, O. E. Müstecaplıoğlu, C. P. Sun, and L. You, Single-mode approximation in a spinor-1 atomic condensate, *Phys. Rev. A* **66**, 011601 (2002).
- [143] O. E. Müstecaplıoğlu, W. Zhang, and L. You, Quantum dynamics of a spin-1 condensate in a double-well potential, *Phys. Rev. A* **75**, 023605 (2007).
- [144] L.-M. Duan, A. Sørensen, J. I. Cirac, and P. Zoller, Squeezing and entanglement of atomic beams, *Phys. Rev. Lett.* **85**, 3991 (2000).
- [145] H. Pu and P. Meystre, Creating macroscopic atomic Einstein-Podolsky-Rosen states from Bose-Einstein condensates, *Phys. Rev. Lett.* **85**, 3987 (2000).

- [146] L. Duan, J. Cirac, and P. Zoller, Quantum entanglement in spinor Bose-Einstein condensates, *Phys. Rev. A* **65**, 033619 (2002).
- [147] O. Mustecaplioglu, M. Zhang, and L. You, Spin squeezing and entanglement in spinor condensates, *Phys. Rev. A* **66**, 033611 (2002).
- [148] S. Yi and H. Pu, Magnetization, squeezing, and entanglement in dipolar spin-1 condensates, *Phys. Rev. A* **73**, 023602 (2006).
- [149] F. Gerbier, S. Fölling, A. Widera, O. Mandel, and I. Bloch, Probing number squeezing of ultracold atoms across the Superfluid-Mott Insulator transition, *Phys. Rev. Lett.* **96**, 090401 (2006).
- [150] B. Oztop, M. O. Oktel, O. E. Mustecaplioglu, and L. You, Quantum entanglement of spin-1 bosons with coupled ground states in optical lattices, *J. Phys. B-At. Mol. Opt. Phys.* **42**, 145505 (2009).
- [151] T. Gasenzer, Limitations of squeezing due to collisional decoherence in Bose-Einstein condensates, *J. Phys. B-At. Mol. Opt. Phys.* **35**, 2337 (2002).
- [152] J. Dunningham, K. Burnett, and S. Barnett, Interferometry below the standard quantum limit with Bose-Einstein condensates, *Phys. Rev. Lett.* **89**, 150401 (2002).
- [153] Y. Li, Y. Castin, and A. Sinatra, Optimum spin squeezing in Bose-Einstein condensates with particle losses, *Phys. Rev. Lett.* **100**, 210401 (2008).
- [154] Y. Li, P. Treutlein, J. Reichel, and A. Sinatra, Spin squeezing in a bimodal condensate: spatial dynamics and particle losses, *Eur. Phys. J. B* **68**, 365 (2009).
- [155] U. Poulsen and K. Mølmer, Quantum states of Bose-Einstein condensates formed by molecular dissociation, *Phys. Rev. A* **63**, 023604 (2001).
- [156] X. Yi and W. Wang, Creating entangled atomic pairs by photodissociation, *J. Phys. B-At. Mol. Opt. Phys.* **34**, 5087 (2001).
- [157] C. Lee, Adiabatic Mach-Zehnder interferometry on a quantized Bose-Josephson junction, *Phys. Rev. Lett.* **97**, 150402 (2006).
- [158] M. Jaaskelainen and P. Meystre, Coherence dynamics of two-mode condensates in asymmetric potentials, *Phys. Rev. A* **73**, 013602 (2006).
- [159] G.-B. Jo, Y. Shin, S. Will, T. A. Pasquini, M. Saba, W. Ketterle, D. E. Pritchard, M. Vengalattore, and M. Prentiss, Long Phase Coherence Time and Number Squeezing of Two Bose-Einstein Condensates on an Atom Chip, *Phys. Rev. Lett.* **98**, 030407 (2007).
- [160] W. Li, A. K. Tuchman, H.-C. Chien, and M. A. Kasevich, Extended coherence time with atom-number squeezed states, *Phys. Rev. Lett.* **98**, 040402 (2007).
- [161] M. Vengalattore, J. M. Higbie, S. R. Leslie, J. Guzman, L. E. Sadler, and D. M. Stamper-Kurn, High-resolution magnetometry with a spinor Bose-Einstein Condensate, *Phys. Rev. Lett.* **98**, 200801 (2007).
- [162] F. Benatti, R. Floreanini, and U. Marzolino, Sub-shot-noise quantum metrology with entangled identical particles, *Ann. Phys.* **325**, 924 (2010).
- [163] F. Benatti, R. Floreanini, and U. Marzolino, Squeezing inequalities and entanglement for identical particles, *arXiv:1009.0995* (2010).
- [164] X. Wang, A. Sørensen, and K. Mølmer, Spin squeezing in the Ising model, *Phys. Rev. A* **64**, 053815 (2001).
- [165] X. Wang, Entanglement and spin squeezing in the three-qubit transverse Ising model, *Phys. Lett. A* **331**, 164 (2004).
- [166] M. Reboiro, O. Civitarese, and L. Rebon, Study of squeezing in spin clusters, *Phys. Lett. A* **366**, 241 (2007).
- [167] G. S. Agarwal and R. R. Puri, Atomic states with spectroscopic squeezing, *Phys. Rev. A* **49**, 4968 (1994).
- [168] H. P. Yuen, Two-photon coherent states of the radiation field, *Phys. Rev. A* **13**, 2226 (1976).
- [169] D. F. Walls and G. J. Milburn, *Quantum Optics*, (Springer-Verlag, Berlin, 1994).
- [170] M. O. Scully and M. S. Zubairy, *Quantum Optics*, (Cambridge University Press, Cambridge, England, 1997).
- [171] V. Dodonov, 'Nonclassical' states in quantum optics: a 'squeezed' review of the first 75 years, *J. Opt. B-Quantum Semiclassical Opt.* **4**, R1 (2002).
- [172] C. M. Caves, Quantum-mechanical noise in an interferometer, *Phys. Rev. D* **23**, 1693 (1981).
- [173] R. S. Bondurant and J. H. Shapiro, Squeezed states in phase-sensing interferometers, *Phys. Rev. D* **30**, 2548 (1984).
- [174] X. Hu and F. Nori, Squeezed phonon states: Modulating quantum fluctuations of atomic displacements, *Phys. Rev. Lett.* **76**, 2294 (1996).
- [175] X. Hu and F. Nori, Quantum phonon optics: Coherent and squeezed atomic displacements, *Phys. Rev. B* **53**, 2419 (1996).
- [176] X. Hu and F. Nori, Phonon squeezed states generated by second-order Raman scattering, *Phys. Rev. Lett.* **79**, 4605 (1997).
- [177] X. Hu and F. Nori, Phonon squeezed states: quantum noise reduction in solids, *Physica B* **263-264**, 16 (1999).
- [178] A. M. Zagorskin, E. Il'ichev, M. W. McCutcheon, J. F. Young, and F. Nori, Controlled generation of squeezed states of microwave radiation in a superconducting resonant circuit, *Phys. Rev. Lett.* **101**, 253602 (2008).
- [179] A. O. Barut and Girardell, L., New coherent states associated with non-compact groups, *Commun. Math. Phys.* **21**, 41 (1971).
- [180] R. Gilmore, Geometry of symmetrized states, *Ann. Phys.* **74**, 391 (1972).
- [181] A. M. Perelomov, Coherent states for arbitrary Lie group, *Commun. Math. Phys.* **26**, 222 (1972).
- [182] A. M. Perelomov, *Generalized Coherent States and Their Applications*, (Springer-Verlag, Berlin, 1986).
- [183] W.-M. Zhang, D. H. Feng, and R. Gilmore, Coherent states: Theory and some applications, *Rev. Mod. Phys.* **62**, 867 (1990).
- [184] A. Lukš, V. Peřrinová, and J. Perina, Principal squeezing of vacuum fluctuations, *Opt. Commun.* **67**, 149–151 (1988).



- [185] A. Lukš, V. Peřinová, and Z. Hradil, Principal squeezing, *Acta Phys. Pol. A* **74**, 713–721 (1988).
- [186] <http://www.umich.edu/~nori/animations.html>.
- [187] M. Kitagawa and Y. Yamamoto, Number-phase minimum-uncertainty state with reduced number uncertainty in a Kerr nonlinear interferometer, *Phys. Rev. A* **34**, 3974 (1986).
- [188] W. M. Itano, J. C. Bergquist, J. J. Bollinger, J. M. Gilligan, D. J. Heinzen, F. L. Moore, M. G. Raizen, and D. J. Wineland, Quantum projection noise: Population fluctuations in two-level systems, *Phys. Rev. A* **47**, 3554–3570 (1993).
- [189] F. T. Arecchi, E. Courtens, R. Gilmore, and H. Thomas, Atomic coherent states in quantum optics, *Phys. Rev. A* **6**, 2211 (1972).
- [190] D. F. Walls and P. Zoller, Reduced quantum fluctuations in resonance fluorescence, *Phys. Rev. Lett.* **47**, 709 (1981).
- [191] H. Prakash and R. Kumar, Simultaneous squeezing of two orthogonal spin components, *J. Opt. B-Quantum Semiclassical Opt.* **7**, S757 (2005).
- [192] H. Prakash and K. Kumar, Atomic squeezing in assembly of two two-level atoms interacting with a single mode coherent radiation, *Eur. Phys. J. D* **42**, 475 (2007).
- [193] L. Song, X. Wang, D. Yan, and Z. Zong, Spin squeezing properties in the quantum kicked top model, *J. Phys. B-At. Mol. Opt. Phys.* **39**, 559 (2006).
- [194] V. Giovannetti, S. Lloyd, and L. Maccone, Quantum-enhanced measurements: Beating the standard quantum limit, *Science* **306**, 1330 (2004).
- [195] A. Rivas and A. Luis, Characterization of quantum angular-momentum fluctuations via principal components, *Phys. Rev. A* **77**(2), 022105 (2008).
- [196] A. Rivas and A. Luis, Practical schemes for the measurement of angular-momentum covariance matrices in quantum optics, *Phys. Rev. A* **78**(4), 043814 (2008).
- [197] X. Wang, A. Miranowicz, Y. X. Liu, C. P. Sun, and F. Nori, Sudden vanishing of spin squeezing under decoherence, *Phys. Rev. A* **81**, 022106 (2010).
- [198] A. R. U. Devi, X. Wang, and B. C. Sanders, Spin squeezing criterion with local unitary invariance, *Quantum Inf. Process.* **2**, 207 (2003).
- [199] X. Wang, Spin squeezing in nonlinear spin-coherent states, *J. Opt. B-Quantum Semiclassical Opt.* **3**, 93 (2001).
- [200] Y. Liu, The squeezed component of the atomic collective phase quadrature operators with respect to a two-level atomic coherent state, *Phys. Lett. A* **221**, 384 (1996).
- [201] X. Wang and B. C. Sanders, Relations between bosonic quadrature squeezing and atomic spin squeezing, *Phys. Rev. A* **68**, 033821 (2003).
- [202] S. Chumakov, A. Frank, and K. Wolf, Finite Kerr medium: Macroscopic quantum superposition states and Wigner functions on the sphere, *Phys. Rev. A* **60**, 1817 (1999).
- [203] T. Holstein and H. Primakoff, Field dependence of the intrinsic domain magnetization of a ferromagnet, *Phys. Rev.* **58**, 1098 (1940).
- [204] B. C. Sanders, Quantum dynamics of the nonlinear rotator and the effects of continual spin measurement, *Phys. Rev. A* **40**, 2417 (1989).
- [205] J. Wesenberg and K. Mølmer, Mixed collective states of many spins, *Phys. Rev. A* **65**, 062304 (2002).
- [206] S. Oçak and T. Altanhan, The effective potential of squeezed spin states, *Phys. Lett. A* **308**, 17 (2003).
- [207] M. Takeuchi, S. Ichihara, T. Takano, M. Kumakura, T. Yabuzaki, and Y. Takahashi, Spin squeezing via one-axis twisting with coherent light, *Phys. Rev. Lett.* **94**, 023003 (2005).
- [208] G.-R. Jin, Y.-C. Liu, and W.-M. Liu, Spin squeezing in a generalized one-axis twisting model, *New J. Phys.* **11**, 073049 (2009).
- [209] I. D. Leroux, M. H. Schleier-Smith, and V. Vuletić, Implementation of cavity squeezing of a collective atomic spin, *Phys. Rev. Lett.* **104**, 073602 (2010).
- [210] M. H. Schleier-Smith, I. D. Leroux, and V. Vuletić, Squeezing the collective spin of a dilute atomic ensemble by cavity feedback, *Phys. Rev. A* **81**, 021804 (2010).
- [211] A. Rojo, Optimally squeezed spin states, *Phys. Rev. A* **68**, 013807 (2003).
- [212] A. Andre and M. Lukin, Atom correlations and spin squeezing near the Heisenberg limit: Finite-size effect and decoherence, *Phys. Rev. A* **65**, 053819 (2002).
- [213] I. Bouchoule and K. Mølmer, Spin squeezing of atoms by the dipole interaction in virtually excited Rydberg states, *Phys. Rev. A* **65**, 041803 (2002).
- [214] M. Jafarpour and A. Akhound, Entanglement and squeezing of multi-qubit systems using a two-axis countertwisting Hamiltonian with an external field, *Phys. Lett. A* **372**, 2374 (2008).
- [215] A. Andre, L. Duan, and M. Lukin, Coherent atom interactions mediated by dark-state polaritons, *Phys. Rev. Lett.* **88**, 243602 (2002).
- [216] X. Wang and K. Mølmer, Pairwise entanglement in symmetric multi-qubit systems, *Eur. Phys. J. D* **18**, 385 (2002).
- [217] D. Yan, X. Wang, and L. Wu, Spin squeezing and entanglement of many-particle spin-half states, *Chin. Phys. Lett.* **22**, 271 (2005).
- [218] B. Zeng, D. Zhou, Z. Xu, and L. You, Entanglement and spin-squeezing properties for three bosons in two modes, *Phys. Rev. A* **71**, 042317 (2005).
- [219] A. Messikh, Z. Ficek, and M. R. B. Wahiddin, Spin squeezing as a measure of entanglement in a two-qubit system, *Phys. Rev. A* **68**, 064301 (2003).
- [220] A. Messikh, Z. Ficek, and M. Wahiddin, Entanglement and spin squeezing in the two-atom Dicke model, *J. Opt. B-Quantum Semiclassical Opt.* **5**, L1 (2003).
- [221] G. Tóth, C. Knapp, O. Guehne, and H. J. Briegel, Optimal spin squeezing inequalities detect bound entanglement in

- spin models, Phys. Rev. Lett. **99**, 250405 (2007).
- [222] J. Vidal, Phys. Rev. A **73**, 062318 (2006).
- [223] X. Yin, X. Wang, J. Ma, and X. G. Wang, Spin squeezing and concurrence, arXiv:0912.1752 (2009).
- [224] V. Coffman, J. Kundu, and W. K. Wootters, Distributed entanglement, Phys. Rev. A **61**, 052306 (2000).
- [225] C. A. Sackett, D. Kielpinski, B. E. King, C. Langer, V. Meyer, C. J. Myatt, M. Rowe, Q. A. Turchette, W. M. Itano, D. J. Wineland, and C. Monroe, Experimental entanglement of four particles, Nature **404**, 256 (2000).
- [226] M. Seevinck and J. Uffink, Sufficient conditions for three-particle entanglement and their tests in recent experiments, Phys. Rev. A **65**, 012107 (2001).
- [227] A. Sørensen and K. Mølmer, Entanglement and extreme spin squeezing, Phys. Rev. Lett. **86**, 4431 (2001).
- [228] G. Tóth, Entanglement detection in optical lattices of bosonic atoms with collective measurements, Phys. Rev. A **69**, 052327 (2004).
- [229] A. Kuzmich and E. S. Polzik, Atomic Quantum State Teleportation and Swapping, Phys. Rev. Lett. **85**(26), 5639 (2000).
- [230] D. Berry and B. Sanders, Quantum teleportation and entanglement swapping for spin systems, New J. Phys. **4**, 8 (2002).
- [231] L.-M. Duan, G. Giedke, J. I. Cirac, and P. Zoller, Inseparability Criterion for Continuous Variable Systems, Phys. Rev. Lett. **84**(12), 2722 (2000).
- [232] R. Simon, Peres-Horodecki Separability Criterion for Continuous Variable Systems, Phys. Rev. Lett. **84**, 2726 (2000).
- [233] D. Berry and B. Sanders, Equivalence between two-mode spin squeezed states and pure entangled states with equal spin, J. Phys. A-Math. Theor. **38**, L205 (2005).
- [234] M. G. Raymer, A. C. Funk, B. C. Sanders, and H. de Guise, Separability criterion for separate quantum systems, Phys. Rev. A **67**, 052104 (2003).
- [235] D. Berry and B. Sanders, Near-optimal two-mode spin squeezing via feedback, Phys. Rev. A **66**, 012313 (2002).
- [236] C. W. Helstrom, *Quantum Detection and Estimation Theory*, Academic Press, New York, 1976.
- [237] A. S. Holevo, *Probabilistic and Statistical Aspects of Quantum Theory*, (North-Holland, Amsterdam, 1982).
- [238] P. Kok and W. B. Lovett, *Introduction to Optical Quantum Information Processing*, (Cambridge University Press, Cambridge, England, 2010).
- [239] L. Pezzé and A. Smerzi, Entanglement, nonlinear dynamics, and the Heisenberg limit, Phys. Rev. Lett. **102**, 100401 (2009).
- [240] J. Ma and X. Wang, Fisher information and spin squeezing in the Lipkin-Meshkov-Glick model, Phys. Rev. A **80**, 012318 (2009).
- [241] P. Hyllus, L. Pezzé, and A. Smerzi, Entanglement and Sensitivity in Precision Measurements with States of a Fluctuating Number of Particles, Phys. Rev. Lett. **105**, 120501 (2010).
- [242] G. R. Jin, S. Luo, Y. C. Liu, H. Jing, and W. M. Liu, Polarization squeezing and multipartite entanglement of triphoton states, J. Opt. Soc. Am. B **27**, A105 (2010).
- [243] S. L. Braunstein and C. M. Caves, Statistical distance and the geometry of quantum states, Phys. Rev. Lett. **72**, 3439 (1994).
- [244] D. Bures, An extension of Kakutani's theorem on infinite product measures to the tensor product of semifinite  $w^*$ -algebras, Trans. Am. Math. Soc. **135**, 199 (1969).
- [245] W.-L. You, Y.-W. Li, and S.-J. Gu, Fidelity, dynamic structure factor, and susceptibility in critical phenomena, Phys. Rev. E **76**, 022101 (2007).
- [246] B. C. Sanders and G. J. Milburn, Optimal Quantum Measurements for Phase Estimation, Phys. Rev. Lett. **75**(16), 2944 (1995).
- [247] V. Giovannetti, S. Lloyd, and L. Maccone, Quantum Metrology, Phys. Rev. Lett. **96**, 010401 (2006).
- [248] S. Boixo, A. Datta, M. J. Davis, S. T. Flammia, A. Shaji, and C. M. Caves, Quantum Metrology: Dynamics versus Entanglement, Phys. Rev. Lett. **101**, 040403 (2008).
- [249] P. Zanardi, M. G. A. Paris, and L. Campos Venuti, Quantum criticality as a resource for quantum estimation, Phys. Rev. A **78**, 042105 (2008).
- [250] D. Burgarth, K. Maruyama, and F. Nori, Coupling strength estimation for spin chains despite restricted access, Phys. Rev. A **79**, 020305 (2009).
- [251] [http://en.wikipedia.org/wiki/Mean\\_of\\_circular\\_quantities](http://en.wikipedia.org/wiki/Mean_of_circular_quantities).
- [252] D. Leibfried, M. Barrett, T. Schaetz, J. Britton, J. Chiaverini, W. Itano, J. Jost, C. Langer, and D. Wineland, Toward Heisenberg-limited spectroscopy with multiparticle entangled states, Science **304**, 1476 (2004).
- [253] S. Sachdev, *Quantum Phase Transitions*, (Cambridge University Press, Cambridge, England, 1999).
- [254] F. Haake, *Quantum Signature of Chaos*, (Springer - Verlag, Berlin, 1999).
- [255] S.-J. Gu, Fidelity approach to quantum phase transitions, Int. J. Mod. Phys. B **24**, 4371 (2010).
- [256] E. J. Heller, Bound-state eigenfunctions of classically chaotic Hamiltonian systems: Scars of periodic orbits, Phys. Rev. Lett. **53**, 1515 (1984).
- [257] R. Schack, G. M. D'Ariano, and C. M. Caves, Hypersensitivity to perturbation in the quantum kicked top, Phys. Rev. E **50**, 972 (1994).
- [258] S. Chaudhury, A. Smith, B. E. Anderson, S. Ghose, and P. S. Jessen, Quantum signatures of chaos in a kicked top, Nature **461**, 768 (2009).
- [259] H. J. Lipkin, N. Meshkov, and G. A. J., Validity of many-body approximation methods for a solvable model (I). Exact solutions and perturbation theory, Nucl. Phys. **62**, 188 (1965).
- [260] J. Vidal, G. Palacios, and R. Mosseri, Entanglement in a second-order quantum phase transition, Phys. Rev. A **69**, 022107 (2004).
- [261] R. Botet, R. Jullien, and P. Pfeuty, Size Scaling for Infinitely Coordinated Systems, Phys. Rev. Lett. **49**, 478–481 (1982).

- [262] J. I. Cirac, M. Lewenstein, K. Mølmer, and P. Zoller, Quantum superposition states of Bose-Einstein condensates, *Phys. Rev. A* **57**, 1208–1218 (1998).
- [263] N. F. Tsomokos D, Ashhab S, Fully connected network of superconducting qubits in a cavity, *New J. Phys.* **10**, 113020 (2008).
- [264] J. P. Draayer and F. Pan, Analytical solutions for the LMG model, *Phys. Lett. B* **451**, 1 (1999).
- [265] R. H. M. Jon Links, H.-Q. Zhou and M. D. Gould, Algebraic Bethe ansatz method for the exact calculation of energy spectra and form factors: applications to models of Bose-Einstein condensates and metallic nanograins, *J. Phys. A: Math. Gen.* **36**, R63 (2003).
- [266] S. Dusuel and J. Vidal, Continuous unitary transformations and finite-size scaling exponents in the Lipkin-Meshkov-Glick model, *Phys. Rev. B* **71**, 224420 (2005).
- [267] H. Wichterich, J. Vidal, and S. Bose, Universality of the negativity in the Lipkin-Meshkov-Glick model, *Phys. Rev. A* **81**, 032311 (2010).
- [268] R. Orús, S. Dusuel, and J. Vidal, Equivalence of Critical Scaling Laws for Many-Body Entanglement in the Lipkin-Meshkov-Glick Model, *Phys. Rev. Lett.* **101**, 025701 (2008).
- [269] J. Vidal, S. Dusuel, and T. Barthel, Entanglement entropy in collective models, *J. Stat. Mech.-Theory Exp.*, P01015 (2007).
- [270] N. Lambert, C. Emary, and T. Brandes, Entanglement and the phase transition in single-mode superradiance, *Phys. Rev. Lett.* **92**, 073602 (2004).
- [271] N. Lambert, Y.-n. Chen, R. Johansson, and F. Nori, Quantum chaos and critical behavior on a chip, *Phys. Rev. B* **80**, 165308 (2009).
- [272] K. Furuya, M. C. Nemes, and G. Q. Pellegrino, Quantum dynamical manifestation of chaotic behavior in the process of entanglement, *Phys. Rev. Lett.* **80**, 5524 (1998).
- [273] L. Song, D. Yan, J. Ma, and X. Wang, Spin squeezing as an indicator of quantum chaos in the Dicke model, *Phys. Rev. E* **79**, 046220 (2009).
- [274] M. A. M. Deaguiar, K. Furuya, C. H. Lewenkopf, and M. C. Nemes, Chaos in a spin boson system - classical analysis, *Ann. Phys.* **216**, 291 (1992).
- [275] U. Weiss, *Quantum Dissipative Systems*, (World Scientific, Singapore, 1999).
- [276] C. W. Gardiner and P. Zoller, *Quantum noise*, (Springer, Berlin, 2000).
- [277] H.-P. Breuer and F. Petruccione, *The Theory of Open Quantum Systems*, (Oxford university press, Oxford, 2002).
- [278] M. Schlosshauer, *Decoherence and the quantum-to-classical transition*, (Springer, Berlin, 2007).
- [279] J. Stockton, J. Geremia, A. Doherty, and H. Mabuchi, Characterizing the entanglement of symmetric many-particle spin-1/2 systems, *Phys. Rev. A* **67**, 022112 (2003).
- [280] S. Huelga, C. Macchiavello, T. Pellizzari, A. Ekert, M. Plenio, and J. Cirac, Improvement of frequency standards with quantum entanglement, *Phys. Rev. Lett.* **79**, 3865 (1997).
- [281] A. M. Rey, L. Jiang, and M. D. Lukin, Quantum-limited measurements of atomic scattering properties, *Phys. Rev. A* **76**, 053617 (2007).
- [282] M. Koschorreck and M. W. Mitchell, Unified description of inhomogeneities, dissipation and transport in quantum light-atom interfaces, *J. Phys. B* **42**(19), 195502 (2009).
- [283] C. Simon and J. Kempe, Robustness of multiparty entanglement, *Phys. Rev. A* **65**, 052327 (2002).
- [284] J. Preskill, *Lecture Notes for Physics 219: Quantum Information and Computation*, (Caltech, Pasadena, CA, 1999).
- [285] I. K. Kominis, Sub-shot-noise magnetometry with a correlated spin-relaxation dominated alkali-metal vapor, *Phys. Rev. Lett.* **100**, 073002 (2008).
- [286] M. Greiner, O. Mandel, T. Esslinger, T. Hänsch, and I. Bloch, Quantum phase transition from a superfluid to a Mott insulator in a gas of ultracold atoms, *Nature* **419**, 51 (2002).
- [287] C. P. Sun, Y. Li, and X. F. Liu, Quasi-spin-wave quantum memories with a dynamical symmetry, *Phys. Rev. Lett.* **91**, 147903 (2003).
- [288] H. Wang, C.-P. Yang, and F. Nori, Robust and scalable optical one-way quantum computation, *Phys. Rev. A* **81**, 052332 (2010).
- [289] M. Fleischhauer and T. Richter, Pulse matching and correlation of phase fluctuations in Lambda systems, *Phys. Rev. A* **51**, 2430 (1995).
- [290] L. Thomsen, S. Mancini, and H. Wiseman, Spin squeezing via quantum feedback, *Phys. Rev. A* **65**, 061801 (2002).
- [291] W. P. Bowen, R. Schnabel, H.-A. Bachor, and P. K. Lam, Polarization Squeezing of Continuous Variable Stokes Parameters, *Phys. Rev. Lett.* **88**, 093601 (2002).
- [292] J. Heersink, T. Gaber, S. Lorenz, O. Glöckl, N. Korolkova, and G. Leuchs, Polarization squeezing of intense pulses with a fiber-optic Sagnac interferometer, *Phys. Rev. A* **68**, 013815 (2003).
- [293] J. F. Corney, P. D. Drummond, J. Heersink, V. Josse, G. Leuchs, and U. L. Andersen, Many-body quantum dynamics of polarization squeezing in optical fibers, *Phys. Rev. Lett.* **97**, 023606 (2006).
- [294] A. Luis and N. Korolkova, Polarization squeezing and nonclassical properties of light, *Phys. Rev. A* **74**, 043817 (2006).
- [295] C. Marquardt, J. Heersink, R. Dong, M. V. Chekhova, A. B. Klimov, L. L. Sánchez-Soto, U. L. Andersen, and G. Leuchs, Quantum Reconstruction of an Intense Polarization Squeezed Optical State, *Phys. Rev. Lett.* **99**, 220401 (2007).
- [296] L. K. Shalm, R. B. A. Adamson, and A. M. Steinberg, Squeezing and over-squeezing of triphotons, *Nature* (2009).